5-17-2018 2:00 PM

Flexural Behaviour of Reinforced Concrete Elements Retrofitted Using External Unbonded Superelastic Shape Memory Alloy Bars

Yamen Ibrahim Elbahy, *The University of Western Ontario*

Supervisor: Youssef, Maged A., *The University of Western Ontario*

A thesis submitted in partial fulfillment of the requirements for the Doctor of Philosophy degree in Civil and Environmental Engineering

ABSTRACT

Steel reinforced concrete (RC) framed structures are seismically designed for safety, where the earthquake energy is dissipated through yielding of the steel bars. During strong earthquakes, high inelastic deformations are allowed to take place. This allowance results in significant residual deformations. Thus, following an earthquake, the structure might be deemed irreparable, requiring its demolishing and replacement. If the frame can be designed to regain its original shape following an earthquake, then the structure will be repairable. This kind of design can be achieved by using smart materials such as Shape Memory Alloys (SMAs).

SMAs have unique properties, which make them distinctive when compared to other metals and alloys. These properties give them the ability to undergo large deformations and return to their undeformed shape upon unloading (superelasticity). Under cyclic loading, the flag shape stress-strain relationship of SMA provides the ability to dissipate large amounts of energy. In addition, they have good corrosion and fatigue resistance. These unique properties of SMAs have motivated researchers to utilize them as reinforcing bars in RC structures.

The first part of this study aims at providing in-depth understanding of the flexural behaviour of SMA RC beams. A sectional analysis method, that predicts the flexural behaviour of SMA RC beams during both loading and unloading stages, is adopted and validated using available experimental data. A parametric study is then carried out to

investigate the effect of different geometrical properties. Recommendations for the optimum amount and length of SMA bars are drawn based on results of this study.

Retrofitting RC structures can be needed to minimize the seismic residual deformations occurring in the structure following an earthquake event. It can also be needed to upgrade their capacities and/or address the deterioration happening overtime. Innovative and cost effective retrofitting techniques are continuously being developed. In the second part of this study, a new technique for retrofitting RC beams in flexure is introduced. The technique is based on using external unbonded superleastic SMA bars. The technique is first assessed using the Finite Element (FE) method. A simplified sectional analysis approach is then presented, validated, and used to conduct a parametric study. Results of the parametric study are used to develop equations to predict changes in the beam behaviour covering its residual displacement, stiffness, and the dissipated energy because of the suggested retrofitting technique.

Beam-column joints (BCJs) or RC framed structures are designed to satisfy the strong column-weak beam concept, where severe inelastic deformations are allowed to occur in the beam. Minimizing these inelastic deformations can be needed to make the structure repairable. In addition, one of the problems for existing RC structures designed per older standards (pre 1970s) is the inadequate anchorage for the beam reinforcement in the joint area. In the third part of this study, the applicability of using external unbonded SMA bars to retrofit RC BCJs is investigated. A FE model is first developed and validated. A simplified model is then proposed and validated using the developed FE model. The

simplified model is used to conduct a parametric study to investigate the behaviour of SMA retrofitted RC BCJs. Results of the parametric study are used to develop equations to decide the optimum length and amount of the SMA bars.

Superelastic SMA bars can be used to minimize the inelastic deformations happening in RC frame structures after seismic events. Minimizing these inelastic deformations make the structure repairable. In the fourth part of this study, the seismic performance of RC frames retrofitted using external superleastic SMA bars is investigated and compared to the behaviour of a regular steel RC frame structure. Nonlinear time history analysis is performed for a six storey RC frame structure located in high seismic region. After performing the analysis, two retrofitted frames are assumed. Analysis is performed again for the two frames at the load intensities causing failure of the steel RC frame. The performance of the retrofitted frames is compared to the steel RC frame. The retrofitted frames showed lower level of damage at failure and they tolerated higher earthquake intensities. The suggested retrofitting technique reduced the maximum drifts by 10% to 15%, and the residual drifts by 50% to 70%.

Keywords: reinforced concrete (RC), shape memory alloys (SMAs), flexural behaviour, retrofitting, sectional analysis, beam-column Joint, frame structure, seismic performance

CO-AUTHORSHIP

This doctoral thesis has been prepared in accordance with the regulation of manuscript format stipulated by the School of Graduate and Postdoctoral Studies at The University of Western Ontario. Substantial parts of this thesis are submitted for publication to peer-reviewed technical journals and international conferences. All data analysis, modelling process, and writing the initial version of all publications are carried out by the candidate himself. The contribution of his research advisor consisted of either providing advice, and/or helping in the development of final versions of publications:

Submitted Journals Publications

Chapter 3 Elbahy, Y.I. and Youssef, M.A. "Flexural Behaviour of Superleastic Shape Memory Alloy Reinforced Concrete Beams During Loading and Unloading Stages." *Engineering Structures Journal*, Submitted April 2018.

Chapter 4 Elbahy, Y.I. and Youssef, M.A. "Flexural Behaviour of Reinforced Concrete Beams Retrofitted Using External Unbonded Superleastic Shape Memory Alloy Bars." *Journal of Building Engineering*, Submitted April 2018.

Chapter 5 Elbahy, Y.I. and Youssef, M.A. "Flexural Behaviour of Reinforced Concrete Beam-Column Joints Retrofitted Using External Unbonded Superleastic Shape Memory Alloy Bars." *Engineering Structures Journal*, Submitted April 2018.

Chapter 6 Elbahy, Y.I. and Youssef, M.A. "Seismic Performance of Reinforced Concrete Frames Retrofitted Using External Superelastic Shape Memory Alloy Bars." *Bulletin of Earthquake Engineering Journal*, Submitted April 2018.

To: *My father AHMED,*

My mother AMIRA,

My brother HESHAM

My sister Yusra, and

My fiancee Toka

ACKNOWLEDGEMENT

The author would like to convey his sincere appreciation and gratitude to his advisor, Dr. Maged A. Youssef for his guidance, advice and encouragement throughout the course of this research. His mentorship, support and patience was a great essence and is greatly acknowledged.

Special thanks are due to fiancée, Dr. Toka S. Mostafa, for her help with the statistical modeling part and for her continuous and endless support during this long term of study. The author would also like to thank all staff at The Department of Civil and Environmental Engineering who contributed directly or indirectly to the accomplishment of this thesis.

Finally, the author would like to express his genuine gratitude and appreciation for his father, mother, brother, and sister for their continuous support and encouragement.

TABLE OF CONTENT

LIST OF TABLES

LIST OF FIGURES

LIST OF ABBREVIATION, SYMBOLS, AND NOMENCLATURE

A'_s	Cross-sectional area of the internal compressive reinforcement
$Adj\ R^2$	An adjustment of the R-squared that penalizes the addition of extraneous predictors to the model
A_i	Area of layer *i*
As	Cross-sectional area of the internal tensile reinforcement
A_{SMAs}/A_s	Ratio between the amounts of SMAs reinforcement to the amount of steel reinforcement.
$BCJs$	Beam-column joints
df	Degrees of Freedom
E	Modulus of elasticity
$E_{cr\text{-}SMA}$	SMAs austenite modulus of elasticity.
EN_{org}	Amount of dissipated energy by the original BCJ
EN_{rt}	Amount of dissipated energy by the retrofitted BCJ
EN_s	Amount of dissipated energy by the steel RC beam.
EN_{SMAs}	Amount of dissipated energy by the SMAs RC beam.
EN_{SMAs}/EN_s	Ratio between the amount of dissipated energy by the SMAs RC beam and the amount of dissipated energy by the steel RC beam.
E_{p1}	SMAs modulus of elasticity during the stress induced transformation from austenite to martensite phase.
E_{p2}	SMAs martensite modulus of elasticity.
$E_{u\text{-}s}$	Post-yielding modulus of elasticity of steel.
$E_{u\text{-}SMA}$	Post-yielding modulus of elasticity of SMAs.
E_y	Modulus of elasticity
$E_{y\text{-}s}$	Pre-yielding modulus of elasticity of steel.
$F(\ a,\ b)$	F-statistic is the Mean Square Model (MS of model) divided by the Mean Square Residual (MS residuals) yielding F=xx. The numbers in parentheses are the Model and Residual degrees of freedom
f_c	Concrete compressive stress.
f_{cr}	Concrete cracking stress.
$f_{cr\text{-}SMA}$	SMAs critical stress at which stress induced transformation from austenite to martensite phase.
FE	finite element
f_{p1}	SMAs stress after complete stress induced transformation from austenite to martensite phase
$FRPs$	Fibre Reinforced Polymers
f_t	Concrete tensile stress.
$f_{u\text{-}s}$	Steel ultimate stress

$f_{u\text{-}SMAs}$	SMAs ultimate (rupture) stress
f_y	Reinforcement yielding stress.
$f_{y\text{-}s}$	Steel yielding stress
$f_{y\text{-}SMAs}$	SMAs real yielding stress
h/b	Cross-section height-to-width ratio.
L	Full length of the beam
L/h	Beam span-to-depth ratio.
L_{SMAs}	SMAs bars length L_{SMAs}.
L_{SMAs}/L	Ratio between the SMAs bar length and the total cantilever beam length.
M	Cross-section moment
M_{org}	Moment capacity of the original beam or BCJ
M_{rt}	Maximum moment capacity of the retrofitted beam or BCJ
MS	Mean Squares
N.A.	Neutral axis
Ni-Ti	Nickel-Titanium.
NSM	Near Surface Mounted
Number of obs	Number of observations used in the regression analysis
P	Applied load
Prob > F	P-value associated with the F-statistic.
R^2	The proportion of variance in the dependent variable (science) which can be explained by the independent variables (math, female, socst and read)
RC	Reinforced Concrete
RMSE	The standard deviation of the error term, and is the square root of the Mean Square Residual (or Error)
SMAs	Shape Memory Alloys
SS	Sum of Squares
ST_{org}	Initial stiffness of the original beam or BCJ
ST_{rt}	Initial stiffness of the retrofitted beam or BCJ
y_i	Distance between the centre of gravity of layer *i* and the centre of gravity of the concrete cross-section.
Z	Slope of compressive strain softening branch.
$\delta_{cr\text{-}SMAs}$	SMAs RC beam critical displacement - at which SMAs bars reach their critical stress value.
δ_{max}	Maximum applied displacement at the cantilever beam free end.
δ_{max}/L	drift ratio
δ_{max}/δ_y	Ratio between the maximum applied displacement at the beam tip and the displacement at which beam reinforcement starts to yield.
$\delta_{max\text{-}org}$	Maximum displacement applied to the original beam

$\delta_{max\text{-}rt}$	Maximum displacement applied to the retrofitted beam
δ_r	Amount of residual displacement at complete unloading
δ_r/δ_{max}	Ratio between residual displacement and maximum applied displacement.
δ_y	Beam displacement at which reinforcement starts to yield
$\delta_{y\text{-}org}$	Displacement at which internal steel bars started to yield in the original beam.
$\delta_{y\text{-}rt}$	Displacement at which yielding in the external SMAs bars starts to occur
$\delta_{y\text{-}s}$	Steel RC beam yielding displacement - at which steel bars reach their yielding stress limit.
$\delta_{y\text{-}s}/\delta_{cr\text{-}SMAs}$	Inverse of the ratio between the SMAs RC beams critical displacement and the steel RC beams yielding displacement.
ε_0	Concrete strain at maximum compressive loading stress f'_c.
ε_c	Concrete compressive strain.
ε_{cr}	Concrete cracking strain.
$\varepsilon_{cr\text{-}SMA}$	SMAs critical strain.
$\varepsilon_{c\text{-}top}$	Strain of the top compressive concrete layer
ε_{cu}	Ultimate concrete compressive strain.
ε_p	Concrete strain at which first zero-stress value is achieved after unloading starts.
ε_{p1}	SMAs strain after complete stress induced transformation from austenite to martensite phase.
ε_r	Concrete strain at which unloading starts.
$\varepsilon_{SMAs\text{-}ex}$	Unbonded SMAs bars strain
ε_{un}	Strain at which unloading start.
$\varepsilon_{u\text{-}s}$	Steel rupture strain.
$\varepsilon_{u\text{-}SMA}$	SMAs ultimate (rupture) strain
ε_y	Yielding strain
$\varepsilon_{y\text{-}s}$	Yielding strain of steel.
$\varepsilon_{y\text{-}SMA}$	SMAs real yielding strain.
ρ_b	Balanced cross-section reinforcement ratio.
ρ_{int}	Intermediate cross-section reinforcement ratio ($\rho_{int} = 0.5\ \rho_b$).
ρ_{min}	Minimum cross-section reinforcement ratio.
$\rho_{s\text{-}b}$	Reinforcement ratio of balanced steel RC cross-section.
ρ_{SMAs}	Reinforcement ratio of SMAs RC cross-section.
$\rho_{SMAs}/\rho_{s\text{-}b}$	Ratio between the reinforcement ratio of the SMAs RC cross-section and the reinforcement ratio of the balanced steel RC cross-section steel.
$\rho_{SMAs}/\rho_{s\text{-}min}$	the ratio between the SMAs reinforcement ratio and the minimally

	reinforced cross-section steel reinforcement ratio
$\rho_{s\text{-}min}$	Minimum reinforcement ratio of steel RC cross-section.
ϕ	Cross-section curvature

Chapter 1 Introduction

1.1 GENERAL

Most of the modern reinforced concrete (RC) framed structures are seismically designed for safety. This allows high inelastic deformations to occur when exposed to moderate or strong earthquakes. These inelastic deformations allow dissipating the seismic energy on the cost of residual deformations. Severe structural damage is expected in the case of strong earthquakes, which may make the structure irreparable and must be demolished. Thus, there is a need to retrofit exisitng structures to minimize seismic residual deformations, which will make the structure repairable.

Pre-1970s designed and built structures are considered non-ductile, and, thus seismicaly deficient (Hassan et al. 2010). One of the main problems of these structures is the short anchorage of the beam reinforcing bars into the joint area. Retrofitting these structures is needed to achieve safety and ductility considering seismic loads.

There are different methods available in the literature for flexural retrofitting of RC elements (Klaiber et al. 1987). The main retrofitting concept to improve the strength and stiffness of the RC element by adding reinforcement to the concrete tensile surface. Examples are: (i) enlarging the element cross-section by using steel RC (Julio et al. 2005); (ii) attachimg a Steel plate (Aboutaha et al. 1996); (iii) using external post-tensioning; and (iv) applying Fibre Reinforced

Polymer (FRP) sheets or near surface mounted bars (Sharif and Bluch 1996, Castro et al. 1996). New techniques are still being developed and introduced to the market. For example, recent research on Shape Memory Alloys (SMAs) highlighted their potential use as a retrofitting material for RC structures (Alam et al. 2007, Janke et al. 2005).

SMAs are types of alloys with unique properties, which make them distinctive when compared to other metals and alloys (Alam et al. 2007; Janke et al. 2005). Superelasticity, which gives the material the ability to undergo large deformations and return to their undeformed shape upon unloading, is one of these unique properties. SMAs have a flag shaped stress-strain relationship, which gives them the ability to dissipate substantial amounts of energy and release them upon unloading. They also have good resistance to corrosion and fatigue, which make them potential candidates to be used as reinforcing bars.

The unique properties of SMAs have motivated researchers to utilize them as reinforcing bars in RC structures. Saiidi et al. (2007) and Abdulridha et al. (2013) experimentally investigated the use of SMAs as reinforcing bars for RC beams. Elbahy et al. (2008, 2009, 2010a, 2010b) studied the flexural behaviour of SMA RC sections and developed design guidelines and equations for strength and serviceability requirements. Using SMAs in plastic hinge regions of reinforced RC beam-column joints (BCJs) was experimentally investigated by Youssef et al. (2008).

1.2 RESEARCH NEEDS AND MOTIVATION

Recent strong earthquakes showed that public infrastructure can be severely damaged by a strong earthquake. These infrastructures are not expected to be available for a long period of time. This situation leads to health risks, severe business disruptions and closure. Canada should work on reducing the risks associated with severe earthquakes to avoid such situation. One of the methods to achieve this is by minimizing the degree of seismic damage. This can be achieved by retrofitting these structures using smart materials such as SMAs.

SMAs have a great ability to eliminate or reduce the amount of residual deformations upon unloading (superelasticity). If SMA is used as a retrofitting material, it will lead to a structure that can regain its original shape, while minimizing the seismic damage. This study investigates the applicability of using external SMA bars to retrofit RC beams, beam-column joints, and framed structures. It also provides design tools to design such a retrofitting technique.

1.3 SPECIFIC RESEARCH OBJECTIVES

This research program aims at exploring the applicability of using external SMA bars to retrofit RC elements. The specific research goals are:

(1) Investigate the behaviour of RC beams internally reinforced with SMA bars during the loading and unloading stages.

(2) Investigate the behaviour of RC beams retrofitted using external SMA bars during loading and unloading stages.

(3) Investigate the behaviour of RC BCJs retrofitted using external SMA bars during loading and unloading.

(4) Develop equations to determine the optimum number and length of SMA bars for the suggested retrofitting technique.

(5) Investigate the seismic performance of RC frames retrofitted using external SMA bars as compared to regular steel RC frames.

1.4 THESIS OUTLINE

This dissertation has been prepared according to the integrated-article format predefined by the Faculty of Graduate studies at Western University, London, Ontario, Canada. It consists of seven chapters covering the scope of this study:

Chapter 1 provides a brief introduction along with the research motivation and objectives.

Chapter 2 provides a brief literature review that discusses the Canadian Infrastructures status, deficiency of the pre-1970s concrete structures to seismic loads, different retrofitting techniques, and the unique properties of SMAs and their applications.

Chapter 3 investigates the behaviour of RC beams internally reinforced with SMA bars. A sectional analysis method is developed and validated using available experimental results. An extensive parametric study is then carried out to investigate the effect of different geometrical properties. Recommendations for the optimum amount and length of SMA bars are drawn based on results of this study.

Chapter 4 introduces a new technique for retrofitting RC beams in flexure by using external unbonded SMA bars. First, a Finite element (FE) model is developed using ABAQUS software. After validating the model using available experimental results, the model is then used to capture the behaviour of the retrofitted beams. A simplified sectional analysis approach is then presented and validated. An extensive parametric study is then carried out to investigate the optimum amount and length of the added SMA bars. Results of the parametric study are used to develop equations that are capable of predicting the changes in the beam behaviour because of the suggested retrofitting technique.

Chapter 5 investigates the applicability of using external unbonded SMA bars to retrofit RC BCJs. A finite elements (FE) model is first developed using ABAQUS software. After validating the model with available experimental results, a simplified model is assumed and validated. A parametric study is then carried out to investigate the behaviour of retrofitted RC BCJs. Results of the the parametric study are used to develop equations that are capable of predicting the changes in the BCJ behaviour because of the suggested retrofitting technique

Chapter 6 investigates the seismic performance of RC frames retrofitted using external superleastic SMA bars as compared to regular steel RC frames. Two retrofitting schemes are suggested to retrofit a six storey RC frame. The frames are then subjected to seismic excitations scaled to different intensities. The performance of the retrofitted frames is compared to the steel RC frame in terms of the damage level, the Maximum Inter-storey Drift (MID) ratio, Maximum Residual Inter-storey Drift (MRID), Maximum Roof Drift Ratio (MRDR), Residual Roof Drift Ratio (RRDR), and the earthquake intensity at collapse.

Chapter 7 summarizes the research conclusions.

1.5 REFERENCES

Alam, M.S., Youssef, M.A., and Nehdi, M. (2007). “Utilizing Shape Memory Alloys to Enhance the Performance and Safety of Civil Infrastructure: a Review.” Canadian Journal of Civil Engineering, 34(9), 1075-1086.

Elbahy Y.I., Nehdi M., Youssef M.A. (2010b). “Artificial Neural Network Model for Deflection Analysis of Superelastic Shape Memory Alloy Reinforced Concrete Beams.” Canadian Journal of Civil Engineering, 37(6), 855-865.

Elbahy Y.I., Youssef M.A., Nehdi M. (2009). “Stress Block Parameters for Concrete Flexural Members Reinforced with Superelastic Shape Memory Alloys.” Journal of Materials and Structures, 42(10), 1335-1351.

Elbahy Y.I., Youssef M.A., Nehdi M. (2010a). “Deflection of Superelastic Shape Memeory Alloy Renforced Concrete Beams: Assessment of Existing Models.” Canadian Journal of Civil Engineering, 37(6), 842-854.

Elbahy, Y.I., Youssef, M.A., Nehdi, M. (2008). “Flexural Behaviour of Concrete Memebers Reinforced with Shape Memory Alloys.” 2nd Canadian Conference on Effective Design of Structures, McMaster University, Hamilton, Ontario, Canada, 477-486.

Janke, L., Czaderski, C., Motavalli, M., and Ruth, J. (2005). “Applications of Shape Memory Alloys in Civil Engineering Structures - Overview, Limits and New Ideas.” Materials and Structures, 338(279), 578-592.

Saiidi, M.S., Sadrossadat-Zadeh, M., Ayoub, C., Itani, A. (2007). "Pilot Study of Behavior of Concrete Beams Reinforced with Shape Memory Alloys." ASCE, Journal of Materials in Civil Engineering, 19(6), 454-461.

Abdulridha, A., Palermo, D., Foo, S., and Vecchio, F. J. (2013). “Behavior and Modeling of Superelastic Shape Memory Alloys Reinforced Concrete Beams.” Journal of Engineering Structures, 49, 893-904. DOI: 10.1016/j.engstruct.2012.12.041.

Youssef, M.A., Alam, M.S. and Nehdi M. (2008) “Experimental investigation on the seismic behaviour of beam-column joints reinforced with superelastic shape memory alloys.,” Journal of Earthquake Engineering 12(7), 1205-1222.

Chapter 2 Literature Review

2.1 INTRODUCTION

Most of the modern reinforced concrete (RC) structures are seismically designed for safety. The design goal is to achieve an economical design by allowing inelastic deformations under moderate to strong earthquakes. These inelastic deformations allow the structure to dissipate the earthquake energy, but it results in significant residual deformations. If excessive residual deformations occur, the structure may become irreparable. Thus, there is a need to eliminate or minimize these residual deformations. One way to achieve this goal might use smart materials such as Shape Memory Alloys (SMAs).

Several methods for the flexural retrofitting of concrete elements have been introduced (Klaiber et al. 1987). They improve the strength and stiffness of the elements by reinforcing the concrete tensile surface. A simple example is enlarging the cross-section using jacketing (Julio et al. 2005, Julio and Branco 2008, Vandoros and Dritsos 2006a, Julio et al. 2003). Steel plate bending and external steel post-tensioning are widely used techniques (Aboutaha et al. 1996, Belal et al. 2014, He et al. 2016). Fibre Reinforced Polymers (FRPs) are also used in retrofitting concrete structures in the form of plates (externally bonded systems) or bars (near surface mounted systems) (Sharif and Bluch 1996, Castro et al. 1996). New techniques are still being developed and introduced to the construction market.

SMAs have a unique ability to undergo large deformations and return to their undeformed shape upon unloading. They can also dissipate substantial amounts of energy when subjected to cyclic loading. Their good resistance to corrosion and fatigue give them high potential to be used as reinforcing bars in RC structures.

Researchers explored utilizing SMAs in structural engineering applications. This include using SMAs as: anchors for columns (Tamai et al. 2003), restrainers for steel beam-columns joints (Ocel et al. 2004), dampers (Clark et al. 1995, Krumme et al. 1995), ties (Auricchio et al. 2001), and bracing members (Mazzolani et al. 2004). Using SMAs as primary reinforcement in concrete flexural members was experimentally investigated by Saiidi et al. (2007) and Abdulridha et al. (2013). Elbahy et al. (2008, 2009, 2010a, 2010b) studied the flexural behaviour of SMA reinforced concrete (RC) sections and developed design guidelines and equations for strength and serviceability requirements. Using SMAs in plastic hinge regions of reinforced RC beam-column joints (BCJs) was experimentally investigated by Youssef et al. (2008).

2.2 CANADIAN INFRASTRUCTURE STATUS

Most of the Canadian Infrastructure, including roads, bridges, schools, and hospitals, were constructed between the 1950s and 1970s (Mirza and Sipos 2009). Because of aging, over exposure to environmental factors, and underinvestment in maintenance, the conditions of these infrastructure is rapidly deteriorating. This fact makes them vulnerable to major hazards, such as earthquakes. This puts Canada's economy and quality of life at high risk.

2.2.1 Canadian Infrastructure Vulnerability to Damage

Cost of repairing the Canadian infrastructure was estimated in 2009 to be CAD $400 billion (Mirza and Sipos 2009). Deferring the maintenance of these infrastructures increases the maintenance cost to exceed five trillion dollars (The Canadian Council for Public-Private Partnership 2009). These estimated costs do not include the additional costs if a strong earthquake strikes. The upward trend in infrastructures deficiency over the last two decades warns a crisis for our cities and communities (The Federation of Canadian Municipalities 2007).

Lately, the Canadian government started to address these deteriorations by establishing its Building Canada and Economic Action Plan initiatives (See Infrastructure Canada 2007, Finance Canada 2010). However, the deferred maintenance program has been growing for decades.

During the period 1950s up to early 1970s, the Canadian government investments in maintenance of infrastructure were mainly dependent on economy growth and inflation. Starting mid-1970s, the government specified investment of zero to 2% of initial construction cost (See Infrastructure Canada 2007, Finance Canada 2010). However, this percent is far less than the appropriate level which is 2 to 4% of the initial construction cost. Thus, more spending is required to maintain infrastructure systems to achieve the level of service established in 1970s.

According to the Canadian Society of Civil Engineering 2003 report, almost 60% of the Canadian infrastructure were constructed before 1960 (The Canadian Society of Civil Engineering 2003). This means that most of the Canadian infrastructure are vulnerable to seismic

damage, because they were designed and built before modern knowledge of earthquake engineering. This vulnerability is likely to be higher in older communities such as Montreal, than in newer communities such as Vancouver.

Recent strong earthquakes, such as Haiti and Chile earthquakes, showed that public infrastructure can be severely damaged by a strong earthquake. Some of the infrastructure can be restored in a short period. However, many systems like transportation systems (i.e. bridges) will probably not be available for a longer period of time following an earthquake. This in turn causes health risks, severe business disruptions and closure. Canada should learn from Haiti and Chile experiences, and work on reducing the risks associated with severe earthquakes. This can simply be achieved by increasing the investment to restore the health of the public infrastructure.

2.2.2 Risk to Transportation Systems

Transportation systems in Vancouver, Montreal, and Ottawa undergo high stress levels because of the huge traffic loads in these areas. A major earthquake would severely disrupt them for a long period, could reach months (Mirza and Sipos 2009). New systems are expected to perform well because they were designed and constructed after the major developments in earthquake engineering. However, old systems, particularly bridges, are expected to be vulnerable to severe damages as these systems were designed and built without good knowledge of earthquake engineering.

2.2.3 Risk to Schools and Hospitals

Newer versions of the National Building Code of Canada assigned higher safety levels for schools and hospitals. Older schools and hospitals do not include these safety levels (National Building Code of Canada 2015). The Canadian government directed some funds to retrofit schools and hospitals in British Columbia and Quebec. For example, in 2010, the Government of Quebec decided to replace the hospital in Baie-St.-Paul and retrofit the hospital in Malbaie because they are not ductile enough to stand for a strong earthquake (CBC News 2010). In 2008, the Government of British Columbia launched a School Seismic Retrofit Program with secured fund of CAD $ 1.5 billion (Office of the Auditor General of British Columbia 2008). This gives a simple example of the governmental investments to reduce the vulnerability of public infrastructures to earthquake damage.

2.3 RETROFITTING RC STRUCTURES

2.3.1 Historical Background

Retrofitting an existing concrete structure is usually a more economical solution than demolishing the old structure and replacing it with a new one. Several retrofitting techniques of concrete structures have been developed during the last few decades. They aim at extending the service life of existing concrete structures. Klaiber et al. (1987) summarized the most popular retrofitting techniques for retrofitting concrete structures including: external prestressing, shotcrete, and injection techniques. In mid 1960's, retrofitting concrete structures using external bonded steel plates was first developed and introduced to the market. Steel plates are bonded to

the concrete surface using epoxy and/or anchors. This technique gained much popularity because of its ease in installation and low cost. Beber et al. (2001) reported that steel plates glued using epoxy are still functioning well for retrofitted structures in Europe.

Investigating the feasibility of using FRPs as a retrofitting material started in early 1990's. FRPs have high tensile strength, light weight, and high resistance to corrosion, which make them a potential candidate for replacing steel in retrofitting applications. Different types of FRPs are available in the market such as: Aramid (AFRP), Carbon (CFRP), and glass (GFRP) (Kachlakev and McCurry 2000). FRPs are adequate for retrofitting application because of the ease and speed in installation. FRPs can be used to retrofit concrete flexural elements. They can also be used for shear retrofitting (Kachlakev and McCurry 2000). FRPs can extend to include non flexural elements, such as columns. FRPs can be used in the form of wraps to increase the ductility of concrete columns in seismic areas. FRPs differ in their strength, stiffness, and durability. Selecting the type resin is dependent on many factors such as environmental exposure and FRP manufacturing.

Retrofitting of concrete flexural elements and slabs can be performed using unbounded steel prestressing tendons and bars. External prestressing using steel tendons was first used in concrete structures in 1930's in Germany, Belgium, and France (Virlogeux, 1990). Prestressing is considered an effective retrofitting technique (Klaiber et al. 1985). It was widely used to retrofit 25 concrete bridges in Germany (Falkner et al., 1995). In France, more than fifty box girder bridges were retrofitted using unbounded prestressed tendons (Godart, 1995).

2.3.2 External Unbonded Reinforcement

Concrete members are usually designed to satisfy both: serviceability and strength requirements. The design capacities may be inadequate because of a deficient design, an increase in applied loads, or a decrease in load carrying capacity. The flexural capacity is mainly dependent on the tensile reinforcement in these members. Thus, to restore the load-carrying capacity of the damaged members, additional reinforcement may be required. Numerous techniques are available for retrofitting flexural members. Some of these techniques are used in practice, while others are still under research.

Retrofitted beams with unbonded external reinforcement are shown to gain much increase in their ultimate strength (Cairns and Zaho 1993, Cairns and Watson 1993). Retrofitting using external reinforcement can also increase shear strength of the retrofitted element (Cairns and Watson 1993). Since the externally added reinforcement is totally unbounded, no campsite action is expected between the added reinforcement and concrete. The usual design equations of flexural members available in design standards are not applicable to the strengthened members.

Retrofitting concrete flexural members using external unbounded reinforcement has many advantages over other retrofitting techniques such as: speed and simplicity of installation, and minimal disruption to users during installation (Cairns and Zaho 1993). For a simply supported beam, yokes are installed at the end of the beam to anchor the threaded bars on both sides of the beam. Advantage of this technique over external prestressing technique is: eliminating the time of the prestressing operation, eliminating the clearance required around anchorage for prestress

jack, and reducing the cost of the retrofitting process. When compared to externally bonded plates retrofitting techniques, much less surface preparation is required and less impact on the environment as no epoxy is required.

Durability (i.e. corrosion) of this retrofitting system is a major drawback which may limit its use in certain situations. Moreover, steel is a heavy material which requires significant effort for transportation and heavy equipment for placemat. Despite of the drawbacks of this strengthening method, it has successfully used in many field applications (Cairns and Zaho 1993).

2.4 FAILURE OF BEAM-COLUMN JOINTS DURING PAST EARTHQUAKES

2.4.1 Introduction

Beam-Column Joints (BCJs) in concrete structures play a critical role in ensuring the structural integrity of the building performance during an earthquake event. Failure of a BCJ during an earthquake event can result in a partial or full collapse of the structure (Moehle and Mahin 1991). Many earthquakes involved damage of BCJs such as: El-Ansam earthquake (Algeria 1980), Northridge earthquake (California 1994), Tehuacan earthquake (Mexico 1999), Izmit earthquake (Turkey 1999), Athens earthquake (Greece 1999), Chi-Chi earthquake (Taiwan 1999), and Haiti earthquake (Haiti 2010).

An example of a building collapse is the collapse of the Kaiser Permanente building during the 1994 Northridge earthquake, **Fig. 2-1**. The building lateral resisting system was a moment resisting frame with anchored infill walls. The building was designed according to the pre-1970

design standards. Failure of the building occurred as a result of failure of multiple corner BCJs (Hassan et al. 2010).

(a) Full view of the building (b) Close up view of the failed BCJs

Fig. 2-1: Failure of the Kaiser Permanente Building during the 1994 Northridge earthquake (Hassan 2011)

Damage of BCJs can be accompanied by failure of other members in the structure. **Fig. 2-2** shows the partial collapse of a concrete frame building during the 1999 Izmit earthquake in Turkey. The partial collapse occurred due to the damage of BCJs as well as columns. Another example of partial building collapse is shown in **Fig. 2-3**. The buildings failed during the 1999 Chi-Chi earthquake in Taiwan, because of both column and BCJ failure.

(a) Full view of the building

(b) Close up view of the third-level BCJ

(c) Close up view of the second-level BCJ

Fig. 2-2: Partial building collapse during the 1999 Izmit earthquake in Turkey (NISEE 2010)

(a) Full view of the building

(b) Close up view of the failed BCJs

Fig. 2-3: Partial collapse of a 15-storey building in the 1999 Chi-Chi earthquake in Taiwan (Uang et al. 1999)

2.4.2 Seismic Deficiencies of the Pre-1970 BCJs

Design of structures to behave in a ductile manner during an earthquake event was first introduced in California in the 1960s. First informal design standards of ductile frames was introduced by the Structural Engineers Association of California (SEAOC) Blue Book in 1963 and 1965. SEAOC Blue Book included shear strength calculations and joint transverse reinforcement. However, these design provisions were specified for 13 storey (48.80 m) buildings or more (Moehle 1998). Following the 1967 Caracas earthquake and the 1971 San Fernando earthquake, the SEAOC Blue book was modified in 1971 to include the ductile details

requirements of buildings less than 13 stories (48.80 m) in height. The continuous development of the SEAOC during the 1970s helped in developing the first Uniform Building Code (UBC) in 1976. UBC (1976) can be considered as the first official standards of modern design for seismic loads. In other words, it can be considered as the transition from a non-ductile behaviour to a ductile behaviour during an earthquake event (Moehle 1998). With continuous development, the concept of capacity design (i.e. strong column-weak beam) was introduced. This concept is widely used in seismic design in modern design standards.

Since the first UBC was issued in 1976, structures built before this date were not enforced to follow special ductility requirements. Thus it is reasonable to assume that the behaviour of structures designed and built before the 1980s is not ductile. Inelastic mechanisms and inadequate detailing of joints can be considered main deficiencies of these structures. Detailing deficiencies can include insufficient anchorage of the beam reinforcement into the joint.

2.4.3 Bond Slip Failure Mode of Unconfined BCJs

Anchorage failure results from the bond slip failure of the beam bottom reinforcement. Because of the short unhooked embedment length of the beam bottom reinforcement, the reinforcement pullouts from the joint (Hassan 2011). In this failure mode, the full capacity of the joint is not developed. The insufficient embedded length of the beam bottom reinforcement into the joint eliminate the formations of the joint strut in one loading direction, which results in the premature failure of the whole joint. In case of excessive beam rotation due to reinforcement pullout, global instability of the structure becomes an issue of concern.

2.5 RETROFITTING OF SEISMIC DEFICIENT BCJS

Different methods of retrofitting BCJs were suggested in the literature to retrofit deficient BCJs constructed before the recent development in seismic design guidelines (Engindeniz 2008). Suggested strengthening techniques include: (i) epoxy injection; (ii) reinforced or prestressed concrete jacketing; (iii) concrete masonry unit jacketing or partial masonry infills; (iv) steel jacketing and/or addition of external steel elements; and (v) FRPs. Retrofitting techniques are different in the materials used, detailing requirements, labour demand, cost, and disruption to building occupancy. However, the main objective of all retrofitting techniques is to enforce the formation of plastic hinge into the beam rather than into the column. Yielding of the beam reinforcement and formation of plastic hinge ensure a ductile behaviour and eliminate the probability of sudden failure through plastic hinge formation in the column or joint shear failure.

2.6 SHAPE MEMORY ALLOYS

2.6.1 Introduction

SMAs are set of alloys with unique properties. These unique properties give them the ability to undergo large deformations and return to their original undeformed shape upon unloading (superelastic effect). This significantly increased their use in many applications including structural engineering ones. The following subsections introduce the basic characteristics and applications from the structural engineering perspective.

2.6.2 Mechanical Behaviour of SMAs

Several types of SMAs have been developed and introduced to the market in the last decades. Among these different types, superelastic Ni-Ti alloys are the most suitable for structural applications because of their high recoverable strain, durability, and being stable at the austenite phase at ambient temperature (Janke et al 2005).

Ni-Ti stress-strain relationship under tension and/or compression loading consists of four linear branches that are connected by smooth curves, **Fig. 2-4(a)**. As a simplification, the smooth curves can be ignored and the linear branches are assumed to intersect as shown in **Fig. 2-4(a)** and **Fig**. 2-4**(b)** (Alam et al. 2007). The alloy behaves elastically with a modulus of elasticity $E_{cr\text{-}SMA}$ until reaching the SMA critical stress $f_{cr\text{-}SMA}$, which represents the start of the martensite variant reorientation. As the strain ε_{SMA} exceeds the SMA critical strain $\varepsilon_{cr\text{-}SMA}$, the modulus of elasticity E_{p1} becomes 10% to 15% of $E_{cr\text{-}SMA}$. For strains above the martensite stress induced strain ε_{p1}, the material becomes stiffer and the modulus of elasticity E_{p2} reaches about 50 to 60% of $E_{cr\text{-}SMA}$. The final linear branch starts at the SMA yield point with a modulus of elasticity $E_{u\text{-}SMA}$ that is 3 to 8% of $E_{cr\text{-}SMA}$. Typical ranges for young's modulus, critical stress, ultimate strength, and elongation at failure are summarized in **Table 2-1**.

As shown in **Fig. 2-4(b)**, the SMA bar can recover its full deformations upon unloading if the strain ε_{SMA} is less than the martensite stress induced strain ε_{p1} (superelasticity). Reaching the yielding stress $f_{y\text{-}SMA}$ results in losing the material superelasticity. For structural applications, it is

recommended to design SMA RC sections to behave within the superelastic range (Youssef et al. 2008).

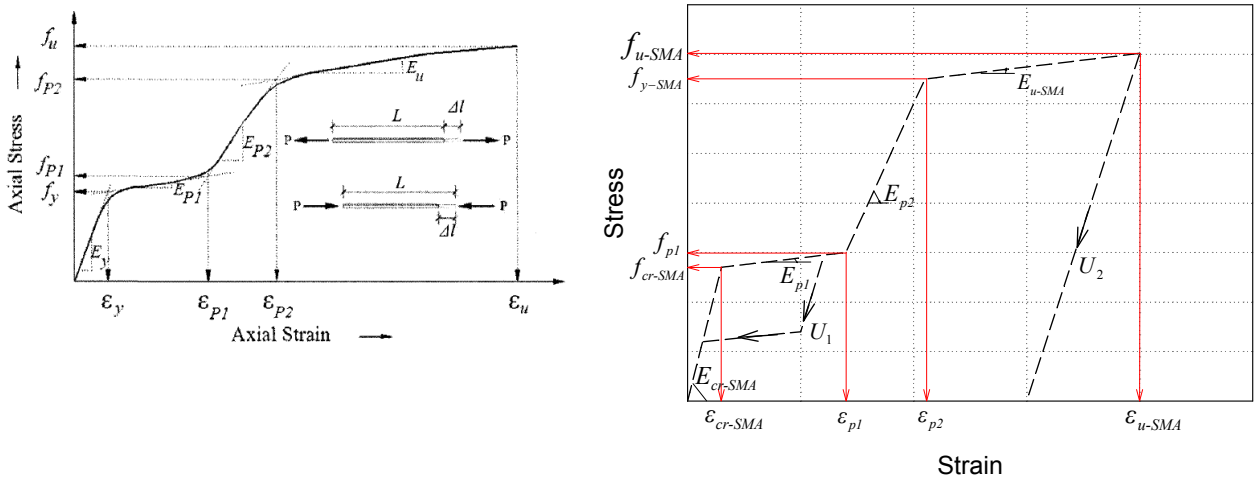

(a) Stress-strain relationship of SMAs under tension or compression (Alam et al. 2007)

(b) Stress-strain relationship of SMAs: Loading and unloading profiles

Fig. 2-4: Stress -strain relationship of SMA

Table 2-1: Properties of structural steel and Ni-Ti SMAs

Property	Structural Steel	NiTi SMA
Density (g/cm^3)	7.85	6.45
Elastic modulus (GPa)	200	30-83
Poisson's ratio	0.27-0.30	0.33
Yield strength (MPa)	248-517	195-690
Ultimate tensile strength (MPa)	448-827	895-1900
Elongation at failure (%)	20	5-50
Recoverable elongation (%)	0.20%	up to 8%

2.6.3 Behaviour of SMAs Under Cyclic Loading

The behaviour of SMAs under cyclic loading makes them very attractive for many engineering applications. An extensive research was performed to investigate the behaviour of SMAs under cyclic loading (Dolce and Cardone 2001). Typical behaviour of SMAs in the austenitic phase under cyclic axial loading is illustrated in **Fig. 2-5**.

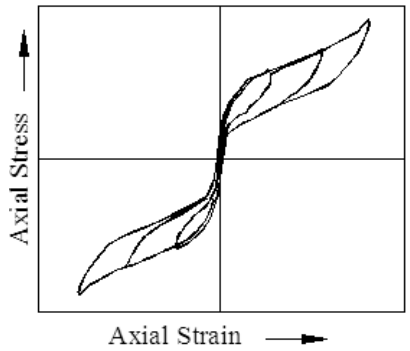

Fig. 2-5: Typical axial stress–strain relationship of superelastic SMA (austenite) under cyclic loading (Dolce and Cardone 2001).

When an SMA sample undergoes a cycle of loading within its superelastic range, it dissipates a certain amount of energy without keeping any permanent deformations. This is attributed to the phase transformation from austenite to martensite during loading and the reverse transformation during the unloading, **Fig. 2-5**. These forward and reversed transformations ensure full release of the dissipated energy during loading.

Although austenitic SMAs (i.e. superelastic) dissipate less amounts of energy when compared to martensitic SMAs, their dominant advantage is dissipating considerable amounts of energy under repeated cyclic loading with negligible residual strains.

2.6.4 Modelling of SMAs

SMAs are of a great potential for seismic design and retrofitting applications of structures because of: (i) their ability to undergo large deformations and return to their undeformed shape upon unloading or through heating; (ii) their ability to dissipate certain amount of energy under repeated cyclic loading without keeping permanent deformations; and (iii) their recentring capability. To facilitate using SMAs in real structures, accurate models need to be introduced. Several studies have been performed to investigate the behaviour of SMAs. According to these studies, three types of models can describe the behaviour of SMAs which are: phenomenological, thermomechanic, and micromechanic models. Only the phenomenological model is explained in this section.

Phenomenological models tend to use a small set of parameters such as: the elastic young's modulus, slope of the plateau, stress at the start and end of the forward and reverse transformations obtained from the experimental test results. Some phenomenological models of SMAs were developed by: Tanaka (1986), Liang and Rogers (1997), Auricchio and Sacco (1997), Lexcellent et all. (2000), Devobsek (2001), Malovrh and Gandhi (2001), and Tamai and Kitagawa (2002).

One-dimensional phenomenological models are considered appropriate for civil engineering applications, because most of these applications use SMA wires and bars. Because of the demand on using SMAs in engineering applications, finite element packages implemented SMA models in their material libraries such as ANSYS (ANSYS Inc. 2018) and Seismostruct (2018). The one dimensional superelastic model implemented in ANSYS is shown in **Fig. 2-6**.

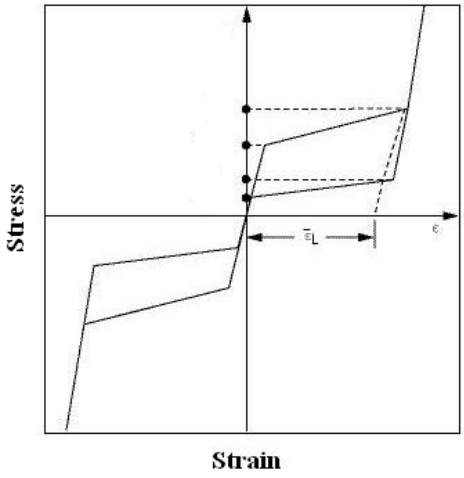

Fig. 2-6: One-dimensional phenomenological model of SMAs (ANSYS 2018)

2.6.5 Strain Rate Effect

Earthquake ground motions usually occur at frequencies ranging between 0.01 Hz to 15.0 Hz. The dominant frequency of the earthquake usually lies between 0.5 Hz to 5.0 Hz. Thus, there is a need to understand the effect of the strain rate on the behaviour of SMAs before using them in seismic applications.

Earlier studies focused on investigating the strain rate effect on the tensile properties of SMAs. Small diameter wires are used in these tests. Tobushi et al. (1998) and Leo et al. (1993) reported an increase in the loading plateau and decrease in the unloading plateau with increasing the cycling rate to 100% strain/min and 50.0 mm/min, respectively. As a result, the amount of dissipated energy is increased with the increase in the strain rate. This increase can be attributed to the increase happening in the wire temperature which cause shift in the transformation stresses (Leo et al. 1993). Tobushi et al. (1998) attributes this increase in the dissipated energy to the increase in the hysteretic area resulting from the high loading speed that does not allow for relaxation during interface movement during the transformation.

For large diameter bars, test results showed increase in the initial modulus of elasticity from 29.7 GPa for the case of quasi-static loading to 32.8 GPa for the case of 1.0 Hz dynamic loading at 2% strain cycles (DesRoches 2004). For the 6% strain cycle, the modulus of elasticity increased by 42%. This increase shows that SMA material will stiffen during seismic loading.

Similarly, the forward transformation stress increases with the increase in the loading rate. Continuous cyclic decreases the forward transformation stress (DesRoches 2004). The overall reduction in the forward transformation stress from the 2% strain cycle to the last 6% strain cycle is found to be 33% for the quasi-static loading, and 24% for the 1.0 Hz dynamic loading. Applying dynamic cyclic load to the test specimen also causes degradation to the transformation stress.

Residual strain is found to be larger (0.88% and 0.83%) under dynamic loading (1.0 Hz and 0.5 Hz) than residual strain observed under quasi-static loading (0.63%). Although applying a dynamic cyclic loading lead to higher residual strain, the value shows a good recentering capability of the SMA following a seismic event.

2.6.6 Applications of SMA Reinforcing Bars

2.6.6.1 Reinforcement for concrete elements

Using the SMAs as longitudinal reinforcing bars in the plastic hinge regions of RC columns was investigated experimentally by Saiidi and Wang (2006). Two quarter-scale spiral RC columns, one with SMA longitudinal reinforcement in the plastic hinge area while the second with conventional steel reinforcement, were designed, constructed, and tested using a shaking table. Details of the tested specimen are shown in **Fig. 2-7**. Test results indicated superior performance of SMA RC columns compared to conventional steel RC columns in limiting relative column top displacement and column residual displacement. The damaged SMA RC column specimen was repaired with engineering cementations composites. The repaired specimen was retested using the same approach as the initial test. Test results showed better performance for the repaired specimen compared to the original specimen in terms of force-displacement capacity and ductility.

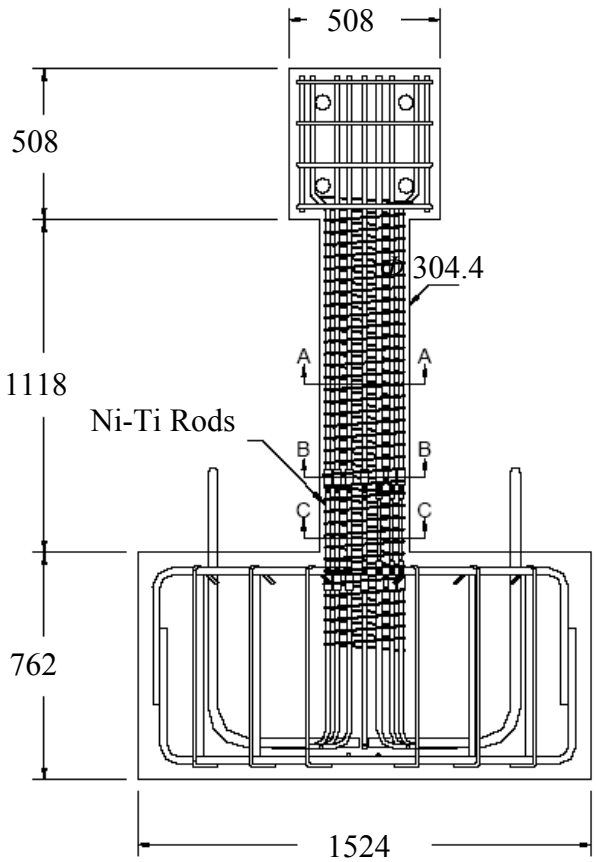

Fig. 2-7: Details of the tested specimen (Saiidi and Wang 2006)

The applicability of using superelastic SMA bars for self-restoration of bridge decks and girders was investigated by Sakai et al. (2003). Three mortar beams, two of them were reinforced with SMA wires while the third was reinforced with steel wires, were tested under static one-point load up to the inelastic range. Test results showed that the SMA reinforced beams were able to return to one-tenth of their maximum deflection. The SMA RC beams reached deflections more than seven times the deflection of the steel RC beams, which indicates much higher ductility. Cracks of the SMA RC beams were almost closed after unloading, **Fig. 2-8**.

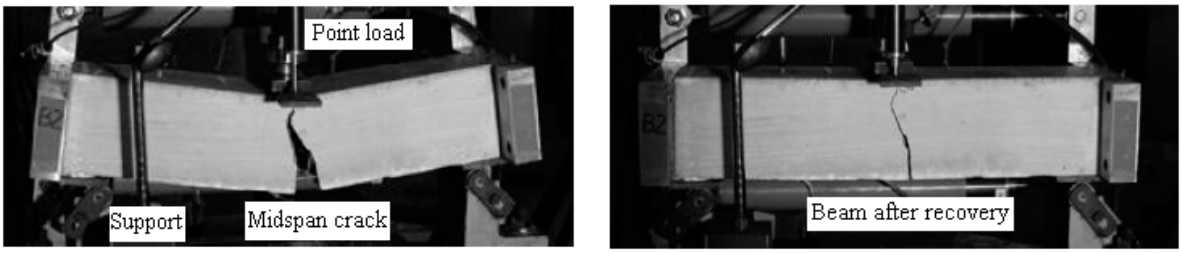

(a) Cracks at maximum deflection (b) Cracks after unloading

Fig. 2-8: Cracking behaviour of SMA mortar beams (Sakai et al. 2003)

The possibility of producing RC beams with variable stiffness and strength was investigated by Czoderski et al. (2005). The experimental program consisted of two RC beams. One beam was reinforced with SMA wires while the second was reinforced with steel wires. The two beams were tested under four-point loading. Heating the SMA wires resulted in phase transformation of the SMAs, and as a result an increase of the beam strength and stiffness. This technique can help designing smart structures, which can intelligently respond to the applied loading.

Saiidi et al. (2007) experimentally investigated the ability of Ni-Ti reinforcement to recover deformations and dissipate energy under cyclic loading. Eight beams that have the same dimensions but differ in the reinforcement type and amount were used in the experimental program. To use the SMA bars with more than one beam, the beams were externally reinforced (**Fig. 2-9**). Test results showed that the average residual deformations in SMA RC beams were much smaller than steel RC beams (one-fifth). Moreover, the SMA bars showed superelastic behaviour when used as longitudinal reinforcement in the beam specimen, as the bars almost recovered the full deformations.

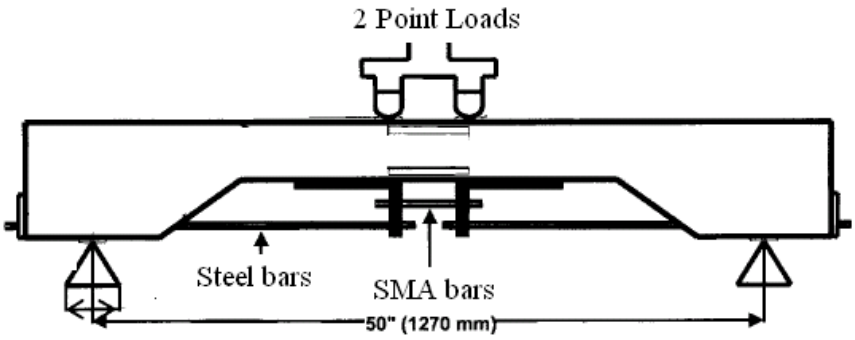

Fig. 2-9: Test setup (Saiidi et al. 2007)

The use of superelastic SMA bars in the critical regions of the beams-column joints was experimentally investigated by Youssef et al. (2008). Two three-quarter scale BCJs were tested under reversed cyclic loading. One of the two joints was reinforced with superelastic SMA bars in the plastic hinge region (**Fig. 2-10**), while the other was reinforced with conventional steel. Test results showed very small residual displacement in case of SMA reinforcement compared to the steel reinforcement case. After the test, the residual strains in the SMA longitudinal bars were negligible, while the longitudinal steel bars experienced much larger strains compared to the SMA bars.

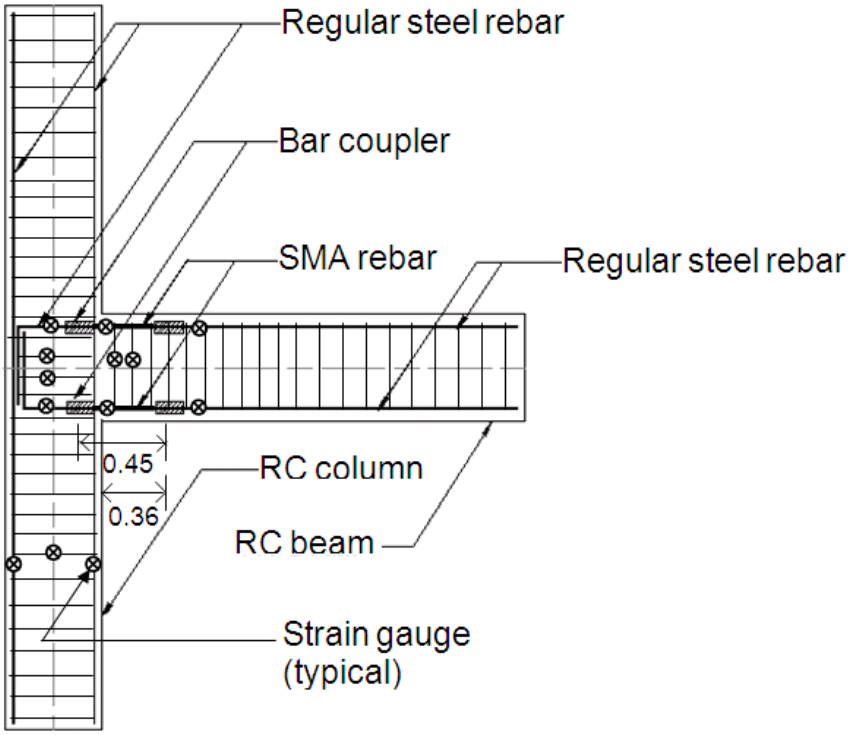

Fig. 2-10: Details of the tested BCJ by Youssef et al. (2008)

2.6.6.2 Prestressing concrete elements

Extensive research has been conducted on utilizing the SMA tendons/wires in prestressing concrete elements. Both pre-tensioning and post-tensioning techniques can be performed using SMAs. Some benefits are associated with using the SMAs in the prestressing process such as: (i) active control on the amount of prestressing, (ii) the absence of jacking or strands cutting process, and (3) elimination of losses associated with elastic shortening, friction, and anchorage losses.

Maji and Negret (1998) utilized the shape memory effect of Ni-Ti strands for prestressing concrete. The SMA strands were elongated beyond their plastic limit, and embedded in the beam

forms. After casting of concrete, the strands were heated to recover the deformations (**Fig. 2-11**). This resulted in a significant prestressing force in concrete. The strands showed good bonding behaviour with concrete.

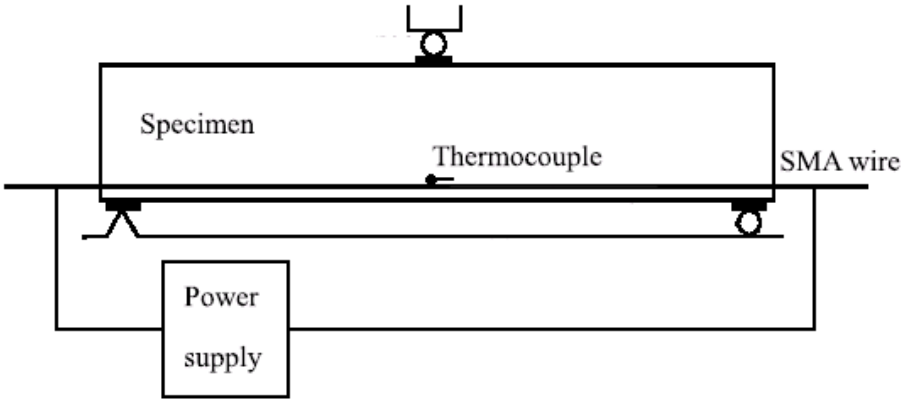

Fig. 2-11: Using SMA in pre-tensioning concrete beams (Li et al. 2007)

El-Tawil and Ortega (2004) studied the availability of using SMAs in permanent prestressing of concrete using post-tensioning technique. Mortar beams with 380 mm x 25mm x 38 mm were used (**Fig. 2-12**). Two types of SMAs were used, Ni-Ti and Ni-Ti-Nb alloys. The second type showed better solution for permanent prestressing as the first type lost the recovery stresses after turning the electric current source off (i.e. temperature drop). The beams were tested under four-point testing, and the test results showed that a significant prestressing was achieved

Opara and Naaman (2000) studied the ability of SMAs to prestress concrete elements by utilizing their ability to recover plastic deformations (**Fig. 2-13**). Plate shaped samples were used in the experimental work. Two of the samples were plain mortar, five were reinforced with steel, and

two were reinforced with SMA. The results from the tests showed that the SMA deformations were fully recovered, and that cracks were fully closed.

(a) SMA Martensite Phase

(b) Pre-stretch SMA at room temperature and transport to construction site

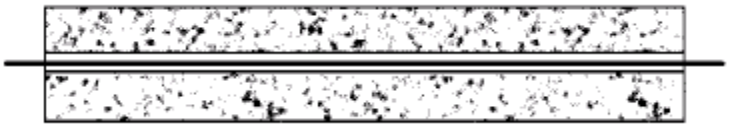

(c) Pour concrete, and after hardening, install tendon in post-tensioning ducts. Alternatively, tendon could be installed in formwork prior to concrete placement.

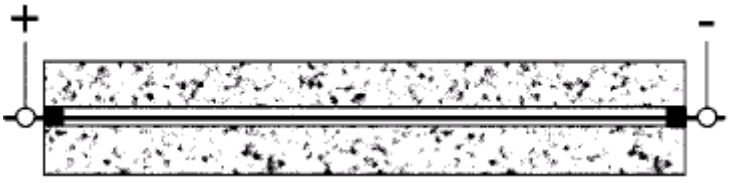

(d) Anchor and trigger tendons using electrical source

Fig. 2-12: Using SMA in post-tensioning concrete beams (El-Tawil and Ortega 2004)

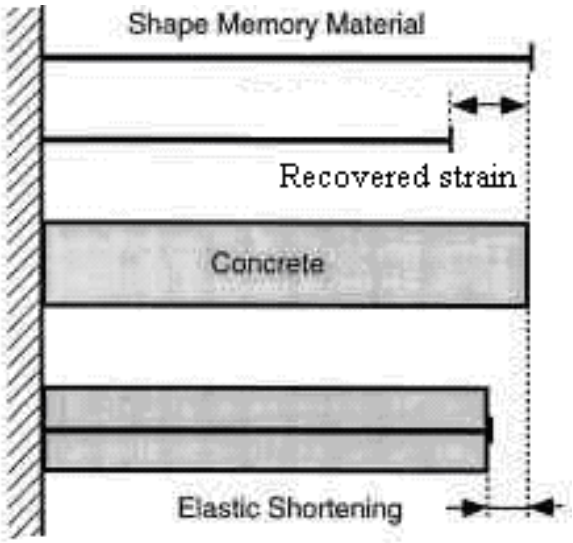

Fig. 2-13: SMA self-healing (Opara and Naaman 2000)

2.6.7 SMA in Retrofitting of Existing Structures

Structures usually need to be retrofitted or rehabilitated because of errors in design and/or construction, changes in structures use or increased loading. Many retrofitting materials have been introduced for strengthening and rehabilitating different kinds of structures such as conventional and high strength steel, and FRPs. FRP is a very brittle material when compared to steel. However, its high resistance to corrosion creates significant advantage over conventional steel reinforcement. Conventional steel has higher modulus of elasticity (i.e. stiffer behaviour) and a yielding plateau, which produces warning prior to failure. Unique properties of SMAs make them potential material for retrofitting and strengthening of existing structures.

The recentring capability and formation of loading plateaus give SMAs the ability to limit the force transfer from the SMA RC member to other members in the structure. The flag shape

stress-strain hysteresis provides high damping ability. The stiffening occuring at high strain levels because of the phase transformation, gives SMAs the ability to support high loads. SMAs have excellent fatigue properties and high resistance to corrosion. All of these properties make SMAs potential candidate for retrofitting applications, especially earthquake retrofitting applications.

2.6.7.1 SMAs as bracing members

Dolce et al. (2004) tested an existing two storey RC frame with SMA bracing members, **Fig. 2-14**. The frame has dimensions of: 3.30 m long, 5.60 m wide, and 3.00 m storey height and is designed according to the 1970's standards. Dolce et al. (2004) aimed at assessing the behaviour of the frame after retrofitting with SMAs bracings. The design of the retrofitting braces was based on the recentring capability. Test results showed an enhanced recentring capability of the frame, increased safety against collapse, and better displacement control.

Fig. 2-14: Retrofitting of a two storey RC frame using SMAs (Dolce et al. 2004)

The advantages of using superelastic SMAs braces over soft iron braces in controlling structure vibrations were experimentally investigated by Ma et al. (2004). A metal frame structure was tested using a shake table simulating the 1994 Northridge earthquake. Shape memory effect was utilized during the test to ensure full recovery of the deformations of the SMA braces. This was achieved by applying an electric current to heat the braces. Test results showed an increase in the first mode frequency with increasing the applied current, which indicates full transformation from the martensitic to austenitic phase. Both austenitic and martensitic SMA braces showed lower top floor displacement and higher acceleration when compared to soft iron steel braces. However, permanent deformation can be recovered in case of martensitic SMA braces by applying an electrical current to the braces. Permanent deformations of soft iron braces can not be recovered.

An analytical investigation was carried out by McCormik and DesRoches (2003) to investigate the efficiency of using large diameter superelastic SMA bars as bracing members in retrofitting RC moment resisting frames. Reduction in inter-storey drifts and column rotation was observed in case of SMA bracing when compared to conventional steel case.

Cortes and Palermo (2018) developed SMA model to simulate the seismic retrofit of squat concrete shear walls with tension-only SMA braces. The model follows a tri-linear envelop to model the flag-shaped behaviour of SMAs. Response of SMA braces is modelled with tension-only truss elements. Results showed satisfactory predictions of strength, drift, damage, energy, and displacement recovery. Moreoer, the effect of the axial load and the size of the SMA on the performance of the retrofitted walls is investigated.

A recently developed Shape Memory Alloy (SMA) model is implemented to simulate the seismic retrofit of squat concrete shear walls with novel tension-only SMA braces. The model follows a tri-linear envelope that captures the flag-shaped behaviour of superelastic SMAs and the accumulation of plastic straining at large strains. The response of the SMA braces is modelled with tension-only truss elements that are assigned the stress-strain parameters obtained from bare brace testing. The results provide satisfactory predictions of strength, drift, damage, energy, and displacement recovery. The effect of axial load and size of the SMA on the performance of the retrofitted walls is assessed through a parametric study.

2.6.7.2 Prestressing

Indirli et al. (2001) used SMAs to rehabilitate the Trignano Giorgio ancient church in Italy. In October 1996, a 4.8 Richter scale earthquake occurred in Italy. As a result, the bell tower of the Trignano Giorgio church was seriously damaged and needed to be retrofitted. The suggested retrofitting system was to use four vertical prestressed steel tie bars at the four corners of the bell tower. Four post-tensioned SMA devices connected in series were attached to the steel tie bars (**Fig. 2-15**). The prestressed steel tie bars were anchored to the foundation and roof of the tower. The steel tie bars function was to increase the flexural resistance of the tower. The SMA devices function was to keep the applied axial load on the tower at the maintained level. This innovative retrofitting technique proved its applicability by supporting the church tower to undergo a 4.5 Richter magnitude earthquake with almost no noticeable damage.

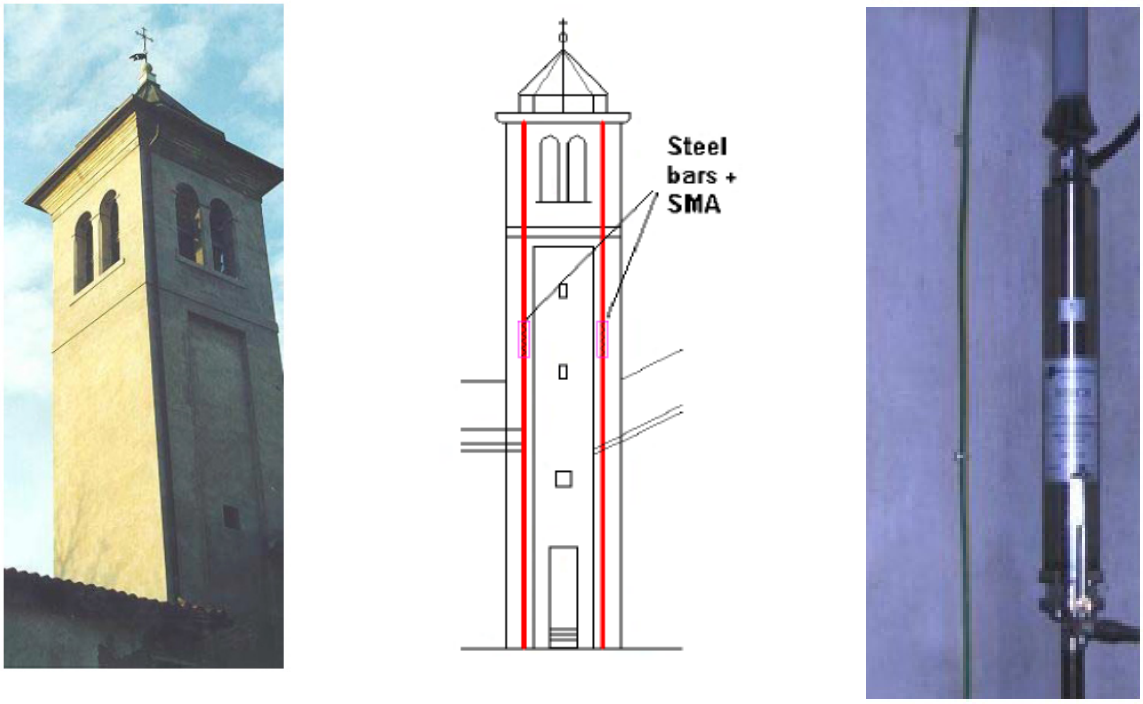

Fig. 2-15: Retrofitting of the Trignano Giorgio ancient church in Italy using SMAs (Indirli et al. 2001)

2.6.7.3 Dampers

Dampers are usually used to limit structural damage during earthquakes. There are several types of dampers such as rubber based dampers, viscous fluid dampers, friction dampers, and viscoelastic dampers. However, many limitations arise on using these types of dampers. Durability, maintenance, and geometry restoration are examples of these limitations (Dolce et al. 2000). SMA based dampers can overcome many of these limitations.

An SMA based device for energy dissipation was first introduced by Clark et al. (1995). The device is mainly composed of two cylindrical posts wrapped by superelastic nitinol wires, **Fig.**

2-16. The device was first experimentally tested. An initial prestressing was applied at 2.75% strain, then the device was subjected to in plan cyclic loading. Experimental results showed good hysteresis results. The device was then used in an analytical model simulating the response of a six storey steel frame. Analytical results showed reduction in the displacement and acceleration responses by one third to one half of the original structure undergoing earthquake event.

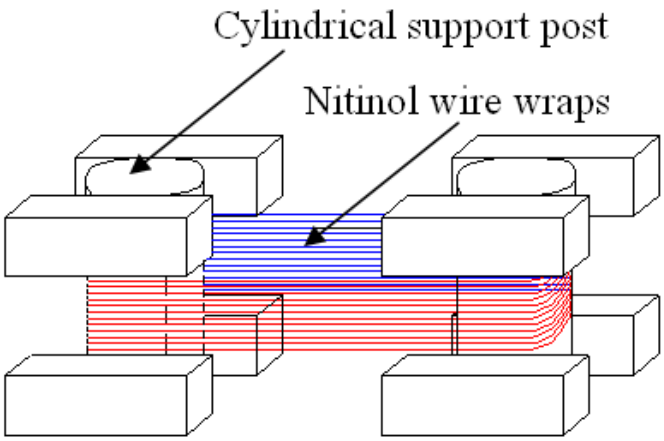

Fig. 2-16: SMA based dampers (Clark et al. 1995)

Another SMA based damper was developed by Mao and Li (2004). The developed device (180 cm x 180 cm in plan x 415 cm in height) was attached to five storey steel frame. The frame was tested using a shaking table. Test results showed huge reduction in the storey drift by values up to 28%.

The damping capacity of SMA wires in the martensitic, austenitic, and martensitic-austentic co-exist phases were measured experimentally by Ma and Song (2005). Test results showed better

performance for the austenitic-martensitic co-exist phases in suppressing repeated vibration compared to other phases.

2.7 SUMMARY AND CONCLUSIONS

Most of the Canadian civil infrastructures are constructed between 1950s and 1970s. Because of aging, fatigue, over exposure to environmental factors, and underinvestment in maintenance, these structures rapidly deteriorate and become more vulnerable to catastrophic failure. In addition, structures built before the 1970s are not designed for ductility requirements, and thus can be considered deficient when subjected to seismic loads. Thus, these structures need to be retrofitted to keep them at the accepted performance level and to follow the current design standards. Several methods for retrofitting of RC elements have been introduced, while others are still being developed. For example, recent research on SMA bars highlighted the potential of using them as retrofitting material for RC structures.

SMAs are set of alloys with unique properties when compared to other metals and alloys. They can undergo large deformations and return to their undeformed shape upon unloading (superelasticity). When subjected to cyclic loading, they have the ability to dissipate large amounts of energy and release them upon unloading. They also have good resistance to fatigue and corrosion. All of these unique properties motivated researchers to utilize them in structural engineering applications. They have been used as anchors for columns, restrainers for BCJs, dampers, and bracing members. This study focuses on using SMAs as a retrofitting material. They have been used to replace regular steel bars in critical regions of the structure.

2.8 REFERENCES

Abdulridha, A., Palermo, D., Foo, S., and Vecchio, F. J. (2013). “Behavior and Modeling of Superelastic Shape Memory Alloys Reinforced Concrete Beams.” Journal of Engineering Structures, 49, 893-904. DOI: 10.1016/j.engstruct.2012.12.041.

Abdulridha, A., Palermo, D., Foo, S., and Vecchio, F. J. (2013). “Behavior and Modeling of Superelastic Shape Memory Alloys Reinforced Concrete Beams.” Journal of Engineering Structures, 49, 893-904. DOI: 10.1016/j.engstruct.2012.12.041.

Aboutaha, R.S., Engelhardt M.D., Jirsa J.O., and Kreger M.E. (1996). "Retrofit of concrete columns with inadequate lap splices by the use of rectangular steel jackets." Earthquake Spectra, 12(4): 693-714.

Alam, M.S., Youssef, M.A., Nehdi, M. (2007). “Utilizing Shape Memory Alloys to Enhance the Performance and Safety of Civil Infrastructure: a Review.” Canadian Journal of Civil Engineering, 34(9), 1075-1086.

Alam, M.S., Youssef, M.A., Nehdi, M. (2007). “Utilizing Shape Memory Alloys to Enhance the Performance and Safety of Civil Infrastructure: a Review.” Canadian Journal of Civil Engineering, 34(9), 1075-1086.

ANSYS, Inc. Version 16.0 (2018). Southpointe, Canonsburg, PA, USA.

ANSYS, Inc. Version 16.0 (2018). Southpointe, Canonsburg, PA, USA.

Auricchio, F. and Lubliner, J. (1997). “Uniaxial model for shape-memory alloys.” International Journal of Solids and Structures, 34, 3601-3618.

Auricchio, F. and Lubliner, J. (1997). “Uniaxial model for shape-memory alloys.” International Journal of Solids and Structures, 34, 3601-3618.

Auricchio, F., Faravelli, L., Magonette, G. and Torra, V. (2001). “Shape Memory Alloys: Advances in Modelling and Applications.” Artes Graficas Torres, 17, 08029, Barcelona, Spain.

Auricchio, F., Faravelli, L., Magonette, G. and Torra, V. (2001). “Shape Memory Alloys: Advances in Modelling and Applications.” Artes Graficas Torres, 17, 08029, Barcelona, Spain.

Beber, A. J., Filho, A. C., and Campagnolo (2001) “CFRP in the strengthening of reinforced concrete beams.” Proceedings of the International Conference on FRP Composites in Civil Engineering, Hong Kong, China, PP. 391-398.

Beber, A. J., Filho, A. C., and Campagnolo (2001) “CFRP in the strengthening of reinforced concrete beams.” Proceedings of the International Conference on FRP Composites in Civil Engineering, Hong Kong, China, PP. 391-398.

Belal, M.F., Mohamed H.M., and Morad S.A. (2014). "Behavior of reinforced concrete columns strengthened by steel jacket." HBRC Journal, 11(2): 201-212.

Castro, A., Kim, R.Y., Fowler, C., and Mistretta, J.P. (1996), “Rehabilitation of Concrete Bridges Beams with Externally-Bonded Composite Plates. Parti” Proceeding of the First International Conference on Composites in Infrastructure (ICCI-96), Tucson, Arizona, pp. 857-869.

Castro, A., Kim, R.Y., Fowler, C., and Mistretta, J.P. (1996), “Rehabilitation of Concrete Bridges Beams with Externally-Bonded Composite Plates. Parti” Proceeding of the First International Conference on Composites in Infrastructure (ICCI-96), Tucson, Arizona, pp. 857-869.

CBC News (2010). “2 Quebec Hospitals to Close – Buildings Do Not Meet Quake Standards.” Sept 5, 2010.

CBC News (2010). “2 Quebec Hospitals to Close – Buildings Do Not Meet Quake Standards.” Sept 5, 2010.

Clark, P.W., Aiken, I.D., Kelly, J.M., Higashino, M. and Krumme, R.C. (1995). “Experimental and Analytical Studies of Shape Memory Alloy Dampers for Structural Control.” Smart Structures and Materials: Passive Damping, Proceedings of SPIE, 2445, 241-251.

Clark, P.W., Aiken, I.D., Kelly, J.M., Higashino, M. and Krumme, R.C. (1995). “Experimental and Analytical Studies of Shape Memory Alloy Dampers for Structural Control.” Smart Structures and Materials: Passive Damping, Proceedings of SPIE, 2445, 241-251.

Czaderski. C., Hahnebach. B., and Motavalli, M. (2006). “RC Beam with Variable Stiffness and Strength.” Construction and Building Materials, 20, 824-833.

Czaderski. C., Hahnebach. B., and Motavalli, M. (2006). “RC Beam with Variable Stiffness and Strength.” Construction and Building Materials, 20, 824-833.

Dobovsek, I. (2001). “Phenomenological Modeling of Shape Memory Effect Using the Concept of Orientational Back Stress.” Journal de Physique IV, 11(8), Pr8–59–Pr8–64.

Dobovsek, I. (2001). “Phenomenological Modeling of Shape Memory Effect Using the Concept of Orientational Back Stress.” Journal de Physique IV, 11(8), Pr8–59–Pr8–64.

Dolce, M., and Cardone, D. (2001). “Mechanical Behaviour of Shape Memory Alloys for Seismic Application 1: Martensite and Austenite NiTi Bars Subjected to Torsion.” International Journal of Mechanical Sciences, 43, 2631–56.

Dolce, M., and Cardone, D. (2001). “Mechanical Behaviour of Shape Memory Alloys for Seismic Application 1: Martensite and Austenite NiTi Bars Subjected to Torsion.” International Journal of Mechanical Sciences, 43, 2631–56.

Dolce, M., Cardone, D., and Marnetto, R. (2000). “Implementation and Testing of Passive Control Devices Based on Shape Memory Alloys.” Earthquake Engineering and Structural Dynamics, 29, 945–968.

Dolce, M., Cardone, D., and Marnetto, R. (2000). “Implementation and Testing of Passive Control Devices Based on Shape Memory Alloys.” Earthquake Engineering and Structural Dynamics, 29, 945–968.

Dolce, M., Cardone, D., Marnetto, R., Mucciarelli, M., Nigro, D., Ponzo, F.C., and Santarsiero, G. (2004). “Experimental Static and Dynamic Response of a Real RC Frame Upgraded with

SMA Re-Centering and Dissipating Braces." Proceedings of the 13th World Conference on Earthquake Engineering, Canada, Paper no. 2878.

Dolce, M., Cardone, D., Marnetto, R., Mucciarelli, M., Nigro, D., Ponzo, F.C., and Santarsiero, G. (2004). "Experimental Static and Dynamic Response of a Real RC Frame Upgraded with SMA Re-Centering and Dissipating Braces." Proceedings of the 13th World Conference on Earthquake Engineering, Canada, Paper no. 2878.

Elbahy, Y.I., Youssef, M.A., and Nehdi, M. (2008). "Flexural Behaviour of Concrete Memebers Reinforced with Shape Memory Alloys." 2nd Canadian Conference on Effective Design of Structures, McMaster University, Hamilton, Ontario, Canada.

Elbahy, Y.I., Youssef, M.A., and Nehdi, M. (2008). "Flexural Behaviour of Concrete Memebers Reinforced with Shape Memory Alloys." 2nd Canadian Conference on Effective Design of Structures, McMaster University, Hamilton, Ontario, Canada.

Elbahy, Y.I., Youssef, M.A., and Nehdi, M. (2009) "Stress Block Parameters for Concrete Flexural Members Reinforced with Superelastic Shape Memory Alloys." Materials and Structures Journal, 42(10), 1335-1351.

Elbahy, Y.I., Youssef, M.A., and Nehdi, M. (2009) "Stress Block Parameters for Concrete Flexural Members Reinforced with Superelastic Shape Memory Alloys." Materials and Structures Journal, 42(10), 1335-1351.

Elbahy, Y.I., Youssef, M.A., and Nehdi, M. (2010a) "Deflection of Superelastic Shape Memory Alloy Reinforced Concrete Beams: Assessment of Existing models." Canadian Journal of Civil Engineering, 37(6), 842-854.

Elbahy, Y.I., Youssef, M.A., and Nehdi, M. (2010a) "Deflection of Superelastic Shape Memory Alloy Reinforced Concrete Beams: Assessment of Existing models." Canadian Journal of Civil Engineering, 37(6), 842-854.

Elbahy, Y.I., Youssef, M.A., and Nehdi, M. (2010b) "Artificial Neural Network Model for Deflection Analysis of Superelastic Shape Memory Alloys Reinforced Concrete Beams." Canadian Journal of Civil Engineering, 37(6), 855-865.

Elbahy, Y.I., Youssef, M.A., and Nehdi, M. (2010b) “Artificial Neural Network Model for Deflection Analysis of Superelastic Shape Memory Alloys Reinforced Concrete Beams.” Canadian Journal of Civil Engineering, 37(6), 855-865.

El-Tawil, S., and Ortega-Rosales, J. (2004). "Prestressing Concrete using Shape Memory Alloy Tendons." ACI Structural Journal, 101(6), 846-851.

El-Tawil, S., and Ortega-Rosales, J. (2004). "Prestressing Concrete using Shape Memory Alloy Tendons." ACI Structural Journal, 101(6), 846-851.

Engindeniz, M. (2008). “Repair and Strengthening of Pre-1970 Reinforced Concrete Corner Beam-Column Joints Using CFRP Composites.” Ph.D. thesis, Georgia Institute of Technology, Atlanta, GA.

Engindeniz, M. (2008). “Repair and Strengthening of Pre-1970 Reinforced Concrete Corner Beam-Column Joints Using CFRP Composites.” Ph.D. thesis, Georgia Institute of Technology, Atlanta, GA.

Finance Canada (2010) “Leading the way on jobs and growth – Canada’s economic action plan year 2”, Budget 2010, March 4 2010.

Finance Canada (2010) “Leading the way on jobs and growth – Canada’s economic action plan year 2”, Budget 2010, March 4 2010.

Hassan, W.M. “Analytical and Experimental Assessment of Seismic Vulnerability of Beam-Column Joints without Transverse Reinforcement in Concrete Buildings” Ph.D. thesis, University of California at Berkley, USA.

Hassan, W.M. “Analytical and Experimental Assessment of Seismic Vulnerability of Beam-Column Joints without Transverse Reinforcement in Concrete Buildings” Ph.D. thesis, University of California at Berkley, USA.

He, A., Cai J., Chen Q.J., Liu X., and Xu J. (2016). "Behaviour of steel-jacket retrofitted RC columns with preload effects." Thin-Walled Structures, 109: 25-39.

Indirli, M., Castellano, M. G., Clemente, P., and Martelli, A. (2001). “Demo-Application of Shape Memory Alloy Devices: The Rehabilitation of the S. Giorgio Church Bell-Tower.” SPIE Proceedings, 4330. 262–272.

Indirli, M., Castellano, M. G., Clemente, P., and Martelli, A. (2001). “Demo-Application of Shape Memory Alloy Devices: The Rehabilitation of the S. Giorgio Church Bell-Tower.” SPIE Proceedings, 4330. 262–272.

Janke, L., Czaderski, C., Motavalli, M., and Ruth, J. (2005). "Applications of Shape Memory Alloys in Civil Engineering Structures - Overview, Limits and New Ideas." Materials and Structures Journal, 38(279), 578-592.

Janke, L., Czaderski, C., Motavalli, M., and Ruth, J. (2005). "Applications of Shape Memory Alloys in Civil Engineering Structures - Overview, Limits and New Ideas." Materials and Structures Journal, 38(279), 578-592.

Julio, E.N.B.S., and Branco F. (2008). "Reinforced Concrete Jacketing-Interface Influence on Cyclic Loading Response." ACI Structural Journal, 105(4):471.

Julio, E.N.B.S., Branco F., and Silva V.D. (2003). "Structural rehabilitation of columns with reinforced concrete jacketing." Progress in Structural Engineering and Materials, 5(1): 29-37.

Julio, E.N.B.S., Branco F., and Silva V.D. (2005) "Reinforced concrete jacketing-interface influence on monotonic loading response." ACI Structural Journal,102(2): 252-257.

Kachlakev, D., and McCurry, D.D. (2000). “Behaviours of Full-Scale Reinforced Concrete Beams Retrofitted for Shear and Flexural with FRP Laminates.” Journal of Composites, 31(6-7), 445-452.

Kachlakev, D., and McCurry, D.D. (2000). “Behaviours of Full-Scale Reinforced Concrete Beams Retrofitted for Shear and Flexural with FRP Laminates.” Journal of Composites, 31(6-7), 445-452.

Krumme, R., Hayes, J., and Sweeney, S. (1995). “Structural Damping with Shape Memory Alloys: One Class of Devices.” Smart Structures and Materials: Passive Damping, Proceedings of SPIE, 2445, 225-240.

Krumme, R., Hayes, J., and Sweeney, S. (1995). “Structural Damping with Shape Memory Alloys: One Class of Devices.” Smart Structures and Materials: Passive Damping, Proceedings of SPIE, 2445, 225-240.

Lexcellent, C., Leclercq, S., Gabry, B., and Bourbon, G. (2000). “The Two Way Shape Memory Effect of Shape Memory Alloys: an Experimental Study and a Phenomenological Model.” International Journal of Plasticity, 16(10), 1155–1168.

Lexcellent, C., Leclercq, S., Gabry, B., and Bourbon, G. (2000). “The Two Way Shape Memory Effect of Shape Memory Alloys: an Experimental Study and a Phenomenological Model.” International Journal of Plasticity, 16(10), 1155–1168.

Liang, C. and Rogers, C. A. (1997). “One-Dimensional Thermomechanical Constitutive Relations for Shape Memory Alloys.” Journal of Intelligent Material Systems and Structures, 8(4), 285-302.

Liang, C. and Rogers, C. A. (1997). “One-Dimensional Thermomechanical Constitutive Relations for Shape Memory Alloys.” Journal of Intelligent Material Systems and Structures, 8(4), 285-302.

Ma, N., and Song, G. (2005). “Study of Damping Capacities of Nitinol Shape Memory Alloys in Martensite, Austenite, and Martensite-Austenite Co-existence Phases.” Proceedings of SPIE, the international society for optical engineering, 5760, 142-151.

Ma, N., and Song, G. (2005). “Study of Damping Capacities of Nitinol Shape Memory Alloys in Martensite, Austenite, and Martensite-Austenite Co-existence Phases.” Proceedings of SPIE, the international society for optical engineering, 5760, 142-151.

Ma, N., Song, G., and Tarefder, R.A. (2004). “Vibration Control of a Frame Structure Using Shape Memory Alloy Braces.” Proceedings of the 3rd International Conference on Earthquake Engineering, Nanjing University of Technology, China, Chapter 4, Paper No. 12.

Ma, N., Song, G., and Tarefder, R.A. (2004). “Vibration Control of a Frame Structure Using Shape Memory Alloy Braces.” Proceedings of the 3rd International Conference on Earthquake Engineering, Nanjing University of Technology, China, Chapter 4, Paper No. 12.

Maji, A. K., and Negret, I. (1998). "Smart Prestressing with Shape-Memory Alloy." Journal of Engineering Mechanics, 124(10), 1121-1128.

Maji, A. K., and Negret, I. (1998). "Smart Prestressing with Shape-Memory Alloy." Journal of Engineering Mechanics, 124(10), 1121-1128.

Malovrh, B. and Gandhi, F. (2001). “Mechanism-Based Phenomenological Models for the Pseudoelastic Hysteresis Behavior of Shape Memory Alloys.” Journal of Intelligent Material Systems and Structures, 12(1), 21–30.

Malovrh, B. and Gandhi, F. (2001). “Mechanism-Based Phenomenological Models for the Pseudoelastic Hysteresis Behavior of Shape Memory Alloys.” Journal of Intelligent Material Systems and Structures, 12(1), 21–30.

Mao, C, and Li, H. (2004). “Experimental Investigation of Shape Memory Alloy as Passive Energy Dissipation Device for Seismic Response Reduction of Buildings.” Proceedings of the Third International Conference on Earthquake Engineering, Nanjing, China, Chapter no. 4, Paper no. 22.

Mao, C, and Li, H. (2004). “Experimental Investigation of Shape Memory Alloy as Passive Energy Dissipation Device for Seismic Response Reduction of Buildings.” Proceedings of the Third International Conference on Earthquake Engineering, Nanjing, China, Chapter no. 4, Paper no. 22.

Mazzolani, F. M., Corte, G. D., and Faggiano, B. (2004). “Seismic Upgrading of RC Building y Means of Advanced Techniques: The ILVA-IDEM Project.” The proceeding of the 13th World Conference on Earthquake Engineering, Canada , Paper no. 2703.

Mazzolani, F. M., Corte, G. D., and Faggiano, B. (2004). “Seismic Upgrading of RC Building y Means of Advanced Techniques: The ILVA-IDEM Project.” The proceeding of the 13th World Conference on Earthquake Engineering, Canada , Paper no. 2703.

McCormick, J., and DesRoches, R. (2003). “Seismic Response Using Smart Bracing Elements.” Proceedings of the Extreme Loading Conference, Toronto, Canada.

McCormick, J., and DesRoches, R. (2003). “Seismic Response Using Smart Bracing Elements.” Proceedings of the Extreme Loading Conference, Toronto, Canada.

Mirza, S., and Sipos, C. (2009) “Canada’s infrastructure deficit: a sad legacy for future generations.” Municipal Leader, Canada.

Mirza, S., and Sipos, C. (2009) “Canada’s infrastructure deficit: a sad legacy for future generations.” Municipal Leader, Canada.

Ocel, J., DesRoches, R., Leon, R. T., Hess, W. G., Krumme, R., Hayes, J. R., and Sweeney, S. (2004). "Steel Beam-Column Connections using Shape Memory Alloys." ASCE, Journal of Structural Engineering, 130(5), 732-740.

Ocel, J., DesRoches, R., Leon, R. T., Hess, W. G., Krumme, R., Hayes, J. R., and Sweeney, S. (2004). "Steel Beam-Column Connections using Shape Memory Alloys." ASCE, Journal of Structural Engineering, 130(5), 732-740.

Office of the Auditor General of British Columbia (2008). “Planning for School Seismic Safety”.

Office of the Auditor General of British Columbia (2008). “Planning for School Seismic Safety”.

Saiidi, M.S., and Wang, H. (2006). “Exploratory Study of Seismic Response of Concrete Columns with Shape Memory Alloys Reinforcement.” ACI Structural Journal, 103(3), 436-443

Saiidi, M.S., and Wang, H. (2006). “Exploratory Study of Seismic Response of Concrete Columns with Shape Memory Alloys Reinforcement.” ACI Structural Journal, 103(3), 436-443

Saiidi, M.S., Sadrossadat-Zadeh, M., Ayoub, C., and Itani, A. (2007). "Pilot Study of Behavior of Concrete Beams Reinforced with Shape Memory Alloys." ASCE, Journal of Materials in Civil Engineering, 19(6), 454-461.

Saiidi, M.S., Sadrossadat-Zadeh, M., Ayoub, C., and Itani, A. (2007). "Pilot Study of Behavior of Concrete Beams Reinforced with Shape Memory Alloys." ASCE, Journal of Materials in Civil Engineering, 19(6), 454-461.

Sakai, Y., Kitagawa, Y., Fukuta, T., and Iiba, M. (2003). “Experimental Study on Enhancement of Self-Restoration of Concrete Beams Using SMA Wire.” Proceedings of SPIE - The International Society for Optical Engineering, 5057, 178-186.

Sakai, Y., Kitagawa, Y., Fukuta, T., and Iiba, M. (2003). “Experimental Study on Enhancement of Self-Restoration of Concrete Beams Using SMA Wire.” Proceedings of SPIE - The International Society for Optical Engineering, 5057, 178-186.

See Infrastructure Canada (2007). “Building Canada: Modern Infrastructure for a Strong Canada.” Cat. No. lu154-4/2007.

See Infrastructure Canada (2007). “Building Canada: Modern Infrastructure for a Strong Canada.” Cat. No. lu154-4/2007.

SeismoStruct Help file (2018). available at http://www.seismosoft.com/SeismoStruct/index.htm.

Sharif, A., and Baluch, M.H. (1996) “External FRP Plates to Strengthen Reinforced Concrete Beams.” Proceeding of the First International Conference on Composites in Infrastructure (ICCI-96), Tucson, Arizona, pp. 814-828.

Sharif, A., and Baluch, M.H. (1996) “External FRP Plates to Strengthen Reinforced Concrete Beams.” Proceeding of the First International Conference on Composites in Infrastructure (ICCI-96), Tucson, Arizona, pp. 814-828.

Tamai, H. and Kitagawa, Y. (2002). “Pseudoelastic Behavior of Shape Memory Alloy Wire and its Application to Seismic Resistance Member for Building.” Computational Materials Science, 25, 218–227.

Tamai, H. and Kitagawa, Y. (2002). “Pseudoelastic Behavior of Shape Memory Alloy Wire and its Application to Seismic Resistance Member for Building.” Computational Materials Science, 25, 218–227.

Tamai, H., Miura, K., Kitagawa, Y., and Fukuta, T. (2003). "Application of SMA Rod to Exposed-Type Column Base in Smart Structural System." Proceedings, Smart Structures and Materials: Smart Systems and Nondestructive Evaluation for Civil Infrastructures, The International Society for Optical Engineering, 169-177.

Tamai, H., Miura, K., Kitagawa, Y., and Fukuta, T. (2003). "Application of SMA Rod to Exposed-Type Column Base in Smart Structural System." Proceedings, Smart Structures and Materials: Smart Systems and Nondestructive Evaluation for Civil Infrastructures, The International Society for Optical Engineering, 169-177.

Tanaka, K. (1986). “A Thermomechanical Sketch of Shape Memory Effect: One-Dimensional Tensile Behavior.” Res Mechanica, 18, 251–263.

Tanaka, K. (1986). “A Thermomechanical Sketch of Shape Memory Effect: One-Dimensional Tensile Behavior.” Res Mechanica, 18, 251–263.

The Canadian Council for Public-Private Partnership (2009). “Canadian Infrastructure Crisis still Critical”.

The Canadian Council for Public-Private Partnership (2009). “Canadian Infrastructure Crisis still Critical”.

The Canadian Society of Civil Engineering (2003). “Civil Infrastructure Systems Technology Roadmap 2003-2013”.

The Canadian Society of Civil Engineering (2003). “Civil Infrastructure Systems Technology Roadmap 2003-2013”.

The Federation of Canadian Municipalities (2007). “Danger Ahead: The Coming Collapse of Canada’s Municipal Infrastructure”.

The Federation of Canadian Municipalities (2007). “Danger Ahead: The Coming Collapse of Canada’s Municipal Infrastructure”.

Vandoros, K.G., and Dritsos S.E. (2006). "Axial preloading effects when reinforced concrete columns are strengthened by concrete jackets." Progress in Structural Engineering and Materials, 8(3): 79-92.

Youssef , M.A., Alam M.S., and Nehdi, M. (2008). “Experimental Investigation on the Seismic Behaviour of Beam-Column Joints Reinforced with Superelastic Shape Memory Alloys.” Journal of Earthquake Engineering, 12(7), 1205-1222.

Youssef , M.A., Alam M.S., and Nehdi, M. (2008). “Experimental Investigation on the Seismic Behaviour of Beam-Column Joints Reinforced with Superelastic Shape Memory Alloys.” Journal of Earthquake Engineering, 12(7), 1205-1222.

Chapter 3 Flexural Behaviour of Superelastic Shape Memory Alloys Reinforced Concrete Beams During Loading and Unloading Stages

3.1 INTRODUCTION

As a part of a moment resisting frame, Reinforced Concrete (RC) beams can be subjected to reversed cyclic bending moments during earthquake events. These moments can lead to permanent deformations and rotations, which complicate future retrofit efforts or make the damaged structure irreparable.

Superelastic Shape Memory Alloys (SMAs) are set of smart alloys that can undergo large deformations and return to their undeformed shapes upon unloading. They also have exceptional behaviour under cyclic loads (i.e. flag shaped stress-strain). They can undergo large number of inelastic loading/unloading cycles, while keeping zero or very small residual deformations upon load removal (Alam et al. 2007). In addition, SMAs have exceptional resistance to corrosion and fatigue loads (Janke et al. 2005). These unique properties have motivated researchers to utilize SMAs in different engineering applications. Yet, the use of SMAs in the structural engineering field is considered relatively new.

The use of SMAs as primary reinforcing bars in RC structures is a potential application. Up to now, this application is mainly covered in the research field with few field applications. For example, Saiidi et al. (2007) tested simply supported beams that have external SMA

reinforcement in the mid-span region. Test results showed that the use of SMA bars led to significantly reduced residual deformations upon unloading as compared to conventional steel bars. Elbahy et al. (2008, 2009, 2010a, 2010b) conducted extensive analytical studies to develop design equations of SMA RC members. The developed equations serve both strength and serviceability requirements. In real applications, SMAs have been used in the rehabilitation of the S. Giorgio Church Bell-Tower in Italy (Indirli et al. 2001) and a RC bridge in Michigan. (Soroushian 2001).

The high cost of SMAs as compared to conventional steel bars and the large size of civil structures limit their use as primary reinforcement. To overcome this problem, researchers suggested limiting the length and position of SMA bars to critical regions of the structure (Youssef et al. 2008; Abdulridha et al. 2013). This suggestion facilitates using SMA bars in real applications. However, there are no guidelines or standards to estimate the needed amount and length of the SMA reinforcement. Thus, the aim of this study is to develop such guidelines.

In this study, a sectional analysis method is developed to predict the flexural behaviour of SMA RC beams during loading and unloading stages. Results of the developed analysis method are then validated through comparison with available experimental work. A parametric study is carried out. Results of the parametric study are used in multiple linear regression analysis do develop equations that can predict the optimum amount and length os the used SMA bars/

3.2 ANALYSIS METHOD

The flexural behaviour of steel and SMA RC cross-sections is analytically investigated in this chapter. The analysis method is based on the sectional analysis approach, which uses fibre modelling (Youssef and Rahman 2007; Elbahy et al. 2009). The main idea lies in dividing the studied cross-section into discrete number of horizontal fibres. Utilizing the one-dimensional constitutive relationship of each fibre, and taking into account the cross-section equilibrium and kinematics, the mechanical behaviour of the cross-section is obtained.

A displacement-controlled loading technique is used in the analysis, where the cross-section is subjected to curvature values in an incremental way. During the unloading stage, the load is also incrementally removed. Two main assumptions are made: (i) plane sections remain plane (i.e. linear strain distribution); and (ii) perfect bond exists between concrete and the reinforcement. More details about the developed analysis method are given in **Appendix I**.

Four different materials models are implemented in the developed program. These models represent the behaviour of concrete, steel, and SMA under tensile and compressive loadings. Brief description of these models is introduced in the following subsections.

3.2.1 Concrete under Compression

The model developed by Scott et al. (1982), **Fig. 3-1(a)**, is used to model the concrete behaviour under compression. This model represents a good balance between accuracy and simplicity. During the unloading stage, behaviour of concrete is assumed to follow the model proposed by

Karsan and Jirsa (1969). When unloading starts, the material follows linear straight path that connects the strain at the unloading start, ε_r, to the unloading strain at zero-stress, ε_p. After reaching ε_p, the strains continue to reduce while keeping the stress value equal to zero. This continues till reaching the point of zero strain.

3.2.2 Concrete under Tension

Behaviour of concrete under tension is assumed to follow the model proposed by Stevens et al. (1987) and simplified by Youssef and Ghobarah (1999), **Fig. 3-1(b)**. In the pre-cracking zone, the concrete behaves in a linear fashion up to the cracking stress f_{cr}. This is followed by significant reduction in the stress values.

If unloading starts before reaching f_{cr}, the concrete behaves in a linear fashion similar to the loading stage. If unloading starts after reaching f_{cr}, the material follows a linear path with a slope equal to the modulus of elasticity of concrete. After reaching the zero-stress point, the strain continues to decrease while the stress is kept equal to zero. This continues until reaching the point of zero-strain.

3.2.3 Steel Bars

The behaviour of the steel material is assumed to follow a bilinear stress-strain relationship under both tension and compression loadings, **Fig. 3-1(c)**. The material behaves elastically until reaching its yielding strain, $\varepsilon_{y\text{-}s}$. Then, the modulus of elasticity is significantly reduced to around 10% of its original value.

If unloading starts within the pre-yielding zone, the material behaves in an elastic manner similar to the loading stage with no residual deformations at complete unloading. If the unloading starts within the post-yielding zone, the material follows a linear unloading path until yielding on the other side (tension or compression).

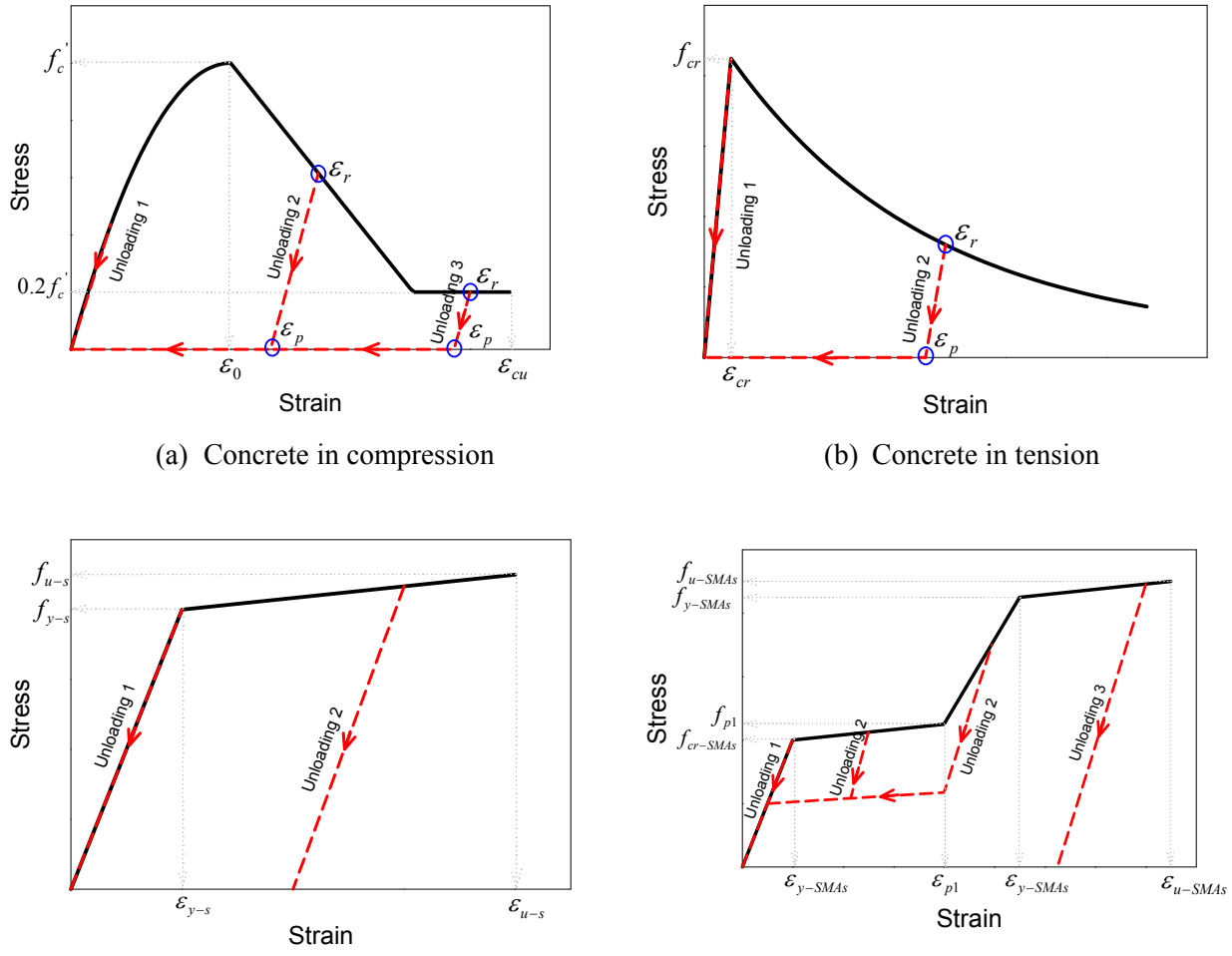

(a) Concrete in compression

(b) Concrete in tension

(c) Steel in tension/compression

(d) SMAs in tension/compression

Fig. 3-1: Stress-strain models during loading and unloading stages

3.2.4 Superelastic SMA Bars

The stress-strain model of Nickel-Titanium (Ni-Ti) SMAs consists of four linear branches that are connected by smooth curves (Alam et al. 2007), **Fig. 3-1(d)**. To simplify the modelling process, the smooth curves are ignored and the linear branches are assumed to directly intersect. The material behaves elastically until reaching the SMA critical stress $f_{cr\text{-}SMAs}$, which represents the start of the martensite stress induced transformation. Exceeding this limit, the material stiffness significantly reduces to about 10% of its initial value. If loading continues until full transformation to martensite phase occurs, the material regains about 50% of its initial stiffness. Then another significant reduction in the material stiffness occurs at yielding.

The behaviour of SMAs during the unloading stage is illustrated in **Fig. 3-1(d)**. If unloading starts before reaching SMA critical stress, the material behaves in an elastic manner similar to the loading stage (i.e. unloading path 1). If unloading starts when the stress in the material is in between the critical and yielding stresses, the material follows a flag shaped stress-strain relationship (i.e. unloading path 2). If unloading starts after the material reaches its yielding limit), the material follows a linear unloading path (i.e. unloading path 3). More details about the material models and their equations are given in **Appendix I**.

It is clear from the figure that allowing the SMA material to reach yielding results in eliminating one of its main advantages, which is superelasticity. Thus, it is not practical to allow SMAs to yield. In the following sections, the SMA critical stress $f_{cr\text{-}SMAs}$ is referred to as yielding.

3.3 DEFLECTION CALCULATIONS

The moment-area method is utilized to calculate the rotation and deflection values. Steps involved in this method include: (i) perform moment-curvature analysis of the different cross-sections; (ii) obtain the curvature distribution along the length of the member; (iii) calculate rotation by integrating the area under the curvature distribution and deflection by calculating the moment of the integrated area.

3.4 EXPERIMENTAL VALIDATION

The experimental work performed by Abdulridha (2013) and Abdulridha et al. (2013) is used to validate the accuracy of using the developed program to predict the flexural behaviour of SMA RC beams. The beams have similar dimensions: 2800 mm length, 2400 mm span, 125 mm cross-section width, and 250 mm cross-section height. The beams differ in the type of flexural reinforcement at the mid-span section (steel or SMAs), and the type of applied loading (monotonic or cyclic). The SMA RC beams are reinforced with SMA bars over a length of 600 mm centred at the mid-span, and 15M steel bars elsewhere. Mechanical couplers connect the steel and SMA bars. The diameter of the middle 300 mm of the SMA bars is reduced to 9.50 mm. Details of the tested beams are summarized in **Table 3-1**. All beams are tested under two central point loads spaced at 125 mm around mid-span. The average concrete compressive strength is 32.7 MPa for the SMAs RC beams and 34.6 MPa for the steel RC beam. Envelopes of SMA and steel stress-strain tests results are used to develop idealized stress-strain relationships as shown in **Fig. 3-2**.

Table 3-1: Details of beams tested by Abdulridha (2013)

Specimen	Loading type	Reinforcement type	Longitudinal Reinforcement	
			Bottom	Top
B1-SM	Monotonic	Steel	2 bars, 10M	2 bars, ϕ = 6.35 mm
B2-SC	Cyclic	Steel	2 bars, 10M	2 bars, ϕ = 6.35 mm
B3-SR	Cyclic	Steel	2 bars, 10M	2 bars, 10M
B4-NM	Monotonic	SMAs	2 bars, ϕ = 9.5 mm	2 bars, ϕ = 6.35 mm
B6-NR	Cyclic	SMAs	2 bars, ϕ = 9.5 mm	2 bars, ϕ = 9.5 mm
B7-NCM	Cyclic	SMAs	2 bars, ϕ = 9.5 mm	2 bars, ϕ = 9.5 mm

The developed program is used to perform moment-curvature analysis of the different cross-sections of the studied beams. The moment-curvature diagrams for three different cross-sections of B6-NR are shown in **Fig. 3-3**: (i) 2-9.5mm SMA RC cross-section; (ii) 2-12.7 mm SMA RC cross-section; and (iii) 2-15M steel RC cross-section. The moment-curvature analysis of each cross-section is performed up to the experimental unloading moment. Experimental load-displacement results are plotted versus the analytically obtained results for all beams in **Fig. 3-4** Very good agreement between the experimental and analytical results is obtained for all beams. Other experimental validations are discussed in **Appendix II**.

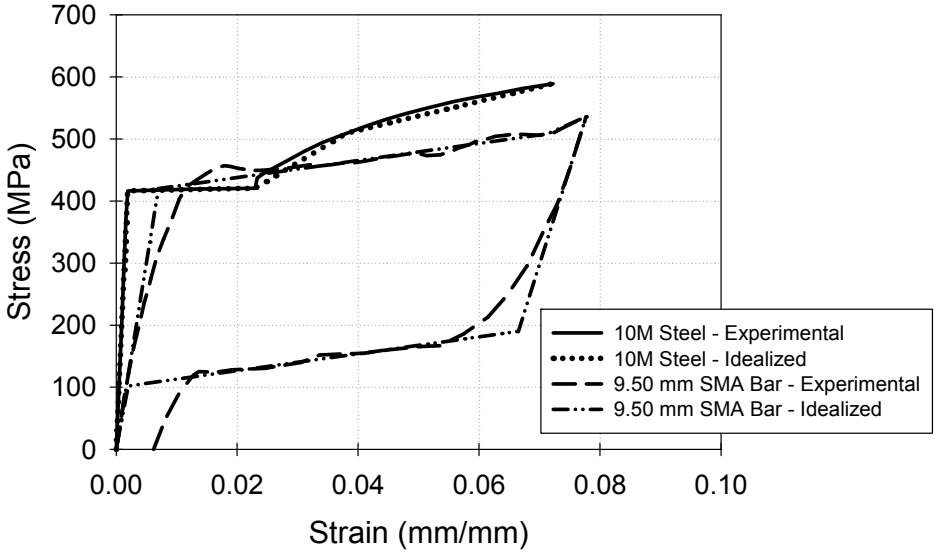

Fig. 3-2: Idealized stress-strain models for steel and SMAs bars.

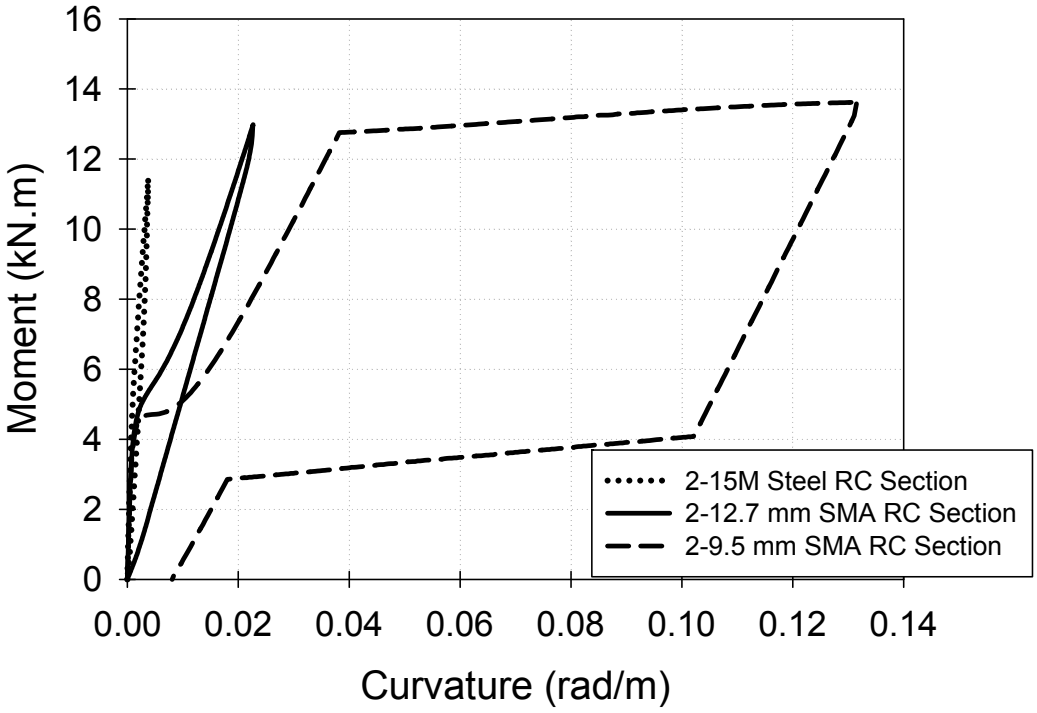

Fig. 3-3: Moment-curvature analysis for steel and SMAs RC cross-sections.

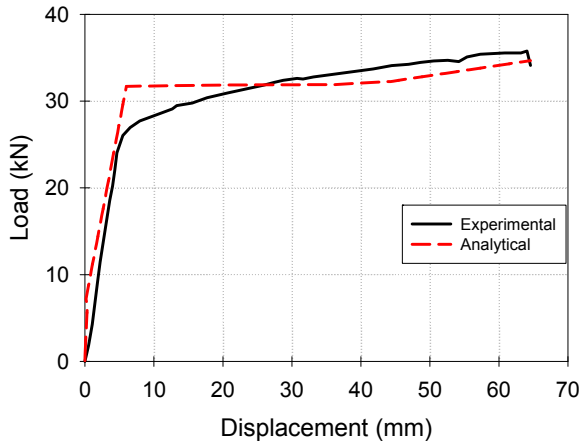

(a) B1-SM

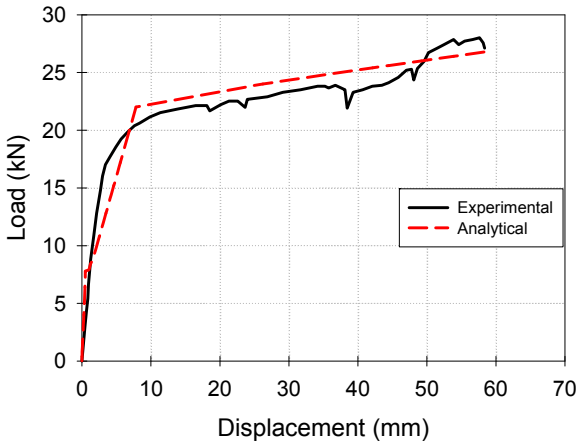

(b) B4-NM

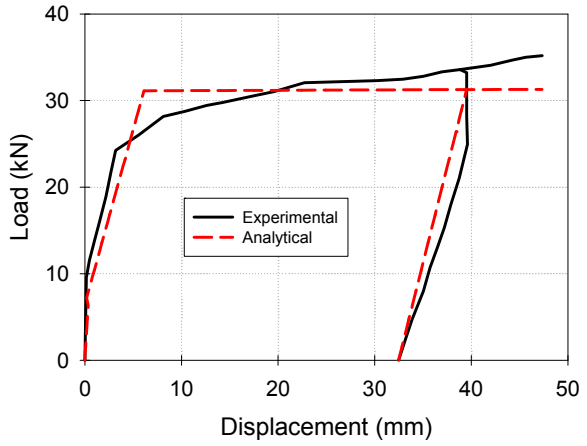

(c) B2-SC

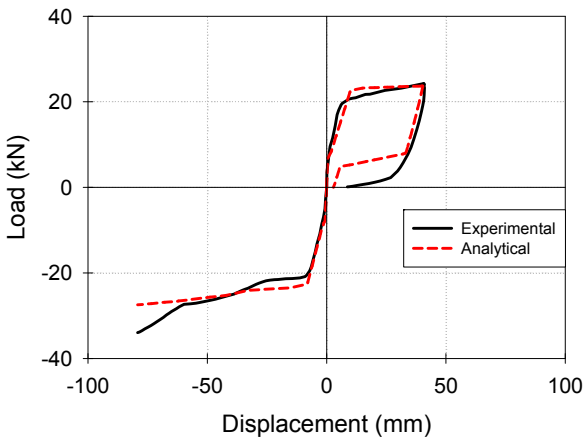

(d) B7-NC

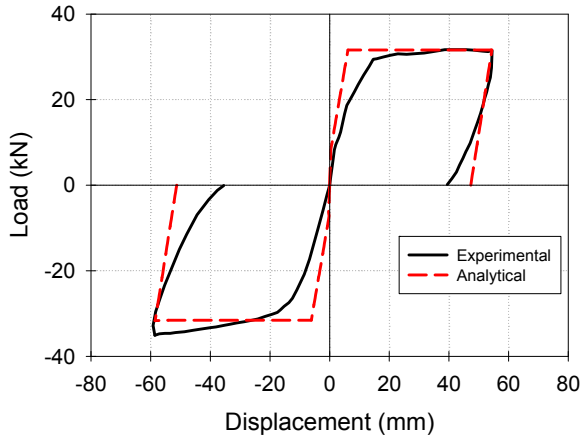

(e) B3-SR

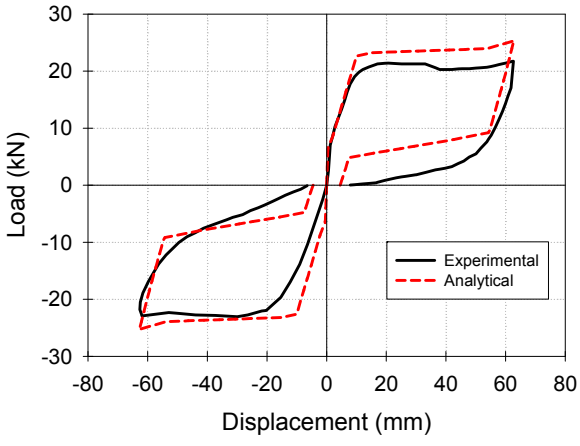

(f) B6-NR

Fig. 3-4: Experimental vs. Analytical load-displacement relationships

3.5 PARAMETRIC STUDY

A parametric study is carried out to investigate the effect of different geometrical and cross-sectional parameters on the overall behaviour of SMA RC beams during loading/unloading stages. Studied parameters include: (i) cross-section reinforcement ratio (ρ_{SMAs}); (ii) ratio between the amount of SMA reinforcement to the amount of steel reinforcement (A_{SMAs}/A_s); (iii) cross-section height-to-width ratio (h/b); (iv) beam span-to-depth ratio (L/h); and (v) concrete compressive strength (f'_c). **Fig. 3-5** shows a sketch of the studied beams.

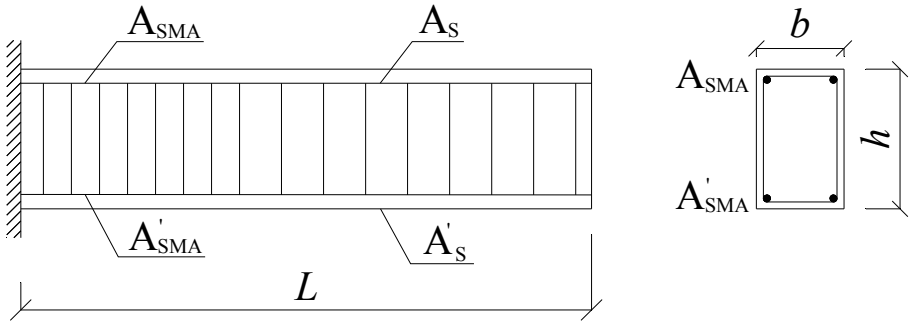

Fig. 3-5: Sketch of the studied beams

The parametric study is performed on cantilever beams. The beams are reinforced with SMA bars at the fixed end of the beams and regular steel bars elsewhere. For each of the studied parameters, nine different lengths are considered for the SMA bars. The considered lengths are: $L/20$, $L/10$, $L/8$, $L/6$, $L/4$, $L/3$, $L/2$, and $L/1$, where L is the full length of the studied beam. The beams are loaded with single point loads applied at their free ends. Details of the studied beams and cross-sections are given in **Table 3-2**.

The amount of compression reinforcement is chosen equal to the amount of the tensile reinforcement, so that the cross-section is capable of resisting the reversed moment. Effect of concrete confinement is considered in the analysis. It is calculated from the equations of the concrete stress-strain model. The number of layers is chosen equal to the height of the beam (i.e. each layer is 1 mm in height).

For each of the studied beams, the developed program is used to obtain the moment-curvature relationships of its cross-sections. The moment-area method is then used to obtain the load-displacement relationship. Results are then assessed based on: (i) load-displacement relationship; (ii) amount of residual deformations; (iii) change in flexural stiffness; and (iv) amount of dissipated energy. Detailed discussion of the parametric study results is given in the following section.

Table 3-2: Details of studied beams and cross-sections

Studied parameter	L/h	h/b	f'_c	A_{SMAs}/A_s	$\rho_{SMAs}/\rho_{s\text{-}min}$	$\rho_{SMAs}/\rho_{s\text{-}b}$	Loading level (δ_{max}/δ_y)
ρ_{SMAs}	4	2.0	40	1.0	1.0	0.09	10
	4	2.0	40	1.0	5.5	0.50	10
	4	2.0	40	1.0	11.0	1.0	10
A_{SMAs}/A_s	3	2.3	50	0.5	0.88	0.075	6
	3	2.3	50	1.0	1.76	0.15	8
	3	2.3	50	2.0	3.52	0.30	8
	3	2.3	50	4.0	7.04	0.60	8
h/b	5	1.0	35	1.0	1.4	0.13	6
	5	2.0	35	1.0	2.8	0.27	6
	5	3.0	35	1.0	4.2	0.40	6
L/h	3	3.5	30	1.0	4.0	0.42	7
	6	3.5	30	1.0	4.0	0.42	7
	9	3.5	30	1.0	4.0	0.42	7
f'_c	6	1.5	20	1.0	7.0	0.88	5
	6	1.5	45	1.0	7.0	0.88	5
	6	1.5	65	1.0	7.0	0.88	5

Where: $\rho_{SMAs}/\rho_{s\text{-}min}$ = ratio between the SMAs reinforcement ratio and the minimally reinforced cross-section steel reinforcement ratio; $\rho_{SMAs}/\rho_{s\text{-}b}$ = ratio between the reinforcement ratio of the SMAs RC cross-section and the reinforcement ratio of the balanced steel RC cross-section; δ_{max}/δ_y = the ratio between the maximum applied displacement at the beam tip and the displacement at which reinforcement starts to yield.

3.6 RESULTS AND DISCUSSION

3.6.1 Reinforcement Ratio (ρ_{SMAs})

Three different cross-section reinforcement ratios are used: (i) minimum reinforcement ratio (ρ_{min}); (ii) balanced reinforcement ratio (ρ_b); and (iii) intermediate value between the ρ_{min} and ρ_b (ρ_{int} = 0.5 ρ_b). Values of the ρ_{min} and ρ_b are determined using the Canadian standards (CSA-A23.3-14 2014) for steel RC cross-sections.

Obtained load-displacement relationships of the three beams are shown in **Fig. 3-6**. Similar behaviour is observed for the three ρ_{SMAs}. As expected, a significant increase in the cross-section yield and maximum capacity is achieved by increasing the cross-section reinforcement ratio.

Residual displacement at complete unloading is shown **Fig. 3-7(a)**. Ratio of residual displacement to maximum applied displacement (δ_r/δ_{max}) is plotted on the Y-axis versus the ratio of the SMA bar length to the total cantilever beam length (L_{SMAs}/L) on the X-axis. Increasing in the SMA bar length reduces the amount of residual displacement at complete unloading. However, the rate of reduction is not constant. For example, significant reduction in the residual displacement (80%) can be observed with the increase of the SMA bar length from 0.00 L to 0.167 L. Increasing the SMA bar length beyond the 0.167 L has very minor effect on the amount of residual deformations.

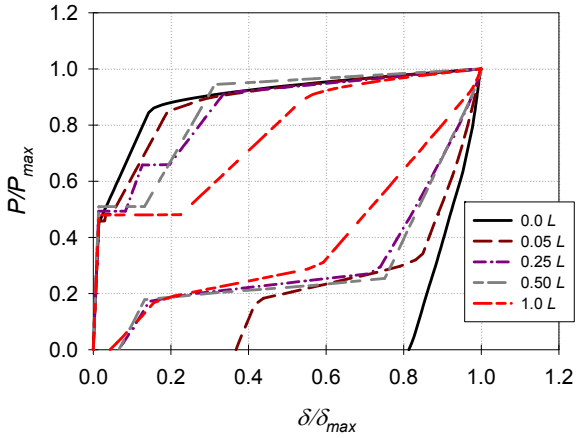

(a) $\rho = \rho_{s\text{-}min}$

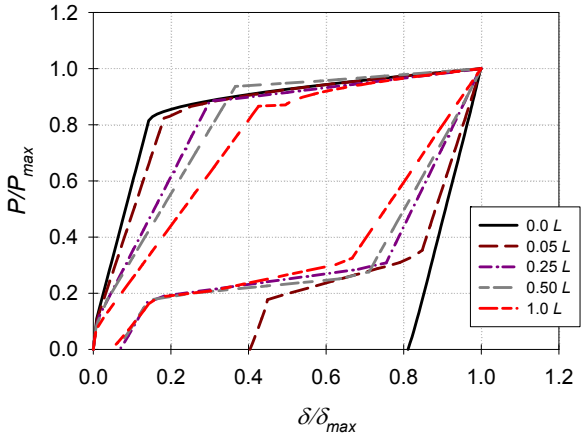

(b) $\rho = \rho_{s\text{-}int}$

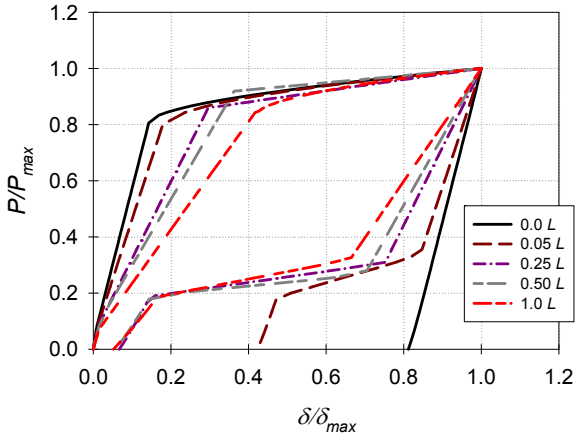

(c) $\rho = \rho_{s\text{-}b}$

Fig. 3-6: Effect of varying the cross-section reinforcement ratio on the load-displacement relationships of steel and SMA RC beams for L_{SMAs} = 0.00 L, 0.05 L, 0.25 L, 0.50 L, and 1.0 L

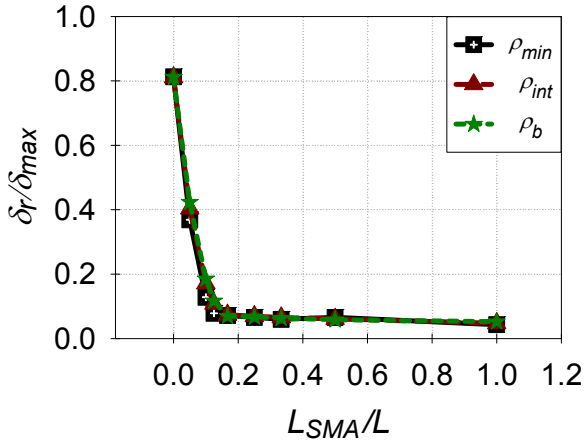

(a) Residual displacements

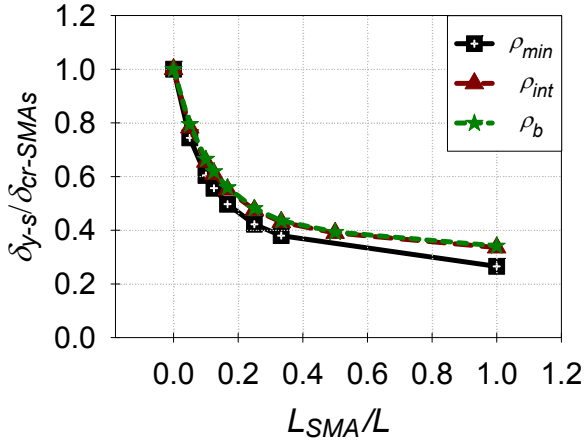

(b) Flexural stiffness

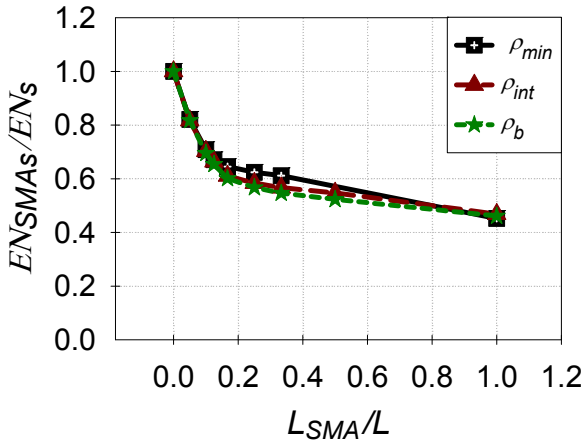

(c) Dissipated energy

Fig. 3-7: Effect of varying the cross-section reinforcement ratio on: (a) residual displacements; (b) flexural stiffness; (c) dissipated energy

Effect of varying the SMA bar length on the intial flexural stiffness of the SMA RC cantilever beams is shown in **Fig. 3-7(b)**. The flexural stiffness of the SMA RC beams relative to the steel RC beams is represented by the ratio $\delta_{y\text{-}s}$ to $\delta_{cr\text{-}SMAs}$. As the SMA bar length increases, flexural stiffness of the cantilever beams decreases. For example, increasing the SMA bar length from 0.00 *L* to 0.50 *L* decreased the flexural stiffness of the SMA RC beam by 60% compared to the steel RC beam. This significant reduction in stiffness is attributed to the difference between the modulus of elasticity of steel and SMAs.

Effect of replacing steel bars with SMAs bars on the amount of dissipated energy is shown in **Fig. 3-7(c)**. Ratio between the amount of dissipated energy by the SMA RC beam to the amount of dissipated energy by the steel RC beam (EN_{SMAs}/EN_s) is plotted on the Y-axis, while the ratio of the SMA bar length to the total cantilever beam length (L_{SMA}/L) is plotted on the X-axis. Significant reduction in the amount of dissipated energy (40%) is observed when the SMA bar length increases from 0.00 *L* to 0.20 *L*. The rate of reduction in amount of dissipated energy is then reduced. Changing the SMAs bar length from 0.20 *L* to 1.00 *L* (80%) results in only 15% additional reduction in the amount of dissipated energy.

3.6.2 Ratio between the Amount of SMA Bars and the Amount of Steel Bars (A_{SMAs}/A_s)

Four cantilever beams with four different A_{SMAs}/A_s ratios (0.5, 1.0, 2.0, and 4.0) were considered in the analysis. Obtained load-displacement relationships of the four beams are presented in **Fig. 3-8**. Varying the A_{SMAs}/A_s ratio significantly affects the load-displacement behaviour. The effect

is more pronounced during the unloading stage. Flexural capacity of the steel RC beam (L_{SMAs} = 0.0) is the highest. As the length of the SMA bar increases, the flexural capacity decreases.

Different load-displacement behaviour is observed when A_{SMAs}/A_s = 2.0 and A_{SMAs}/A_s = 4.0 values are used, **Fig. 3-8**. Yielding load of the beam increases when the length of the SMA bar increases. This different trend in behaviour as compared to cases of A_{SMAs}/A_s = 0.5 and A_{SMAs}/A_s = 1.0 is attributed to the significant increase in the amount of SMA reinforcement in the maximum moment area near the support.

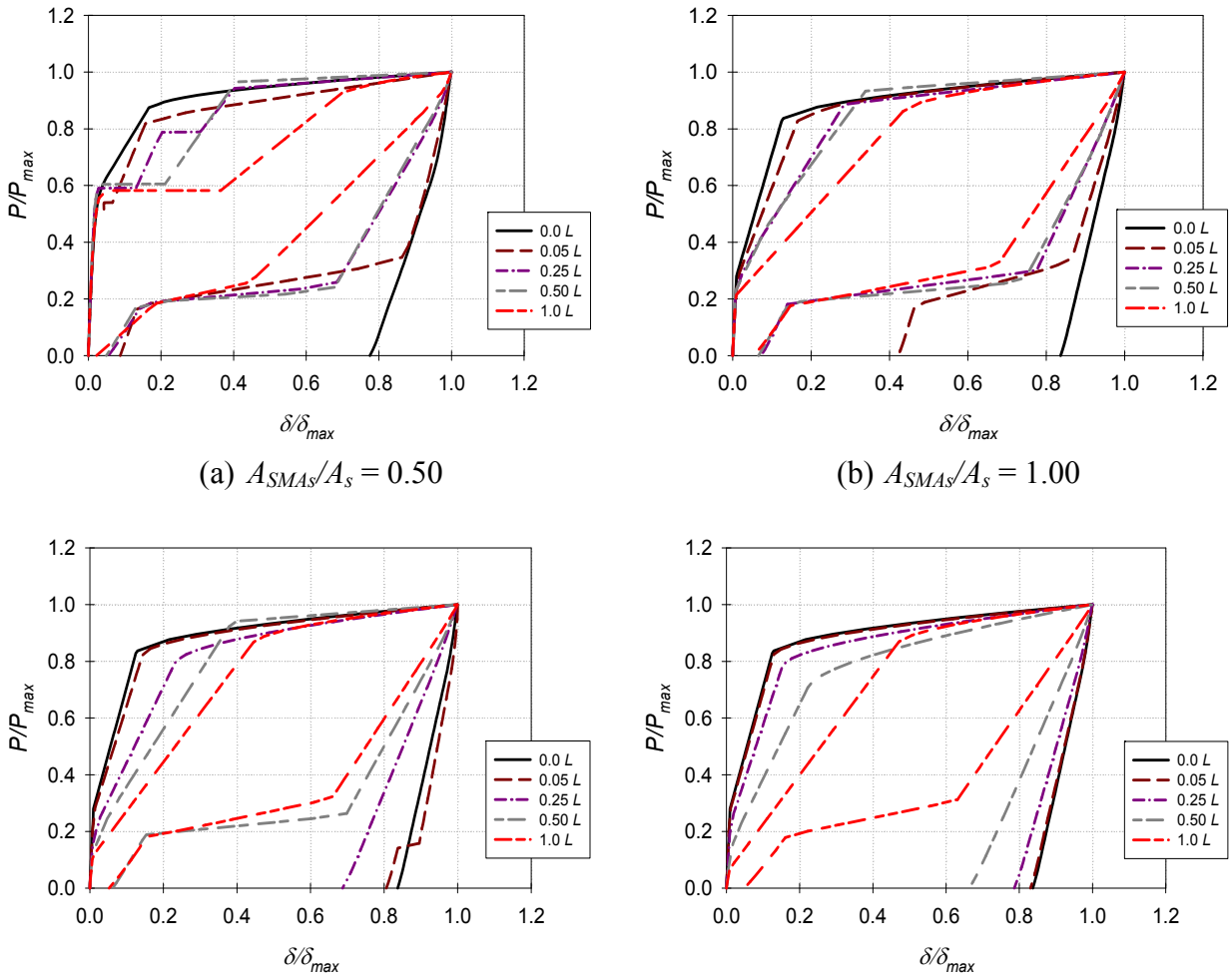

(a) $A_{SMAs}/A_s = 0.50$ (b) $A_{SMAs}/A_s = 1.00$

(c) $A_{SMAs}/A_s = 2.00$ (d) $A_{SMAs}/A_s = 4.00$

Fig. 3-8: Effect of varying the A_{SMAs}/A_s ratio on the load-displacement relationships of steel and SMA RC beams for L_{SMAs} = 0.00 L, 0.05 L, 0.25 L, 0.50 L, and 1.0 L

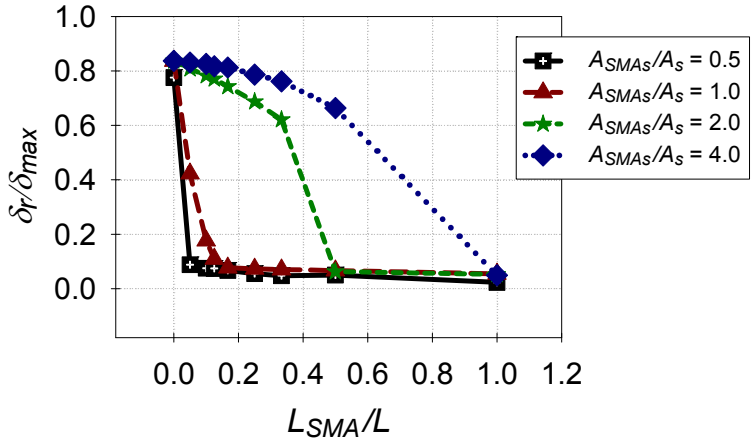

(a) Residual displacements

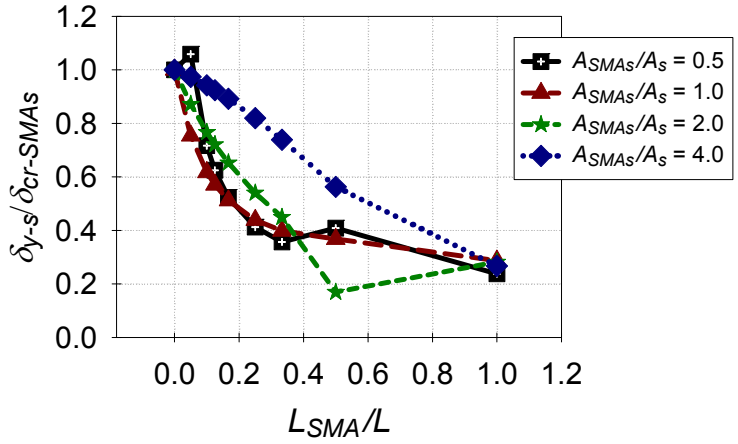

(b) Flexural stiffness

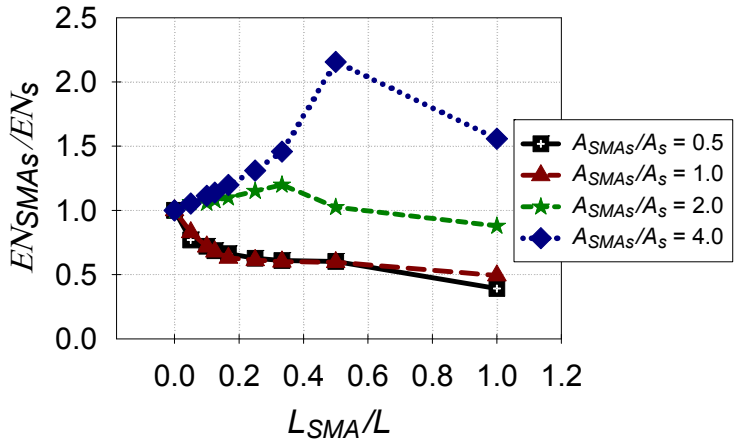

(c) Dissipated energy

Fig. 3-9: Effect of varying the A_{SMAs}/A_s ratio on: (a) residual displacements; (b) flexural stiffness; (c) dissipated energy

Amount of residual displacement at complete unloading is significantly affected by varying the A_{SMAs}/A_s value as shown in **Fig. 3-9(a)**. SMA RC beams with A_{SMAs}/A_s = 0.5 recover high portion of the maximum applied displacement at complete unloading. When 0.05 *L* of the steel bars are replaced with SMA bars, residual displacement is reduced by 88%. This reduction is attributed to the intense yielding (i.e. critical stress) happening in the SMA bars at A_{SMAs}/A_s = 0.5. For higher A_{SMAs}/A_s ratio, the percentage decrease in the residual displacement is reduced.

Flexural stiffness of the studied beams is also affected by changing the A_{SMAs}/A_s ratio. As shown in **Fig. 3-9(b)**, significant reduction in the flexural stiffness of the beams is observed when the A_{SMAs}/A_s = 0.5 and A_{SMAs}/A_s = 1.0 ratios are used. For example, using SMA bar length equal to 0.33 *L* causes a 300% reduction in the flexural stiffness in case of A_{SMAs}/A_s = 0.5 and a 240% in case of A_{SMAs}/A_s = 1.0.

As shown in **Fig. 3-9(b)**, increasing A_{SMAs}/A_s ratio significantly lowers the reduction in the flexural stiffness of the beams. For example, using SMAs bar length equal to 0.33 *L* reduces the flexural stiffness by 55% in case of A_{SMAs}/A_s = 2.0 and by 15% in case of A_{SMAs}/A_s = 4.0.

Effect of varying the A_{SMAs}/A_s ratio on the amount of dissipated energy is illustrated in **Fig. 3-9(c)**. As shown in the figure, the amount of dissipated energy significantly decreases with the increase in the SMA bars length for A_{SMAs}/A_s = 0.5 and A_{SMAs}/A_s = 1.0. Reduction in dissipated energy reaches a value of almost 50% when the steel bars are replaced with full length SMA bars. For A_{SMAs}/A_s = 2.0, the amount of dissipated energy is increased by increasing the length of SMA bars up to 0.33 *L*. After reaching 125% increase in the amount of dissipated energy when

using SMA bars length of 0.33 *L*, amount of dissipated energy started to decrease with further increase in the SMA bars length. It reached a value of 105% at SMA bars length equal to 0.5 *L* and 90% at 1.0 *L* SMA bars length. Similar behaviour is observed for A_{SMAs}/A_s = 4.0. The increase in the amount of dissipated energy in case of A_{SMAs}/A_s = 2.0 and A_{SMAs}/A_s = 4.0 is attributed to the increase in the area bounded by the load-displacement curve at small lengths of SMA bars.

3.6.3 Cross-section Height-to-Width Ratio (*h/b*)

Three beams with three different *h/b* values are used in this study: *h/b* = 1.0, *h/b* = 2.0, and *h/b* = 3.0. Calculated load-displacement relationships of the three beams considering different SMA bar lengths are shown in **Fig. 3-10**. It is clear from the figures that changing the cross-section dimensions (*b* or *h*) do not have a noticeable effect on the unloading behaviour of the beams. Residual displacement at complete unloading is almost identical for the three beams, **Fig. 3-11(a)**. This is because the amount of residual displacement is mainly dependent on the number and length of the SMA bars. Increasing the SMA bar length significantly reduces the amount of residual displacements. For example, residual displacement at complete unloading is reduced from 80% to 10% of the maximum applied displacement when the length of the SMA bars increased from 0.0 *L* to 0.167 *L*. Extending the SMA bars beyond the 0.167 *L* length limit has a very minor effect on the residual displacement.

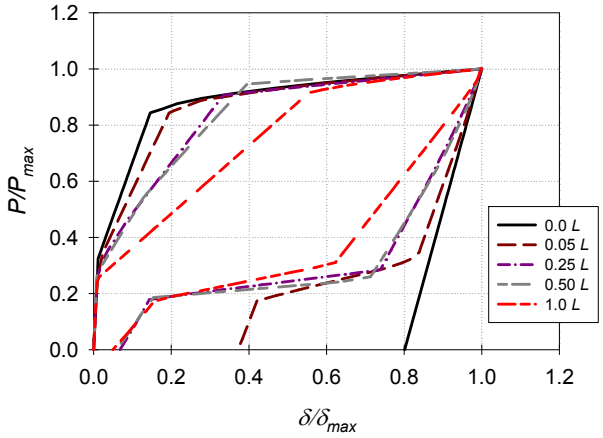

(a) h/b = 1.00

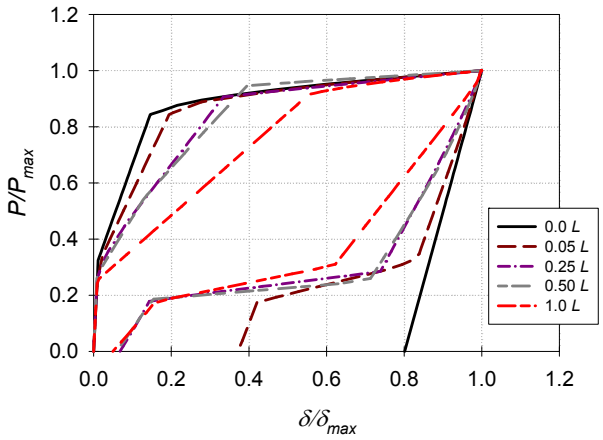

(b) h/b = 2.00

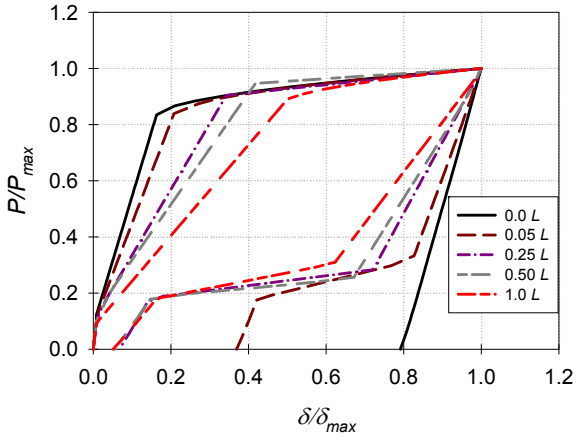

(c) h/b = 3.00

Fig. 3-10: Effect of varying the h/b ratio on the load-displacement relationships of steel and SMA RC beams for L_{SMAs} = 0.00 L, 0.05 L, 0.25 L, 0.50 L, and 1.0 L

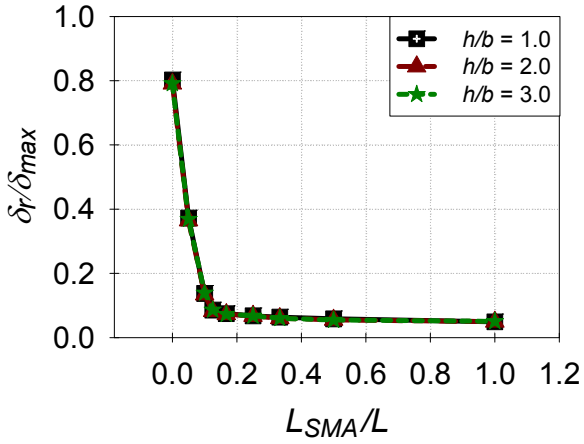

(a) Residual displacements

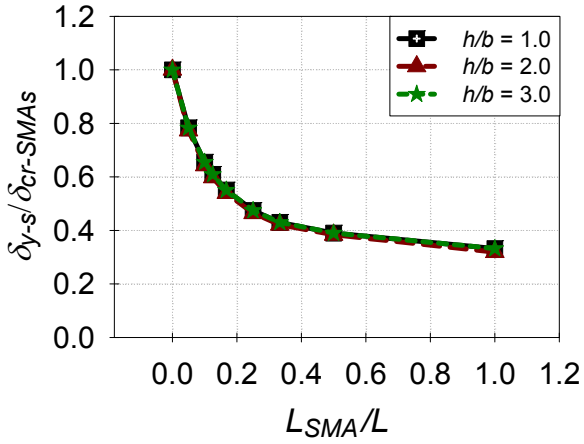

(b) Flexural stiffness

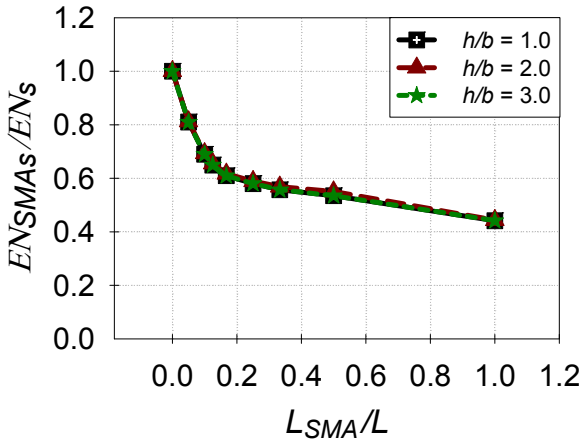

(c) Dissipated energy

Fig. 3-11: Effect of varying the cross-section height-to-width ratio (*h/b*) on: (a) residual displacements; (b) flexural stiffness; (c) dissipated energy

Effect of increasing the SMA bar length on the flexural stiffness of the beams is shown in **Fig. 3-11(b)**. Increasing the length of the SMA bars reduces the flexural stiffness of the cantilever beams. This is attributed to the difference in the modulus of elasticity value between steel and SMA materials. Beams with h/b = 2.0 and h/b = 3.0 have almost identical change in stiffness with the change in the SMA bar length. For h/b = 1.0, similar trend in stiffness is observed. However, more pronounced reduction in flexural stiffness is observed when the steel bars are replaced with full length SMA bars. When SMA bar length of 1.0 L is used, flexural stiffness reduction of 400% is observed in case of h/b = 1.0 compared to 300% and 310% in case of h/b = 3.0 and h/b = 2.0, respectively.

Trend of variation in the amount of dissipated energy with the increase in the length of the SMA bars is plotted in **Fig. 3-11(c)**. Increasing the length of the SMA bars decreases the amount of dissipated energy. Trend of reduction is identical for the three studied beams. Increasing the SMA bar length from 0.0 L to 0.20 L decreases the amount of dissipated energy by 40%. Replacing steel bars with full length (1.0 L) SMA bars results in 55% reduction in the amount of dissipated energy.

3.6.4 Beam Span-to-Depth Ratio (L/h)

Three cantilever beams with: L/h = 3.0, L/h = 6.0, and L/h = 9.0 are considered. **Fig. 3-12** illustrates the load-displacement response of the three beams when different lengths of the SMA bars are considered. Increasing the L/h ratio significantly reduces the yielding and maximum capacity of the beams.

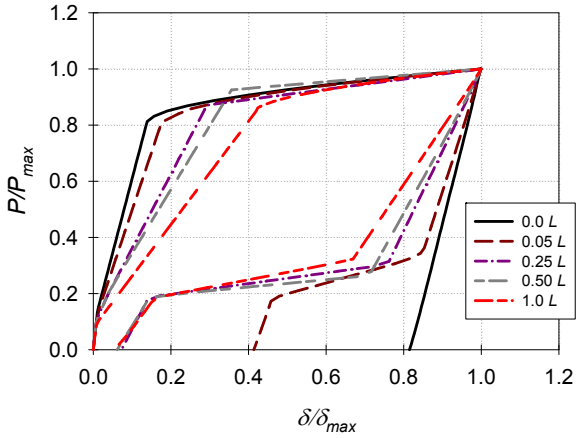

(a) L/h = 3.00

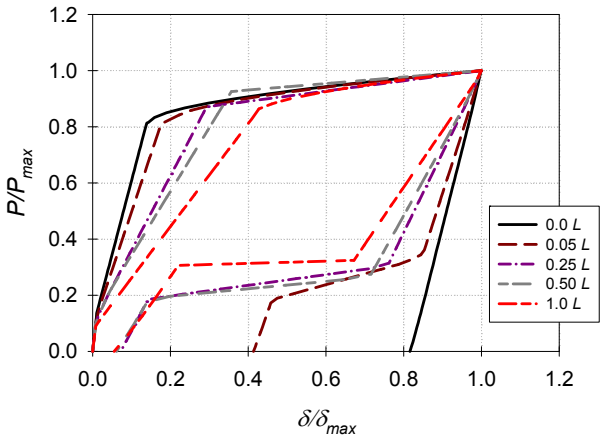

(b) L/h = 6.00

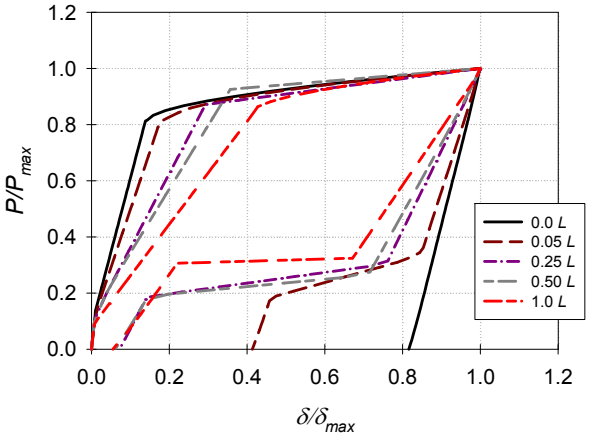

(c) L/h = 9.00

Fig. 3-12: Effect of varying the L/h ratio on the load-displacement relationships of steel and SMA RC beams for L_{SMAs} = 0.00 L, 0.05 L, 0.25 L, 0.50 L, and 1.0 L

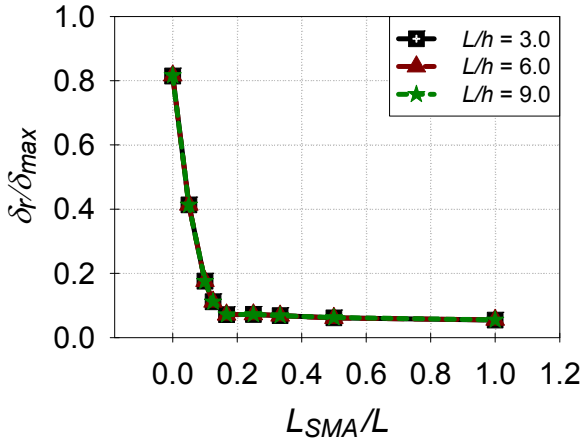

(a) Residual displacements

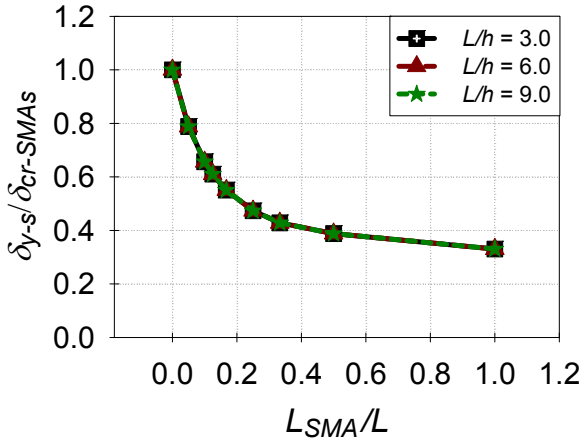

(b) Flexural stiffness

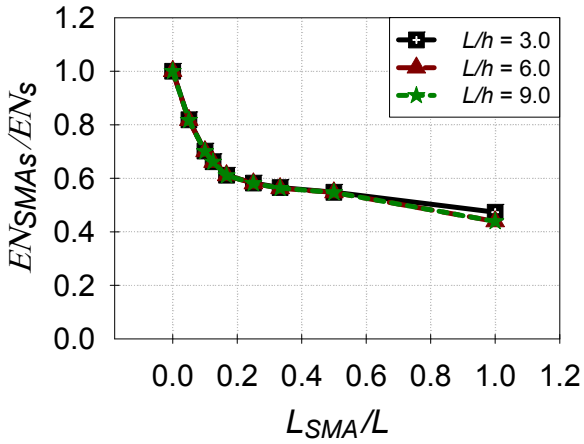

(c) Dissipated energy

Fig. 3-13: Effect of varying the beam span-to-depth ratio (L/h) on: (a) residual displacements; (b) flexural stiffness; (c) dissipated energy

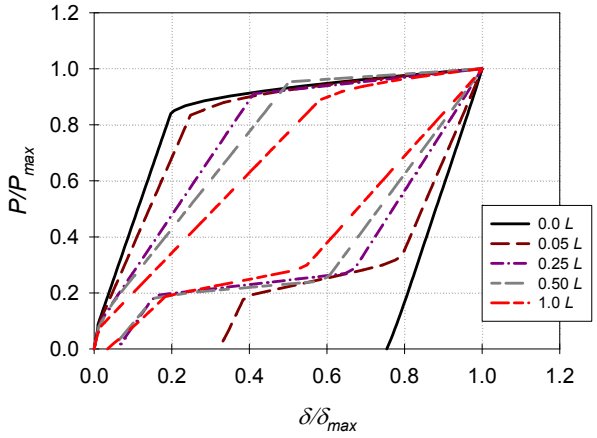

(a) $f_c^{'}$ = 20 MPa

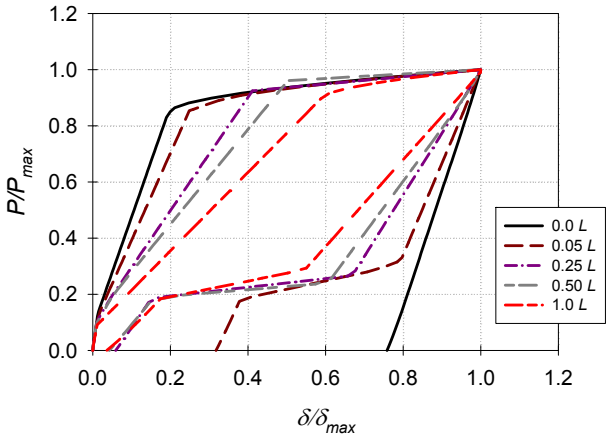

(b) $f_c^{'}$ = 45 MPa

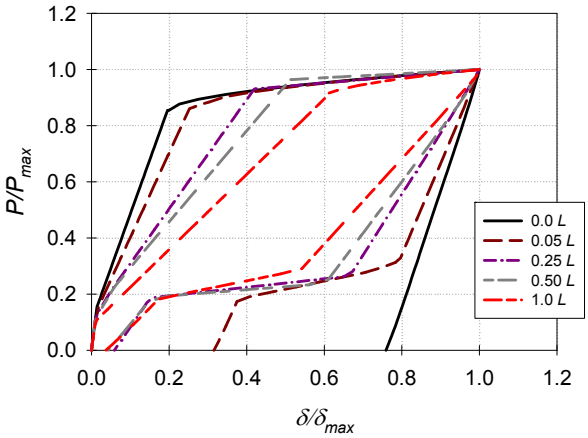

(c) $f_c^{'}$ = 65 MPa

Fig. 3-14: Effect of varying the concrete compressive strength on the load-displacement relationships of steel and SMA RC beams for L_{SMAs} = 0.00 L, 0.05 L, 0.25 L, 0.50 L, and 1.0 L

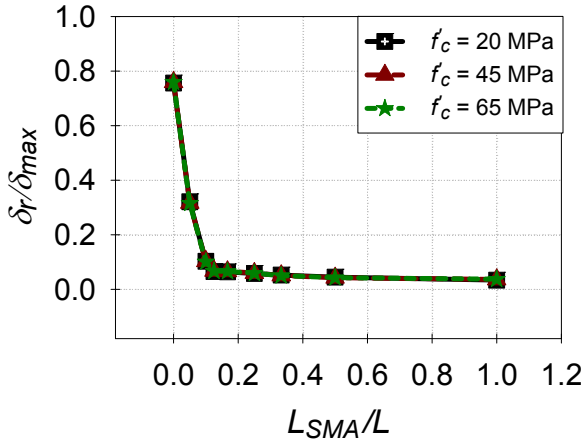

(a) Residual displacements

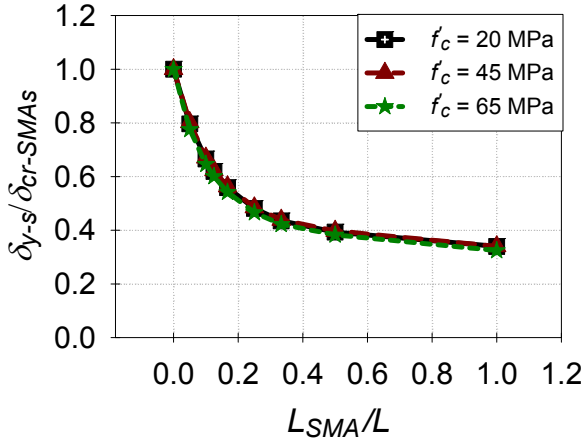

(b) Flexural stiffness

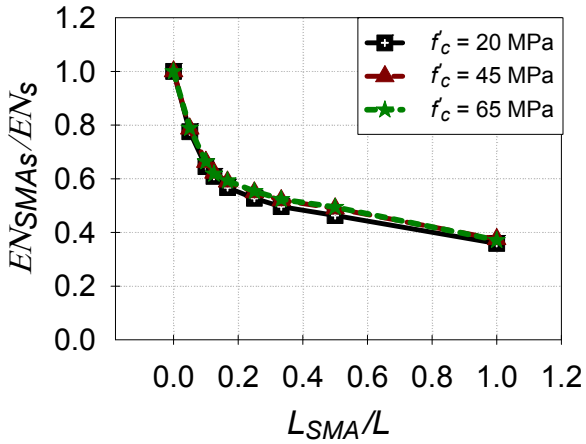

(c) Dissipated energy

Fig. 3-15: Effect of varying the A_{SMAs}/A_s ratio on: (a) residual displacements; (b) flexural stiffness; (c) dissipated energy

Fig. 3-13(a) shows that increasing the length of the SMA bars significantly reduces the amount of residual displacements. Since the reduction in the amount of residual displacement is similar for the three beams, it can be concluded that varying the *L/h* ratio has no effect on changing the amount of residual displacements at complete unloading. Using SMA bar length of 0.167 *L* reduces the amount of residual displacement at complete unloading by 90%. Increasing the SMA bar length beyond 0.167 *L* is found to have a negligible effect on the residual displacements.

Increasing the length of the SMA bar significantly decreases the flexural stiffness as shown in **Fig. 3-13(b)**. The increased SMA bar length significantly reduces the effect of *L/h* ratio. Replacing the steel bars with full length (1.0 *L*) SMA bars reduces the flexural stiffness by 200%. Increasing the SMA bar length significantly reduces the effect of *L/h* ratio on the amount of dissipated energy, **Fig. 3-13(c)**. SMA bar length is the main controlling parameter of the reduction occurring in the amount of dissipated energy. For example, the amount of dissipated energy is reduced by 55% when the steel bars are replaced with a full length (1.0 *L*) SMA bars.

3.6.5 Concrete Compressive Strength (f'_c)

Three cantilever beams with: f'_c = 20 MPa, f'_c = 45 MPa, and f'_c = 65 MPa are used. Load-displacement responses of the three beams with different lengths of SMA bars are plotted in **Fig. 3-14**. Varying the concrete compressive strength has a minor effect on the yielding and maximum capacities of the beams. Maximum displacement is reduced by almost 15% when the f'_c value increased from 20 MPa to 65 MPa. The amount of residual displacement is also not affected by varying the f'_c as shown in **Fig. 3-15(a)**. The residual displacement changes when the

length of the SMA bars is increased. Trend of change is identical for the three beams. Increasing the length of the SMA bars from 0.0 *L* to 0.167 *L* reduces the residual displacements by 90%

Fig. 3-15(b) shows that varying the $f_c^{'}$ value has no effect on the reduction happening in the flexural stiffness. As shown in the figure, using SMA bars with length 0.5 *L* reduces the flexural stiffness by 60%, while replacing the steel bars with length *L* SMA bars reduces the flexural stiffness by 65%.

Fig. 3-15(c) clearly indicates the negligible effect of changing the $f_c^{'}$ value on the amount of dissipated energy. The three beams have a sudden drop (40%) in the amount of dissipated energy when the SMA bar length increased from 0.0 *L* to 0.167 *L*. Increasing the SMA bar length beyond the 0.167 L has minor effect on the amount of dissipated energy. For instance, replacing the steel bars with full length SMA bars results in only 63% reduction in the amount of dissipated energy as compared to the steel RC beams.

3.7 CHOICE OF SMA LENGTH

There are only few real applications that utilized SMA bars as primary reinforcing bars. This section provides equations that can predict the residual displacements at complete unloading, the change in the beam stiffness, and the dissipated energy when regular steel bars are replaced with SMA bars. Multiple linear regression technique is used to determine these equations. Linear, quadratic power and logarithmic models are examined.

The backward elimination stepwise regression is adopted (Dunlop and Smith 2003). All explanatory variables (inputs) are included at the beginning. The non-significant variables are then eliminated one at a time. By the end of the analysis, the remaining variables are only the statistically significant ones.

The database used in the analysis is created from the results obtained from the parametric study. The inputs used in the analysis are: L_{SMAs}/L, A_{SMAs}/A_s, $\rho_{SMAs}/\rho_{s\text{-}min}$, $\rho_{SMAs}/\rho_{s\text{-}b}$, f'_c, h/b, LL, L/h. The outputs used in the analysis are: δ_r/δ_{max}, ($\delta_{y\text{-}s}/\delta_{cr\text{-}SMAs}$), and EN_{SMAs}/EN_s. Descriptive statistics of the used data are presented in **Table 3-3**.

Table 3-3: Descriptive statistics of the used data

Variable	Number of Observations	Mean	Standard Deviation	Minimum value	Maximum value
δ_r/δ_{max}	144	0.2455369	0.2872124	0.0228764	0.8367937
$\delta_{y\text{-}s}/\delta_{cr\text{-}SMAs}$	144	0.7231725	0.2538049	0.3590281	2.156095
EN_{SMAs}/EN_s	144	0.5904093	0.2191969	0.1694713	1.058578
L_{SMAs}/L	144	0.2805556	0.2937315	0	1
A_{SMAs}/A_s	144	1.21875	0.7726051	0.5	4
$\rho_{SMAs}/\rho_{s\text{-}min}$	144	4.112833	2.506175	0.83077	10.958
$\rho_{SMAs}/\rho_{s\text{-}b}$	144	0.4028801	0.2516064	0.07538	1
f'_c	144	40.3125	10.71269	20	65
h/b	144	2.270833	0.7429741	1	3.5
Load level (δ_{max}/δ_y)	144	6.6	1.0209	5	8
L/h	144	4.6875	1.614916	3	9

Table 3-4: Correlation coefficients between all variables

	δ_r/δ_{max}	$\delta_{y\text{-}s}/\delta_{cr\text{-}SMAs}$	EN_{SMAs}/EN_s	L_{SMAs}/L	A_{SMAs}/A_s	$\rho_{SMAs}/\rho_{s\text{-}min}$	$\rho_{SMAs}/\rho_{s\text{-}b}$	f'_c	h/b	LL	L/h
δ_r/δ_{max}	1.00										
$\delta_{y\text{-}s}/\delta_{cr\text{-}SMAs}$	0.79	1.00									
EN_{SMAs}/EN_s	0.83	0.60	1.00								
L_{SMAs}/L	-0.46	-0.38	-0.76	1.00							
A_{SMAs}/A_s	0.51	0.70	0.23	0.00	1.00						
$\rho_{SMAs}/\rho_{s\text{-}min}$	0.10	0.09	0.10	0.00	0.27	1.00					
$\rho_{SMAs}/\rho_{s\text{-}b}$	0.07	0.04	0.08	0.00	0.21	0.97	1.00				
f'_c	0.16	0.25	0.06	0.00	0.26	-0.18	-0.32	1.00			
h/b	0.05	0.04	0.02	0.00	0.02	-0.02	-0.02	-0.3	1.00		
LL	0.32	0.42	0.08	0.00	0.47	0.00	-0.08	0.06	0.52	1.00	
L/h	-0.21	-0.32	-0.06	0.00	-0.30	0.09	0.17	-0.36	0.09	-0.44	1.00

The analysis starts with investigating the correlation between each pair of the variables. Highly correlated pairs and their signs are noted. Correlation matrix is determined and is shown in **Table 3-4**. **Table 3-5** to **Table 3-10** present the final regression models for the three outputs. All the variable coefficients reported in these tables are statistically significant from zero at 95% confidence level because the associated p-values of all the coefficients are less than 0.05.

Regression results also include standard errors (Std. Err.) associated with each coefficient, the t-statistics (t) that is used to evaluate whether the estimated coefficients are significantly different from zero or not, and the 2-tailed p-values (p>t) used to test the null hypothesis that the coefficient is zero using an alpha of 0.05 (i.e. 95% confidence level). Analysis of variance (ANOVA) results are also summarized in each table reporting the variance breakdown of the output explained by the model and the residuals. ANOVA results include the sum of squares (SS), degrees of freedom (df) and mean square (MS) associated with three sources of variance: Model, residuals, and total variances.

The overall model fitness is also reported with the model results. F-test is used to test the null hypothesis that all model coefficients are statistically significant from zero. Prob>F=0 indicates that all model coefficients are statistically significant from zero. R-squared is the coefficient of determination that represents the proportions of the variance in the dependent variable explained by the independent variables. R-squared is used to assess the overall model goodness-of-fit. The closer the R-squared value to 1.0 the better the model fitness is.

Adjusted R-squared is an adjustment of the R-squared to account for the addition of the explanatory variables and their effect on the model fitness. Root Mean Square Error (Root MSE)

is another measure of the model goodness-of-fit. It is the standard deviation of residuals to indicate how close the linear regression model is to the measured data points. The smaller the Root MSE is, the closer the model fit to the observed data. All the reported models are considered to be with very good fit as their R-squared values vary from 0.7 to 0.9. Furthermore, the values of MSE range from 0.05 to 0.39 confirming also a very good model fit (Montgomery et al. 2012).

For example, **Table 3-5** presents a linear regression model of δ_r/δ_{max} when $L_{SMAs}/L \leq 0.14$. The model defines the linear relationship between the dependent variable δ_r/δ_{max} and the second order transformation of the three independent variables (L_{SMAs}/L, A_{SMAs}/A_s, and L/h). The coefficient for each independent variable is estimated. The final suggested regression models are summarized in **Equations [3-1]** to **[3-3]**.

$$\delta_r/\delta_{max} = -9.38644 \times (L_{SMAs}/L) + 35.56246 \times (L_{SMAs}/L)^2 + 0.6020821 \times (A_{SMAs}/A_s) - 0.0932349 \times (A_{SMAs}/A_s)^2 - 0.1102018 \times (L/h) + 0.0085443 \times (L/h)^2 + 0.5670711 \qquad L_{SMAs}/L \leq 0.14 \qquad \textbf{[3-1a]}$$

$$\ln(\delta_r/\delta_{max}) = -0.9008659 \times (L_{SMAs}/L) + 1.213188 \times (A_{SMAs}/A_s) - 0.4609012 \times (L/h) + 0.0353669 \times (L/h)^2 - 1.027448 \qquad L_{SMAs}/L > 0.14 \qquad \textbf{[3-1b]}$$

$$\ln(\delta_{y\text{-}s}/\delta_{cr\text{-}SMAs}) = -2.871903 \times (L_{SMAs}/L) + 0.3076423 \times (A_{SMAs}/A_s) - 0.0438487 \times (A_{SMAs}/A_s)^2 - 0.0896358 \times (L/h) + 0.0066686 \times (L/h)^2 - 0.0422848 \qquad L_{SMAs}/L \leq 0.14 \qquad \textbf{[3-2a]}$$

Table 3-5: Regression model for δ_r/δ_{max} when $L_{SMAs}/L \leq 0.14$

Source	SS	df	MS			
				Number of obs	=	64
Model	5.40512271	6	0.900853784	F(6, 57)	=	86.64
				Prob > F	=	0
Residual	0.592698607	57	0.010398221	R-squared	=	0.9012
				Adj R-squared	=	0.8908
Total	5.99782131	63	0.095203513	Root MSE	=	0.10197

δ_r/δ_{max}	Coef.	Std. Err.	t	P>t	[95% Conf.	Interval]
L_{SMAs}/L	-9.38644	1.010386	-9.29	0	-11.4097	-7.363177
$(L_{SMAs}/L)^2$	35.56246	7.852247	4.53	0	19.83861	51.28632
A_{SMAs}/A_s	0.6020821	0.0976462	6.17	0	0.406549	0.7976151
$(A_{SMAs}/A_s)^2$	-0.0932349	0.0205793	-4.53	0	-0.1344443	-0.0520255
L/h	-0.1102018	0.0431388	-2.55	0.013	-0.1965858	-0.0238178
$(L/h)^2$	0.0085443	0.0038105	2.24	0.029	0.0009139	0.0161747
Constant	0.5670711	0.1381184	4.11	0	0.2904937	0.8436485

Table 3-6: Regression model for δ_r/δ_{max} when $L_{SMAs}/L > 0.14$

Source	SS	df	MS			
				Number of obs	=	80
Model	32.2004529	4	8.05011323	F(4, 75)	=	52.44
				Prob > F	=	0
Residual	11.5134861	75	0.153513148	R-squared	=	0.7366
				Adj R-squared	=	0.7226
Total	43.713939	79	0.553341	Root MSE	=	0.39181

$\ln(\delta_r/\delta_{max})$	Coef.	Std. Err.	t	P>t	[95% Conf.	Interval]
L_{SMAs}/L	-0.9008659	0.1478548	-6.09	0.000	-1.195408	-0.606324
$\ln(A_{SMAs}/A_s)$	1.213188	0.1097809	11.05	0.000	0.9944934	1.431883
L/h	-0.4609012	0.14432	-3.19	0.002	-0.7484014	-0.1734009
$(L/h)^2$	0.0353669	0.0128571	2.75	0.007	0.0097542	0.0609796
Constant	-1.027448	0.3825008	-2.69	0.009	-1.789429	-0.2654676

Table 3-7: Regression model for $\delta_{y\text{-}s}/\delta_{cr\text{-}SMAs}$ when $L_{SMAs}/L \leq 0.14$

Source	SS	df	MS			
Model	1.85713726	5	0.371427452	Number of obs	=	64
				F(5, 58)	=	56.64
				Prob > F	=	0
Residual	0.380350649	58	0.00655777	R-squared	=	0.83
				Adj R-squared	=	0.8154
Total	2.23748791	63	0.035515681	Root MSE	=	0.08098

$\ln(\delta_{y\text{-}s}/\delta_{cr\text{-}SMAs})$	Coef.	Std. Err.	t	P>t	[95% Conf.	Interval]
L_{SMAs}/L	-2.871903	0.2108541	-13.62	0	-3.293974	-2.449833
A_{SMAs}/A_s	0.3076423	0.077545	3.97	0	0.1524191	0.4628655
$(A_{SMAs}/A_s)^2$	-0.0438487	0.0163429	-2.68	0.009	-0.0765626	-0.0111347
L/h	-0.0896358	0.0342584	-2.62	0.011	-0.1582114	-0.0210602
$(L/h)^2$	0.0066686	0.0030261	2.2	0.032	0.0006112	0.012726
Constant	-0.0422848	0.1092839	-0.39	0.7	-0.2610404	0.1764707

Table 3-8: Regression model for $\delta_{y\text{-}s}/\delta_{cr\text{-}SMAs}$ when $L_{SMAs}/L > 0.14$

Source	SS	df	MS			
Model	7.16349661	4	1.79087415	Number of obs	=	80
				F(4, 75)	=	133.48
				Prob > F	=	0
Residual	1.00627315	75	0.013416975	R-squared	=	0.8768
				Adj R-squared	=	0.8703
Total	8.16976976	79	0.103414807	Root MSE	=	0.11583

$\ln(1/(\delta_{cr\text{-}SMAs}/\delta_{y\text{-}s}))$	Coef.	Std. Err.	t	P>t	[95% Conf.	Interval]
$(L_{SMAs}/L)^2$	-0.2967487	0.035693	-8.31	0	-0.3678527	-0.2256447
A_{SMAs}/A_s	0.3830598	0.0181175	21.14	0	0.3469678	0.4191518
$\rho_{SMAs}/\rho_{s\text{-}b}$	-0.7221479	0.1910504	-3.78	0	-1.10274	-0.341556
$(\rho_{SMAs}/\rho_{s\text{-}b})^2$	0.4479831	0.1747933	2.56	0.012	0.099777	0.7961892
Constant	-0.6942598	0.0418022	-16.61	0	-0.777534	-0.6109856

Table 3-9: Regression model for EN_{SMAs}/EN_s when $L_{SMAs}/L \leq 0.14$

Source	SS	df	MS	Number of obs =		64
Model	1.47433386	3	0.49144462	F(3, 60)	=	172.52
				Prob > F	=	0
Residual	0.17091711	60	0.002848619	R-squared	=	0.8961
				Adj R-squared	=	0.8909
Total	1.64525097	63	0.026115095	Root MSE	=	0.05337

EN_{SMAs}/EN_s	Coef.	Std. Err.	t	P>t	[95% Conf.	Interval]
L_{SMAs}/L	-4.246152	0.528841	-8.03	0	-5.303991	-3.188312
$(L_{SMAs}/L)^2$	10.20425	4.109903	2.48	0.016	1.983215	18.42528
$(A_{SMAs}/A_s)^2$	0.0130695	0.0018159	7.2	0	0.0094371	0.0167019
Constant	0.9730266	0.0137205	70.92	0	0.9455814	1.000472

Table 3-10: Regression model for EN_{SMAs}/EN_s when $L_{SMAs}/L > 0.14$

Source	SS	df	MS	Number of obs	=	80
Model	0.866746838	4	0.21668671	F(4, 75)	=	74.75
				Prob > F	=	0
Residual	0.217402194	75	0.002898696	R-squared	=	0.7995
				Adj R-squared	=	0.7888
Total	1.08414903	79	0.013723405	Root MSE	=	0.05384

EN_{SMAs}/EN_s	Coef.	Std. Err.	t	P>t	[95% Conf.	Interval]
L_{SMAs}/L	-0.8652805	0.1159677	-7.46	0	-1.0963	-0.634261
$(L_{SMAs}/L)^2$	0.4895451	0.0946956	5.17	0	0.3009019	0.6781883
$(A_{SMAs}/A_s)^2$	0.0141995	0.0016721	8.49	0	0.0108685	0.0175305
$\rho_{SMAs}/\rho_{s\text{-}b}$	0.057189	0.0245013	2.33	0.022	0.0083799	0.1059981
Constant	0.6334503	0.0280425	22.59	0	0.5775868	0.6893138

$$\ln(\delta_{y\text{-}s}/\delta_{cr\text{-}SMAs}) = -0.2967487 \times (L_{SMAs}/L)^2 + 0.3830598 \times (A_{SMAs}/A_s) - 0.7221479 \times (\rho_{SMAs}/\rho_{s\text{-}b}) + 0.4479831 \times (\rho_{SMAs}/\rho_{s\text{-}b})^2 - 0.6942598 \qquad L_{SMAs}/L > 0.14 \qquad \textbf{[3-2b]}$$

$$EN_{SMAs}/EN_s = -4.246152x\ (L_{SMAs}/L) + 10.20425 \times (L_{SMAs}/L)^2 + 0.0130695 \times (A_{SMAs}/A_s)^2 + 0.9730266 \qquad L_{SMAs}/L \leq 0.14 \qquad \textbf{[3-3a]}$$

$$EN_{SMAs}/EN_s = -0.8652805x\ (L_{SMAs}/L) + 0.4895451x\ (L_{SMAs}/L)^2 + 0.0141995 \times (A_{SMAs}/A_s)^2 + 0.057189 \times (\rho_{SMAs}/\rho_{s\text{-}b}) + 0.6334503 \qquad L_{SMAs}/L > 0.14 \qquad \textbf{[3-3b]}$$

For example, if only 10% of the length of the steel bars of a cantilever beam (L/h = 5.0) is replaced with SMA bars (i.e. L_{SMAs}/L =0.10), and the cross-sectional areas of the bars are the same (A_{SMAs}/A_s = 1.0), then this beam will keep only 15.5% of the applied displacement (i.e. δ_r/δ_{max} = 15.5%). The stiffness of the beam will be reduced by 29.3% (i.e. $\delta_{y\text{-}s}/\delta_{cr\text{-}SMAs}$ = 70.7%), while the amount of dissipated energy by the beam will be reduced by 33.6% (i.e. EN_{SMAs}/EN_s = 66.4%) compared to the steel RC beam.

3.8 CONCLUSIONS

In this study, flexural behaviour of SMA RC beams during loading/unloading stages is investigated. Analysis method, that is based on the sectional analysis approach, is used to investigate the flexural behaviour of steel and SMA RC beams. First, the applicability of using the moment-area method with SMA RC beams is validated using available experimental results.

An extensive parametric study is then carried out to investigate the effect of different geometrical and cross-sectional parameters on the flexural behaviour of SMA RC beams. Studied parameters

are: (i) cross-section reinforcement ratio; (ii) ratio between the amounts of SMA reinforcement to the amount of steel reinforcement; (iii) cross-section height-to-width ratio; (iv) beam span-to-depth ratio; and (v) concrete compressive strength. For each of the studied parameters, nine load-displacement responses are calculated assuming different lengths of the SMA bars.

Increasing the SMA bar length up to 0.167 L significantly reduces the amount of residual displacements at complete unloading. In addition, the flexural stiffness is found to decrease significantly by increasing the SMA bar length. Amount of dissipated energy is also found to be dependent on the length of the SMA bars. However, it is noted that the rate of reduction of the flexural stiffness and the dissipated energy reduces as the length of SMA bars increase.

Four out of the five considered parameters in the parametric study are found to have minor or negligible effect on the beams behaviour. The ratio between the amounts of SMA reinforcement to the amount of steel reinforcement is the only parameter that caused a significant change in behaviour in terms of amount of residual displacement, change in flexural stiffness, and change in amount of dissipated energy.

All results of the parametric study are then used for multiple linear regression analysis. Results of the regression analysis are used to develop equations to help designers address the change occurring in the beam behaviour when regular steel reinforcing bars are replaced with SMA reinforcing bars. Changes in the amounts of residual displacements, flexural stiffness and dissipated energy can be estimated using the developed equations.

3.9 REFERENCES

Abdulridha, A. (2013). "Performance of Superelastic Shape Memory Alloy Reinforced Concrete Elements Subjected to Monotonic and Cyclic Loading." PhD Thesis, Department of Civil Engineering, University of Ottawa, Ottawa, Ontario, Canada, 346 pp.

Abdulridha, A., Palermo, D., Foo, S., and Vecchio, F. J. (2013). "Behavior and Modeling of Superelastic Shape Memory Alloys Reinforced Concrete Beams." Journal of Engineering Structures, 49, 893-904. DOI: 10.1016/j.engstruct.2012.12.041.

Alam, M.S., Youssef, M.A., and Nehdi, M. (2007). "Utilizing Shape Memory Alloys to Enhance the Performance and Safety of Civil Infrastructure: a Review." Canadian Journal of Civil Engineering, 34(9), 1075-1086.

Dunlop, P, and Simon, S. (2003) "Estimating key characteristics of the concrete delivery and placement process using linear regression analysis." Journal of Civil Engineering and Environmental Systems, 20(4), 273-290.

Elbahy, Y.I., Youssef, M.A., Nehdi, M. (2008). "Flexural Behaviour of Concrete Memebers Reinforced with Shape Memory Alloys." 2nd Canadian Conference on Effective Design of Structures, McMaster University, Hamilton, Ontario, Canada, 477-486.

Elbahy Y.I., Nehdi M., Youssef M.A. (2010b). "Artificial Neural Network Model for Deflection Analysis of Superelastic Shape Memory Alloy Reinforced Concrete Beams." Canadian Journal of Civil Engineering, 37(6), 855-865.

Elbahy Y.I., Youssef M.A., Nehdi M. (2009). "Stress Block Parameters for Concrete Flexural Members Reinforced with Superelastic Shape Memory Alloys." Journal of Materials and Structures, 42(10), 1335-1351.

Elbahy Y.I., Youssef M.A., Nehdi M. (2010a). "Deflection of Superelastic Shape Memeory Alloy Renforced Concrete Beams: Assessment of Existing Models." Canadian Journal of Civil Engineering, 37(6), 842-854.

Janke, L., Czaderski, C., Motavalli, M., and Ruth, J. (2005). “Applications of Shape Memory Alloys in Civil Engineering Structures - Overview, Limits and New Ideas.” Materials and Structures, 338(279), 578-592.

Karsan, I. D., and Jirsa, J. O. (1969). “Behavior of Concrete under Compressive Loading.” ASCE Journal (Structural Division), 95(12), 2543-2563.

Montgomery, D. C., Peck, E. A., and Vining, G. G. (2012). “Introduction to linear regression analysis.” John Wiley & Sons, Vol. 821.

Saiidi, M.S., Sadrossadat-Zadeh, M., Ayoub, C., Itani, A. (2007). "Pilot Study of Behavior of Concrete Beams Reinforced with Shape Memory Alloys." ASCE, Journal of Materials in Civil Engineering, 19(6), 454-461.

Scott, B.D.; Park, R.; and Priestley, M.J.N. (1982). “Stress-Strain Behavior of Concrete Confined by Overlapping Hoops at Low and High Strain Rates.” ACI journal, 79(1), 13-27.

Soroushian, P., Ostowari, K., Nossoni, A., and Chowdhury, H. (2001). “Repair and Strengthening of Concrete Structures through Application of Corrective Posttensioning Forces with Shape Memory Alloys,” Transportation Research Record: Journal of the Transportation Research Board, 1770, 20-26.

Stevens, N.J., Uzumeri, S.M., and Collins, M.P. (1987). “Analytical Modeling of Reinforced Concrete Subjected to Monotonic and Reversed Loading.” Publication No. 87-1, University of Toronto, 3634 pp.

Youssef, M., and Ghobarah, A. (1999). “Strength Deterioration due to Bond Slip and Concrete Crushing in Modeling of Reinforced Concrete Members.” ACI Structural Journal, 96(6), 956-967.

Youssef, M.A., and Rahman, M. (2007). “Simplified seismic modeling of reinforced concrete flexural members.” Magazine of Concrete Research, 59(9), 639-649.

Youssef MA, Alam MS, Nehdi M. (2008). "Experimental Investigation on the Seismic Behaviour of Beam-Column Joints Reinforced with Superelastic Shape Memory Alloys." Journal of Earthquake Engineering, 12(7), 454-461.

Chapter 4 Flexural Behaviour of Reinforced Concrete Beams Retrofitted using External Unbonded Superelastic Shape Memory Alloy Bars

4.1 INTRODUCTION

The civil infrastructure systems constitute a large portion of the national wealth. Because of ageing and exposure to the environment, they rapidly deteriorate and become more vulnerable to catastrophic failure. Therefore, these structures might need retrofitting to extend their service life. Retrofitting might also be needed to correct design and/or construction errors and to allow changing the structure function.

Examples of available retrofitting techniques for Reinforced Concrete (RC) sections are: (i) concrete jacketing; (ii) attaching steel plates; (iii) applying external post-tensioning; and (iv) using Fibre Reinforced Polymers (FRPs). Flexural retrofitting of RC beams using superelastic Shape Memory Alloy (SMA) bars is another potential technique. Main advantages of superelastic SMA bars are: (i) ability to undergo large deformations and return to their undeformed shape upon unloading (i.e. superelasticity); (ii) ability to dissipate large amounts of energy and release them upon unloading (i.e. flag shape stress-strain relationship) (iii) high resistance to corrosion; and (iv) high resistance to fatigue (Alam et al. 2007, Janke et al. 2005).

In this study, the possibility of using unbonded SMA bars to retrofit RC beams is analytically investigated. A Finite element (FE) model is first developed and validated using ABAQUS software (ABAQUS 2018). A simplified sectional method is then introduced. Results of the suggested method are validated using the FE model. A parametric study is then carried out using the simplified method. Results of the parametric study are used to develop design equations that can capture the change in the flexural behaviour of beams retrofitted using external unbonded SMA bars.

4.2 FINITE ELEMENT SIMULATION

Three-dimensional FE models are developed in this study to investigate the behaviour of RC beams retrofitted using external SMA bars during the loading/unloading stages. Analysis is performed using the commercial FE program ABAQUS Version 6.9 (ABAQUS 2018).

Hexahedral (8-node) isoparametric linear solid elements with reduced integration (C3D8R) are used to model the RC beams. Same element type is used to model the internal and external reinforcement, and external angles.

4.2.1 Concrete under Compression

The model developed by Scott et al. (1982), **Fig. 4-1(a)**, is used to model the concrete behaviour under compression loading. This model represents a good balance between accuracy and simplicity. During the unloading stage, behaviour of concrete in compression is assumed to follow the model proposed by Karsan and Jirsa (1969). When unloading starts, the material

follows linear straight path that connects the strain at the unloading start, ε_r, to the unloading strain at zero-stress, ε_p. After reaching ε_p, the strains continue to reduce while keeping the stress value equal to zero. This continues till reaching the point of zero strain.

4.2.2 Concrete under Tension

Behaviour of concrete under tension loading is assumed to follow the model proposed by Stevens et al. (1987) and simplified by Youssef and Ghobarah (1999), **Fig. 4-1(b)**. In the pre-cracking zone, the concrete behaves in a linear fashion up to the cracking stress f_{cr}. This is followed by significant reduction in the stress value.

If unloading starts before reaching f_{cr}, the concrete behaves in a linear fashion similar to the loading stage. If unloading starts after reaching f_{cr}, the material follows a linear path with a slope equal to the modulus of elasticity of concrete. After reaching the zero-stress point, the strain continues to decrease while the stress is kept equal to zero. This continues until reaching the point of zero-strain.

4.2.3 Steel Bars

The behaviour of the steel material is assumed to follow a bilinear stress-strain relationship under both tension and compression loadings, **Fig. 4-1(c)**. The material behaves elastically until reaching its yielding strain, $\varepsilon_{y\text{-}s}$. Then, the modulus of elasticity is significantly reduced.

If unloading starts within the pre-yielding zone, the material behaves in an elastic manner similar to the loading stage with no residual deformations at complete unloading. If the unloading starts within the post-yielding zone, the material follows a linear unloading path until yielding on the other side (tension or compression).

4.2.4 Superelastic SMA Bars

The stress-strain model of SMA consists of four linear branches that are connected by smooth curves (Alam et al. 2007), **Fig. 4-1(d)**. To simplify the modelling process of the SMA material, the smooth curves are ignored and linear branches are assumed to directly intersect. The material behaves elastically until reaching the SMA critical stress $f_{cr\text{-}SMA}$ which represents the start of the martensite stress induced transformation. Exceeding this limit, the material stiffness significantly reduces to about 10% of its initial value. If loading continues until full transformation to martensite phase occurs, the material regains about 50% of its initial stiffness. If loading continues to the real yielding limit, another significant reduction in the material stiffness occurs.

The behaviour of SMAs during the unloading stage is illustrated in **Fig. 4-1(d)**. If unloading starts before reaching SMAs critical stress, the material behaves in an elastic manner similar to the loading stage (i.e. unloading path 1). If unloading starts when the stress in the material is in between the critical and yielding stresses, the material follows a flag shaped stress-strain relationship (i.e. unloading path 2). If unloading starts after the material reaches its yielding limit), the material follows a linear unloading path (i.e. unloading path 3).

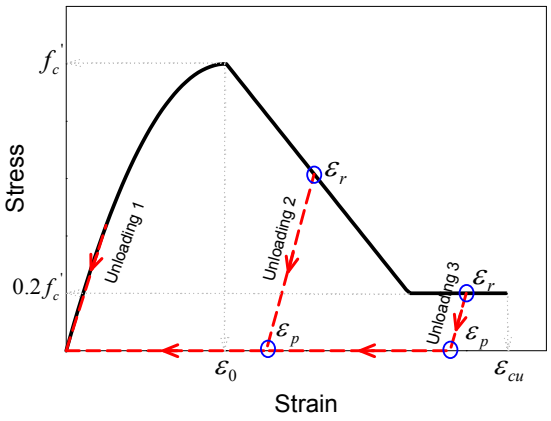

(e) Concrete in compression

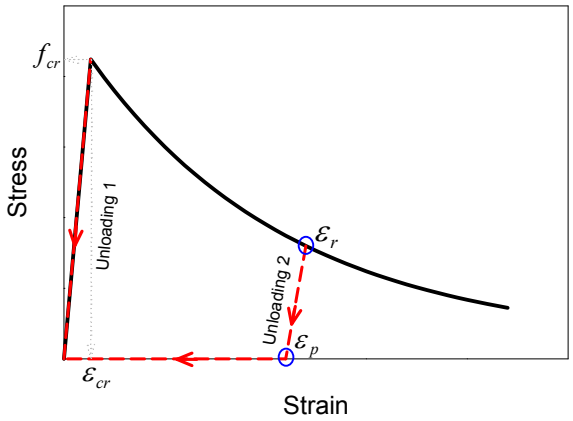

(f) Concrete in tension

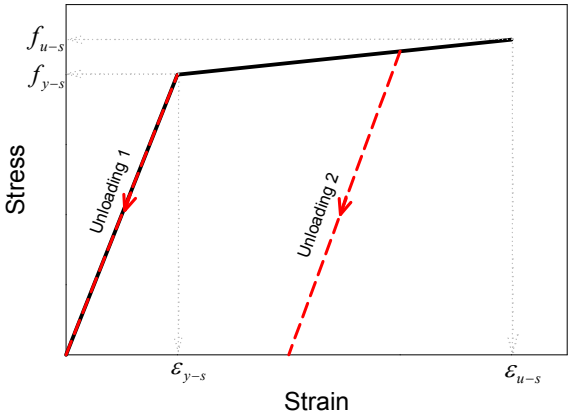

(g) Steel in tension/compression

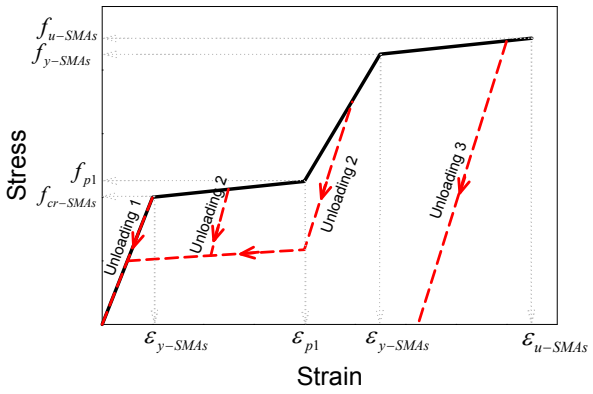

(h) SMA in tension/compression

Fig. 4-1: Stress-strain models during loading and unloading stages; (a) Concrete in compression; (b) Concrete in tension; (c) Steel in tension/compression; (d) SMA in tension/compression.

4.3 EXPERIMENTAL VALIDATION

The experimental work performed by Abdulridha (2013) and Abdulridha et al. (2013) is used to validate the developed model. Six simply supported beams with dimensions of 2800 mm length, 2400 mm span, 125 mm cross-section width, 250 mm cross-section height, and reinforced with SMA and/or steel bars are experimentally tested. All beams are tested under two central point loads spaced at 125 mm around mid-span.

The clear concrete cover of the beams is 20 mm. The average concrete compressive strength is 32.7 MPa for the SMA RC beams and 34.6 MPa for the steel RC beam. The beams are transversely reinforced with 6.35 mm wires spaced at 100 mm.

The length of the SMA bars is 600 mm centred at the mid-span of the beams. The diameter of the middle 300 mm of the SMA bars is reduced to 9.50 mm. M15 steel bars connected the SMA bar using mechanical couplers are used to reinforce the remaining length of the beam. Reinforcement details of the tested beams are summarized in **Table 4-1**.

Table 4-1: Details of the tested beams by Abdulridha et al. (2013)

Specimen	Loading type	Reinforcement type at mid-span	Longitudinal reinforcement at mid-span	
			Bottom	Top
B1-SM	Monotonic	Steel	2 bars, 10M	2 bars, ϕ = 6.35 mm
B2-SC	Cyclic	Steel	2 bars, 10M	2 bars, ϕ = 6.35 mm
B3-SR	Cyclic	Steel	2 bars, 10M	2 bars, 10M
B4-NM	Monotonic	SMAs	2 bars, ϕ = 9.5 mm	2 bars, ϕ = 6.35 mm
B6-NR	Cyclic	SMAs	2 bars, ϕ = 9.5 mm	2 bars, ϕ = 9.5 mm
B7-NCM	Cyclic	SMAs	2 bars, ϕ = 9.5 mm	2 bars, ϕ = 9.5 mm

Mesh sensitivity analysis is performed to determine the appropriate element size. Four element different sizes (61.25, 43.75, 26.25 and 17.5 mm) are examined considering beam B6-NR, **Fig. 4-2**. It is found that element size of 17.5 mm is appropriate for the analysis. Obtained load-displacement relationships are compared with the experimental results in case of monotonic loading, and with experimental envelopes in case of cyclic and reversed-cyclic loading. Experimental load-displacement results are plotted versus the numerically obtained results in **Fig. 4-3** and **Fig. 4-4** for steel and SMA RC beams, respectively. As shown in the figure, very good agreement between experimental and analytical results is obtained for all beams.

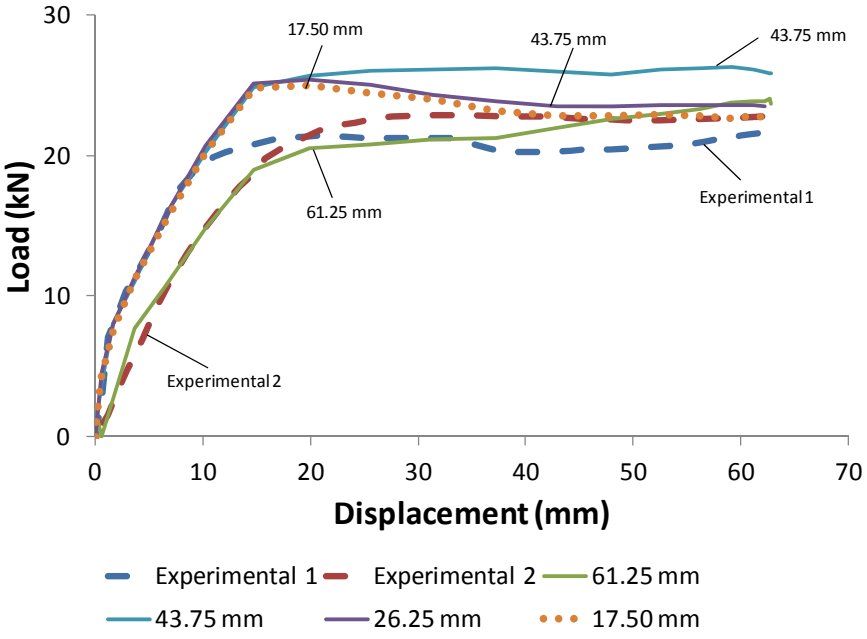

Fig. 4-2: Mesh sensitivity analysis for the FE model.

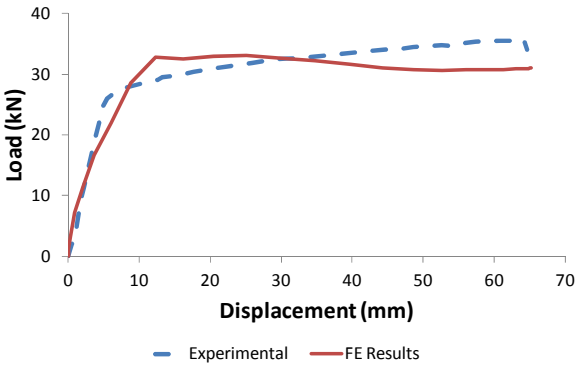

(a) B1-SM results

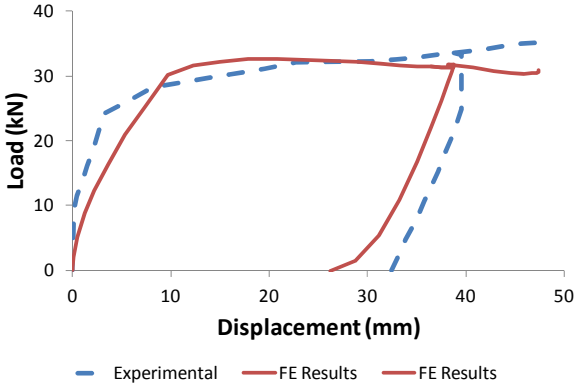

(b) B2-SC results

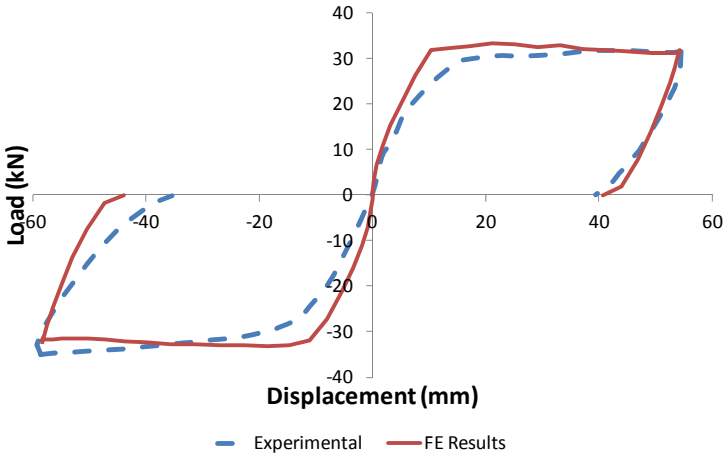

(c) B3-SR results

Fig. 4-3: Experimental vs. numerical load-displacement results of steel RC beams tested by Abdulridha (2013); (a) B1-SM results; (b) B2-SC results; (c) B3-SR results.

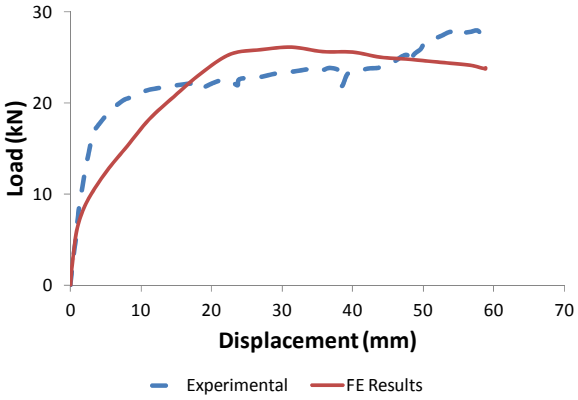

(a) B4-NM results

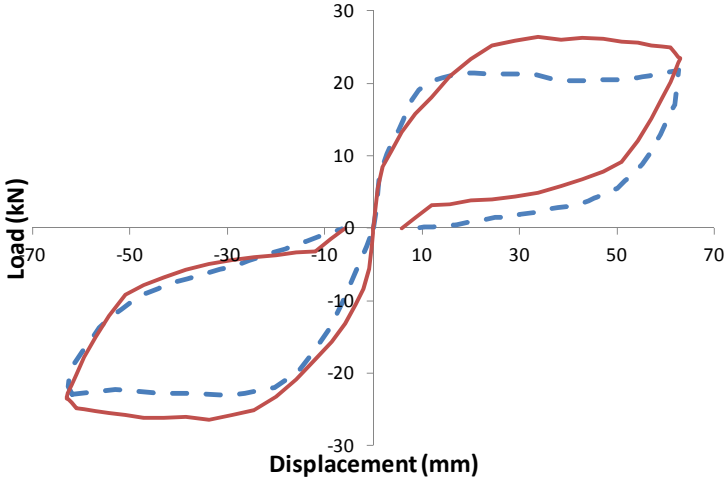

(b) B6-NR results

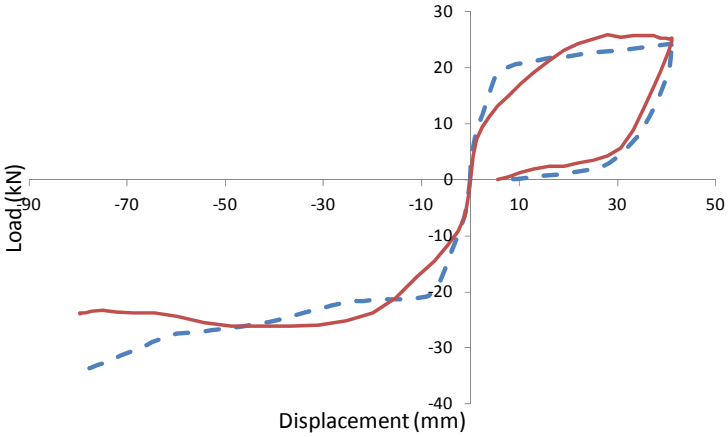

(c) B7-NCM results

Fig. 4-4: Experimental vs. numerical load-displacement results of SMA RC beams tested by Abdulridha (2013); (a) B4-NM results; (b) B6-NR results; (c) B7-NCM results.

The experimental work by Saiidi et al. (2007) is also used to validate the FE model. They tested eight RC beams under quasi-static loading. The beams have the same dimensions. Four beams are reinforced with SMA bars at mid-span, while the other four are reinforced with conventional steel bars. Details of the types and amounts of reinforcement used in the eight beams are summarized in **Table 4-2.**

The beams are 1530 mm long. The beams have cross-sectional dimensions of 127x152 mm at mid-span and 127x305 mm at the ends, **Fig. 4-5**. The main external reinforcement is attached to the beam using external angles. The beams are tested under two point loads.

Mesh sensitivity analysis is first performed to determine the appropriate element size. Four element sizes are examined, **Fig. 4-6**. It is found that reducing the element size beyond 25.4 mm has negligible effect on the predicted results. Results of the analysis are plotted in **Fig. 4-7** for the SMA RC beams and in **Fig. 4-8** for the steel RC beams. As shown in the figures, good agreement between the experimental and analytical results is observed for both steel and SMA RC beams.

Table 4-2: Properties of the tested beams by Saiidi et al. (2007)

Specimen	Mid-span reinforcement	ε_y (mm/mm)	f_y (MPa)	E (MPa)
BNL1	1 ϕ 6.40 mm	0.013	400	34078
BNL2	2 ϕ 6.40 mm	0.013	400	34078
BNH1	1 ϕ 9.50 mm	0.013	510	39245
BNH2	2 ϕ 9.50 mm	0.013	510	39245
BSL1	1 # 3 bars	0.0021	440	209524
BSL2	2 # 3 bars	0.0021	440	209524
BSH1	1 # 4 bars	0.0009	420	466667
BSH2	2 # 4 bars	0.0009	420	466667

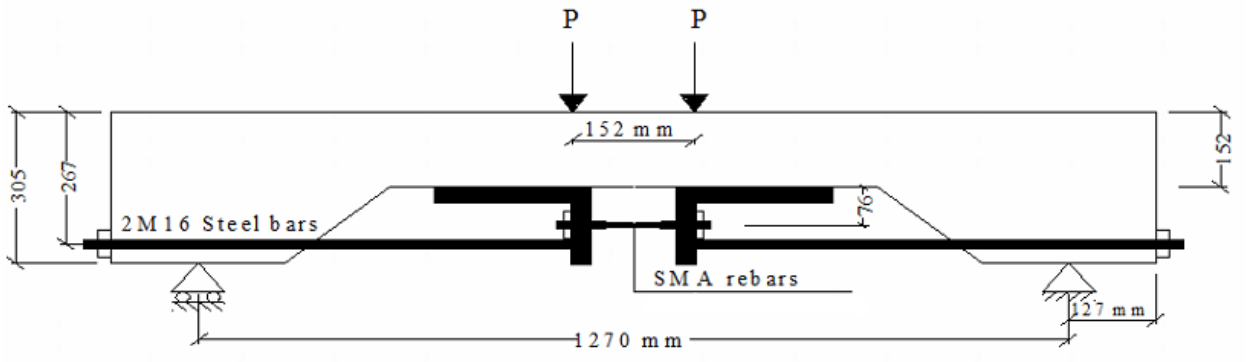

Fig. 4-5: Dimensions and test setup of beams tested by Saiidi et al. (2007).

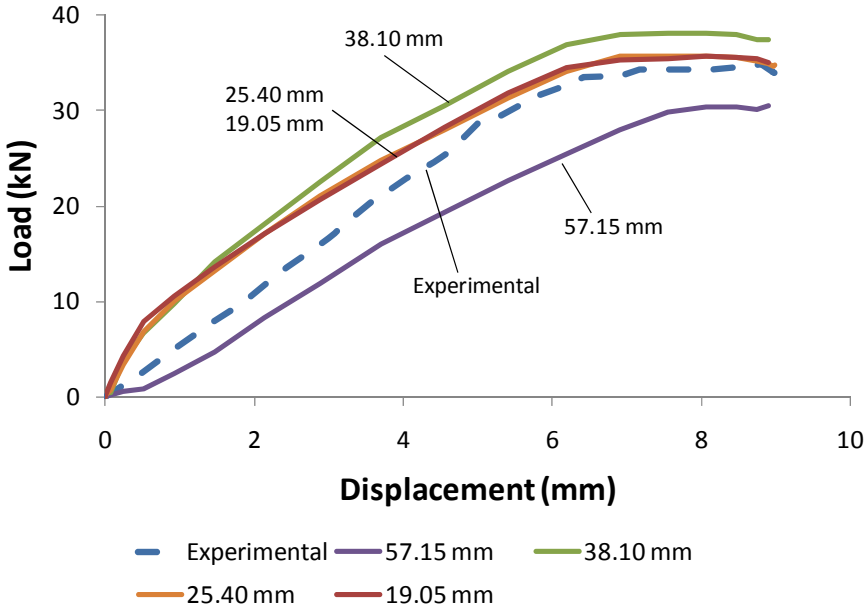

Fig. 4-6: Mesh sensitivity analysis for beam BNH1.

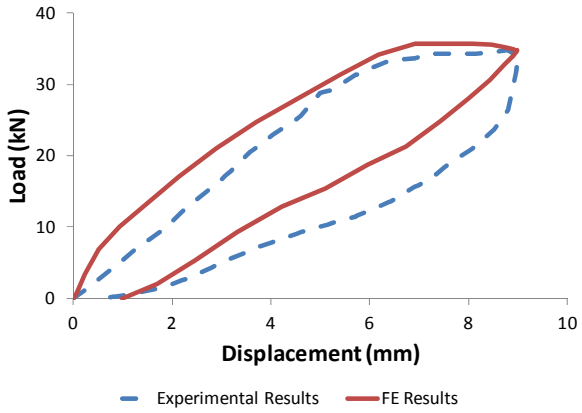

(a) BNH1 results

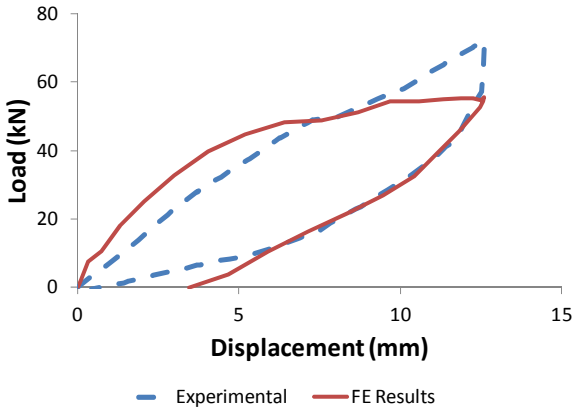

(b) BNH2 results

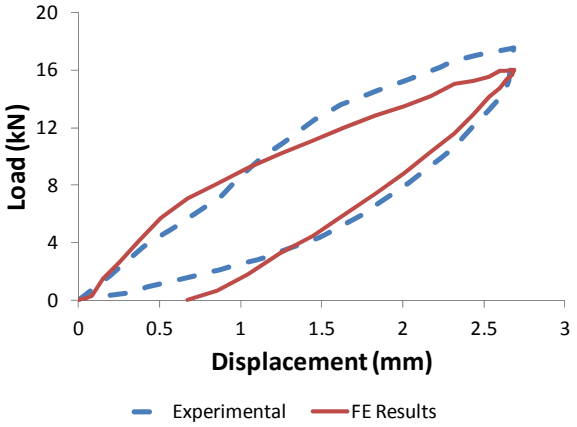

(c) BNL1 results

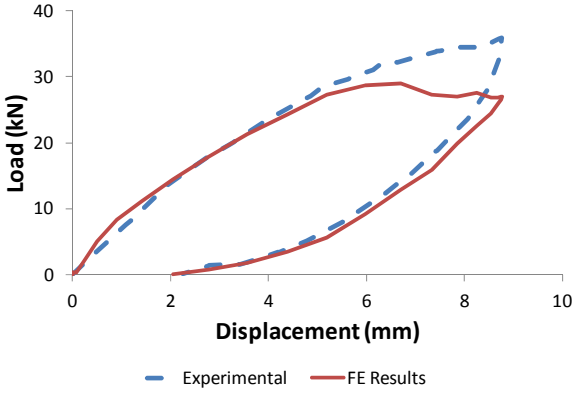

(d) BNL2 results

Fig. 4-7: Experimental vs. analytical load-displacement results of the SMA RC beams tested by Saiidi et al. (2007); (a) BNH1 results; (b) BNH2 results; (c) BNL1 results; (d) BNL2 results.

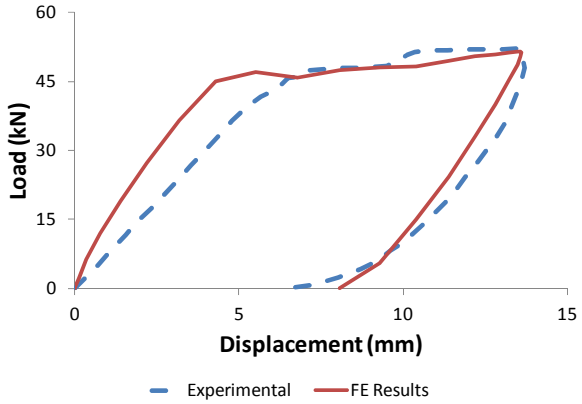

(a) BSH1 results

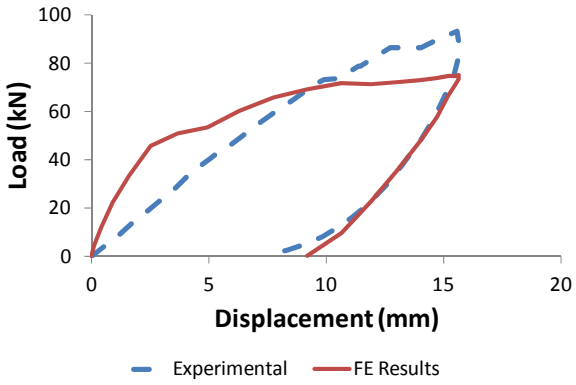

(b) BSH2 results

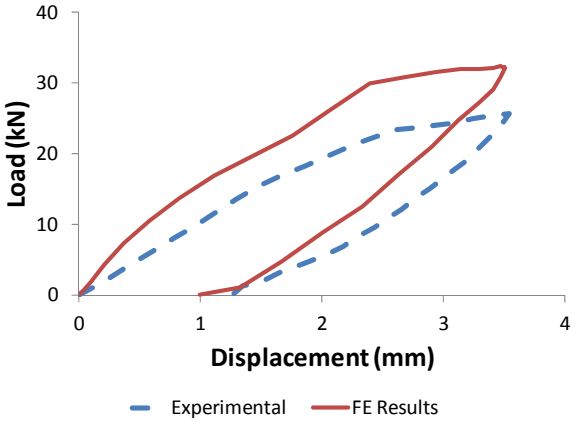

(c) BSL1 results

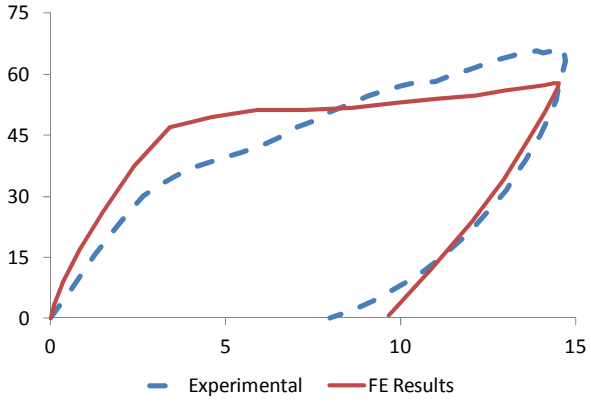

(d) BSL2 results

Fig. 4-8: Experimental vs. analytical load-displacement results of the steel RC beams tested by Saiidi et al. (2007); (a) BSH1 results; (b) BSH2 results; (c) BSL1 results; (d) BSL2 results.

4.4 SUGGESTED RETROFITTING TECHNIQUE

Fig. 4-9 shows the suggested retrofitting technique. Two angles are first attached to the ends of the beam using steel bolts. The angles are then connected with SMA-steel bars. Each bar is made of a middle SMA bar connected using two mechanical couplers to two steel bars. The use of steel bars minimizes the length of the SMA bars, and, thus their cost. Hold down angles can be used along the length of the beam to enforce the external bars follow the curvature of the beam.

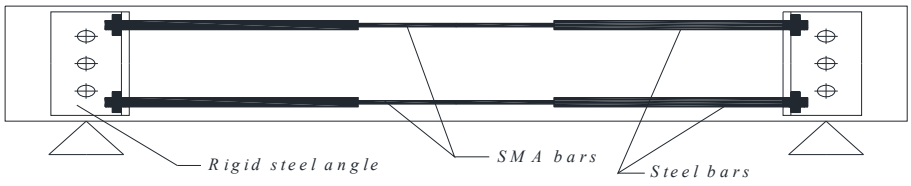

Fig. 4-9: Suggested strengthening technique.

The modulus of elasticity of steel is about 4 times the modulus of elasticity of SMAs. Thus, attaching a small or moderate ratio of SMA will improve the beam strength, but is not expected to reduce the residual deformations. Thus, it is proposed to cut the internal tensile steel at the mid-span section as it is being replaced by the external SMA bars.

To investigate the structural performance of the proposed system, a RC beam is assumed to have a cross-section of 125x250 mm and a span of 1200 mm, **Fig. 4-10**. The beam is internally reinforced with 2-10M steel bars at top and bottom. The concrete compressive strength is

assumed to be 32.70 MPa. An external angle with dimensions of 110x110x40 mm is attached to the beam near the support section using 3 bolts. The bolts are assumed to be 91 mm in length and 12.7 mm in diameter. Another angle with the same size is used as a deflector near the mid-span section to have the external bar follow the beam as it deflects when loaded. External SMA bars are coupled to steel bars with larger cross-section and attached to the external angles using end couplers.

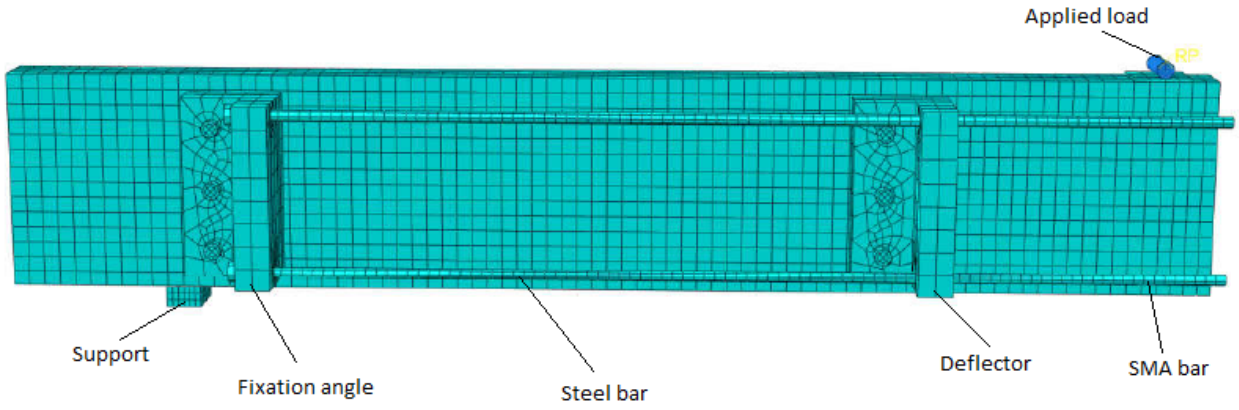

Fig. 4-10: FE model of half the strengthened beam

FE analysis is performed for the retrofitted beam. Four element different sizes (61.25, 43.75, 26.25, and 17.5 mm) are first considered to determine the appropriate mesh size. It is found that element size of 17.5 mm gives good results and further refinement of the mesh does not noticeably change the behaviour.

Fig. 4-11 shows the load-displacement relationship of the retrofitted beam vs. the original beam. The maximum moment capacity of the beam increased from 20 kN.m to 24 kN.m. The pre-yielding stiffness of the beam reduced significantly due to replacing the internal steel bars with

SMA bars. Suggested retrofitting technique reduced the amount of residual displacement from 32 mm to 5 mm (84%). Thus, it is clear that SMA can be used to reduce seismic residual deformations. However, such use affects the stiffness and strength of the retrofitted element. The following sections present a simplified method that is used to conduct a parametric study and develop simplified equations to evaluate effects of the suggested retrofitting technique.

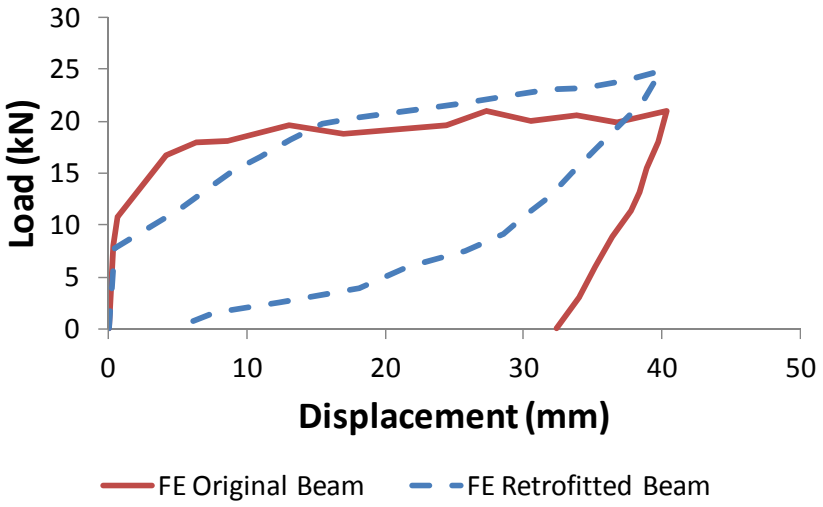

Fig. 4-11: Load displacement results of the retrofitted beam vs. the original beam.

4.5 SIMPLIFIED ANALYSIS METHOD

A simplified method is introduced in this section. A computer program is first developed using JAVA programming to predict the flexural behaviour of RC beams retrofitted using unbonded superelastic SMAs bars. The program is based on the sectional analysis methodology, where the cross-section of the retrofitted beam is divided into a discrete number of horizontal layers, **Fig. 4-12**. Using the predefined stress-strain relationship of each layer, and considering the cross-section equilibrium and kinematics, the flexural behaviour of the retrofitted beam can be predicted (Youssef and Rahman 2007; Elbahy et al. 2008, 2009, 2010a, and 2010b). Two main assumptions are proposed in the suggested analysis procedure: (i) plane sections remain plane (i.e. linear strain distribution); and (ii) perfect bond exists between concrete and internal reinforcement layers.

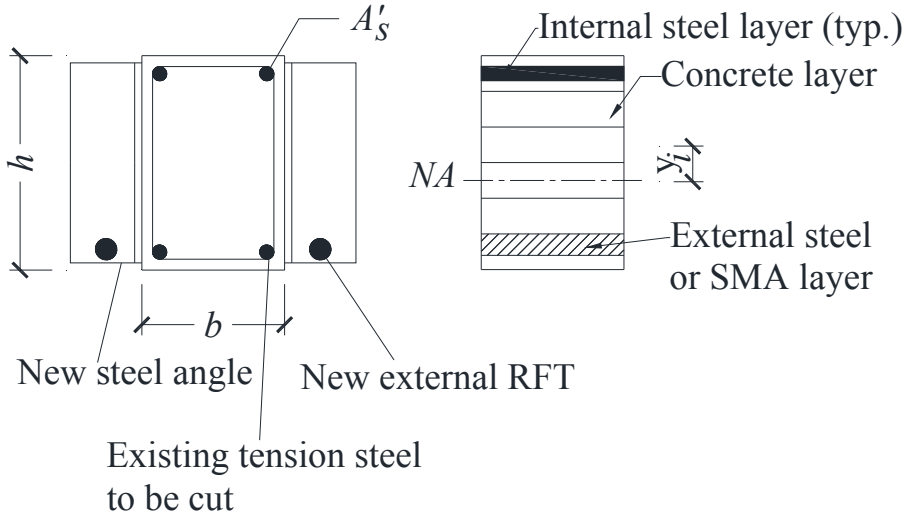

Fig. 4-12: Fibre Model.

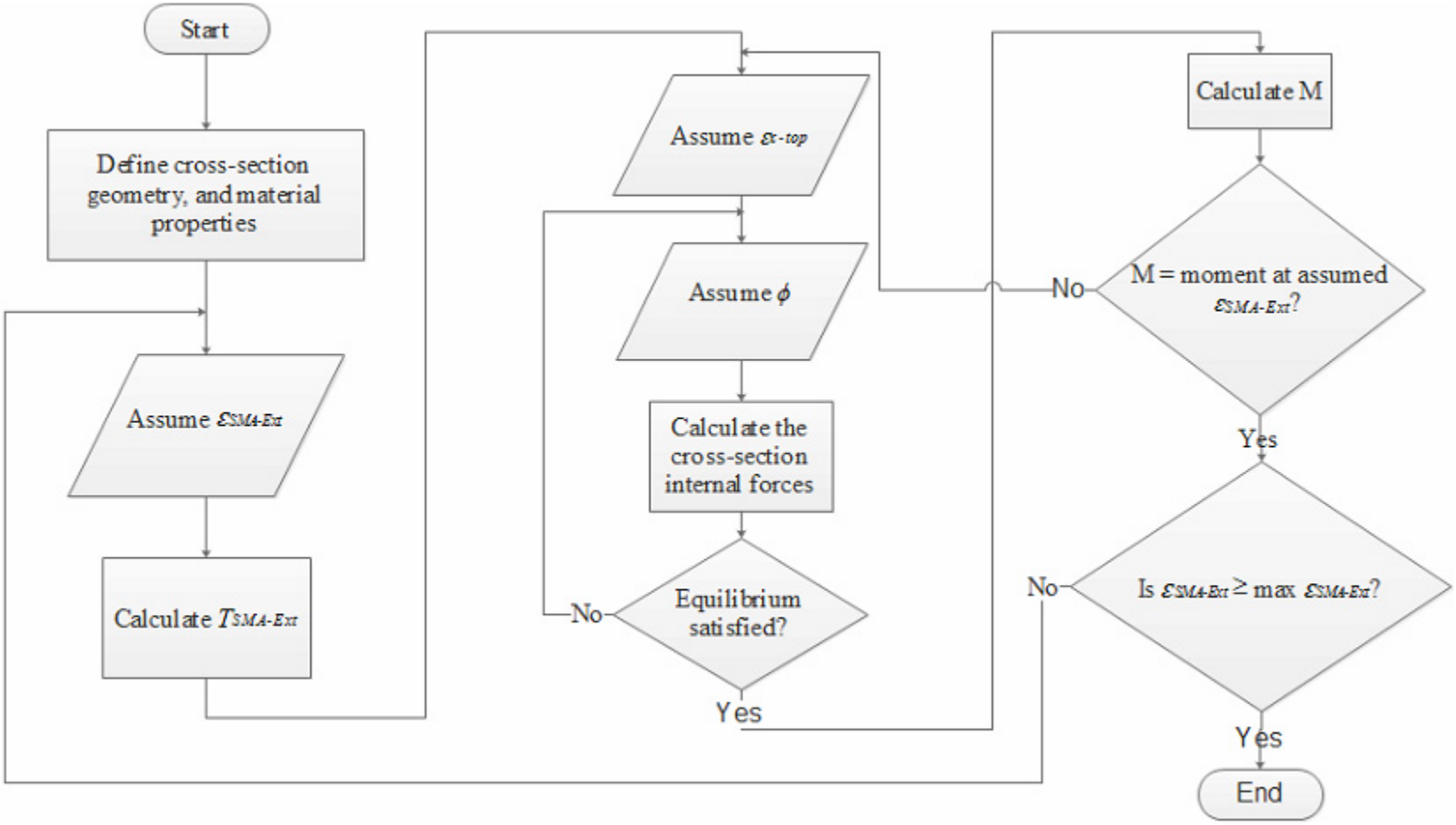

(a) Loading stage

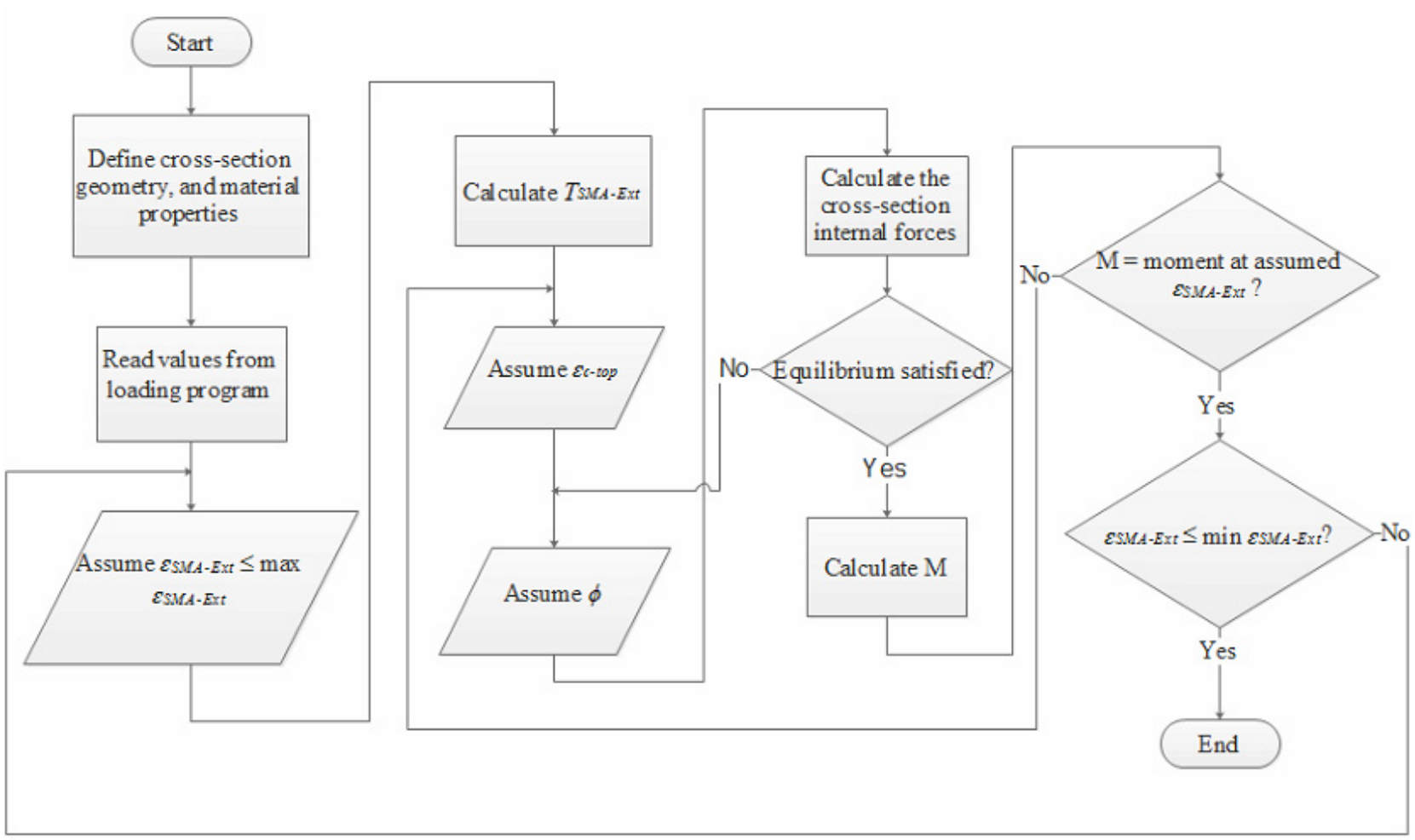

(b) Unloading stage

Fig. 4-13: Flow chart of the developed program; (a) Loading stage; (b) Unloading stage.

Fig. 4-13(a) illustrates a flow chart of the developed program during the loading stage. Steps of the analysis are: (i) The analysis starts by assuming an initial strain for the unbonded SMA bars; (ii) using the predefined SMA stress-strain relationship, the force in the unbonded SMA bars is then calculated; (iii) a compressive strain value, $\varepsilon_{c\text{-}top}$, is assumed for the top concrete layer; (iv) cross-section curvature, ϕ, is then iterated until equilibrium is achieved; (v) the corresponding cross-section moment, M, is then calculated; (vi) analysis is repeated for a range of top compressive strains $\varepsilon_{c\text{-}top}$ until reaching a moment value that corresponds to the assumed $\varepsilon_{SMA\text{-}ext}$. The final moment and curvature represent one point on the desired moment-curvature relationship. This procedure is repeated for different strain values $\varepsilon_{SMA\text{-}ext}$.

Fig. 4-13(b) shows a flow chart of the program during the unloading stage. Steps of the analysis are: (i) read the values corresponding to the point of unloading from the loading program ($\varepsilon_{SMA\text{-}ext}$, moment, curvature, layer stress, layer strain); (ii) unloading analysis starts by assuming a smaller $\varepsilon_{SMA\text{-}ext}$ in the unbonded SMA bar; (iii) using the predefined unloading stress-strain relationship of the SMA bar, the force in the unbonded SMA bar is calculated; (iv) the compressive strain value in the top layer $\varepsilon_{c\text{-}top}$ recorded at the maximum loading level is used as an initial top strain value for the unloading analysis; (v) using the predefined stress-strain relationship of each layer and the recorded stress and strain of each layer, the cross-section curvature ϕ is iterated until the cross-section equilibrium is achieved; and (vi) the corresponding cross-section moment and curvature are calculated and recorded. Analysis is then repeated for a range of smaller top compressive strains $\varepsilon_{c\text{-}top}$ and $\varepsilon_{SMA\text{-}ext}$.

The Four material models introduced in the Finite Element simulation section are implemented in the developed program. These models represent the behaviour of concrete, steel, and SMA materials under tensile and compressive loadings.

4.6 DEFLECTION CALCULATIONS

The moment-area method is utilized to calculate the rotation and deflection values. Steps involved in this method includes: (i) perform moment-curvature analysis of different cross-sections defining the structural element; (ii) the bending moment distribution is used in conjunction with the moment-curvature relationship to obtain the curvature distribution along the length of the member; (iii) rotation of any part of the element can be calculated by integrating the area under the curvature distribution, while deflection can be obtained by calculating the moment of the integrated area about the target location.

4.7 PROGRAM VALIDATION

The FE model is used in this section to validate the results obtained using the simplified sectional analysis method. The load-displacement relationship of the ABAQUS model is plotted versus the load-displacement relationship obtained using the simplified sectional analysis method in **Fig. 4-14**. The FE model showed good agreement with the simplified method. Therefore, the simplified method is used in the analysis of the following sections of the paper. Additional validations of the developed program are given in **Appendix III**.

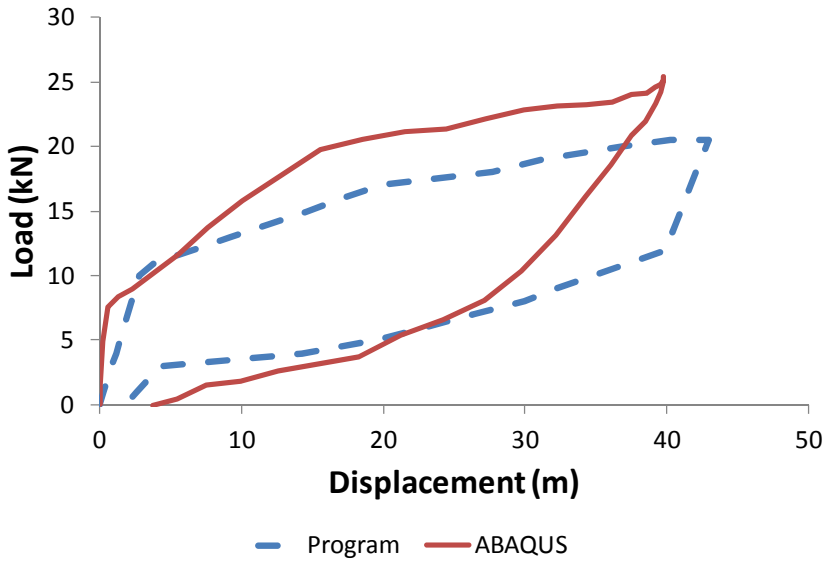

Fig. 4-14: Load-displacement relationship of the FE method vs. the developed program.

4.8 PARAMETRIC STUDY

A parametric study is carried out in this section to investigate the behaviour of RC beams retrofitted using unbonded SMA bars. Analysis is performed for the loading and unloading stages. Three parameters are investigated: (i) the ratio between the added external SMA reinforcement to the amount of internal steel reinforcement in the beam (A_{SMA}/A_s); (ii) applied load level (ratio between the maximum applied displacement to the displacement at which yielding of the external reinforcement occurs δ_{max}/δ_y); and (iii) ratio between the length of the used SMA bars to the span of the beam (L_{SMA}/L).

The parametric study is performed on simply supported beams with cross-sectional dimensions of 300 mm by 700 mm and span of 7,000 mm. The beams are loaded/unloaded under either one or two point loads. For each of the studied parameters, the parameter under investigation is

varied within the desired range while keeping all other parameters constant during the analysis. While varying A_{SMA}/A_s and load level, the length of the SMA bars is assumed equal to the full length of the beam. For the third parameter (L_{SMA}/L), nine different lengths of the SMA bars are investigated (0.05 *L*, 0.10 *L*, 0.125 *L*, 0.167 *L*, 0.25 *L*, 0.33 *L*, 0.50 *L*, 0.67 *L*, and 0.75 *L;* where *L* is the span of the studied beams). The parametric study is repeated two times: (i) assuming the beams are externally reinforced with SMA bars and the internal steel bars are not cut; and (ii) assuming the beams are externally reinforced with steel bars and the internal steel bars are not cut. Results of the two cases are provided in **Appendices IV, V** and **VI**.

4.9 RESULTS AND DISCUSSIONS

4.9.1 A_{SMA}/A_s Parameter

Seven different A_{SMA}/A_s ratios are used in the analysis. These ratios are: A_{SMA}/A_s = 0.5, 1.0, 2.0, 3.0, 4.0, 5.0, and 6.0. **Fig. 4-15(a)** shows the effect of increasing the A_{SMA}/A_s on the amount of residual displacement upon unloading. It is clear from the figure that the amount residual displacement is independent of increasing the A_{SMA}/A_s ratio at different load levels. The ratio δ_r/δ_{max} varies from 0% to 3% when the A_{SMA}/A_s ratio increased from 0.50 to 6.0. This negligible δ_r/δ_{max} is attributed to the full deformation recovery of the SMA bars after load removal.

Increasing the A_{SMA}/A_s ratio resulted in significant increase in the maximum moment capacity ratio M_{rt}/M_{org}, **Fig. 4-15(b)**. The increase happens in a linear fashion. However, it should be noted that using A_{SMA}/A_s less than 1.0 results in reduction in the maximum moment capacity of the beam compared to the original one.

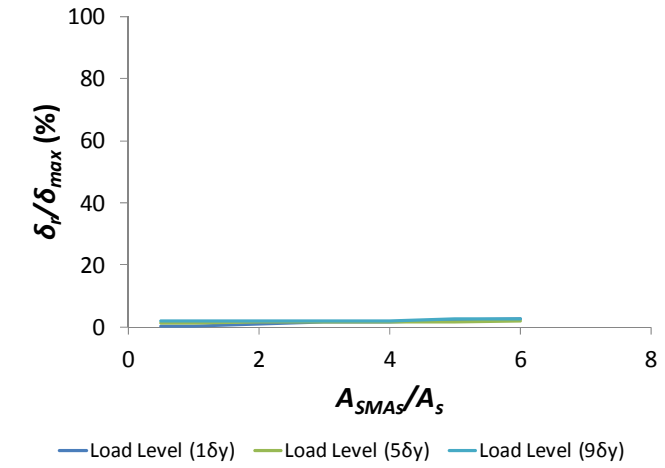

(a) Residual displacements

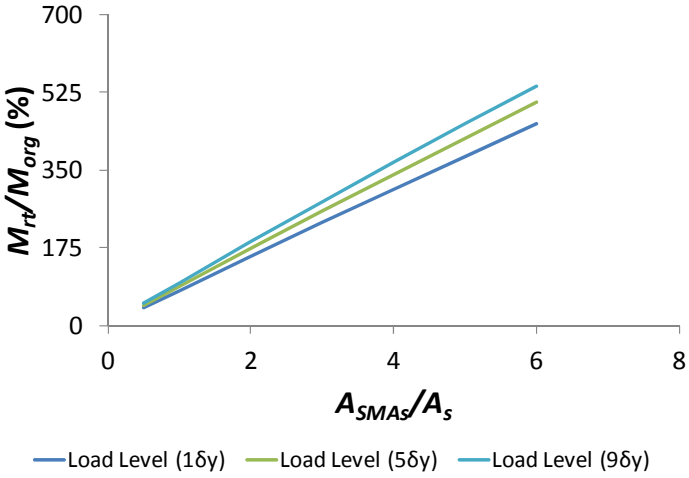

(b) Moment capacity

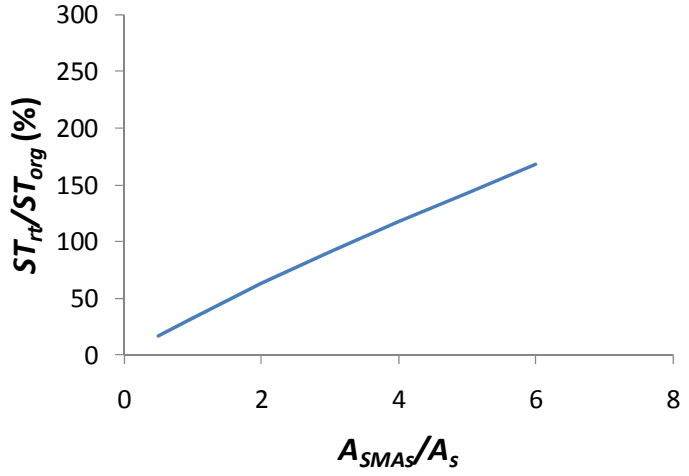

(c) Initial stiffness

Fig. 4-15: Effect of varying the A_{SMAs}/A_s ratio on the retrofitted beam behaviour; (a) Residual displacements; (b) Moment capacity; (c) Initial stiffness.

Initial stiffness decreases to less than 25% of its original value if A_{SMA}/A_s ratio of 0.5 is used, **Fig. 4-15(c)**. Increasing A_{SMA}/A_s ratio to 3.0 can help the beam to regain its initial stiffness. Increasing A_{SMA}/A_s ratio beyond this limit results in a more stiff behaviour of the retrofitted beam compared to the original one.

4.9.2 Load Level Parameter (δ_{max}/δ_y)

The effect of varying the applied load level (δ_{max}/δ_y) on the behaviour of RC beams retrofitted using external SMA bars is investigated in this subsection. The analysis is performed for different values of A_{SMA}/A_s ratios. **Fig. 4-16** shows the results of the analyzed beams.

Fig. 4-16(a) shows that the effect of increasing the load level on the amount of residual deformations is negligible. This is because the overall behaviour of the beam is controlled by the behaviour of the external SMA bars at all A_{SMA}/A_s ratios.

Increasing the load level shows increase in the moment capacity of the beams, **Fig. 4-16(b)**. This is attributed to the strain hardening in SMA stress-strain models. Significant reduction (33% to 65%) in the overall moment capacity of the beams with low A_{SMA}/A_s ratio (i.e. A_{SMA}/A_s = 0.50 to 2.0) can be observed.

Fig. 4-16(c) confirms that the initial stiffness of the beams are not affected by the applied load level. However, the initial stiffness of the beams with low A_{SMA}/A_s ratio (i.e. A_{SMA}/A_s = 0.50 to A_{SMA}/A_s = 2.0) is much lower than the initial stiffness value of the original beam.

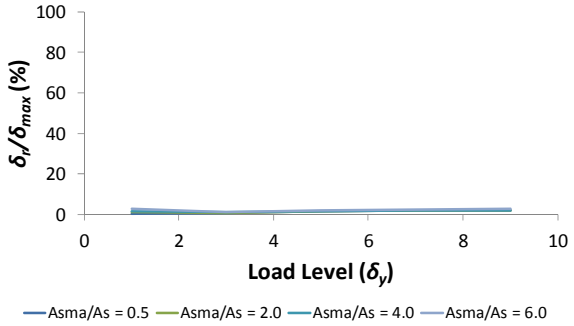

(a) Residual Displacement

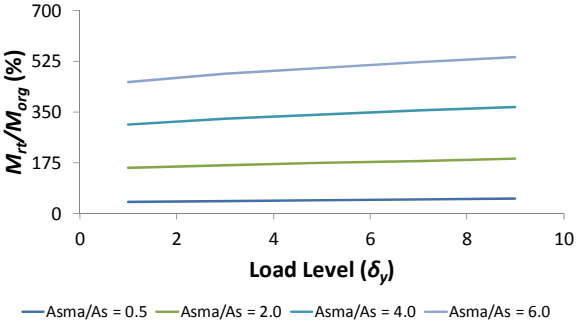

(b) Moment capacity

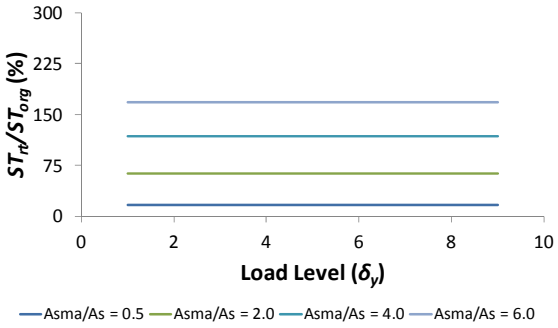

(c) Initial stiffness

Fig. 4-16: Effect of varying the applied load level on the retrofitted beam behaviour ; (a) Residual displacements; (b) Moment capacity; (c) Initial stiffness.

4.9.3 L_{SMA}/L Parameter

The effect of varying the external SMA bar length on the behaviour of the retrofitted beams is investigated in this subsection. SMA bar length is represented by the ratio (L_{SMA}/L). Nine different SMA bar lengths are assumed in the analysis. Each length is analyzed at different A_{SMA}/A_s ratios and at different load levels.

Fig. 4-17 and **Fig. 4-18** show the effect of varying the L_{SMA}/L ratio on the amount of residual displacements upon unloading for different A_{SMA}/A_s ratios and for different load levels. The amount of residual displacement is significantly reduced (i.e. 2% to 5%). The dependency of L_{SMA}/L on the A_{SMA}/A_s ratio and the load level is eliminated. **Fig. 4-19** shows that the retrofitted beam strength is not affected by increasing the L_{SMA}/L ratio. The reason behind this is that the SMA bars are coupled to regular steel bars with bigger cross-sectional area to ensure that most of the deformations and failure occur in the SMA region. Thus, the maximum strength of the beam is equal to the strength of SMA RC section and is independent of the SMA bar length.

The effect of varying the L_{SMA}/L ratio on the initial stiffness of the beam is also studied. As shown in **Fig. 4-20**, increasing the length of the SMA bars reduces the initial stiffness of the beam. This reduction is very significant (700%) in case of low A_{SMA}/A_s ratios, and less significant (100%) at high A_{SMA}/A_s values.

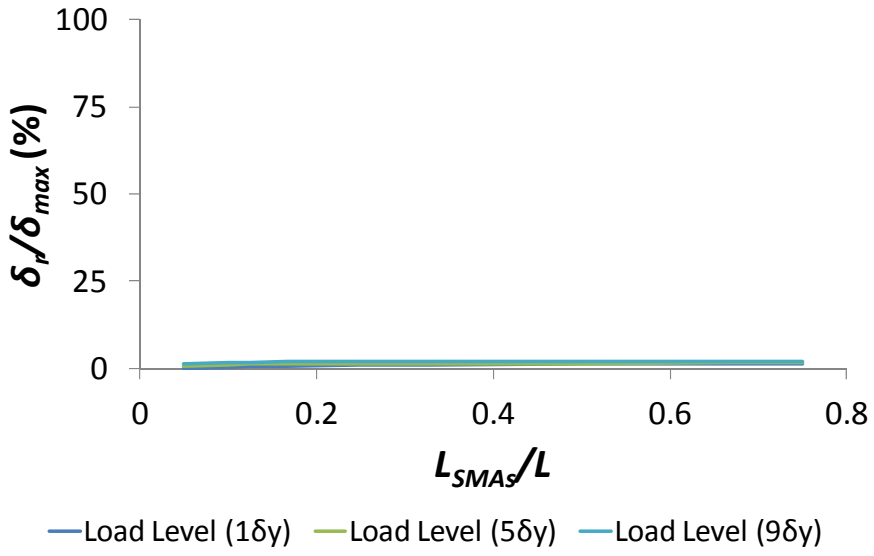

Fig. 4-17: Effect of varying the L_{SMA}/L ratio on the amount of residual displacements in the strengthened beams at A_{SMA}/A_s =3.0.

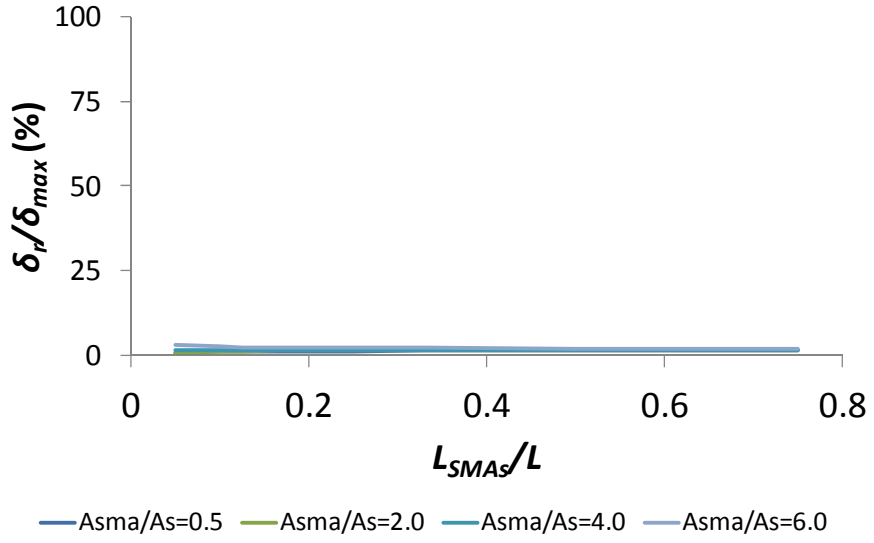

Fig. 4-18: Effect of varying the L_{SMA}/L ratio on the amount of residual displacements in the retrofitted beams at load level = 5.0 δ_y.

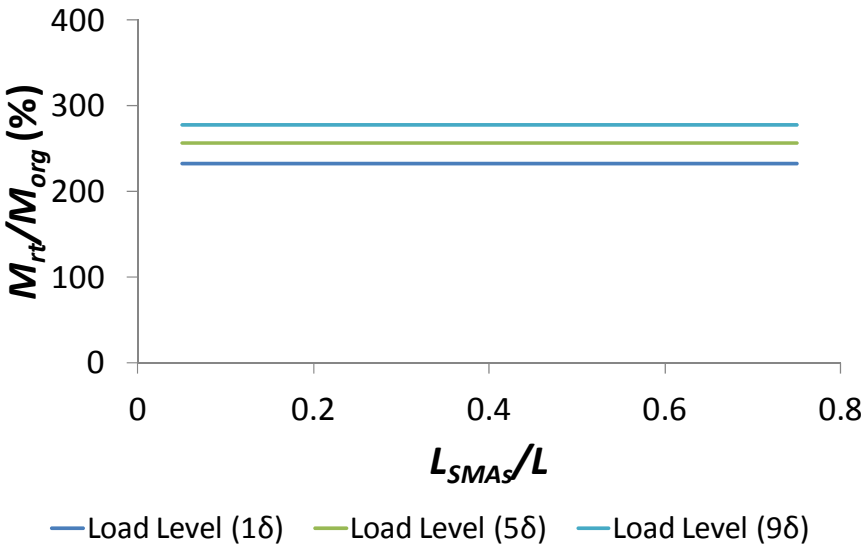

Fig. 4-19: Effect of varying the L_{SMA}/L ratio on the moment capacity of the retrofitted beams at $A_{SMAs}/A_s = 3.0$.

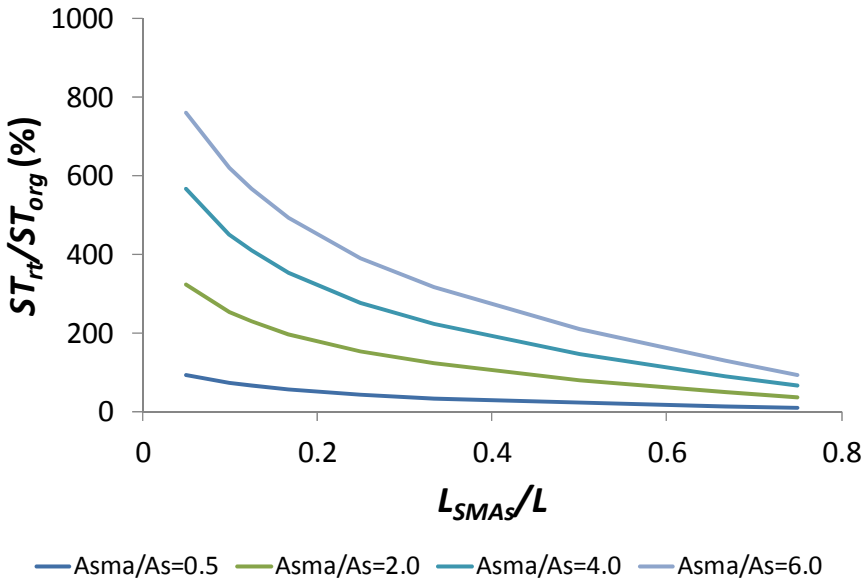

Fig. 4-20: Effect of varying the L_{SMA}/L ratio on the initial stiffness of the retrofitted beams.

The effect of varying the length of the external SMA bars on the displacement at which yielding in the external SMA bars starts is also introduced in this study. Increasing the length of the SMA bars resulted in increasing the $\delta_{y\text{-}rt}/\delta_{y\text{-}org}$ ratio, **Fig. 4-21**. This increase is insignificant at the small L_{SMA}/L values, and increases as the length of the SMA bars increase. The rate of increasing is higher for beams with low A_{SMA}/A_s. The ratio $\delta_{y\text{-}rt}/\delta_{y\text{-}org}$ is independent of the load level, and, thus the load level effect is not investigated.

The effect of varying the length of the external SMA bars on the maximum displacement of the retrofitted beam is shown in **Fig. 4-22**. Increasing the length of the SMA bars increases the $\delta_{max\text{-}rt}/\delta_{max\text{-}org}$ ratio. This increase is more pronounced in case of low A_{SMA}/A_s. Similar trend is observed at different loading levels. Similar to the yielding displacements, the rate of increase in $\delta_{max\text{-}rt}/\delta_{max\text{-}org}$ is more significant in case of low A_{SMA}/A_s.

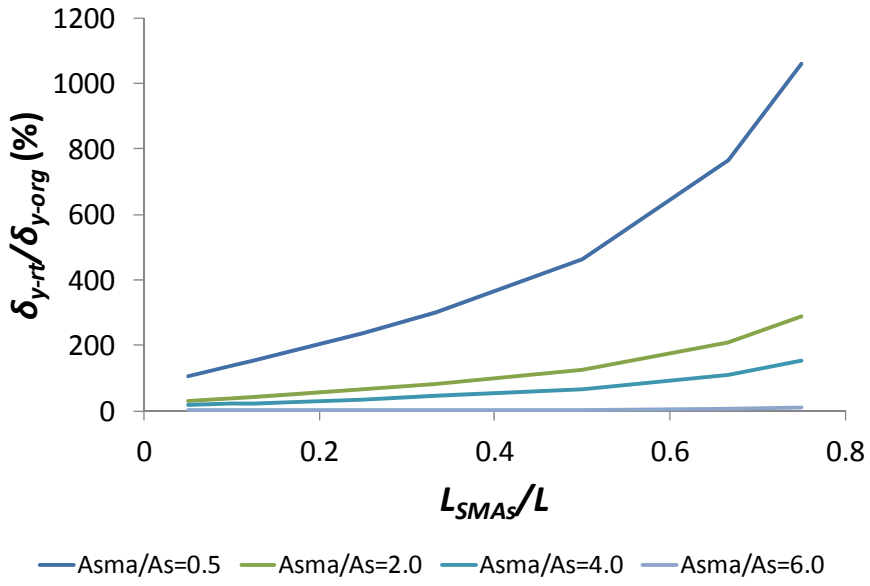

Fig. 4-21: Effect of varying the L_{SMA}/L ratio on the displacement at which yielding in the external SMA bar starts to occur in the retrofitted beams.

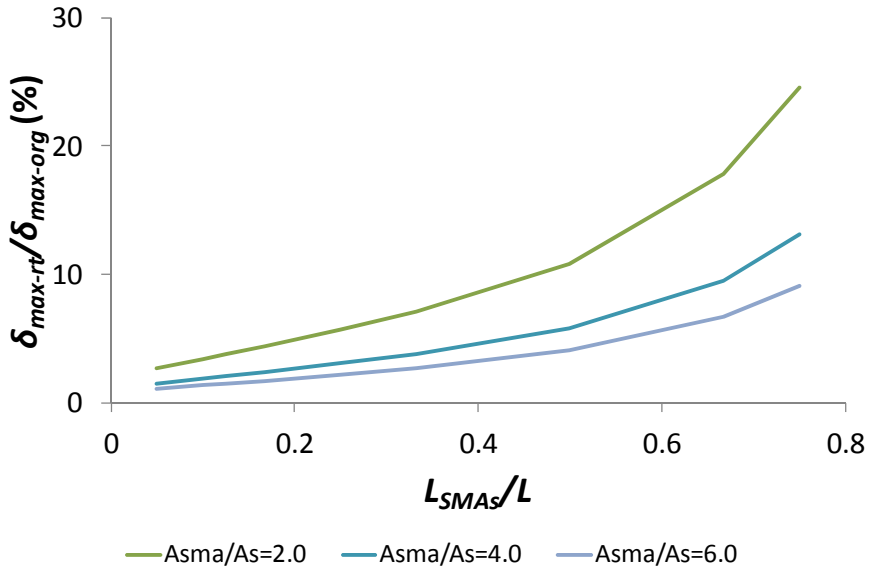

Fig. 4-22: Effect of varying the L_{SMA}/L ratio on the maximum displacement of the retrofitted beams.

4.10 CHOICE OF SMA BARS

Multiple linear regression is used to model the relationship between the outputs and the inputs obtained from the parametric study. After trying numerous number of models that utilize different transformations (i.e. linear transformation, quadratic power transformation, and logarithmic transformation), the best five models for the five outputs are noted and presented in this section.

In the used backward elimination stepwise regression (Dunlop and Smith 2003), all explanatory variables (inputs) are included in the model at the beginning. Then, the non-significant variables are eliminated one at a time. At the end of the analysis, the reported remaining variables are only the statistically significant ones.

The data used in this analysis are the data obtained from the parametric study. A total of 350 data sets are used in the models. All parameters (i.e. inputs and outputs) are non-dimensional parameters. The inputs are: L_{SMA}/L, A_{SMA}/A_s, and load level. The outputs of the parametric study are: δ_r/δ_{max}, M_{rt}/M_{org}, ST_{rt}/ST_{org}, $\delta_{y\text{-}rt}/\delta_{y\text{-}org}$, and $\delta_{max\text{-}rt}/\delta_{max\text{-}org}$. Descriptive statistics of the used data are presented in **Table 4-3**. Analysis of the data starts with investigating the correlation between each pair of the variables and noting the highly correlated pairs and their signs. Correlation matrix is determined using the STATA software V.12 (STATA 2018) and is shown in **Table 4-4**.

Table 4-3: Descriptive statistics of the used data

Variable	Number of Observations	Mean	Standard Deviation	Minimum value	Maximum value
L_{SMAs}/L	700	0.3942	0.3056	0.0500	1.0000
A_{SMAs}/A_s	700	3.0714	1.8993	0.5000	6.0000
Load level (δ_y)	700	5.0000	2.8305	1.0000	9.0000
δ_r/δ_{max} **(%)**	700	22.1472	30.0816	0.0246	93.3457
M_{rt}/M_{org} **(%)**	700	301.4610	162.5948	40.0022	622.2005
ST_{rt}/ST_{org} **(%)**	700	264.9297	200.8122	9.5681	899.7625
$\delta_{y\text{-}rt}/\delta_{y\text{-}org}$ **(%)**	700	58.1500	39.4430	1.0000	127.0000
$\delta_{max\text{-}rt}/\delta_{max\text{-}org}$ **(%)**	700	280.9829	193.6878	1.0000	622.0000

Table 4-4: Correlation coefficients between all variables

	L_{SMA}/L	A_{SMA}/A_s	Load level	δ_r/δ_{max}	M_{rt}/M_{org}	ST_{rt}/ST_{org}	$\delta_{y\text{-}rt}/\delta_{y\text{-}org}$	$\delta_{max\text{-}rt}/\delta_{max\text{-}org}$
L_{SMA}/L	1.00							
A_{SMA}/A_s	0.00	1.00						
Load level	0.00	0.00	1.00					
δ_r/δ_{max}	0.08	-0.43	0.13	1.00				
M_{rt}/M_{org}	0.00	0.96	0.11	-0.22	1.00			
ST_{rt}/ST_{org}	-0.63	0.55	0.00	-0.08	0.61	1.00		
$\delta_{y\text{-}rt}/\delta_{y\text{-}org}$	-0.20	-0.16	0.00	0.08	-0.15	-0.24	1.00	
$\delta_{max\text{-}rt}/\delta_{max\text{-}org}$	-0.05	-0.29	0.01	0.08	-0.30	-0.50	0.74	1.00

Table 4-5 to **Table 4-9** present the final regression models for the five outputs. These models are the most statistically significant models. All the variable coefficients reported in these tables are statistically significant from zero at 95% confidence level because the associated p-values of all the coefficients are less than 0.05. Measures of model goodness-of-fit (represented by *R-squared*, *Adj R-squared,* and *Root Mean Square Error (MSE)*) are also reported in each table. All the reported models are considered to be with very good fit as their *R-squared* values vary from 0.67 to 0.99. Furthermore, the values of MSE range from 0.24 to 9.60 confirming also a very good model fit (Montgomery et al. 2012).

Equations [4-1] to **[4-5]** represent the summary of the final regression models for the five outputs.

$$\delta_r/\delta_{max} = -0.14318 \times A_{SMAs}/A_s + 0.061737 \times (A_{SMAs}/A_s)^2 + 0.013083 \times (\text{Load level})^2 + 0.751673 \quad \textbf{[4-1]}$$

$$M_{rt}/M_{org} = 82.72809 \times (A_{SMAs}/A_s) + 5.773622 \times (\text{Load level}) - 23.0628 \quad \textbf{[4-2]}$$

$$\ln(ST_{rt}/ST_{org}) = -0.71767 \times \ln(L_{SMAs}/L) + 0.88563 \times \ln(A_{SMAs}/A_s) + 3.210665 \quad \textbf{[4-3]}$$

$$\ln(\delta_{y\text{-}rt}/\delta_{y\text{-}org}) = 8.336842 \times (L_{SMAs}/L) - 11.2 \times (L_{SMAs}/L)^2 + 0.408727 \times (A_{SMAs}/A_s) - 0.06615 \times (A_{SMAs}/A_s)^2 + 2.603485 \quad \textbf{[4-4]}$$

$$\ln(\delta_{max\text{-}rt}/\delta_{max\text{-}org}) = 14.02687 \times (L_{SMAs}/L) - 17.2568 \times (L_{SMAs}/L)^2 - 0.14746 \times (A_{SMAs}/A_s) + 4.255832 \quad \textbf{[4-5]}$$

For example, if a simply supported beam is to be retrofitted using the suggested technique. If the amount of external SMA reinforcement is equal to the amount of internal steel reinforcement (A_{SMAs}/A_s = 1.0), the SMA bars covers only 20% of the span (L_{SMAs}/L = 0.20), and the beam is loaded to a displacement that is equal to six times the yielding displacement, then the amount of residual deformation of the retrofitted beam will be equal to 1.14% of the maximum applied displacement. The moment capacity of the retrofitted beam will be 94% of the original beam. The initial stiffness will be reduced by 21%. Yielding of the SMA bars will start at a displacement equal to 64% of the yielding displacement of the original beam.

Table 4-5: Regression model for δ_r/δ_{max}

Source	**SS**	**df**	**MS**	Number of obs	=	350
Model	141.1401	3	47.0467	F(3, 346)	=	243.48
				Prob > F	=	0
				R-squared	=	0.6786
Residual	66.85632	346	0.193226	Adj R-squared	=	0.6758
Total	207.9964	349	0.595978	Root MSE	=	0.43958

δ_r/δ_{max}	**Coef.**	**Std. Err.**	**t**	**P>t**	**[95% Conf. Interval]**	
A_{SMAs}/A_s	-0.14318	0.052947	-2.7	0.007	-0.24732	-0.03904
$(A_{SMAs}/A_s)^2$	0.061737	0.008069	7.65	0	0.045866	0.077608
(Load level)^2	0.013083	0.000808	16.18	0	0.011493	0.014673
Constant	0.751673	0.074234	10.13	0	0.605666	0.89768

Table 4-6: Regression model for M_{rt}/M_{org}

Source	SS	df	MS			
Model	8721587	2	4360793	Number of obs	=	350
				F(2, 347)	=	47192.31
				Prob > F	=	0
				R-squared	=	0.9963
Residual	32064.44	347	92.40474	Adj R-squared	=	0.9963
Total	8753651	349	25082.1	Root MSE	=	9.6127

M_{rt}/M_{org}	Coef.	Std. Err.	t	P>t	[95% Conf.	Interval]
A_{SMAs}/A_s	82.72809	0.270732	305.57	0	82.19561	83.26057
Load level	5.773622	0.181664	31.78	0	5.416322	6.130923
Constant	-23.0628	1.334355	-17.28	0	-25.6872	-20.4384

Table 4-7: Regression model for ST_{rt}/ST_{org}

Source	SS	df	MS			
Model	349.8711	2	174.9356	Number of obs	=	350
				F(2, 347)	=	2911.59
				Prob > F	=	0
				R-squared	=	0.9438
Residual	20.84864	347	0.060083	Adj R-squared	=	0.9434
Total	370.7198	349	1.062234	Root MSE	=	0.24512

$\ln(ST_{rt}/ST_{org})$	Coef.	Std. Err.	t	P>t	[95% Conf.	Interval]
$\ln(L_{SMAs}/L)$	-0.71767	0.01408	-50.97	0	-0.74536	-0.68997
$\ln(A_{SMAs}/A_s)$	0.88563	0.015595	56.79	0	0.854957	0.916303
Constant	3.210665	0.02609	123.06	0	3.159351	3.261978

Table 4-8: Regression model for $\delta_{y\text{-}rt}/\delta_{y\text{-}org}$

Source	SS	df	MS			
				Number of obs	=	350
Model	529.6073	4	132.4018	F(4, 345)	=	231.82
				Prob > F	=	0
				R-squared	=	0.7288
Residual	197.0443	345	0.571143	Adj R-squared	=	0.7257
Total	726.6516	349	2.082096	Root MSE	=	0.75574

$\ln(\delta_{y\text{-}rt}/\delta_{y\text{-}org})$	Coef.	Std. Err.	t	P>t	[95% Conf.	Interval]
L_{SMAs}/L	8.336842	0.527699	15.8	0	7.298929	9.374754
$(L_{SMAs}/L)^2$	-11.2	0.51597	-21.71	0	-12.2148	-10.1851
A_{SMAs}/A_s	0.408727	0.09103	4.49	0	0.229683	0.58777
$(A_{SMAs}/A_s)^2$	-0.06615	0.013873	-4.77	0	-0.09343	-0.03886
Constant	2.603485	0.149139	17.46	0	2.310149	2.896821

Table 4-9: Regression model for $\delta_{max\text{-}rt}/\delta_{max\text{-}org}$

Source	SS	df	MS			
				Number of obs	=	350
Model	971.7832	3	323.9277	F(3, 346)	=	572.24
				Prob > F	=	0
				R-squared	=	0.8323
Residual	195.8593	346	0.566067	Adj R-squared	=	0.8308
Total	1167.643	349	3.345681	Root MSE	=	0.75237

$\ln(\delta_{max\text{-}rt}/\delta_{max\text{-}org})$	Coef.	Std. Err.	t	P>t	[95% Conf.	Interval]
L_{SMAs}/L	14.02687	0.525349	26.7	0	12.99359	15.06015
$(L_{SMAs}/L)^2$	-17.2568	0.513672	-33.59	0	-18.2671	-16.2465
A_{SMAs}/A_s	-0.14746	0.02119	-6.96	0	-0.18914	-0.10578
Constant	4.255832	0.117638	36.18	0	4.024456	4.487209

4.11 CONCLUSIONS

The use of external unbonded SMA bars to retrofit RC beams is investigated in this study. A FE model is first developed to simulate the behaviour of the retrofitted beams and validated using available experimental results. Experimental results included RC beams that are internally and externally reinforced using SMA and steel bars. Good agreement between experimental and analytical results is observed. A simplified method is then developed to capture the flexure behaviour of the retrofitted beams. The method is based on the sectional analysis technique for unbonded bars. Results obtained from the developed program/method are validated using FE results.

An extensive parametric study is then carried out to investigate the flexural behaviour of RC beams retrofitted using SMA bars. Effect of varying three different parameters is studied. These parameters are: A_{SMA}/A_s, load level (δ_{max}/δ_y), and L_{SMA}/L. For each of the studied parameters, the load-displacement relationship is constructed using the moment-area method. Out of the different load-displacement relationships, δ_r/δ_{max}, M_{rt}/M_{org}, ST_{rt}/ST_{org}, $\delta_{y\text{-}rt}/\delta_{y\text{-}org}$, and $\delta_{max\text{-}rt}/\delta_{max\text{-}org}$ are used to highlight the changes happening in the behaviour due to varying one of the parameters.

Results of the parametric study are then used in multiple linear regression analysis. Numerous number of models are first developed for the five outputs. Best five models for the five outputs are then reported. The five models are summarized in the form of simple equations to help engineers decide the optimum amount and length of needed SMA bars.

4.12 REFERENCES

ABAQUS, F.E. A. (2018) "ABAQUS Analysis user's manual." Dassault Systemes,Vélizy Villacoublay, France.

Alam, M.S., Youssef, M.A., and Nehdi, M. (2007). "Utilizing Shape Memory Alloys to Enhance the Performance and Safety of Civil Infrastructure: a Review." Canadian Journal of Civil Engineering, 34(9), 1075-1086.

Deshpande, N., Londhe, S., and Kulkarni, S. (2014). "Modeling compressive strength of recycled aggregate concrete by Artificial Neural Network, Model Tree and Non-linear Regression." International Journal of Sustainable Built Environment, 3(2), 198-198.

Dunlop, P, and Simon, S. (2003) "Estimating key characteristics of the concrete delivery and placement process using linear regression analysis." Journal of Civil Engineering and Environmental Systems, 20(4), 273-290.

Elbahy Y.I., Nehdi M., Youssef M.A. (2010b). "Artificial Neural Network Model for Deflection Analysis of Superelastic Shape Memory Alloy Reinforced Concrete Beams." Canadian Journal of Civil Engineering, 37(6), 855-865.

Elbahy Y.I., Youssef M.A., Nehdi M. (2009). "Stress Block Parameters for Concrete Flexural Members Reinforced with Superelastic Shape Memory Alloys." Journal of Materials and Structures, 42(10), 1335-1351.

Elbahy Y.I., Youssef M.A., Nehdi M. (2010a). "Deflection of Superelastic Shape Memeory Alloy Renforced Concrete Beams: Assessment of Existing Models." Canadian Journal of Civil Engineering, 37(6), 842-854.

Elbahy, Y.I., Youssef, M.A., Nehdi, M. (2008). "Flexural Behaviour of Concrete Memebers Reinforced with Shape Memory Alloys." 2nd Canadian Conference on Effective Design of Structures, McMaster University, Hamilton, Ontario, Canada, 477-486.

Janke, L., Czaderski, C., Motavalli, M., and Ruth, J. (2005). "Applications of Shape Memory Alloys in Civil Engineering Structures - Overview, Limits and New Ideas." Materials and Structures, 338(279), 578-592.

Karsan, I. D., and Jirsa, J. O. (1969). "Behavior of Concrete under Compressive Loading." ASCE Journal (Structural Division), 95(12), 2543-2563.

Montgomery, D. C., Peck, E. A., and Vining, G. G. (2012). "Introduction to linear regression analysis." John Wiley & Sons, Vol. 821.

Saiidi,M.S., Sadrossadat-Zadeh, M., Ayoub,C., and Itani,A. (2007). "Pilot study of behavior of concrete beams reinforced with shape memory alloys." Journal of Materials in Civil engineering, American Society of Civil Engineering, 19(6): 454-461.

Scott, B.D.; Park, R.; and Priestley, M.J.N. (1982). "Stress-Strain Behavior of Concrete Confined by Overlapping Hoops at Low and High Strain Rates." ACI journal, 79(1), 13-27.

Stevens, N.J., Uzumeri, S.M., and Collins, M.P. (1987). "Analytical Modeling of Reinforced Concrete Subjected to Monotonic and Reversed Loading." Publication No. 87-1, University of Toronto, 3634 p.

Youssef, M., and Ghobarah, A. (1999). "Strength Deterioration due to Bond Slip and Concrete Crushing in Modeling of Reinforced Concrete Members." ACI Structural Journal, 96(6), 956-967.

Youssef, M.A., and Rahman, M. (2007). "Simplified seismic modeling of reinforced concrete flexural members." Magazine of Concrete Research, 59(9), 639-649.

Chapter 5 Flexural Behaviour of Reinforced Concrete Joints Retrofitted Using External Superelastic Shape Memory Alloy Bars

5.1 INTRODUCTION

It is acceptable to assume that pre-1970s Reinforced Concrete (RC) structures are deficient under seismic loads. These structures are not designed for ductile behaviour. Insufficient anchorage of the beam reinforcement into the beam-column joint (BCJ) can be considered a main deficiency for these structures. Thus, there is an urgent need to retrofit these structures to ensure safety of the occupants.

Newly built structures may also need to be retrofitted to accommodate changes in their use or loading. Different retrofitting materials and techniques are suggested in the literature to retrofit RC BCJs such as: (i) epoxy repairs (Mohle and Mahin 1991, French et al. 1990, Beres et al. 1992, Filiatrault and Lebrub 1996); (ii) concrete jackets (Corazao and Durrani 1989, Alcocer and Jirsa 1993); (iii) reinforced masonary blocks (Bracci et al. 1995); (iv) steel jackets and steel elements (Corazao and Durrani 1989, Ghobarah et al. 1997, Biddah et al. 1997); and (v) fibre reinforced polymers (FRP) (Antonopoulous and Triantafillou 2002, Ghobarah and Said 2002, Gergely et al. 1998, karayannis and Sirjelis 2002, clyde and Pantelides 2002). Although steel is a commonly used material, it has a major disadvantage, which is the large permanent seismic deformations.

Superelastic Shape Memory Alloys (SMAs) can undergo large strains and return to their undeformed shape upon unloading. The flaged shape stress-strain hysteresis gives them some damping ability, **Fig. 5-1**. Also, SMAs have excellent fatigue properties and high corrosion resistance. All of these unique properties make them potential candidate for retrofitting RC BCJs (Janke et al. 2005, Alam et al. 2007).

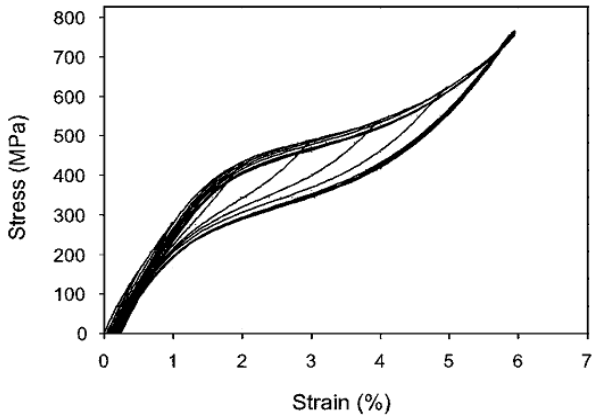

Fig. 5-1: Stress-strain relationships for an SMA bar (McCormick et al., 2006)

In this study, the applicability of retrofitting RC BCJs using external unbonded SMA bars is investigated. First, a Finite Element (FE) model is developed and validated using available experimental results. Then, a simplified model is suggested and validated using the FE model. An extensive parametric study is then carried out to investigate the behaviour of retrofitted RC BCJs. Results of the parametric study are used to develop equations that address the change in the behaviour of the retrofitted BCJs.

5.2 FINITE ELEMENT SIMULATION

Three-dimensional FE models are developed to investigate the behaviour of RC BCJs retrofitted using external SMA bars during the loading/unloading stages. Analysis is performed using the commercial FE program ABAQUS Version 6.9 (ABAQUS 2018). 8-node hexahedral isoparametric linear solid elements with reduced integration (C3D8R) are used in the modelling process of the concrete, internal and external reinforcement, and external angles. Different element sizes are first considered to determine the appropriate mesh size.

5.3 EXPERIMENTAL VALIDATION

Results of the experimental work performed by Youssef et al. (2008) are used to validate the accuracy of the developed FE model. Two large scale BCJs are constructed and tested under reversed-cyclic loading. The two joints are identical in dimensions and reinforcement details except the type of reinforcement. In the plastic hinge region, one joint (BCJ1) is reinforced with regular steel bars, while the second (BCJ2) is reinforced with superelastic SMA bars.

As shown in **Fig. 5-2**, the beams of the two joints have a length of 1830 mm, 400 mm cross-section height, and 250 mm cross-section width. Amounts and arrangements of transverse reinforcement are also identical for the two beams. Stirrups are 10M in diameter and are spaced at 80 mm for the 800 mm length adjacent to the column and spaced at 120 mm elsewhere. The longitudinal top and bottom steel for the beam of BCJ1 is 2-20M. For BCJ2, Two superelastic SMAs bars (20.6 mm diameter) are used to replace the top and bottom steel bars at the plastic

hinge region. Regular 2-20M steel bars are used outside the plastic hinge region of BCJ2 beam. Steel couplers are used to connect the SMA bars to the steel bars.

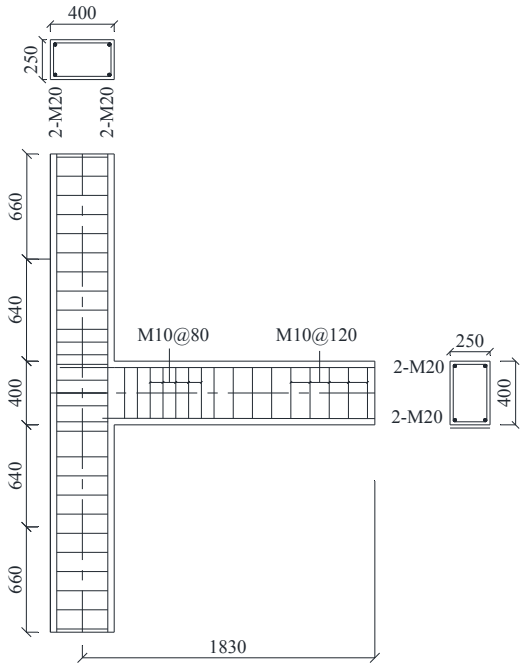

Fig. 5-2: Details of the two BCJs tested by Youssef et al. (2008)

Average concrete compressive strength is 53.50 MPa for BCJ1 and 53.70 MPa for BCJ2. Average split cylinder tensile strength is 3.50 MPa for BCJ1 and 2.80 MPa for BCJ2. Steel Reinforcing bars of BCJ1 have yield strength of 520 MPa, ultimate strength of 653 MPa, and a modulus of elasticity of 198 GPa. Steel reinforcing bars of BCJ2 have yield strength of 450 MPa, ultimate strength 650 MPa, and a modulus of elasticity of 193 GPa. Stirrups have a yield strength of 422 MPa and ultimate strength of 682 MPa.

Youssef et al. (2008) determined the mechanical properties of the superelastic SMA bars by experimentally testing them under cyclic loading. It is reported that the SMA bars critical stress is 401 MPa at a critical strain of 0.75%. The modulus of elasticity is evaluated as 62.5 GPa. The residual strain is determined as 0.73%, when the SMA bar was loaded up to 6.0% strain.

Different element sizes (46.88, 39.07, 31.25, 25.40 and 19.05 mm) are first considered to determine the appropriate mesh size for the two BCJs. As shown in **Fig. 5-3**, element size of 25.4 mm gives good results and further refinement of the mesh does not noticeably change the behaviour. As shown in **Fig. 5-4**, good agreement between the experimental and analytical results can be observed for the two BCJs.

The work done by Saiidi et al. (2007) is used to validate the model accuracy in predicting the behaviour of RC beams externally reinforced with steel or SMA bars. Saiidi et al. (2007) tested eight reinforced concrete beams under quasi-static loading. The eight beams are different in the type and amount of reinforcement at the mid-span as summarized in **Table 5-1**. Four beams are reinforced with SMA bars at mid-span, while the other four are reinforced with conventional steel bars.

The beams are 1530 mm long. They have cross-sectional dimensions of 127x152 mm at mid-span and 127x305 mm at the ends (i.e. outer-sections), **Fig. 5-5**. The beams are tested under two point symmetric loads that are placed 152 mm apart. The reinforcement at mid-span is attached to the beam using external angles. The internal reinforcement is cut at the mid-span section to ensure that the behaviour is controlled by the external reinforcement.

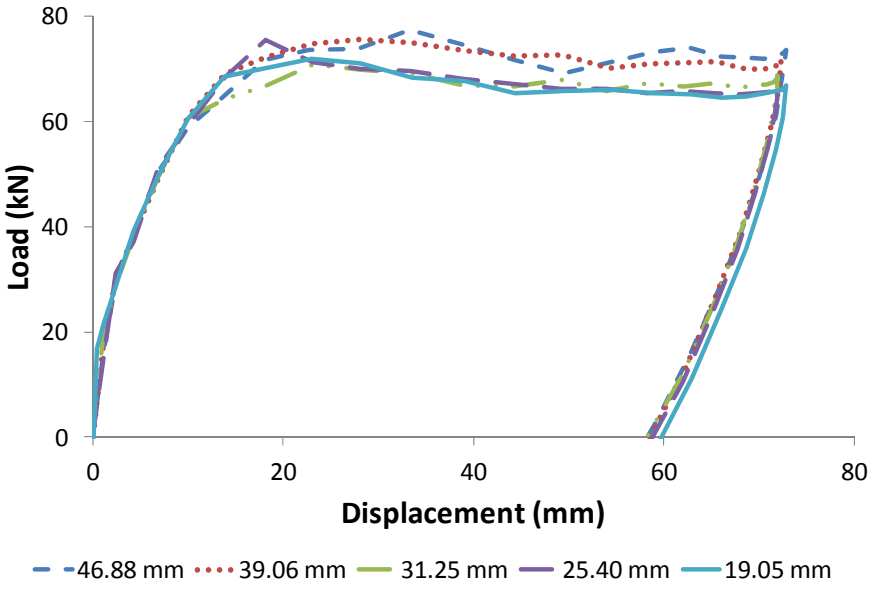

(a) BCJ1

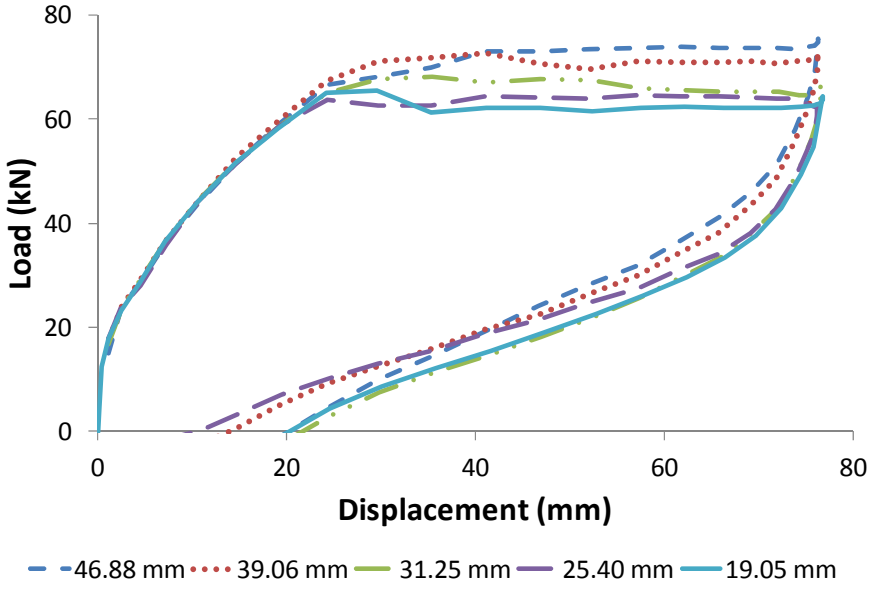

(b) BCJ2

Fig. 5-3: Mesh sensitivity analysis for the FE analysis of the BCJ; (a) BCJ1; and (b) BCJ2

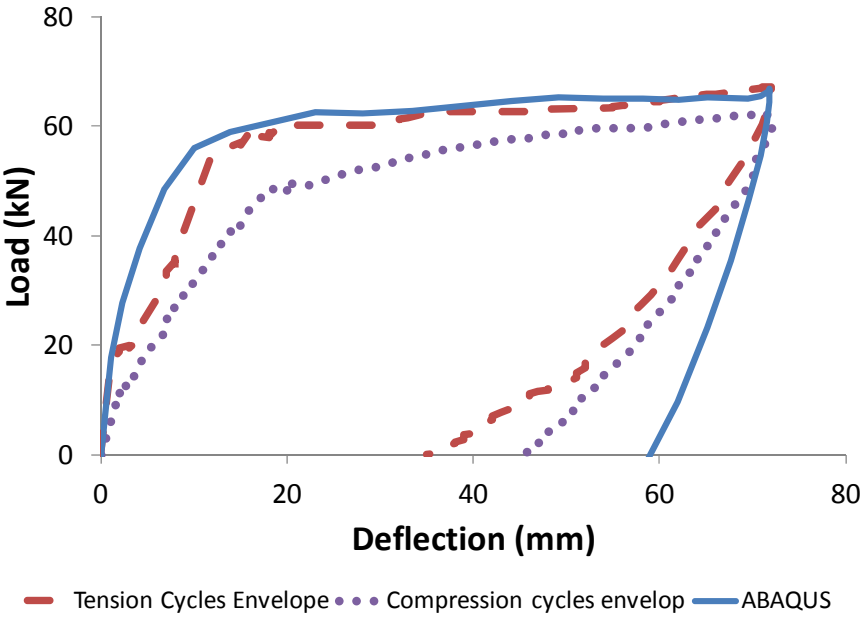

(a) BCJ1

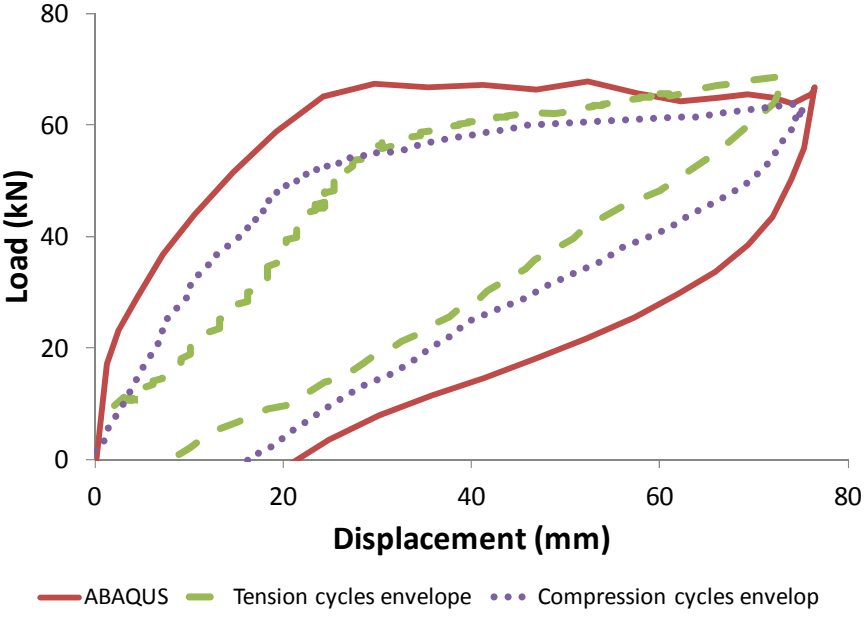

(b) BCJ2

Fig. 5-4: Experimental vs. FE load-displacement results for the BCJs tested by Youssef et al. (2008); (a) BCJ1; and (b) BCJ2

Table 5-1: Properties of the beams tested by Saiidi et al. (2007)

Specimen	Mid-span reinforcement	ε_y (mm/mm)	f_y (MPa)	E_y (MPa)
BNL1	1 Φ 6.40 mm	0.013	400	34,078
BNL2	2 Φ 6.40 mm	0.013	400	34,078
BNH1	1 Φ 9.50 mm	0.013	510	39,245
BNH2	2 Φ 9.50 mm	0.013	510	39,245
BSL1	1 Φ 9.53 mm	0.0021	440	209,524
BSL2	2 Φ 9.53 mm	0.0021	440	209,524
BSH1	1 Φ 12.70 mm	0.0009	420	466,667
BSH2	2 Φ 12.70 mm	0.0009	420	466,667

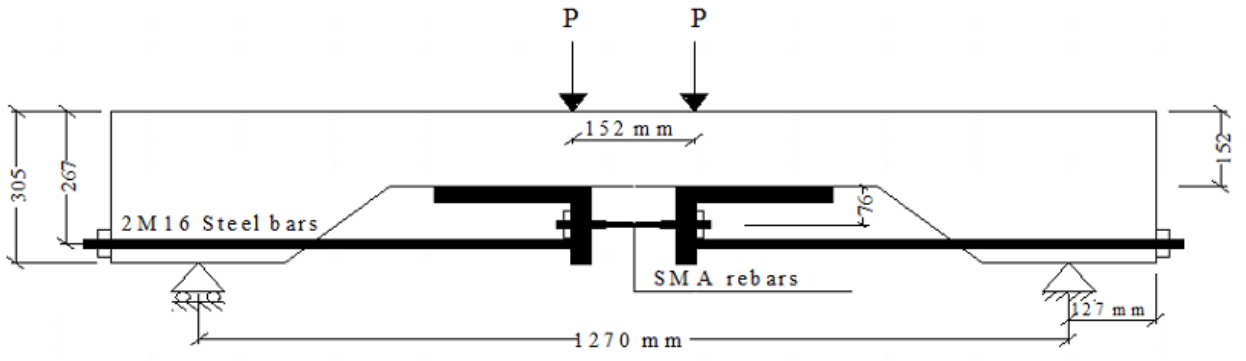

Fig. 5-5: Beams dimensions and test setup

Mesh sensitivity analysis is performed to determine the appropriate element size. As shown in **Fig. 5-6**, four element sizes are used in the analysis. It is found that reducing the element size beyond the 25.4 mm has negligible effect on the predicted results. Results of the analysis are plotted in **Fig. 5-7** for the SMA RC beams and in **Fig. 5-8** for the steel RC beams. As shown in the figures, good agreement between the experimental and analytical results is observed for both steel and SMA RC beams.

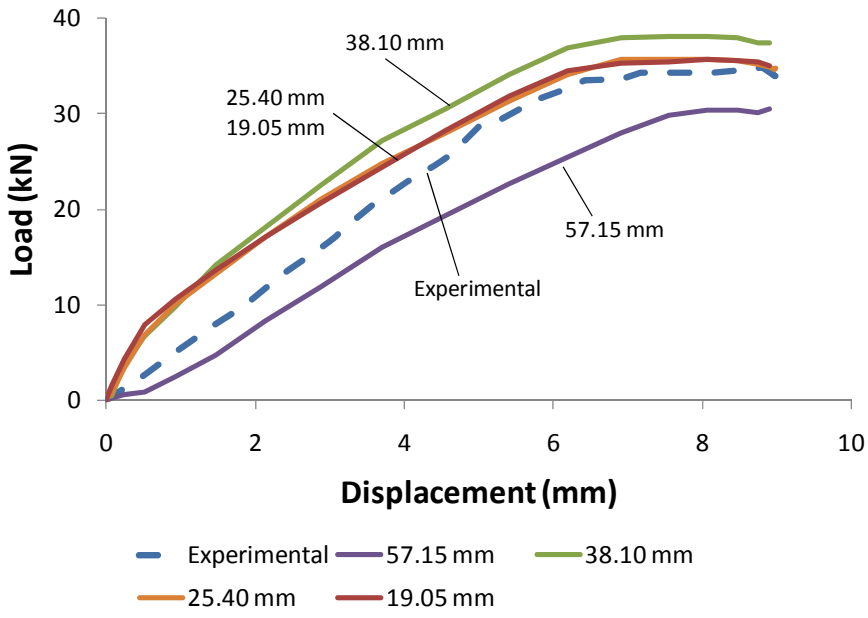

Fig. 5-6: Mesh sensitivity analysis for beam BNH1

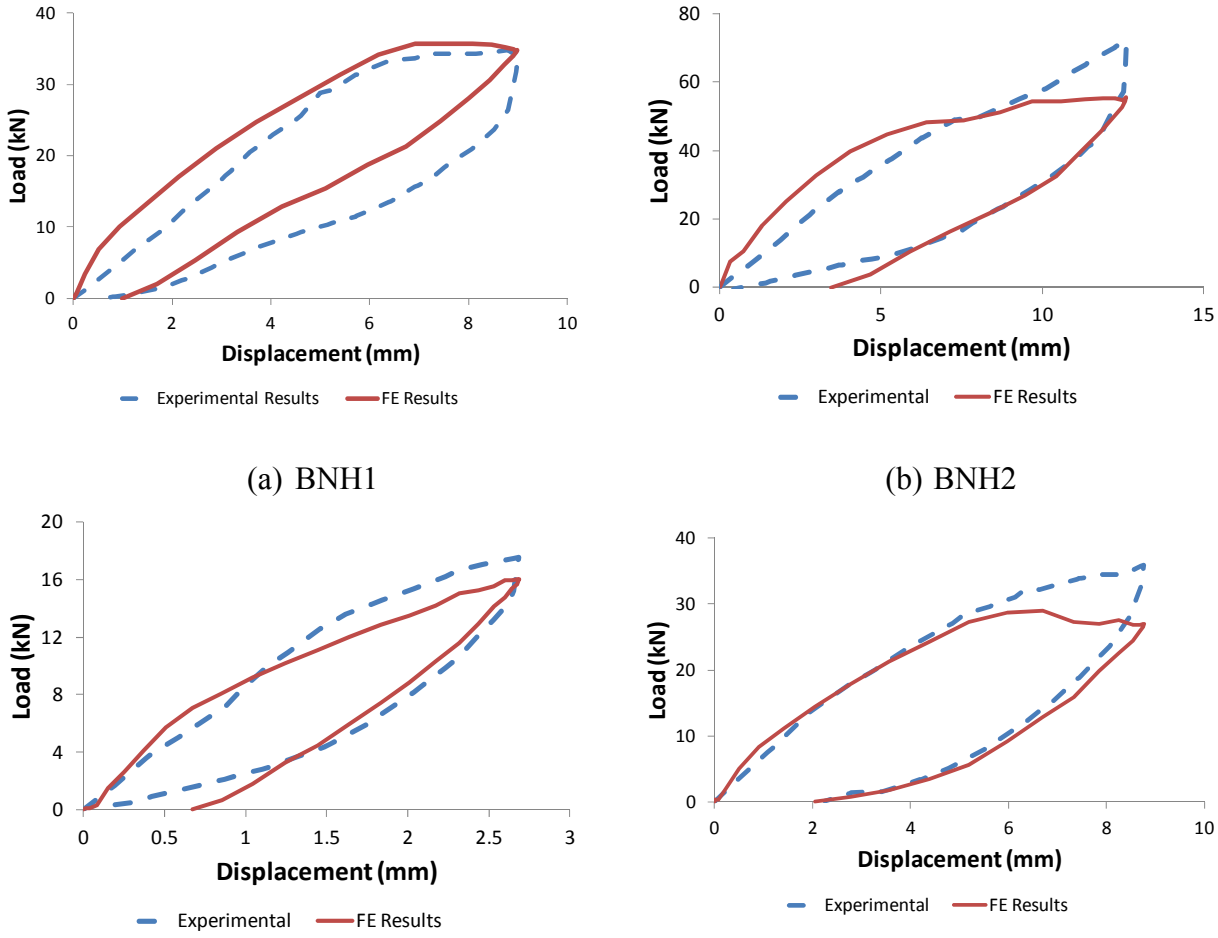

Fig. 5-7: Experimental vs. analytical results for SMA RC beams; (a) BNH1; (b) BNH2; (c) BNL1; and (d) BNL2

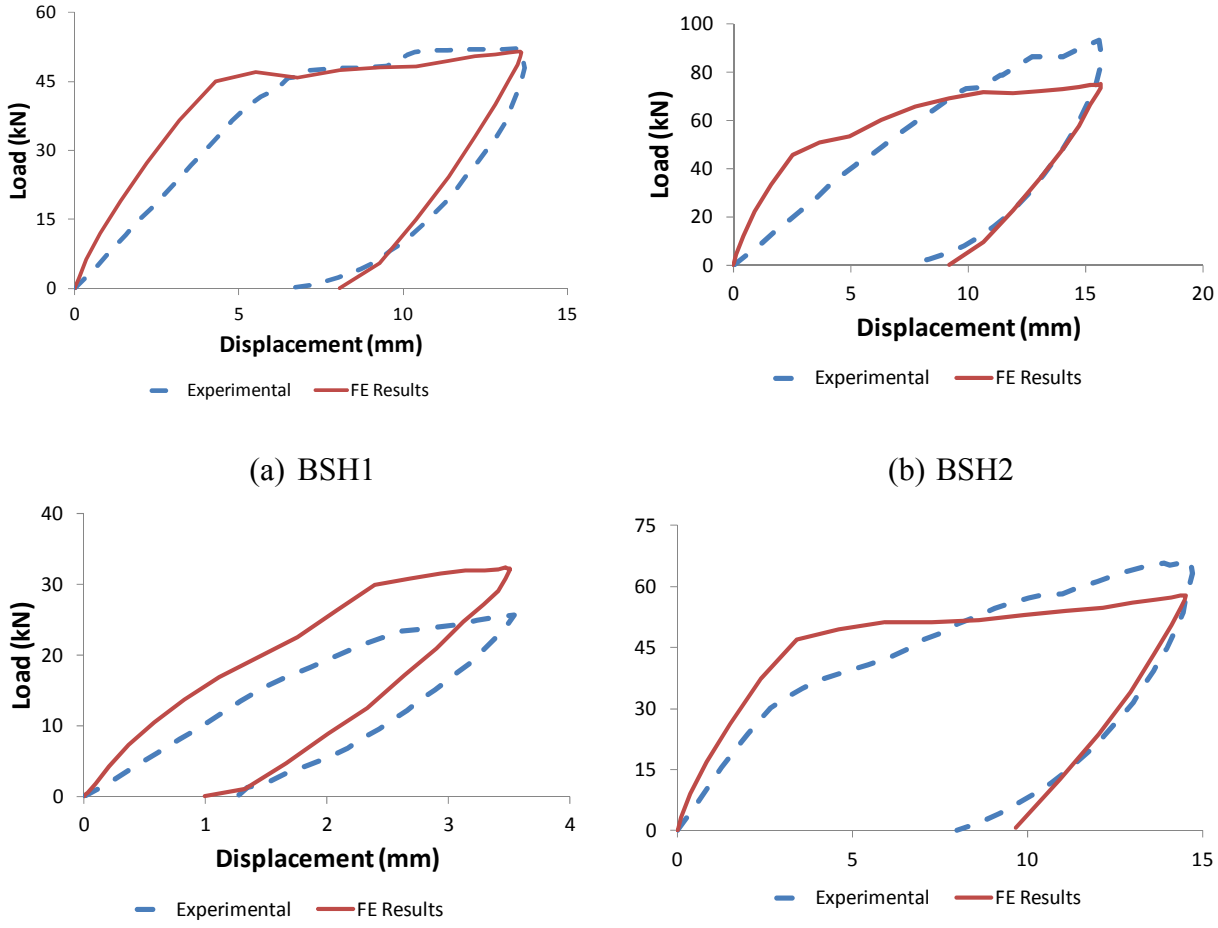

Fig. 5-8: Experimental vs. analytical results for steel RC beams; (a) BSH1; (b) BSH2; (c) BSL1; and (d) BSL2

5.4 PROPOSED RETROFITTING TECHNIQUE

The proposed retrofitting technique is based on attaching external SMA bars to the RC BCJ. As shown in **Fig. 5-9**, the bars are attached to the BCJ using external steel angles. The steel angles are attached to the BCJ using steel bolts. One angle is attached to the BCJ joint area, while the second angle is attached to the beam. Hold down angles can be used for big lengths of the SMA bars to enforce the bars to follow the beam deflection.

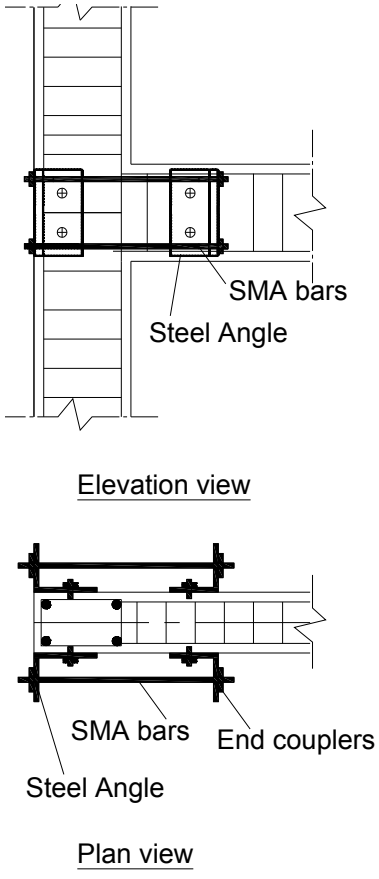

Fig. 5-9: Proposed retrofitting technique

5.5 RETROFITTED BCJ

A RC BCJ is assumed for the analysis in this section. The beam of the BCJ has a cross-section of 250x400 mm and a span of 1830 mm. The column has similar cross-section dimensions and is 1200 mm in height. The BCJ is supported using top and bottom plates representing roller and hinge supports, respectively. The plates have dimensions equal to 250x400x100.The external angles have dimensions of 90x90x20 mm and are attached to the BCJ using 8 bolts. The bolts are assumed to be 71 mm in length and 12.7 mm in diameter. The external SMA bars are attached to the external angles using end couplers. The added external SMA bars are equal to the internal steel reinforcement.

FE analysis is performed for the retrofitted BCJ. **Fig. 5-10** shows a sketch of the retrofitted BCJ while **Fig. 5-11** shows the FE model of the retrofitted BCJ. **Fig. 5-12** shows the load-displacement relationship of the retrofitted BCJ vs. the original BCJ. The maximum moment capacity of the beam increased from 70 kN to 85 kN due to retrofitting. The initial stiffness of the beam is almost not affected by retrofitting. The amount of residual displacement is reduced from 72 mm to 60 mm. Amount of dissipated energy is increased.

It is clear from the figure that adding external SMA bars reduced the amount of residual displacement by 17%. This small effect is attributed to the low modulus of elasticity for the SMA bars that is much lower (1/5 to 1/3) than that of the regular steel. Thus, attaching a small to moderate ratio of SMA will improve the strength of the BCJ, but it is not expected to reduce the residual deformations. Thus, it is proposed to cut the internal steel bars of the beam at the face of

the column and replace them with the external SMA bars. This ensures that the BCJ behaviour is governed by the external SMA bars rather than the internal steel bars.

FE analysis is performed again for the BCJ assuming cutting the internal steel reinforcement. Analysis of the results is illustrated in **Fig. 5-13**. As shown in the figure, significant reduction in the amount of residual displacement (98%) is observed in this case. On the other hand, the total moment capacity of the beam is reduced by 31% due to the cut of the internal steel bars. Initial stiffness of the beam is also significantly reduced. These disadvantages can be overcome by increasing the amount of the external SMA bars as will be investigated in the following sections.

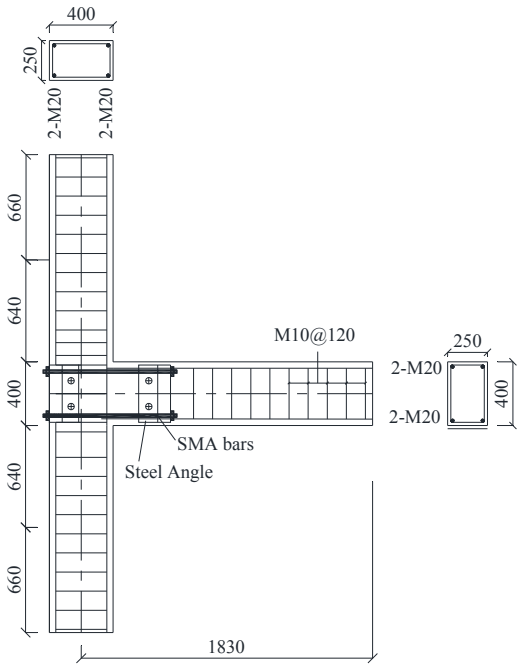

Fig. 5-10: sketch of the retrofitted BCJ

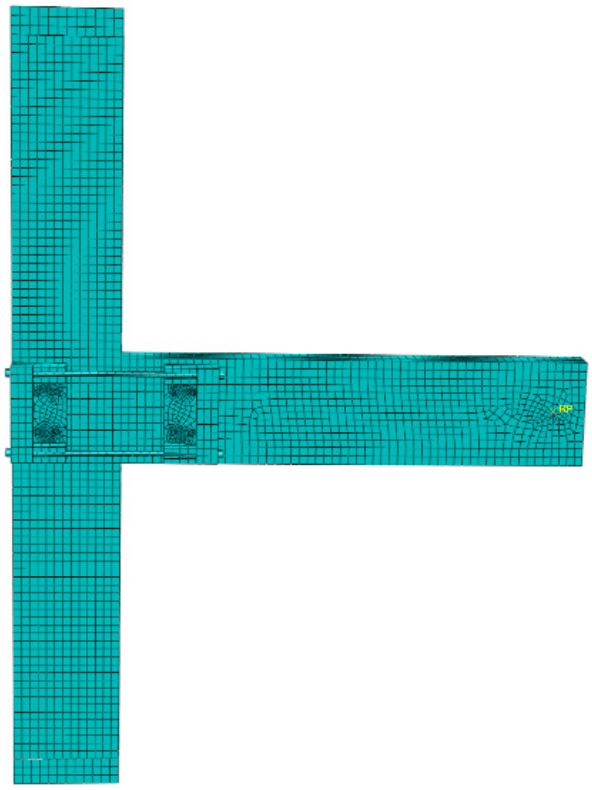

Fig. 5-11: FE Model of the retrofitted BCJ

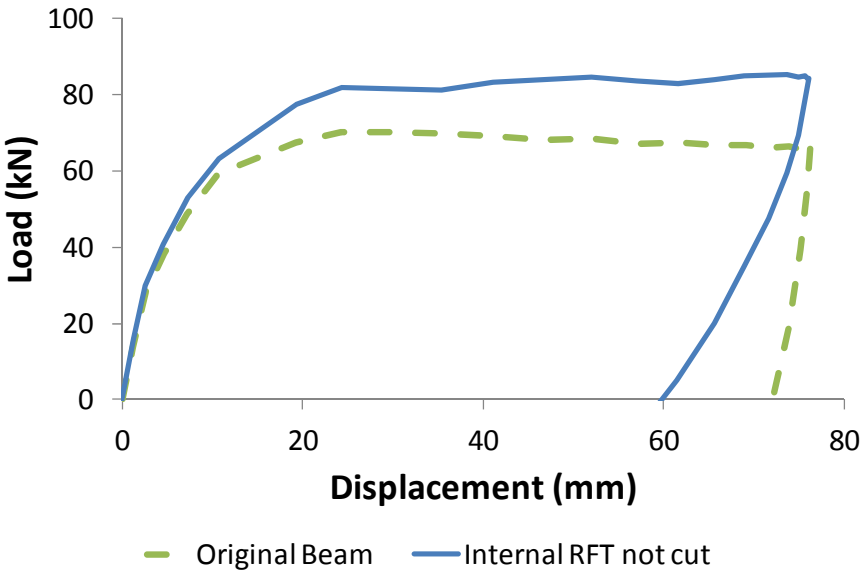

Fig. 5-12: FE load-displacement relationship for the original BCJ vs. the retrofitted BCJ

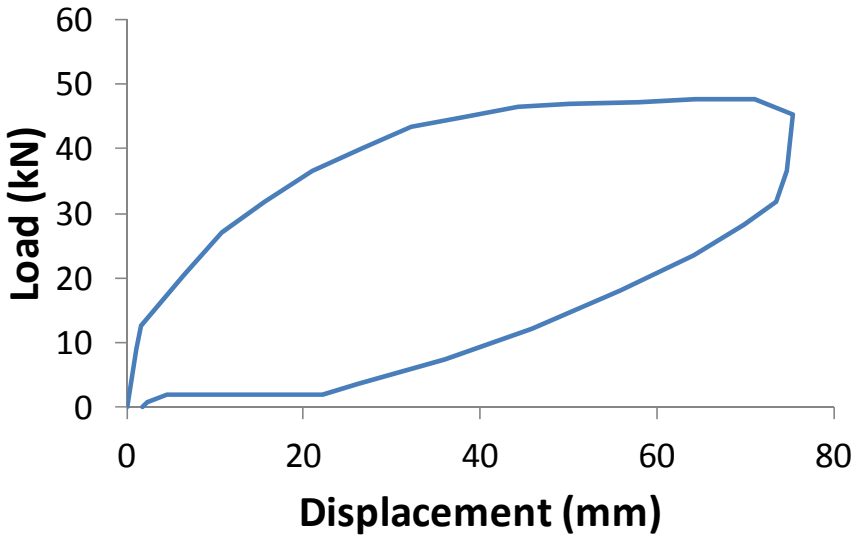

Fig. 5-13: FE load-displacement relationship for the original BCJ vs. the retrofitted BCJ with internal steel bars are cut

5.6 SIMPLIFIED MODEL

Modelling the retrofitted BCJ using ABAQUS is a complex process. Thus, a simplified model for the retrofitted BCJ is proposed in this section. The simplified model is developed using Seismostruct software v.6 (Seismostruct 2018). The special technique used to model the connection include: (i) modelling the SMA bars using inelastic truss elements; (ii) modelling the superelastic behaviour of the SMA bars using the uniaxial material model proposed by Auricchio and Sacco (1997); (iii) modelling the concrete beam and column using displacement based inelastic frame elements; and (iv) modelling the external angles that supports the SMA bars using rigid arms connected to the concrete beam and column.

As shown in **Fig. 5-14**, the beam and the column of the BCJ are modelled using frame elements. Two rigid arms are connected to the beam near the face of the column representing the angle supported in the joint area. Another two rigid arms are connected to the beam at a distance equal to the length of the required SMA bars. The SMA bars are connected between the rigid arms and are modelled using truss elements. The reinforcement in the beam element is cut in between the rigid arms to eliminate any contribution from it to the strength, stiffness and residual deformation of the joint.

To validate the assumed simplified model, a comparison between the load-displacement results of the simplified model developed using Seismostruct software and the actual model developed using ABAQUS is shown in **Fig. 5-15**. Very good agreement between the two results is achieved.

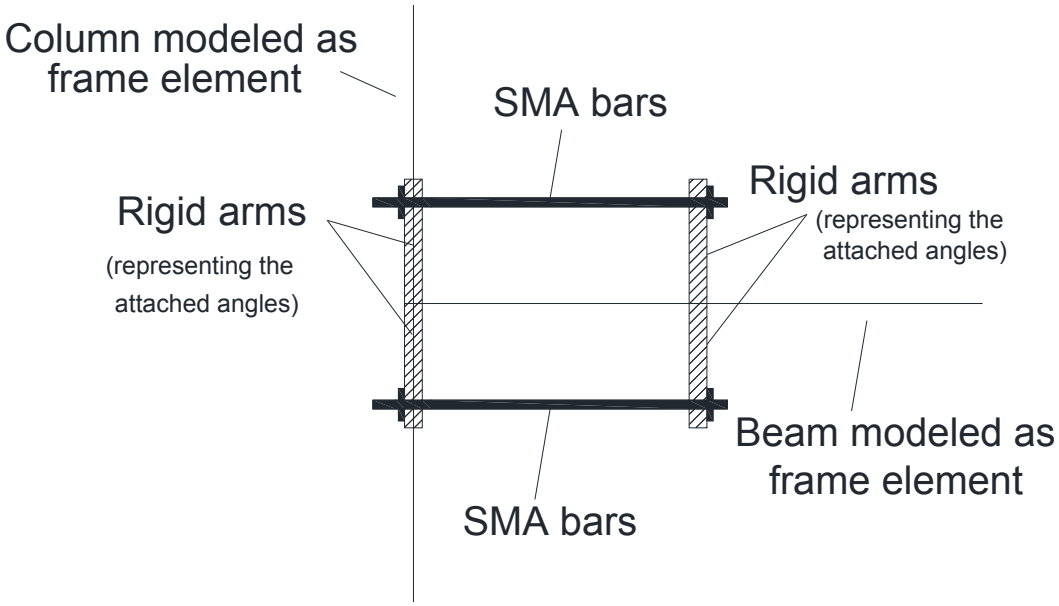

Fig. 5-14: Sketch of the simplified model

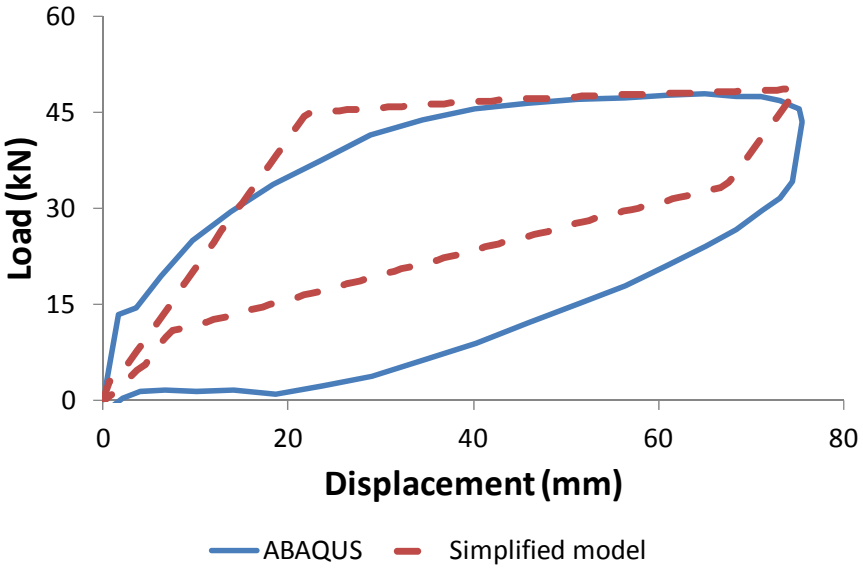

Fig. 5-15: Load-displacement results of the ABAQUS model vs. the simplified Seismostruct model

5.7 PARAMETRIC STUDY

A parametric study is carried out in this section to further investigate the behaviour of RC BCJs retrofitted using external SMA bars. The analysis is performed using the developed simplified model for both loading and unloading stages. Three different parameters are investigated in this study: (i) the ratio between the added external SMA reinforcement to the amount of internal steel reinforcement in the beam (A_{SMA}/A_s); (ii) ratio between the length of the used SMA bars to the length of the beam (L_{SMA}/L); and (iii) drift ratio (δ_{max}/L).

The parametric study is performed on BCJs with geometrical dimensions similar to that presented in the Finite Element Simulation section. The beams are loaded/unloaded using a point load applied at the cantilever tip. For each of the studied parameters, the parameter under investigation is varied within the desired range while keeping all other parameters constant during the analysis. Four different outputs are used to compare the results of the parametric study. These outputs are: (i) the ratio between the amount of residual displacement upon complete unloading (δ_r) and the maximum displacement applied to the beam tip (δ_{max}); (ii) the ratio between the maximum moment capacity of the retrofitted BCJ (M_{rt}) to the moment capacity of the original BCJ (M_{org}); (iii) the ratio between the secant stiffness of the retrofitted BCJ (ST_{rt}) to the secant stiffness of the original BCJ (ST_{org}); and (iv) the amount of dissipated energy by the retrofitted BCJ (EN_{rt}) to the amount of dissipated energy by the original BCJ (EN_{org}). Internal steel reinforcement is assumed to be cut in all of the studied BCJs. Detailed results of the parametric study are introduced in the following section.

5.8 RESULTS AND DISCUSSIONS

5.8.1 A_{SMAs}/A_s Parameter

Ten different A_{SMAs}/A_s ratios are used in the analysis. These ratios are: A_{SMA}/A_s = 0.5, 1.0, 1.5, 2.0, 2.5, 3.0, 3.5, 4.0, 4.5, and 5.0. The analysis is performed for nine SMA lengths ranging between 0.125L to 1.0L. Results of the analysis are plotted in **Fig. 5-16**.

The amount of residual displacement at complete unloading from the failure point is found to be negligible at small A_{SMAs}/A_s ratios. As the A_{SMAs}/A_s ratio increased from 2.0 to 3.0, the δ_r/δ_{max} ratio increased from 1.0% to almost 53% in case of L_{SMAs}/L = 0.125. For L_{SMAs}/L = 0.25, the increase in the amount of residual displacement (30%) occurred when the A_{SMAs}/A_s ratio increased from 3.0 to 3.5. This increase in the amount of residual displacements can be attributed to the change happening in the cross-section status from an under reinforced section to an over reinforced section. For L_{SMAs}/L = 0.50 and higher, the amount of residual displacement is kept minimum at δ_r/δ_{max} = 2.0%.

The moment capacity of the BCJ is found to increase with the increase in the A_{SMAs}/A_s ratio. The rate of increase significantly varies with the L_{SMAs}/L ratio. Higher rate of increase in case of L_{SMAs}/L = 0.125 and 0.25 is observed. For case of L_{SMAs}/L = 0.125, the increase occurred to M_{rt}/M_{org} ratio of almost 200%. Further increase in the A_{SMAs}/A_s ratio does not increase the moment capacity. This means that the failure in the BCJ is governed by the concrete crushing rather than the yielding of the SMA bars.

The initial stiffness of the BCJ is found to increase with the increase in the A_{SMAs}/A_s ratio for all L_{SMAs}/L ratios. However, the rate and amount of increase significantly varies with the length of the SMA bars. It can also be noted from the figure that the initial stiffness is smaller than that of the original BCJ except for small L_{SMAs}/L ratios (0.125 and 0.25).

Amount of dissipated energy is found to slightly increase with the increase in the A_{SMAs}/A_s ratio. For case of L_{SMAs}/L = 0.125 and 0.25, there is a sudden change in the amounts of dissipated energy at A_{SMAs}/A_s values ranging between 2.0 and 3.5. This sudden change is attributed to the mode of failure of the cross-section which changed from SMA bars yielding to concrete crushing.

5.8.2 L_{SMAs}/L Parameter

SMA bars length is represented by the ratio (L_{SMAs}/L), which is the ratio between the length of the used SMA bars to the total length of the beam. Nine different SMA bar lengths are assumed in the analysis. These lengths are: L_{SMAs}/L = 0.125, 0.167, 0.20, 0.25, 0.333, 0.50, 0.667, 0.75, and 1.0. Each length is analyzed at different A_{SMAs}/A_s ratios (A_{SMAs}/A_s = 0.50, 1.0, 1.5, 2.0, 2.5, 3.0, 3.5, 4.0, 4.5, and 5.0). Results of the analysis are presented in **Fig. 5-17**.

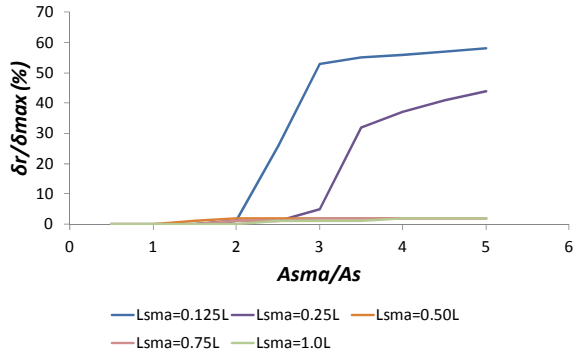

(a) Residual displacement

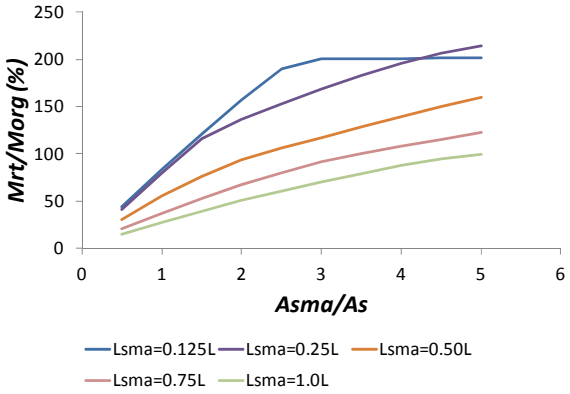

(b) Moment capacity

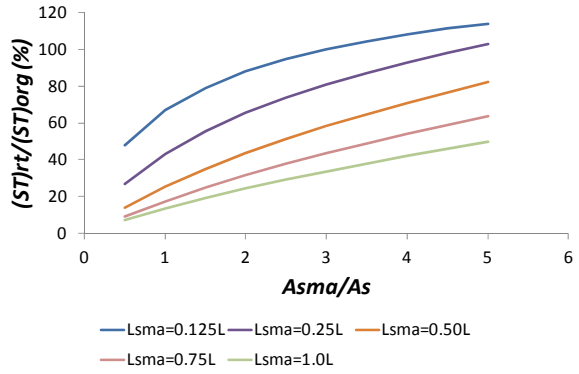

(c) Initial stiffness

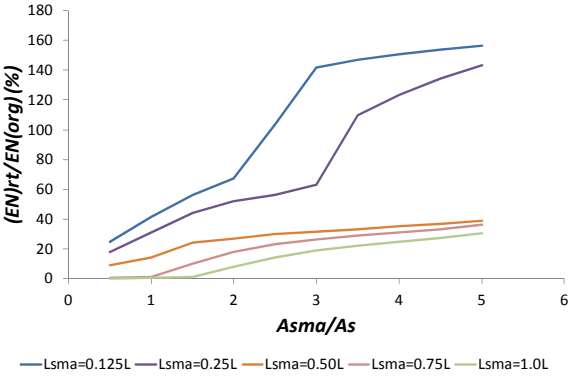

(d) Dissipated energy

Fig. 5-16: Effect of varying the A_{SMA}/A_s ratio on: (a) residual displacement; (b) moment capacity; (c) initial stiffness; and (d) dissipated energy.

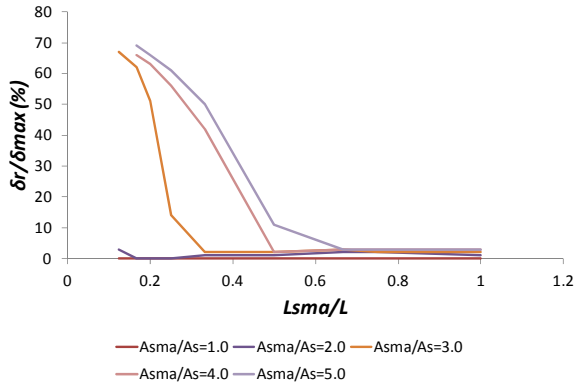

(a) Residual displacement

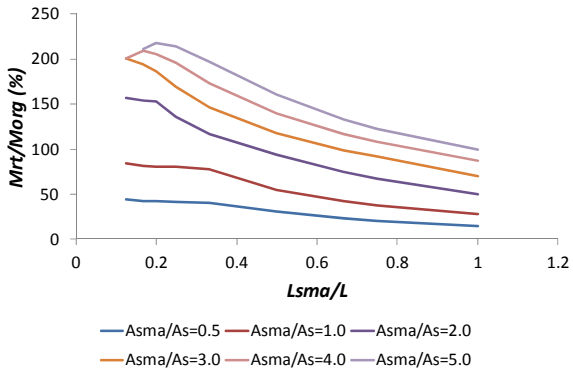

(b) Moment capacity

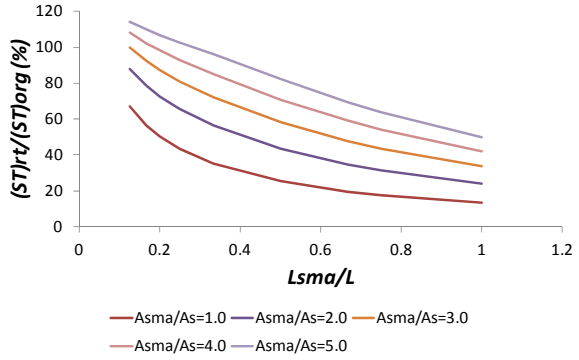

(c) Initial stiffness

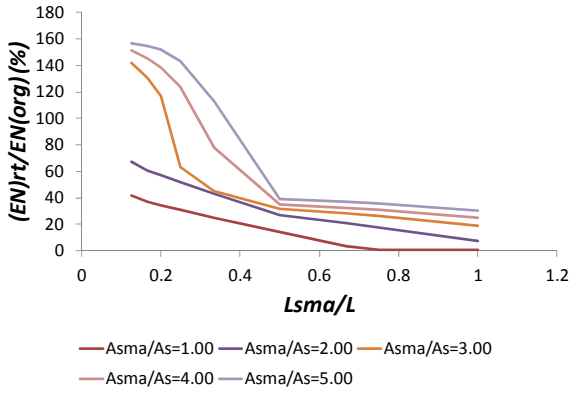

(d) Dissipated energy

Fig. 5-17: Effect of varying the L_{SMA}/L ratio on: (a) residual displacement; (b) moment capacity; (c) initial stiffness; and (d) dissipated energy.

Increasing the length of the SMA bars results in significant reduction in the amount of residual deformations. The ratio δ_r/δ_{max} reduced from 70% to 3% when the SMA bars length ratio increased from 0.125 to 0.333 in case of A_{SMAs}/A_s = 3.0. For A_{SMAs}/A_s = 1.0 and 2.0, almost no change in the amount of residual deformation is noted. The moment capacity of the retrofitted BCJs is found to decrease with the increase in the L_{SMAs}/L ratio. The reduction occurred for all ratios of A_{SMAs}/A_s. However, the rate and amount of reduction varies with the A_{SMAs}/A_s values. For example, the moment capacity is reduced from 220% to almost 100% in case of A_{SMAs}/A_s = 5.0, while it is reduced only from 80% to 30% in case of A_{SMAs}/A_s = 1.0.

The initial stiffness of the retrofitted BCJ is found to decrease with the increase in the L_{SMAs}/L ratio. Similar behaviour is observed for all values of the A_{SMAs}/A_s. The ST_{rt}/ST_{org} ratio is reduced from 120% to 50% when the L_{SMAs}/L ratio increased from 0.125 to 1.0 in case of A_{SMAs}/A_s =5.0 and from 70% to 10% in case of A_{SMAs}/A_s = 1.0. Amount of dissipated energy is found to significantly decrease with the increase in the L_{SMAs}/L ratio. The EN_{rt}/EN_{org} is decreased from 160% to 30% when the L_{SMAs}/L ratio increased from 0.125 to 1.0 in case of A_{SMAs}/A_s = 5.0, and from 40% to 0% in case of A_{SMAs}/A_s = 1.0.

5.8.3 Drift Ratio Parameter

The effect of varying the drift ratio on the behaviour of RC BCJs retrofitted using external SMA bars is investigated in this subsection. The analysis is performed for different values of A_{SMAs}/A_s ratios at different drift ratios. The drift ratio is represented by the ratio between the beam-tip

maximum deflection (δ_{max}) to the length of the beam (L). The analysis is performed for three different drift ratios. **Fig. 5-18** illustrates the results of the analysis.

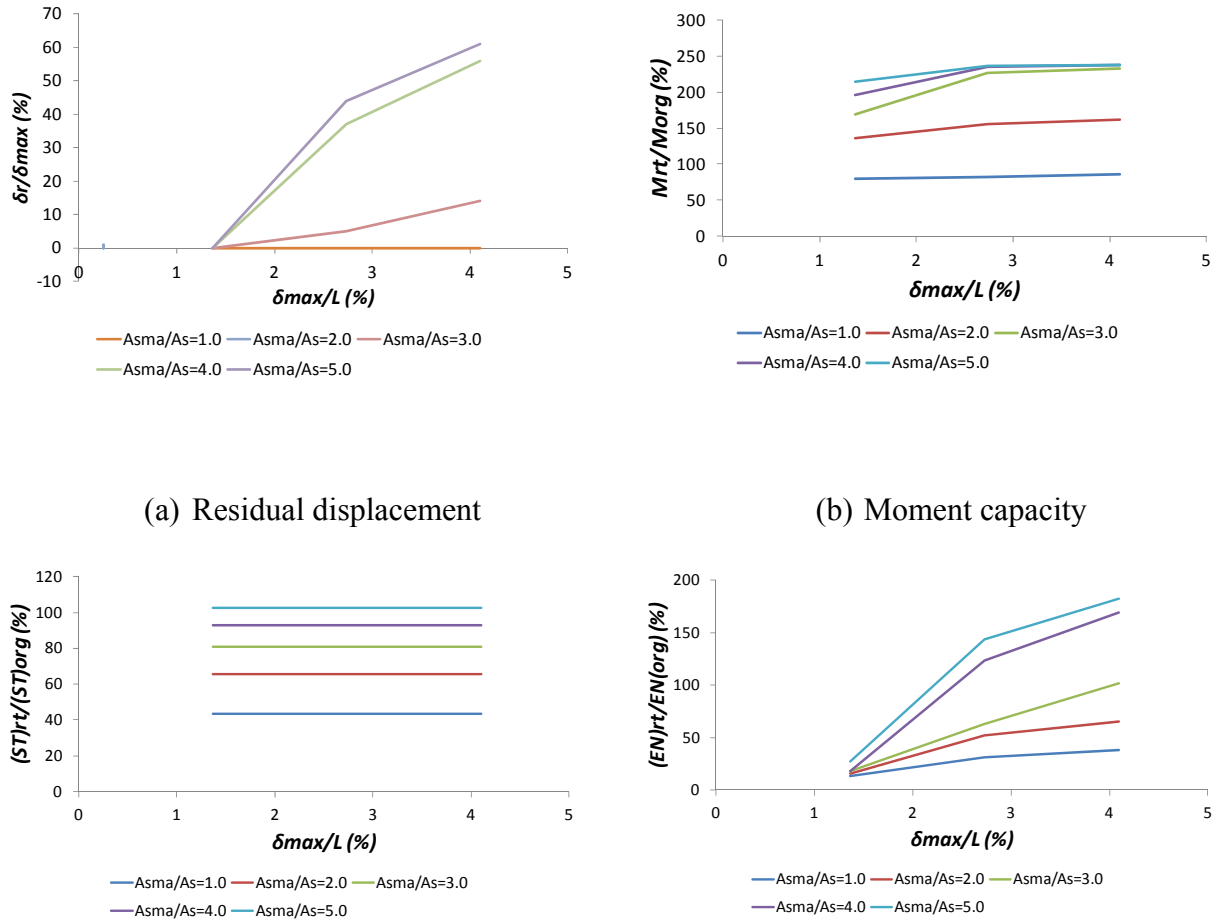

(a) Residual displacement

(b) Moment capacity

(c) Initial stiffness

(d) Dissipated energy

Fig. 5-18: Effect of varying the drift ratio on: (a) residual displacement; (b) moment capacity; (c) initial stiffness; and (d) dissipated energy.

The amount of residual displacements is found to significantly increase (60%) with the increase in the drift ratio for A_{SMAs}/A_s = 4.0 and 5.0. The increase is smaller (15%) in case of A_{SMAs}/A_s =3.0. For cases with low A_{SMAs}/A_s ratios (i.e. 1.0 and 2.0), no change in the amount of residual displacement is observed. Slight increase in the BCJ moment capacity occurs with the increase in the drift ratio. This slight increase is attributed to the strain hardening of the SMA bars. The initial stiffness of the BCJ is found to be independent of the drift ratio. Amount of dissipated energy increases with the increase in the drift ratio. The rate and amount of increase in the dissipated energy is dependent on A_{SMAs}/A_s ratio. The higher the A_{SMAs}/A_s ratio, the larger the amount of dissipated energy.

5.9 CHOICE OF SMA BARS LENGTH

After performing the parametric study, the results are then arranged in a database format with all records of the study. Multiple linear regression technique is then used to determine the relationships between the inputs and outputs of the study. Numerous number of models based on different transformations (i.e. linear transformations, quadratic power transformation, and logarithmic transformation) are first tried. The best models that relate the parametric study inputs to outputs are then chosen and reported in this study. A total of four models for the four outputs are reported.

The used regression analysis methodology is called backward elimination stepwise regression (Dunlop and Smith 2003). In this technique, all explanatory variables (inputs) are included in the model at the beginning. Then, the non-significant variables are eliminated one at a time in each

trial. At the end of the analysis, the reported remaining variables are only the statistically significant ones.

A total of 524 data sets are used in establishing the statistical models. These data represents all the data obtained from the parametric study. All inputs and outputs of this study are kept dimensionless. The inputs of the models are: (i) internal reinforcement status (bars are cut or not cut); (ii) A_{SMAs}/A_s ratio; (iii) L_{SMAs}/L ratio; and (iv) drift ratio. The outputs of the parametric study are: δ_r/δ_{max}, M_{rt}/M_{org}, ST_{rt}/ST_{org}, and EN_{rt}/EN_{org}. Descriptive statistics of the used data are presented in **Table 5-2**.

Table 5-2: Descriptive statistics of the used data

Variable	Obs	Mean	Std. Dev.	Min	Max
RFT Status	524	0.51	0.50	0	1
δ_{max} /L	524	2.70	1.11	1.37	4.10
L_{SMAs}/L	524	0.44	0.28	0.13	1
A_{SMA}/A_s	524	2.74	1.44	0.5	5
δ_r/δ_{max}	524	31.07	28.61	-1.42E-13	83
M_{rt}/M_{org}	524	181.42	67.76	14.77	354.78
ST_{rt}/ST_{org}	524	97.61	44.57	7.20	180.74
EN_{rt}/EN_{org}	524	100.82	69.90	0.03	260.50

Correlation analysis is first used with the data to determine the correlation between each pair of the variables and noting the highly correlated ones and their signs. The correlation matrix is determined using the STATA software V.12 and is shown in **Table 5-3**. **Table 5-4** to **Table 5-7** present the final regression models for the four outputs. These models are the most statistically significant models. All the variable coefficients reported in these tables are statistically significant from zero at 95% confidence level because the associated p-values of all the coefficients are less than 0.05. Measures of model goodness-of-fit (represented by *R-squared*, *Adj R-squared,* and *Root Mean Square Error (MSE)*) are also reported in each table. All the reported models are considered to be with very good fit as their *R-squared* values vary from 0.72 to 0.98. Furthermore, the values of MSE range from 0.16 to 15.0 confirming also a very good model fit (Montgomery et al. 2012). **Equations [5-1:5-4]** represent the summary of the final statistical models for the four outputs.

$$(\delta_r/\delta_{max}) = -43.8554 \times (\text{Reinforcement status}) - 3.05824 \times (\delta_{max}/L)^2 + 24.97149 \times (\delta_{max}/L) + 48.73263 \times (L_{SMAs}/L)^2 - 63.5142 \times (L_{SMAs}/L) + 0.299076 \times (A_{SMA}/A_s)^2 + 23.85597 \quad \textbf{[5-1]}$$

$$\ln (M_{rt}/M_{org}) = 0.351534 \times (\delta_{max}/L) - 0.03753 \times (\delta_{max}/L)^2 - 0.70269 \times (L_{SMAs}/L)^2 + 0.736527 \times \ln (A_{SMA}/A_s) + 3.829082 \quad \textbf{[5-2]}$$

$$(ST_{rt}/ST_{org}) = 63.86686 \times (L_{SMAs}/L) + 24.46517 \times (L_{SMAs}/L)^2 - 1.92955 \times (A_{SMAs}/A_s)^2 + 56.02788 \quad \textbf{[5-3]}$$

$$\ln (EN_{rt}/EN_{org}) = 2.085338 \times (\delta_{max}/L) - 0.25739 \times (\delta_{max}/L)^2 - 4.36291 \times (L_{SMAs}/L) + 0.985633 \times (L_{SMAs}/L)^2 + 1.194 \times \ln (A_{SMAs}/A_s) + 0.415448 \quad \textbf{[5-4]}$$

Let's assume a steel RC BCJ is to be retrofitted with the suggested retrofitting technique. If the length of the SMA bars is limited to 0.20 of the full beam length (L_{SMAs}/L = 20%), the ratio between the added external SMA reinforcement to the internal steel reinforcement is 1.50 (A_{SMAs}/A_s = 150%), and the BCJ is loaded to a drift ratio equal to 2.0% (δ_{max}/L = 2.0%), then this BCJ will keep residual displacement at complete unloading that is equal to only 7% of the maximum applied displacement. The moment capacity of the BCJ will be improved by 5%, and the initial stiffness of the BCJ will be reduced to 66% of its original value. The amount of dissipated energy by the BCJ will be reduced to 25% of its original value.

Table 5-3: Correlation coefficients between all variables

	RFT Status	δ_{max}/L	L_{SMAs}/L	A_{SMA}/A_s	δ_r/δ_{max}	M_{rt}/M_{org}	ST_{rt}/ST_{org}	EN_{rt}/EN_{org}
RFT Status	1							
δ_{max}/L	0.02	1						
L_{SMAs}/L	0.03	-0.01	1					
A_{SMA}/A_s	0.00	-0.01	-0.01	1				
δ_r/δ_{max}	-0.76	0.31	-0.14	0.07	1			
M_{rt}/M_{org}	-0.48	0.21	-0.22	0.66	0.47	1		
ST_{rt}/ST_{org}	-0.83	-0.02	-0.16	0.40	0.74	0.79	1	
EN_{rt}/EN_{org}	-0.75	0.35	-0.22	0.30	0.90	0.71	0.85	1

Table 5-4: Regression model for δ_r/δ_{max}

Source	SS	df	MS	Number of obs	=	524
Model	311799.6	6	51966.6	F(6, 517)	=	230.77
				Prob > F	=	0
				R-squared	=	0.7281
Residual	116419.6	517	225.183	Adj R-squared	=	0.725
Total	428219.2	523	818.7748	Root MSE	=	15.006

δ_r/δ_{max}	Coef.	Std. Err.	t	P>t	[95% Conf.	Interval]
RFT Status	-43.8554	1.312181	-33.42	0	-46.4333	-41.2775
$(\delta_{max}/L)^2$	-3.05824	0.743889	-4.11	0	-4.51965	-1.59682
(δ_{max}/L)	24.97149	4.095759	6.1	0	16.92511	33.01787
$(L_{SMAs}/L)^2$	48.73263	9.739459	5	0	29.59885	67.86641
(L_{SMAs}/L)	-63.5142	10.60582	-5.99	0	-84.35	-42.6784
$(A_{SMA}/A_s)^2$	0.299076	0.081117	3.69	0	0.139717	0.458436
Constant	23.85597	5.454152	4.37	0	13.14094	34.57099

Table 5-5: Regression model for M_{rt}/M_{org}

Source	SS	df	MS	Number of obs	=	268
Model	90.04619	4	22.51155	F(4, 263)	=	853.29
				Prob > F	=	0
				R-squared	=	0.9285
Residual	6.938488	263	0.026382	Adj R-squared	=	0.9274
Total	96.98468	267	0.363238	Root MSE	=	0.16243

ln (M_{rt}/M_{org})	Coef.	Std. Err.	t	P>t	[95% Conf.	Interval]
(δ_{max}/L)	0.351534	0.062099	5.66	0	0.229259	0.473809
$(\delta_{max}/L)^2$	-0.03753	0.011257	-3.33	0.001	-0.0597	-0.01536
$(L_{SMAs}/L)^2$	-0.70269	0.031461	-22.34	0	-0.76464	-0.64075
ln (A_{SMA}/A_s)	0.736527	0.014268	51.62	0	0.708432	0.764621
Constant	3.829082	0.076069	50.34	0	3.679301	3.978863

Table 5-6: Regression model for ST_{rt}/ST_{org}

Source	SS	df	MS	Number of obs	=	268
Model	216748.4	4	54187.1	F(4, 263)	=	3315.53
				Prob > F	=	0
				R-squared	=	0.9806
Residual	4298.316	263	16.34341	Adj R-squared	=	0.9803
Total	221046.7	267	827.8903	Root MSE	=	4.0427

ST_{rt}/ST_{org}	Coef.	Std. Err.	t	P>t	[95% Conf.	Interval]
(L_{SMAs}/L)	-137.331	3.967807	-34.61	0	-145.144	-129.518
$(L_{SMAs}/L)^2$	63.86686	3.612979	17.68	0	56.75282	70.98091
(A_{SMA}/A_s)	24.46517	0.766933	31.9	0	22.95506	25.97528
$(A_{SMA}/A_s)^2$	-1.92955	0.136156	-14.17	0	-2.19764	-1.66146
Constant	56.02788	1.221183	45.88	0	53.62334	58.43242

Table 5-7: Regression model for EN_{rt}/EN_{org}

Source	SS	df	MS	Number of obs	=	268
Model	585.3854	5	117.0771	F(5, 262)	=	300.65
				Prob > F	=	0
				R-squared	=	0.8516
Residual	102.0269	262	0.389415	Adj R-squared	=	0.8487
Total	687.4122	267	2.574578	Root MSE	=	0.62403

ln (EN_{rt}/EN_{org})	Coef.	Std. Err.	t	P>t	[95% Conf.	Interval]
(δ_{max}/L)	2.085338	0.238586	8.74	0	1.615549	2.555128
$(\delta_{max}/L)^2$	-0.25739	0.043251	-5.95	0	-0.34255	-0.17222
(L_{SMAs}/L)	-4.36291	0.612504	-7.12	0	-5.56897	-3.15686
$(L_{SMAs}/L)^2$	0.985633	0.557721	1.77	0.078	-0.11255	2.083819
ln (A_{SMA}/A_s)	1.194	0.05482	21.78	0	1.086056	1.301944
Constant	0.415448	0.316043	1.31	0.19	-0.20686	1.037756

5.10 CONCLUSIONS

Retrofitting RC BCJs using external unbonded SMA bars is investigated. A three-dimensional FE model using ABAQUS is first developed and validated using available experimental results. Experimental results included RC BCJs internally reinforced with steel and SMA bars, and RC beams externally reinforced with unbonded steel and SMA bars. Good agreement between experimental and analytical results is observed.

A retrofitted BCJ is assumed and analyzed using the developed FE model. Obtained results of the retrofitted BCJ are compared to the results of the original BCJ. An increase of 22% in the beam strength is observed. Residual displacement reduced by only 17% due to retrofitting. This small recovery is attributed to the big difference in the modulus of elasticity between steel and SMA. To increase the amount of recovered displacement at complete unloading, it is proposed to cut the internal steel bars at the face of the column and replace them with external SMA bars. The analysis is performed again for the retrofitted beam after cutting the internal bars. It is found that the residual displacement at complete unloading is only 2% of the maximum applied displacement. Disadvantage of the proposed technique is the reduction in the beam strength and stiffness.

Since it is a complicated process to model the BCJ in ABAQUS, a simplified model using the Seismostruct software is then developed to capture the behaviour of RC BCJs externally reinforced with SMA bars. Results of the simplified model are first validated using the results of the FE model. After validating the simplified model, it is used to carry out an extensive

parametric study to investigate the behaviour of RC BCJs retrofitted using external SMA bars. Three parameters are investigated in this study. These parameters are: (i) ratio between the external SMA reinforcement to the internal steel reinforcement (A_{SMA}/A_s); (ii) ratio between the length of the SMA bars and the full length of the beam (L_{SMAs}/L), and (iii) applied drift ratio (δ_{max}/L). Four outputs are used in the parametric study to capture the change happening in the behaviour due to varying of the parameters. These outputs are: (δ_r/δ_{max}), (M_{rt}/M_{org}), (ST_{rt}/ST_{org}), and (EN_{rt}/EN_{org}).

Results of the parametric study are then used to perform multiple linear regression analysis. Different models with different transformations of the inputs are developed for the four outputs. Results of the regression analysis are then summarized in the form of simple equations to determine the optimum amount and length of the used SMA bars.

5.11 REFERENCES

Abaqus, F.E.A. (2018) "ABAQUS Analysis user's manual." Dassault Systemes,Vélizy-Villacoublay, France, 2006.

Alam, M.S., Youssef, M.A., and Nehdi, M. (2007). "Utilizing Shape Memory Alloys to Enhance the Performance and Safety of Civil Infrastructure: a Review." Canadian Journal of Civil Engineering, 34(9), 1075-1086.

Alcocer, S.M., and Jirsa, J. O. (1993). "Strength of reinforced concrete frame connections rehabilitated by jacketing." ACI Structural Journal, 90(3), 249-261.

Antonopoulos, C. P., and Triantafillou, T. C. (2002). "Analysis of FRP strengthened RC beam-column joints." Journal of Composites for Construction (ASCE), 6(1), 41-51.

Auricchio, F, and Sacco, E. (1997) "Superelastic shape-memory-alloy beam model." Journal of Intelligent Material Systems and Structures, 8(6), 489-501.

Beres, A., El-Borgi, S., White, R. N., and Gergely, P. (1992). Experimental results of repaired and retrofitted beam-column joint tests in lightly reinforced concrete frame buildings, Technical report NCEER-92-0025, State University of New York at Buffalo, Buffalo, NY.

Biddah, A., Ghobarah, A., and Aziz, T. S. (1997). "Upgrading of nonductile reinforced concrete frame connections." Journal of Structural Engineering (ASCE), 123(8), 1001-1009.

Bracci, J. M., Reinhorn, A. M., and Mander, J. B. (1995). "Seismic retrofit of reinforced concrete buildings designed for gravity loads: Performance of structural model." ACI Structural Journal, 92(6), 711-723.

Clyde, C., and Pantelides, C. P. (2002). "Seismic evaluation and rehabilitation of R/C exterior building joints." Proceedings of the Seventh U.S. National Conference on Earthquake Engineering (CD-ROM), Boston, MA.

Corazao, M., and Durrani, A. J. (1989). Repair and strengthening of beam-to-column connections subjected to earthquake loading, Technical report NCEER-89-0013, State University of New York at Buffalo, Buffalo, NY.

Dunlop, P, and Simon, S. (2003) "Estimating key characteristics of the concrete delivery and placement process using linear regression analysis." Journal of Civil Engineering and Environmental Systems, 20(4), 273-290.

Filiatrault, A., and Lebrun, I. (1996). “Seismic rehabilitation of reinforced concrete joints by epoxy pressure injection technique.” Seismic rehabilitation of concrete structures, SP-160, G. M. Sabnis, A. C. Shroff, and L. F. Kahn, eds., American Concrete Institute, Farmington Hills, MI, 73-92.

French, C. W., Thorp, G. A., and Tsai, W. J. (1990). “Epoxy repair techniques for moderate earthquake damage.” ACI Structural Journal, 87(4), 416-424.

Gergely, I., Pantelides, C. P., Nuismer, R. J., and Reaveley, L. D. (1998). “Bridge pier retrofit using fiber-reinforced plastic composites.” Journal of Composites for Construction (ASCE), 2(4), 165-174.

Ghobarah, A., and Said, A. (2002). “Shear strengthening of beam-column joints.” Engineering Structures: The Journal of Earthquake, Wind and Ocean Engineering; 24(7), 881-888.

Ghobarah, A., Aziz, T. S., and Biddah, A. (1997). “Rehabilitation of reinforced concrete frame connections using corrugated steel jacketing.” ACI Structural Journal, 4(3), 283-294.

Janke, L., Czaderski, C., Motavalli, M., and Ruth, J. (2005). “Applications of Shape Memory Alloys in Civil Engineering Structures - Overview, Limits and New Ideas.” Materials and Structures, 338(279), 578-592.

Karayannis, C. G., and Sirkelis, G. M. (2002). “Effectiveness of RC beam-column connections strengthening using carbon-FRP jackets.” Proceedings of the Twelfth European Conference on Earthquake Engineering (CD-ROM), London, PR 549.

McCormick, J., Desroches, R., Fugazza, D. and Auricchio, F. (2006) “Seismic vibration control using superelastic shape memory alloys.” Journal of Engineering Material and technology 128(3), 294-301.

Moehle, J. P., and Mahin, S. A. (1991). “Observations on the behavior of reinforced concrete buildings during earthquakes.” Earthquake-resistant concrete structures: Inelastic response and design, SP-127, S. K. Ghosh, ed., American Concrete Institute, Farmington Hills, MI, 67-89.

Saiidi,M.S., Sadrossadat-Zadeh, M., Ayoub,C., and Itani,A. (2007). “Pilot study of behavior of concrete beams reinforced with shape memory alloys.” Journal of Materials in Civil engineering, American Society of Civil Engineering, 19(6), 454-461.

SeismoSoft (2018) "SeismoStruct - A computer program for static and dynamic nonlinear analysis of structures." Available from URL: http://www.seismosoft.com.

Youssef, M.A., Alam, M.S. and Nehdi M. (2008) “Experimental investigation on the seismic behaviour of beam-column joints reinforced with superelastic shape memory alloys.,” Journal of Earthquake Engineering 12(7), 1205-1222.

Chapter 6 Seismic Performance of Reinforced Concrete Frames Retrofitted Using External Superelastic Shape Memory Alloys Bars

6.1 INTRODUCTION

Reinforced Concrete (RC) frame structures designed and built prior to the 1970s lack ductility, and, thus are unsafe under seismic loads (Hassan 2011). The beam-column joints (BCJs) of these structures are poorly detailed and are considered deficient under lateral loads. Beam reinforcement is insufficiently anchored into the joint area of these structures.

Newly built RC frame structures are designed to dissipate the energy of moderate and strong earthquakes through allowing some inelastic deformations (Engindeni 2008). These inelastic deformations result in permanent deformations in the structure, and in some cases may require demolishing the damaged structure. Thus, there is a need to retrofit the pre-1970s structures to be able to resist the seismic loads, and to reduce the permanent deformations of the newly built structures. One of the methods to achieve this goal is by utilizing smart materials such as superelastic Shape Memory Alloys (SMAs) (Alam et al. 2009, Youssef and ElFeki 2012).

Superleastic SMA bars have unique properties compared to the usual steel reinforcement. They have the ability to undergo large deformations and return to their undeformed shape upon unloading (Alam et al. 2007). They also have good resistance to fatigue and corrosion and high

damping ability (Janke et al. 2005). So using superleastic SMA bars to enhance the seismic performance of these structures can be ideal (Alam et al. 2009, Youssef and ElFiki 2012).

Youssef and Elfeki (2012) studied the behaviour of RC frame structures internally reinforced with SMA bars at the critical locations of the structure. Seven different arrangements for the SMA bars are selected resulting in seven different frames. Nonlinear dynamic analyses are performed to select the frames with the best seismic performance. It is found that the frames with SMA reinforcement in the BCJs of the first floor, and in the BCJs of the first and fourth floors give the best seismic performance.

This paper investigates the seismic performance of RC frame structures retrofitted using external superleastic SMA bars. A six storey steel RC frame located in high seismic region is used as the reference frame. Two potential retrofit schemes that utilize superelastic SMA bars are assumed. Nonlinear dynamic analyses are performed for the three frames using Seismistruct software (Seismostruct 2018). Results of the analysis are then used to compare the seismic performance of the three frames in terms of the damage level, the Maximum Inter-storey Drift (MID) ratio, Maximum Residual Inter-storey Drift (MRID), Maximum Roof Drift Ratio (MRDR), Residual Roof Drift Ratio (RRDR), and the earthquake intensity at collapse.

6.2 PROPOSED RETROFITTING TECHNIQUE

The idea of the proposed retrofitting technique is based on attaching external SMA bars to the RC BCJ. As shown in **Fig. 6-1**, the bars are attached to the BCJ using external steel angles. The

steel angles are attached to the BCJ using steel bolts. One angle is attached to the BCJ joint area, while the second angle is attached to the beam. Hold down plates can be used for big lengths of the SMA bars to enforce the bars to deform with the beam.

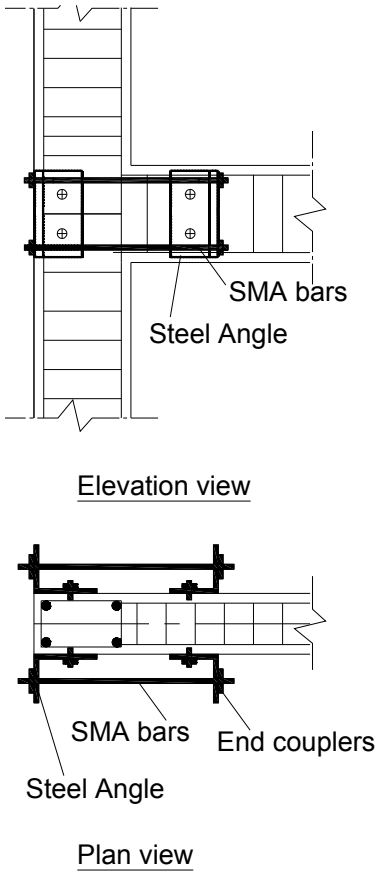

Fig. 6-1: Proposed retrofitting technique

The modulus of elasticity of SMA is much lower (1/5 to 1/3) than that of the regular steel. Thus, attaching a small to moderate ratio of SMA will improve the strength and the stiffness of the BCJ, but it is not expected to reduce the residual deformations at complete unloading. Thus, it is proposed to cut the internal steel bars of the beam at the face of the column and replace it with

the external SMA bars. This ensures that the BCJ behaviour is governed by the external SMA bars rather than the internal steel bars, and thus minimum residual deformations are expected at complete unloading.

6.3 SIMPLIFIED MODEL

A simplified model for the retrofitted BCJ is proposed. The simplified model is developed using Seismostruct software v.6 (Seismostruct 2018). The special technique used to model the connection include: (i) modelling the SMA bars using inelastic truss elements; (ii) modelling the superelastic behaviour of the SMA bars using the uniaxial material model proposed by Auricchio and Sacco (1997); (iii) modelling the concrete beam and column using displacement based inelastic frame elements; and (iv) modelling the external angles that supports the SMA bars using rigid arms connected to the concrete beam and column.

As shown in **Fig. 6-2**, the beam and the column of the BCJ are modelled using frame elements. Two rigid arms are connected to the beam near the face of the column representing the angle supported in the joint area. Another two rigid arms are connected to the beam at a distance equal to the length of the required SMA bars. The SMA bars are connected between the rigid arms and are modelled using truss elements. The reinforcement in the beam element is cut in between the rigid arms to eliminate any contribution from it to the strength, stiffness and residual deformation of the joint.

To validate the assumed simplified model, a comparison between the load-displacement results of the simplified model developed using Seismostruct software and the actual model developed using ABAQUS (ABAQUS 2018) is shown in **Fig. 6-3**. Very good agreement between the two results is achieved.

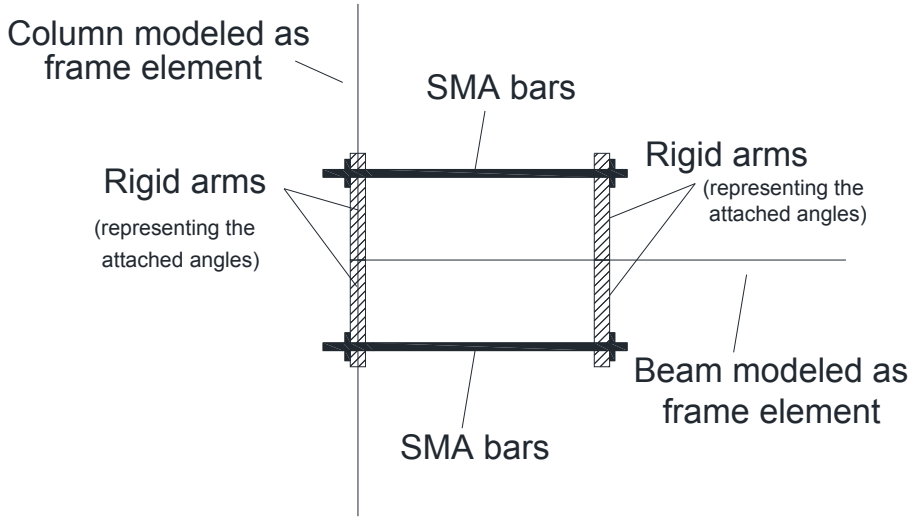

Fig. 6-2: Sketch of the simplified model

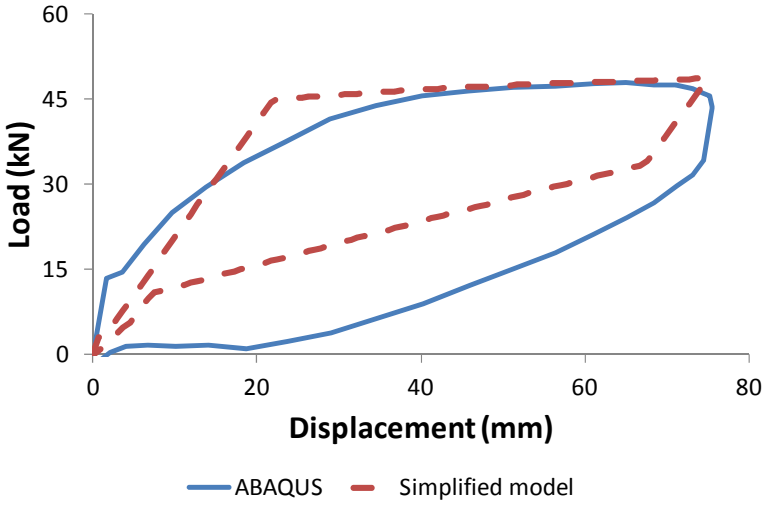

Fig. 6-3: Load-displacement results of the ABAQUS model vs. the simplified Seismostruct model

6.4 STEEL RC FRAME CHARACTERISTICS AND MODELING

The steel RC frame structure designed by Youssef and Elfeki (2012) is used as the reference frame. The frame (Frame 1) is a symmetric six-storey RC office building located in California (high seismic region). The layout and dimensions of the building are shown in **Fig. 6-4**. It is designed to satisfy the requirements of the International Building Code (IBC 2006) and the American Concrete Institute code (ACI 318 2005). The lateral load resisting system is composed of special moment frames. The cross-section dimensions and the reinforcement details of the frame are shown in **Fig. 6-5**.

Only one special moment frame is selected for the analysis because of the geometrical symmetry. The frame is modeled using Seismostruct software (Seismostruct 2018). The beams and columns are modeled using cubic elasto-plastic elements. The beams are divided in six elements, while the columns are divided in three. The beams are modeled as T-sections, while the beam-column joints are modeled using rigid elements, **Fig. 6-6.** The concrete compressive strength is assumed to be 28 MPa while the steel yielding stress is 400 MPa.

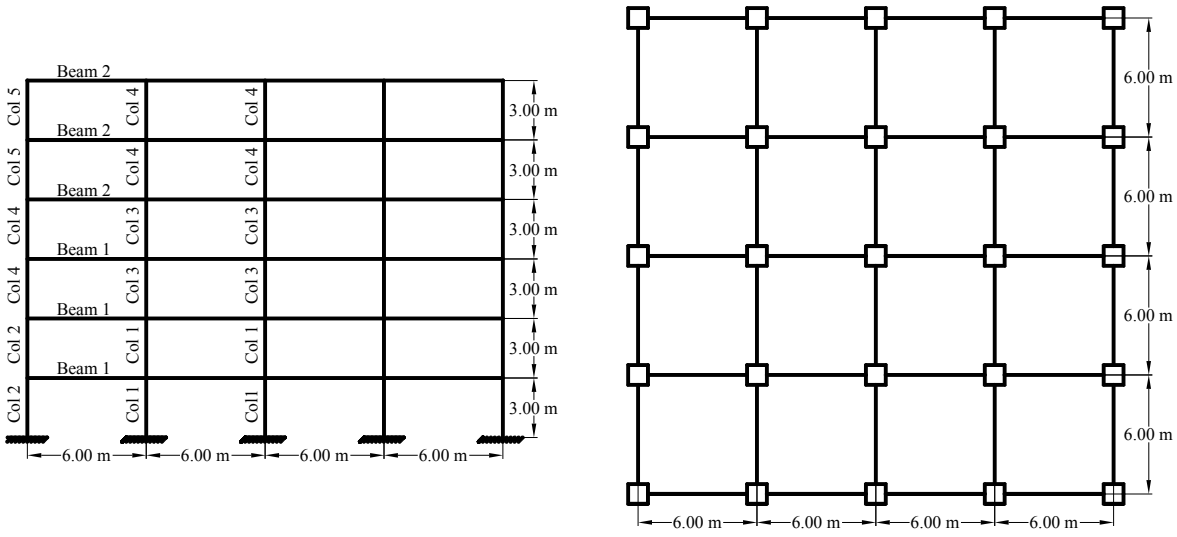

Fig. 6-4: Six-storey RC building Plan and Elevation (Youssef and Elfeki 2012)

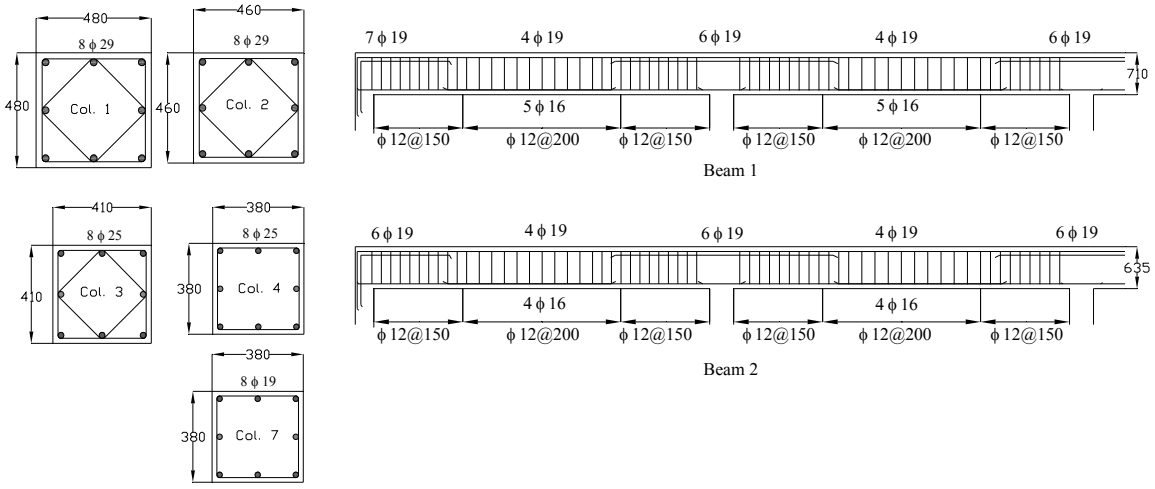

Fig. 6-5: Six-storey RC building cross-sections of beams and columns (Youssef and Elfeki 2012)

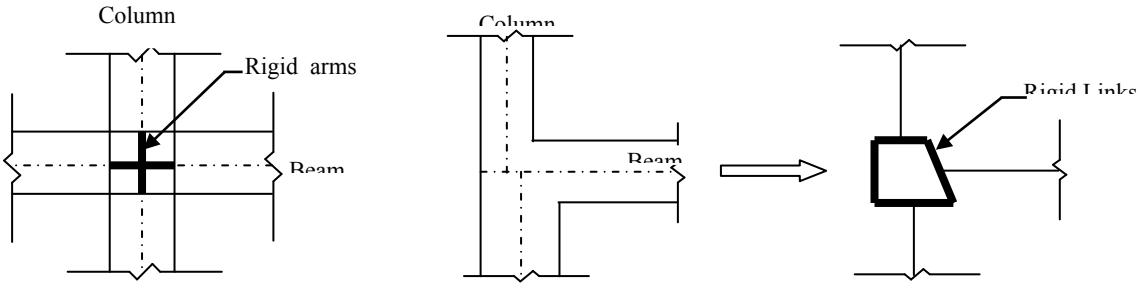

a) Interior beam-column joint b) Edge beam-column joint

Fig. 6-6: Modeling of beam column joints (Youssef and Elfeki 2012)

6.5 SMA RC FRAMES

Superleastic SMA bars are added to the steel RC frames to enhance their seismic performance. The SMA bars are added to the beam-column joints of the first floor for one frame (Frame 2) and to the beam-column joints of the first and fourth floors of the other frame (Frame 3). The choice of these locations is based on the recommendations made by Youssef and Elfeki (2012).The internal steel reinforcement of the retrofitted BCJ is cut at the locations of the added SMA bars. This ensures that the behaviour of the retrofitted BCJs and frame is controlled by the superleastic SMA bars rather than the internal steel bars.

The amount of SMA reinforcement is chosen equal to the amount of internal steel reinforcement. The critical stress, critical strain, modulus of elasticity of the SMA bars is equal to 401 MPa, 0.007, 62.5 GPa respectively. The SMA bars are attached to the frame using external rigid steel angles and bolts. The retrofitted BCJs are modelled in the Seismostruct software using the simplified model.

6.6 LOCAL FAILURE AND COLLAPSE LIMITS

Local yielding of the RC element is assumed to happen when the reinforcement reaches its yielding strain. Yielding strain is defined as 0.002 for steel and as 0.007 for SMAs. Researchers are suggesting different definitions for the failure of concrete. In this paper, Crushing of concrete is assumed to occur either when the confined concrete reaches a value of 0.015 or when the stirrups reach their fracture strain as proposed by Pauley and Priestley (1992). Collapse of the structure is assumed to occur when four of the columns located in the same storey reach their crushing strain (Youssef and Elfeki 2012).

6.7 DYNAMIC ANALYSES

6.7.1 Eigen Value Analysis

Eigen value analysis is performed for the steel RC frame by Youssef and Elfeki (2012). The fundamental period of vibration of the structure is found to be 0.501. The Eigen value analysis is repeated for the two retrofitted frames to investigate the effect of adding external SMA bars on the fundamental period of vibration. No or negligible effect is observed. **Fig. 6-7** shows the first four mode shapes of the studied frames.

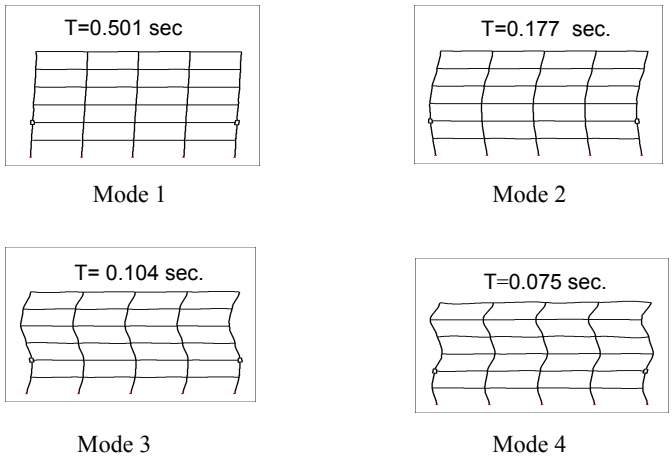

Fig. 6-7: First four mode shapes of the six-storey RC building (Youssef and Elfeki 2012)

6.7.2 Selection of Ground Motion Records

The five ground motion records used by Youssef and Elfeki (2012) are used in this study to perform the dynamic analysis of the frames. The ratio between the peak ground acceleration and the peak ground velocity (A/v) is used to classify the intensity of the used records. These records cover a wide range of ground motion frequencies. A summary of the record characteristics are given in **Table 6-1**. The 5% damped spectral acceleration at the fundamental period of the structure [Sa(T1,5%)] is used to scale the used earthquake records. **Fig. 6-8** shows the scaled earthquake records.

Table 6-1: Chosen earthquake records

Earthquake	Date	Ms Magnitude	Station	PGA (g)	A/v
Northridge USA	17/1/94	6.7	Arleta-Nordhoff	0.340	Inter.
Imperial Valley USA	15/10/79	6.9	El Centro Array #6 (E06)	0.439	Low
Loma Prieta USA	18/10/89	7.1	Capitola (CAP)	0.530	High
Whittier USA	1/10/87	5.7	Whittier Dam	0.316	High
San Fernando	9/2/71	6.6	Pacoima Dam	1.230	Inter.

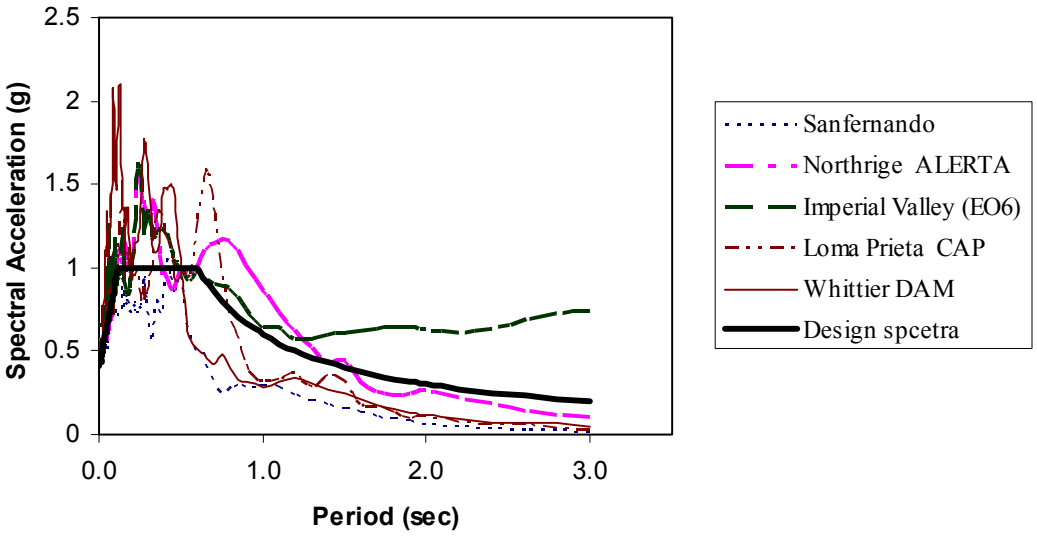

Fig. 6-8: Spectral acceleration diagrams

6.7.3 Incremental Dynamic Analysis (IDA)

Incremental Dynamic analysis is performed for the three frames to observe the effect of increasing the spectral acceleration on the behaviour of the frames.

6.7.4 Time History Analysis at Collapse

The analysis is first performed for Frame 1 (steel RC frame) to determine the intensities for the five earthquakes defining collapse. The analysis is then performed for the other two frames at the defined intensities. Performance of the three frames is illustrated in the following section.

6.8 RESULTS AND DISCUSSIONS

6.8.1 Incremental Dynamic Analysis

Fig. 6-9 to **Fig. 6-13** show the results obtained from the incremental dynamic analysis. **Fig. 6-9** illustrates the behaviour of the three frames when subjected to Imperial record. It is clear from the figure that the three frames experienced similar MID and MRDR at low values of Sa (T1, 5%). At high values of Sa (T1, 5%), Frame 1 experienced much higher MID and MRDR values. This shows the effect of the suggested retrofitting technique on limiting the MID and MRDR values. MRID and RRDR behaviour is similar at low Sa (T1, 5%). However, at high values of Sa (T1, 5%), the suggested retrofitting technique showed much less values of residual drifts. Furthermore, Frame 3 (SMA at first floor only) showed lower residual drifts than Frame 2, which means better arrangement for the SMA bars.

Fig. 6-10 shows the response of the three frames to the Loma Prieta record. In this case, the three frames showed similar values of MID at all levels of Sa (T1, 5%). Frames 2 and 3 showed less values of MRDR close to failure. Frame 3 showed less residual drifts (MRID and RRDR) than frames 1 and 2. Frame 2 has MRID and RRDR values that are almost an average of the two other frames. **Fig. 6-11** shows the response of the three frames to the Northridge record. MID and MRDR values are similar for the three frames at all levels of Sa (T1, 5%). Residual drift (MRID and RRDR) values of frames 2 and 3 are much lower than frame 1 (steel RC frame). Frame 2 shows less MRID value at collapse, while Frame 3 shows less RRDR value at collapse.

Response of the three frames to the San Fernando record is shown in **Fig. 6-12**. The three frames have similar maximum and residual drift ratios at small levels of Sa (T1, 5%). At high levels of Sa (T1, 5%), Frames 1 and 3 show less MID values than frame 2. The difference increases as the Sa (T1, 5%) value increase. MRDR value is similar for the three frames at all levels of Sa (T1, 5%). For residual drifts (MRID and RRDR), the response of the three frames is similar at low values of Sa (T1, 5%) and at collapse. At intermediate values of Sa (T1, 5%), frame 1 shows higher residual drifts than frames 2 and 3.

Fig. 6-13 shows the response of the three frames to Whittier record. Similar response of the three frames is observed for MID and MRDR. At collapse, frame 1 shows higher MID value. Frames 2 and 3 show much less residual drifts at collapse. However, comparable values are observed at low levels of Sa (T1, 5%).

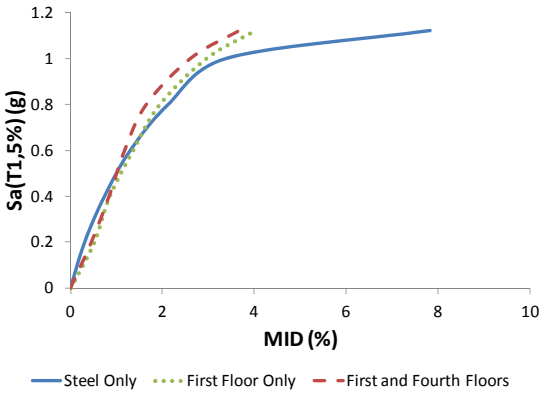

(a) Maximum Inter-storey Drift

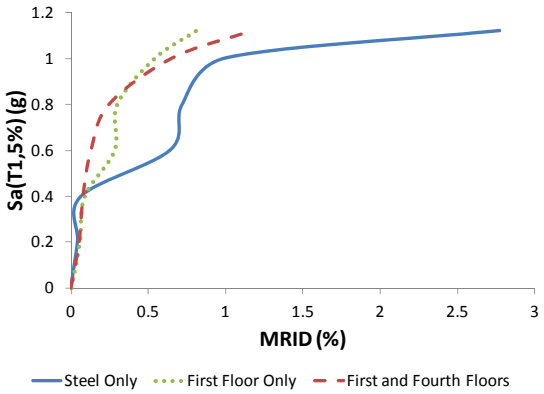

(b) Maximum Residual Inter-storey Drift

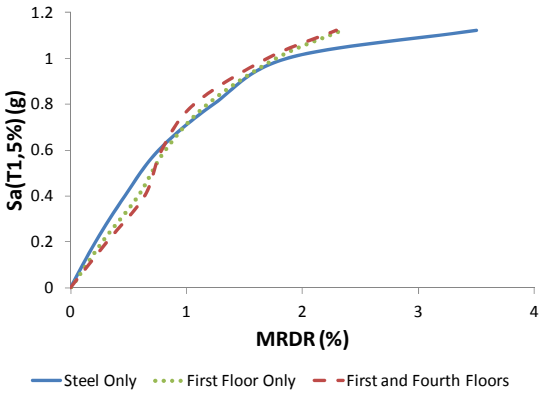

(c) Maximum Roof Drift Ratio

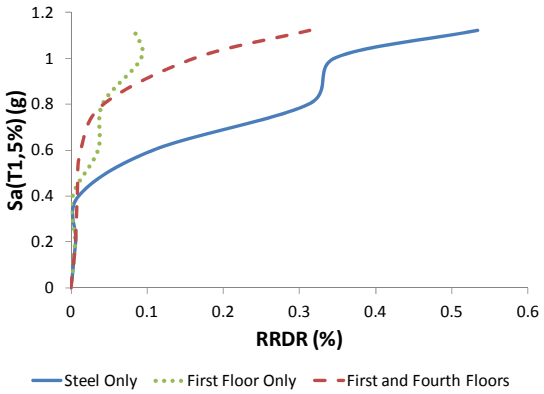

(d) Residual Roof Drift Ratio

Fig. 6-9: Incremental dynamic analysis of the three frames - Imperial Record

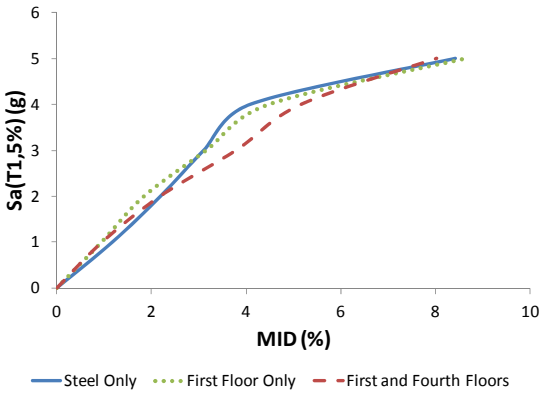

(a) Maximum Inter-storey Drift

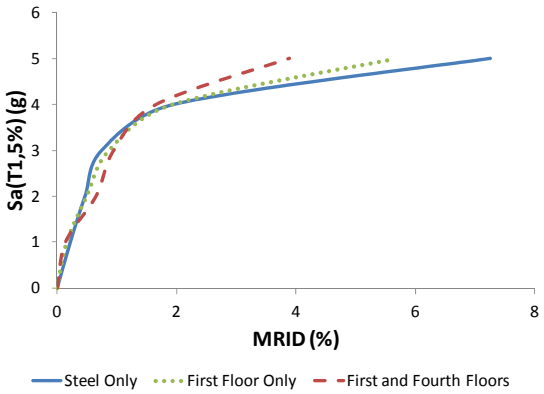

(b) Maximum Residual Inter-storey Drift

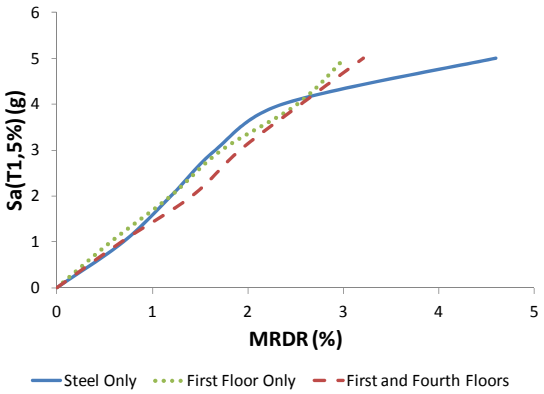

(c) Maximum Roof Drift Ratio

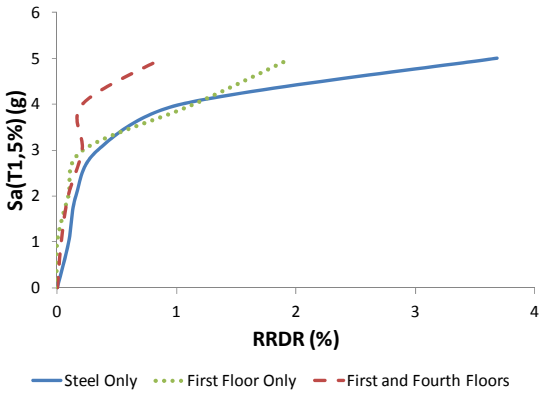

(d) Residual Roof Drift Ratio

Fig. 6-10: Incremental dynamic analysis of the three frames - Loma Prieta Record

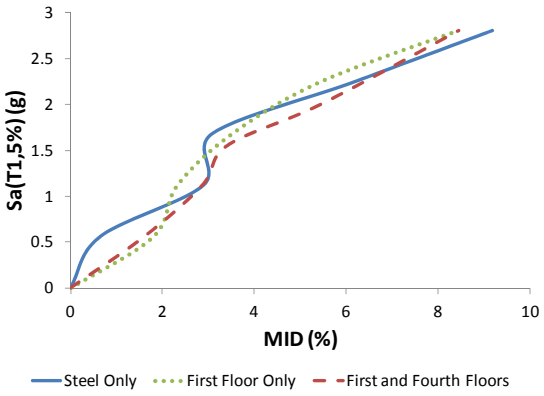

(a) Maximum Inter-storey Drift

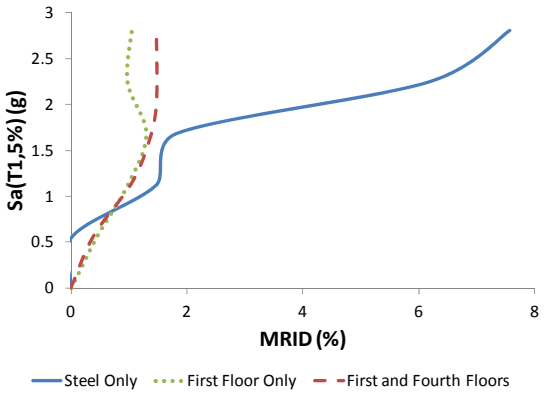

(b) Maximum Residual Inter-storey Drift

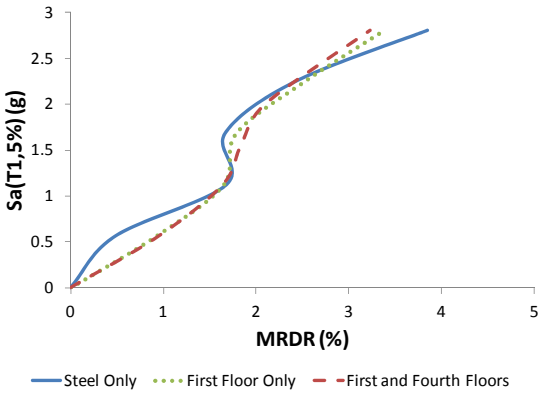

(c) Maximum Roof Drift Ratio

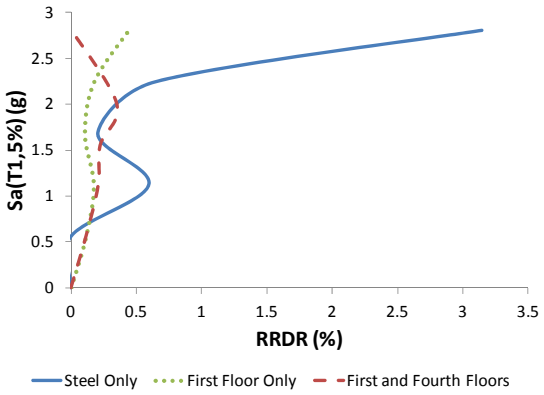

(d) Residual Roof Drift Ratio

Fig. 6-11: Incremental dynamic analysis of the three frames - Northridge Record

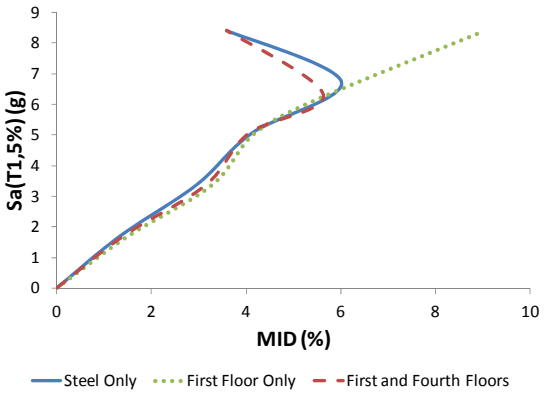

(a) Maximum Inter-storey Drift

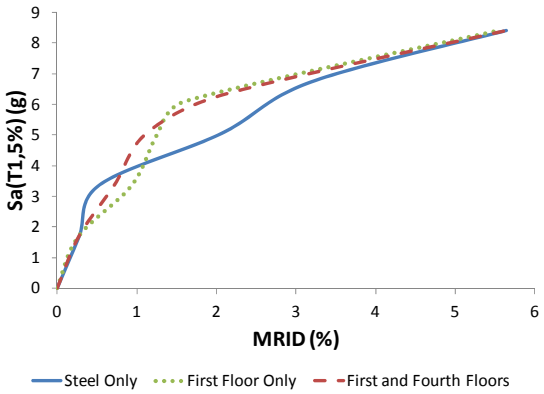

(b) Maximum Residual Inter-storey Drift

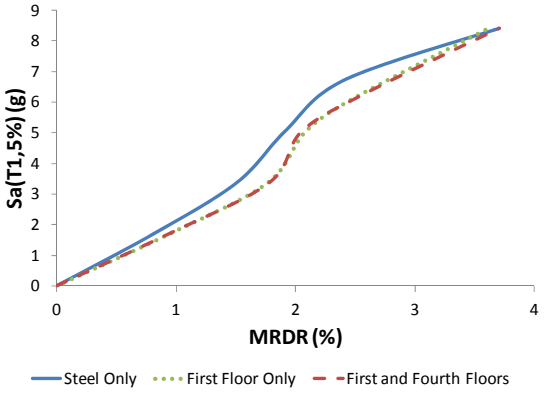

(c) Maximum Roof Drift Ratio

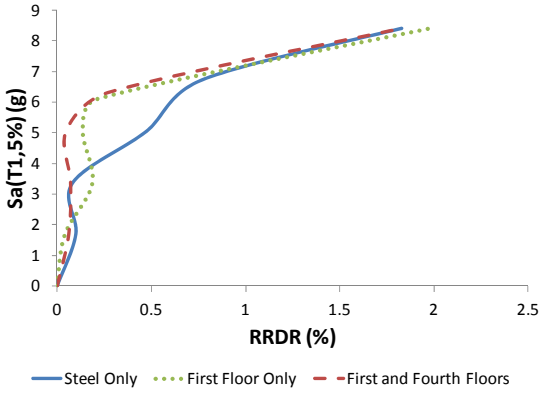

(d) Residual Roof Drift Ratio

Fig. 6-12: Incremental dynamic analysis of the three frames - San Fernando Record

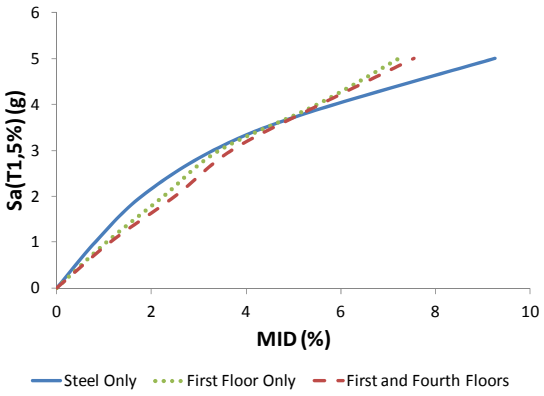

(a) Maximum Inter-storey Drift

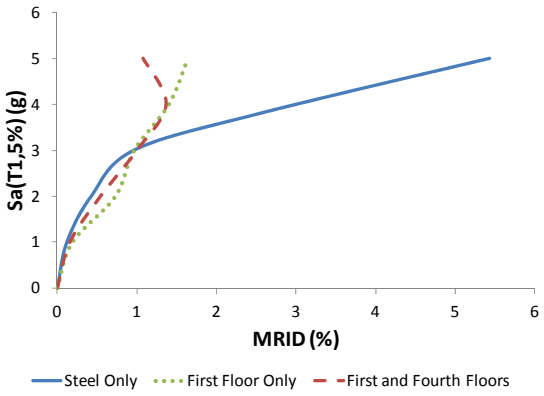

(b) Maximum Residual Inter-storey Drift

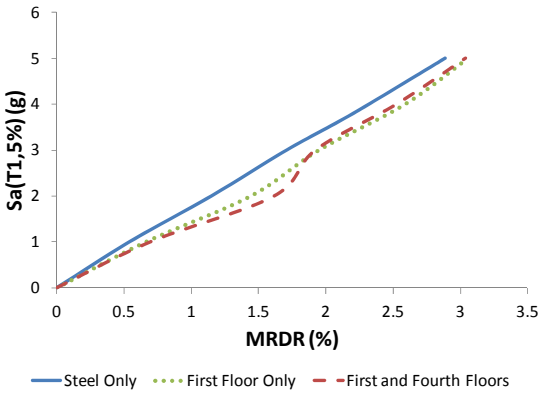

(c) Maximum Roof Drift Ratio

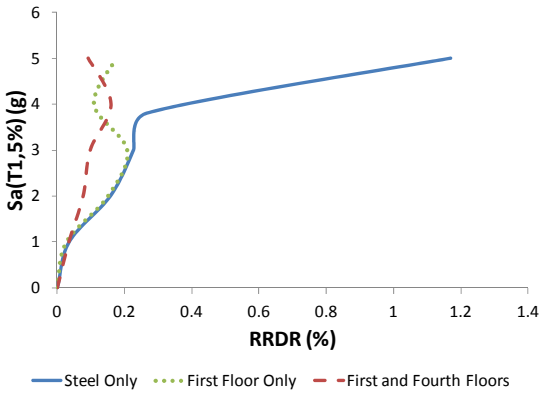

(d) Residual Roof Drift Ratio

Fig. 6-13: Incremental dynamic analysis of the three frames - Whittier Record

6.8.2 Damage Schemes

The damage schemes of the three frames under the five earthquake records are illustrated in **Fig. 6-14** to **Fig. 6-18**. **Fig. 6-14** shows the damage scheme of the three frames when subjected to the Imperial Valley record. It is clear from the figure that Frame 1 (steel RC frame) reached its collapse limit due to the concrete crushing of the lower ends of the first storey columns. Frames 2 and 3 did not reach the collapse limit and can sustain higher loads as only three columns reached their crushing limit. No crushing is observed at higher storey columns. Most of the beams and columns of the three frames reached their yielding limit. First and second floor beams of Frame 1 sustained yielding at their mid-span. All beams of Frame 3 did not reach yielding at their mid-spans.

Fig. 6-15 shows the damage schemes of the three frames when subjected to the Loma Prieta earthquake record. Frame 1 reached its collapse limit by crushing of the lower four ends of the first storey columns. Frames 2 and 3 did not reach their collapse limit and can sustain higher loads. Most of the columns and beams reached their yielding limit. Most of the beams also reached their yielding limit at mid-span.

Damage schemes of the three frames when subjected to Northridge earthquake are shown in **Fig. 6-16**. The three frames reached their collapse limit due to concrete crushing of first storey columns. Three columns of the third storey of Frame 1 reached their crushing limits. Only two out of the three columns reached their crushing limits in Frames 2 and 3. Yielding of beams at

their mid-spans is concentrated at the first two stories of Frame 1, and at the second, third and fourth stories of the other two frames.

The effect of the San Fernando earthquake on the three frames is shown in **Fig. 6-17**. Crushing occurred for first storey columns of Frame 1. In addition, two beams in the first storey reached their crushing limit. Frames 2 and 3 did not reach their collapse limit and resist higher levels of loads. Two columns in the third storey of Frame 2 reached their crushing limit, while only one column in the same location reached its crushing limit in Frame 3. Severe yielding of the beams and columns of the three frames can be observed. Mid-span yielding of the beams of the three frames is also observed.

The damage schemes of the three frames due to the Whittier earthquake are shown in **Fig. 6-18**. Collapse of the three frames occurred due to crushing of the first storey columns. Severe yielding of the beams and columns can be observed. One beam and one column in the second storey of Frame 3 reached their crushing limit. Mid-span yielding of the beams is more pronounced in case of Frames 1 and 2 than the case of Frame 3.

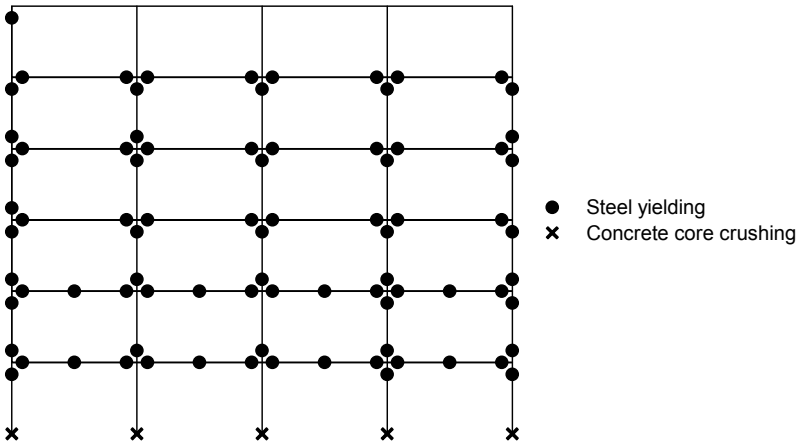

(a) Frame 1 (Steel Only)

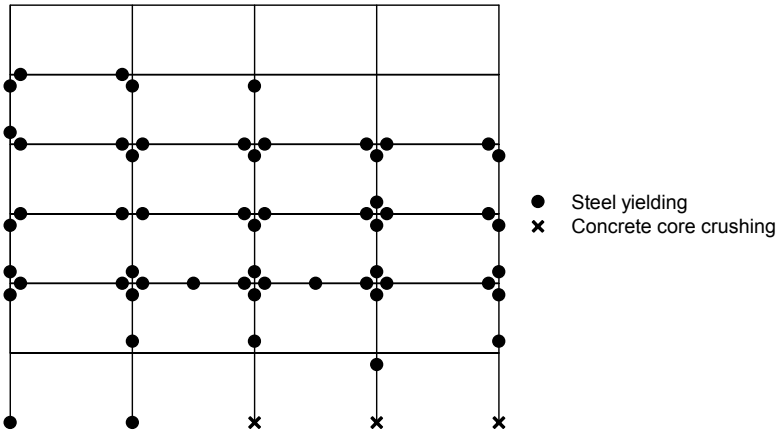

(b) Frame 2 (First Floor Only)

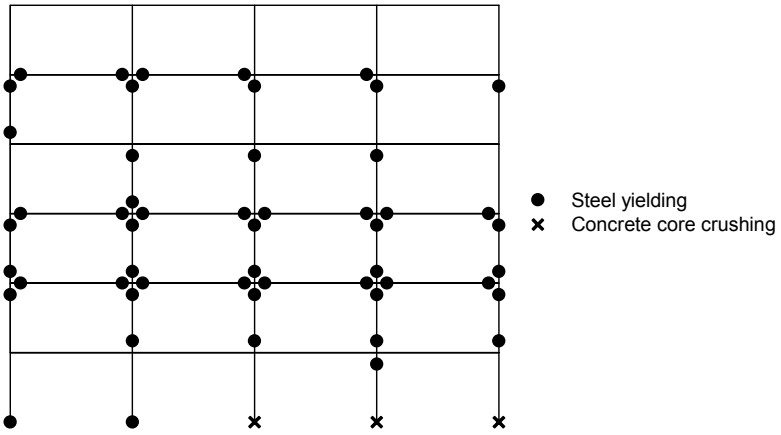

(c) Frame 3 (First and Fourth Floors)

Fig. 6-14: Damage scheme for different frames when subjected to Imperial earthquake record; (a) Frame 1 (Steel Only); (b) Frame 2 (First Floor Only); and (c) Frame 3 (First and Fourth Floors)

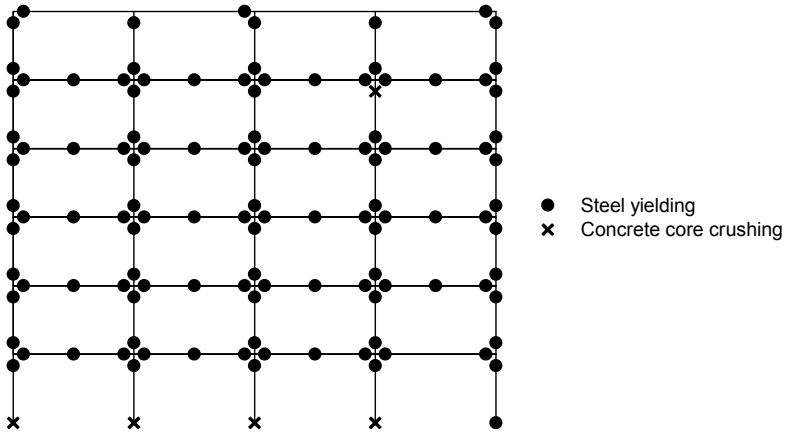

(a) Frame 1 (Steel Only)

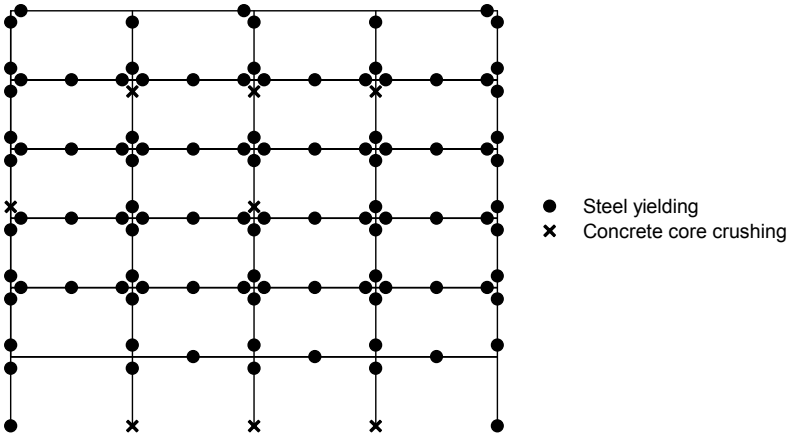

(b) Frame 2 (First Floor Only)

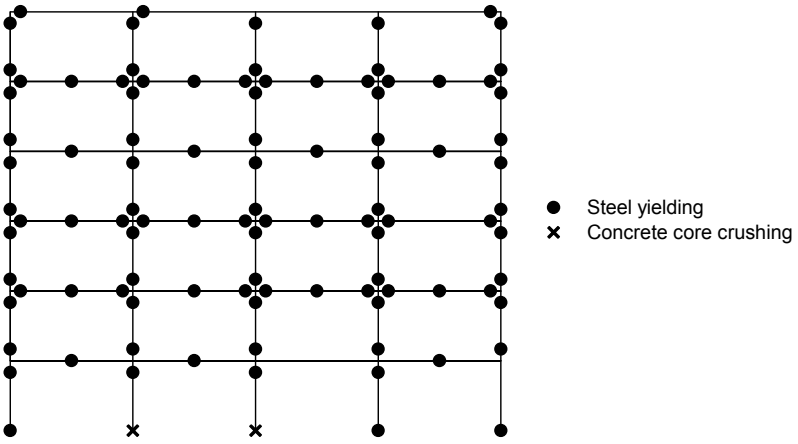

(c) Frame 3 (First and Fourth Floors)

Fig. 6-15: Damage scheme for different frames when subjected to Loma Prieta earthquake record; (a) Frame 1 (Steel Only); (b) Frame 2 (First Floor Only); and (c) Frame 3 (First and Fourth Floors)

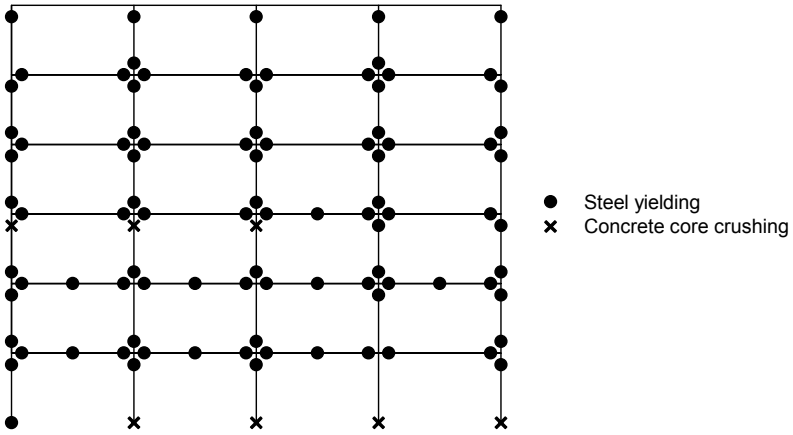

(a) Frame 1 (Steel Only)

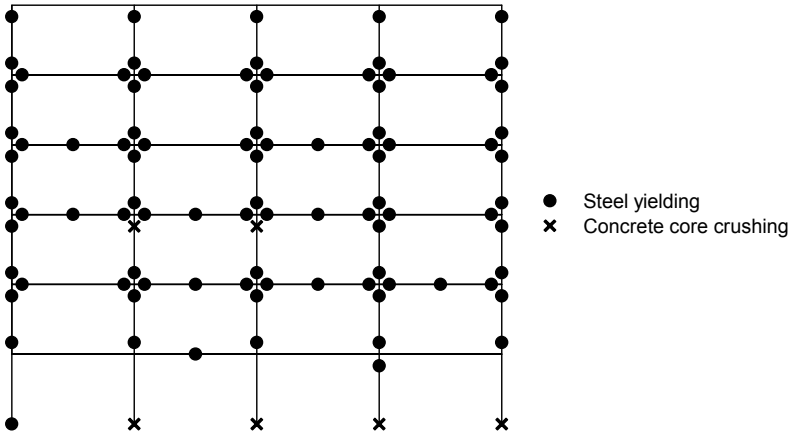

(b) Frame 2 (First Floor Only)

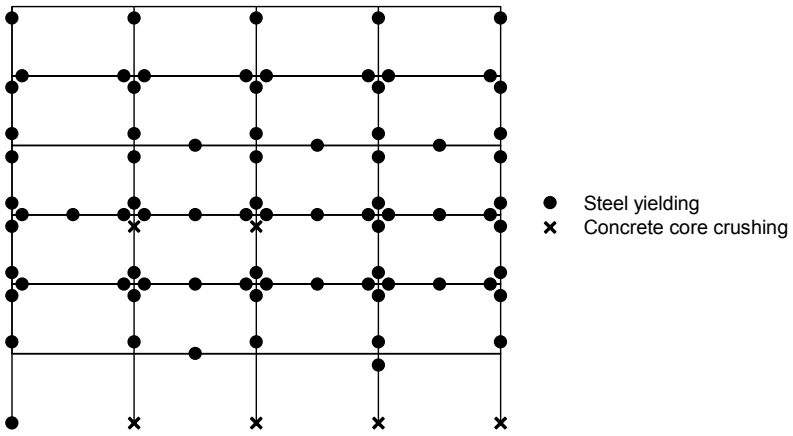

(c) Frame 3 (First and Fourth Floors)

Fig. 6-16: Damage scheme for different frames when subjected to Northridge earthquake record; (a) Frame 1 (Steel Only); (b) Frame 2 (First Floor Only); and (c) Frame 3 (First and Fourth Floors)

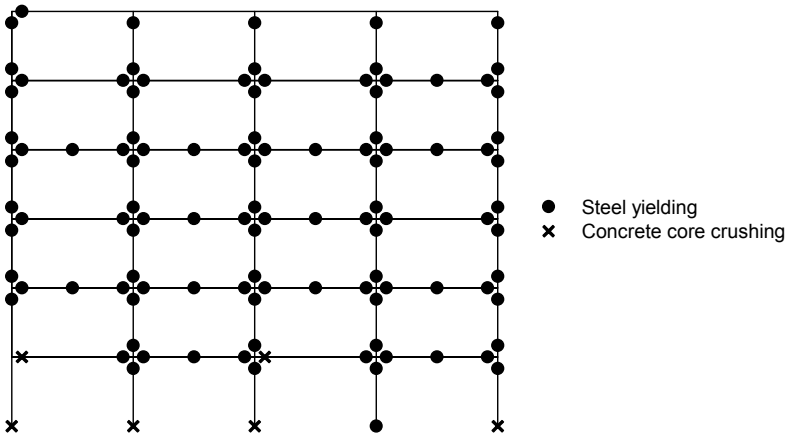

(a) Frame 1 (Steel Only)

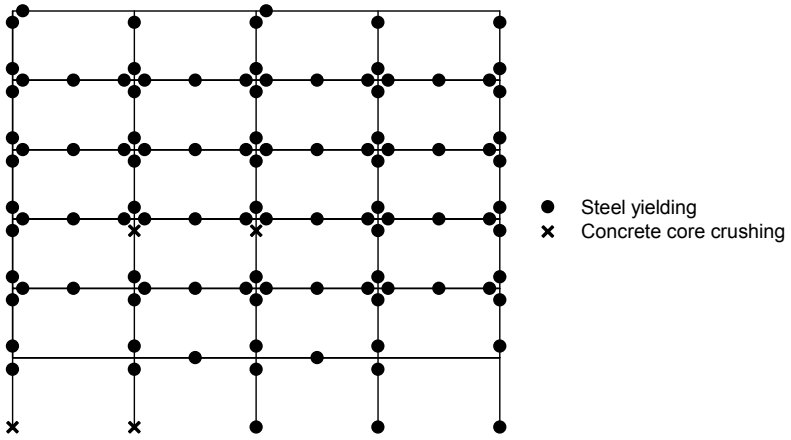

(b) Frame 2 (First Floor Only)

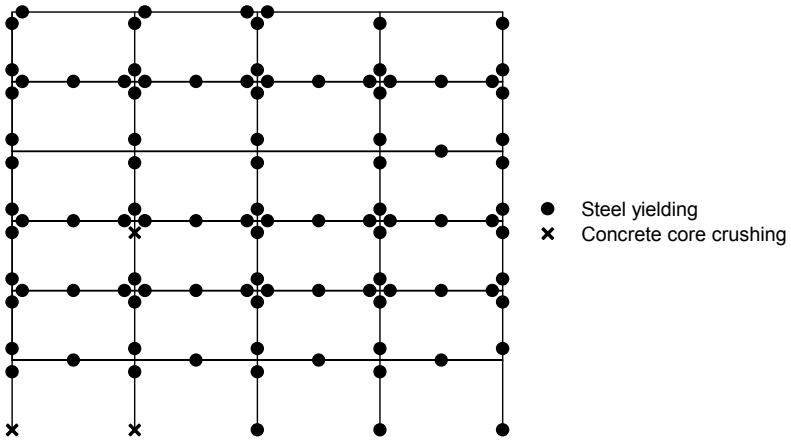

(c) Frame 3 (First and Fourth Floors)

Fig. 6-17: Damage scheme for different frames when subjected to San Fernando earthquake record; (a) Frame 1 (Steel Only); (b) Frame 2 (First Floor Only); and (c) Frame 3 (First and Fourth Floors)

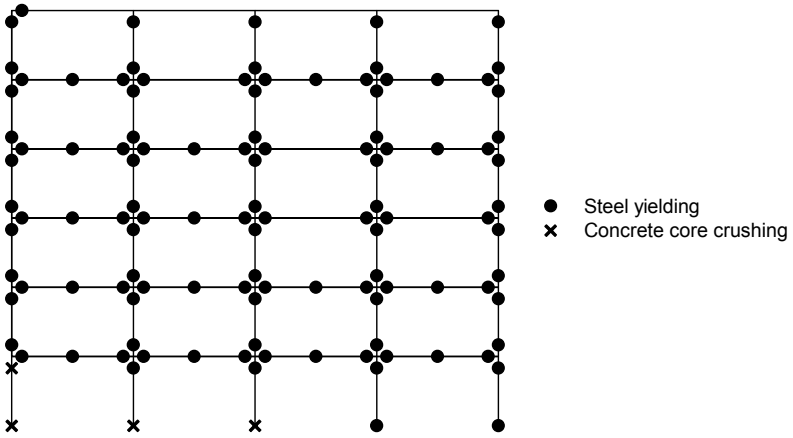

(a) Frame 1 (Steel Only)

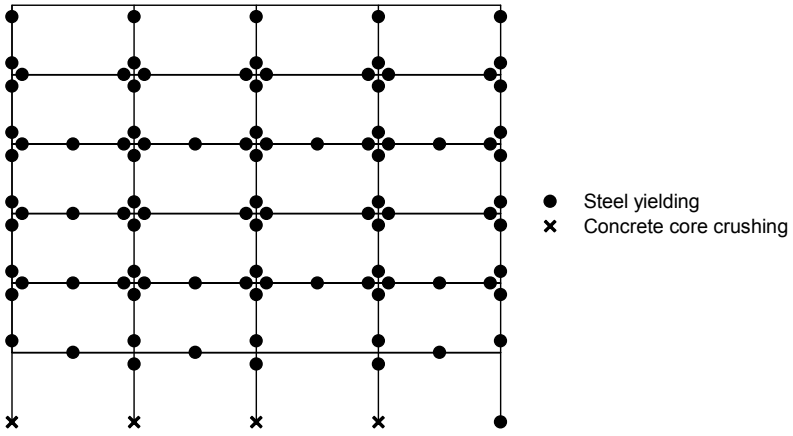

(b) Frame 2 (First Floor Only)

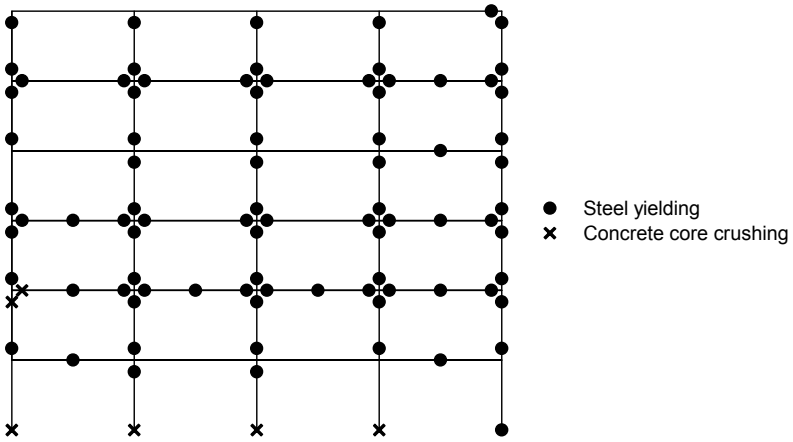

(c) Frame 3 (First and Fourth Floors)

Fig. 6-18: Damage scheme for different frames when subjected to Whittier earthquake record; (a) Frame 1 (Steel Only); (b) Frame 2 (First Floor Only); and (c) Frame 3 (First and Fourth Floors)

6.8.3 Maximum and Residual Drifts

MID, MRID, MRDR, and RRDR values at failure are used in this section to compare the behaviour of the three frames. Results of the three frames are given in **Table 6-2** and are illustrated in **Fig. 6-19**. The average MID for Frame 1 (steel RC frame) is found to be 8.40%. Frames 2 and 3 have lower average MID values 7.46 and 7.43, respectively. This shows the improvement in the frame behaviour by reducing the MID ratio.

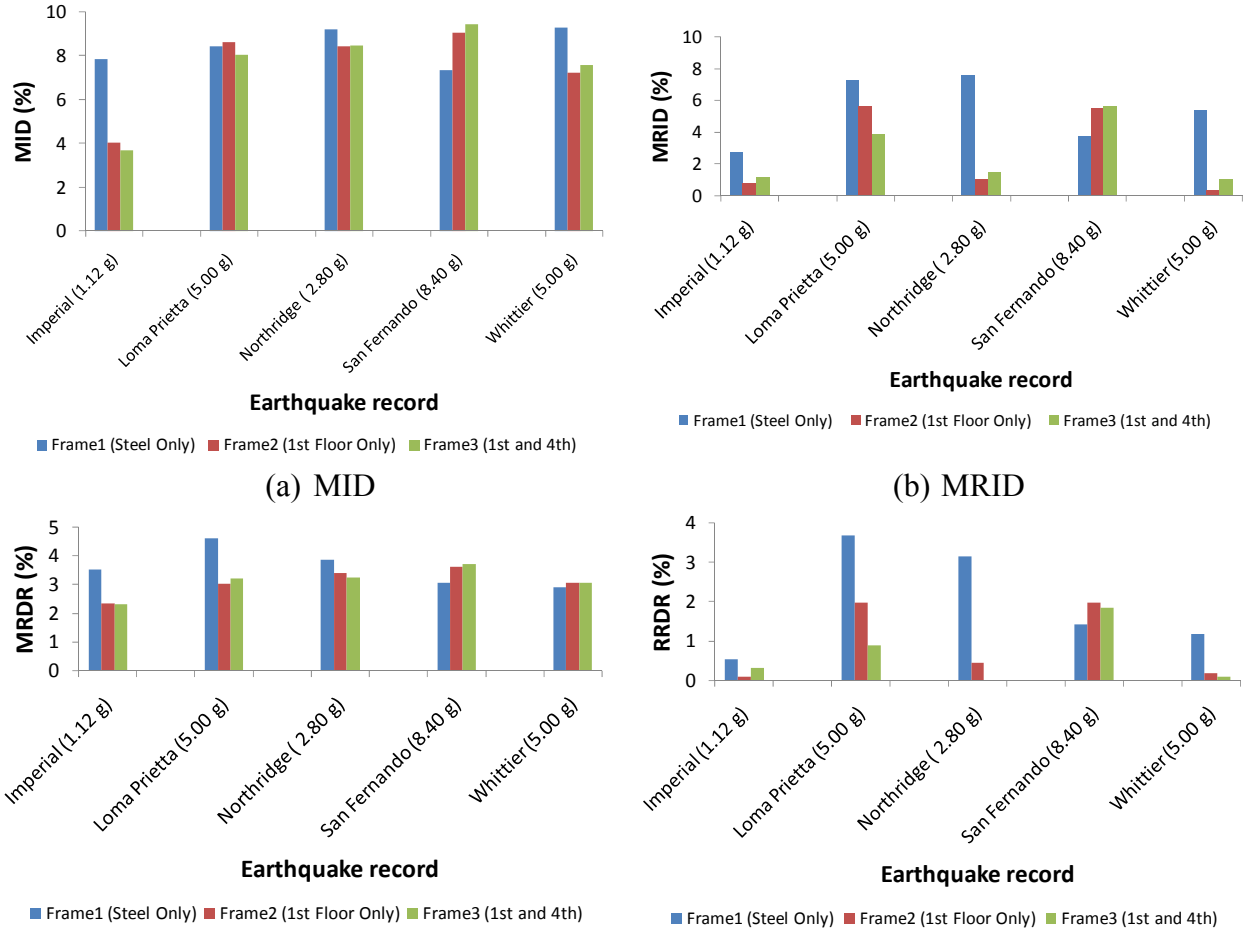

(a) MID (b) MRID

(c) MRDR (d) RRDR

Fig. 6-19: Maximum and residual drift ratios of the studied frames; (a) MID; (b) MRID; (c) MRDR; and (d) RRDR

Table 6-2: Comparison between the seismic performance of the three frames

Earthquake Record	Frame1 (Steel Only)				Frame2 (1st Floor Only)				Frame3 (1st and 4th)			
	MID	MRID	MRDR	RRDR	MID	MRID	MRDR	RRDR	MID	MRID	MRDR	RRDR
Imperial (1.12 g)	7.83	2.77	3.50	0.53	4.01	0.81	2.33	0.08	3.68	1.17	2.29	0.31
Loma Prietta (5.00 g)	8.41	7.25	4.60	3.68	8.60	5.66	3.01	1.96	8.02	3.89	3.21	0.88
Northridge (2.80 g)	9.18	7.56	3.85	3.15	8.43	1.05	3.37	0.44	8.45	1.47	3.23	0.01
San Fernando (8.40 g)	7.33	3.77	3.04	1.42	9.04	5.52	3.61	1.97	9.43	5.64	3.71	1.83
Whietter (5.00 g)	9.26	5.43	2.89	1.17	7.22	0.36	3.05	0.18	7.55	1.08	3.04	0.09
Average Value	8.40	5.36	3.57	1.99	7.46	2.68	3.08	0.93	7.43	2.65	3.10	0.62
Percent of Change	NA	NA	NA	NA	-11.20	-50.00	-13.96	-53.49	-11.63	-50.51	-13.40	-68.63

The improvement in the MRID value for frames 2 and 3 is found to be significant. The average MRID values of Frames 2 and 3 are 2.68% and 2.65% which are much lower (50.00% and 50.51%) of that of Frame 1 (5.36%). These values illustrate the significant improvement in the frame behaviour by adding the external SMA bars to the frame at the right locations.

The average MRDR is found to be 3.57% for Frame 1. This value is reduced by 13.96% for Frame 2 and by 13.40% for Frame 3. This confirms the reduction occurred in the MRID value of the frames. The RRDR significantly improved by adding the external SMA bars. The RRDR reduced from 1.99% for the steel RC frame to 0.93% and 0.62% for frames 2 and 3 respectively. These values correspond to percents of change equal to 53.49% and 68.63% for Frames 2 and 3, respectively.

These drift results in addition to the previously introduced damage schemes show that retrofitting an existing RC frame by adding external SMA bars at the right locations can lead to: (i) lower level of damage; (ii) small reduction in the MID and MRDR values (10%-15%); (iii) significant (50%-70%) reduction in the residual deformations represented by MRID and RRDR; and (iv) tolerating higher intensity earthquakes.

6.9 CONCLUSIONS

This chapter investigates the applicability of using external SMA bars to enhance the seismic performance of steel RC frames. A six-storey steel RC frame building is used as a reference for this study. The frame is assumed to be located in high seismic zone and is subjected to five

different scaled earthquake records. After determining the collapse intensity for each record, the analysis is performed again for other two retrofitted frames. The two frames are retrofitted using the proposed retrofitting technique. The first frame is retrofitted at its first floor, while the second frame is retrofitted at the first and fourth floors.

The performance of the three frames is compared based on the: (i) maximum tolerated earthquake intensity; (ii) level of damage; (iii) maximum drifts represented by MID and MRDR; and (iv) residual drifts represented by MRID and RRDR. The retrofitted frames showed lower level of damage at failure and higher tolerated earthquake intensities. The suggested retrofitting technique reduced the maximum drifts of the frame by 10% to 15%, and reduced the residual drifts by 50% to 70%. The two frames showed a similar behaviour. Thus, it is more economical to use the retrofit scheme of Frame 2, where the BCJs of the first floor only are retrofitted.

6.10 REFERENCES

ABAQUS, F.E.A. (2018) “ABAQUS Analysis user’s manual.” Dassault Systemes,Vélizy-Villacoublay, France, 2006.

ACI Committee 318 (2005) “Building Code Requirements for Structural Concrete (ACI 318-05) and commentary (ACI 318R-05).” American Concrete Institute, Farmington Hills MI, USA, 430 pp.

Alam, M.S., Nehdi, M. and Youssef, M.A. (009) "Seismic Performance of Concrete Frame Structures Reinforced with Superelastic Shape Memory Alloys." Smart Structures and Systems 5(5): 565-585.

Alam, M.S., Youssef, M.A., and Nehdi, M. (2007). “Utilizing Shape Memory Alloys to Enhance the Performance and Safety of Civil Infrastructure: a Review.” Canadian Journal of Civil Engineering, 34(9), 1075-1086.

Auricchio, F, and Sacco, E. (1997) “Superelastic shape-memory-alloy beam model.” Journal of Intelligent Material Systems and Structures, 8(6), 489-501.

Engindeni, M (2008) “Repair and Strengthening of Pre-1970 Reinforced Concrete Corner Beam-Column Joints Using CFRP Composites.” PhD dissertation, Georgia Institute of Technology, USA.

Hassan, W.M. (2011) “Analytical and Experimental Assessment of Seismic Vulnerability of Beam-Column Joints without Transverse Reinforcement in Concrete Buildings.” PhD dissertation, University of California at Berkely, USA.

IBC (2006) International Building Code, International Code Council, ICC, Country Club Hills, IL, USA, 679 pp.

Janke, L., Czaderski, C., Motavalli, M., and Ruth, J. (2005). “Applications of Shape Memory Alloys in Civil Engineering Structures - Overview, Limits and New Ideas.” Materials and Structures, 338(279), 578-592.

Paulay, T. and Priestley, M.J.N. (1992) “Seismic design of reinforced concrete and masonry buildings.” John Wiley & Sons, New York, NY, USA.

SeismoSoft (2018) "SeismoStruct - A computer program for static and dynamic nonlinear analysis of structures." Available from URL: http://www.seismosoft.com.

Youssef, M.A. and Elfeki, M.A. (2012) “Seismic Performance Concrete Frames Reinforced with Superelastic Shape Memory Alloys.” Journal of Smart Structures and Systems, 9(4), 313-333.

Chapter 7 Conclusions and Recommendations

7.1 SUMMARY AND CONCLUSIONS

Shape Memory Alloys (SMAs) have a unique ability to undergo large deformations and return to their undeformed shape upon unloading (superelasticity). Under cyclic loading, they have the ability to dissipate large amounts of energy and release them upon unloading. This is attributed to the flag shape stress-strain behaviour of SMA. In addition, they have good corrosion and fatigue resistance. These unique properties of SMAs have motivated researchers to utilize them as a retrofitting material in structural engineering applications.

This study aimed at proposing new flexural retrofitting technique for Reinforced Concrete (RC) elements. The idea of the proposed technique is based on attaching external unbonded SMA bars to the RC element. Investigation for the behaviour of the members and equations for deciding the optimum amount and length of the SMA bars is addressed in this study.

7.1.1 Flexural Behaviour of Superelastic Shape Memory Alloy Reinforced Concrete Beams during Loading and Unloading Stages

In Chapter 3, the flexural behaviour of SMA RC beams during loading/unloading stages is investigated. Analysis method that is based on the sectional analysis technique is used. The analysis method is first validated using available experimental results. An extensive parametric

study is then carried out to investigate the effect of different geometrical and cross-sectional parameters on the flexural behaviour of SMA RC beams. The studied parameters are: (i) cross-section reinforcement ratio (ρ_{SMAs}); (ii) ratio between the amount of SMA reinforcement to the amount of steel reinforcement (A_{SMAs}/A_s); (iii) cross-section height to width ratio (h/b); (iv) beam span-to-depth ratio (L/h); and (v) concrete compressive strength (f'_c).

The parametric study is performed on cantilever beams that are reinforced with SMA bars at the fixed end of the beams and regular steel bars elsewhere. For each of the studied parameters, nine different lengths are considered for the SMA length. These lengths are: $L/20$, $L/10$, $L/8$, $L/6$, $L/4$, $L/3$, $L/2$, and $L/1$, where L is the full length of the studied beam. For each of the studied beams, the developed sectional analysis method is used to obtain the moment-curvature relationships of its cross-sections. The moment-area method is utilized to obtain the load-displacement behaviour of the beams.

Results of the parametric study are compared based on: (i) load-displacement response; (ii) amount of residual deformations; (iii) change in flexural stiffness; and (iv) amount of dissipated energy. Results of the parametric study are then used in performing multiple linear regression analysis. A database is first created using the 144 beams analyzed in the parametric study. Inputs are chosen as: L_{SMAs}/L, A_{SMAs}/A_s, $\rho_{SMAs}/\rho_{s\text{-}min}$, $\rho_{SMAs}/\rho_{s\text{-}b}$, f'_c, h/b, LL, L/h. Outputs are chosen as: δ_r/δ_{max}, ($\delta_{y\text{-}s}/\delta_{cr\text{-}SMAs}$), EN_{SMAs}/EN_S. Correlation matrix is first determined to get the correlation between each pair of the variables. The final suggested regression models are reported and summarized in the form of simple equations. Changes in the amounts of residual displacements, flexural stiffness and dissipated energy can be estimated using the developed equations.

The use of the developed regression models is limited to slender cantilever beams with equal top and bottom reinforcement.

7.1.2 Flexural Behaviour of Reinforced Concrete Beams Retrofitted using External Unbonded Superelastic Shape Memory Alloy Bars.

In chapter 4, a new retrofitting technique for retrofitting RC beams using external unbonded SMA bars is proposed. The main idea is attaching the external bars to the beam using two external angles. Analysis started with developing a Finite Element (FE) model for the retrofitted beams. The FE model is validated using available experimental results. The experimental results included six internally reinforced RC beams and eight beams that are externally reinforced with steel and SMA bars. Good agreement between the developed FE model and the experimental results is obtained.

The suggested retrofitting technique is expected to improve the beam stiffness and strength, but not expected to reduce the amount of residual displacement at complete unloading. This is attributed the big difference in the modulus of elasticity value of internal steel bars and external SMA bars. Thus it is proposed to cut the internal steel bars and replace them with external SMA bars. Analysis of the original and retrofitted beam shows a reduction in the amount of residual deformations from 32 mm to 5 mm (84%) after cutting the internal steel reinforcement.

A simplified analysis method is then developed to capture the behaviour of the retrofitted beam. The method is based on the sectional analysis technique. The method is capable of analyzing

beams that are internally and/or externally reinforced with steel and/or SMA bars during the loading and unloading stages. Results of the proposed simplified method are first validated using the developed FE model. After validating the results, the simplified method is used to conduct an extensive parametric study.

The parametric study is carried out to investigate the behaviour of RC beams retrofitted using external unbonded SMA bars. The investigated parameters are: (i) the ratio between the added external SMA reinforcement to the amount of internal steel reinforcement in the beam (A_{SMA}/A_s); (ii) applied load level (δ_{max}/δ_y); and (iii) the ratio between the length of the used SMA bars to the span of the beam (L_{SMA}/L). The first two parameters are studied assuming that the length of the SMA bars is equal to the span of the beam. Nine different lengths are considered for the L_{SMA}/L.

Results of the parametric study are then put in a database format and used to perform multiple linear regression analysis. The database consisted of a total of 350 data sets (inputs and outputs). The inputs are: L_{SMA}/L, A_{SMA}/A_s, and load level, while the outputs are: δ_r/δ_{max}, M_{rt}/M_{org}, ST_{rt}/ST_{org}, $\delta_{y\text{-}rt}/\delta_{y\text{-}org}$, and $\delta_{max\text{-}rt}/\delta_{max\text{-}org}$. Correlation analysis is first performed to note the highly correlated parameters and their signs. The most statistically significant models are presented and summarized in the form of simple equations. These equations will help in determining the amount of residual displacement, change in beam strength and capacity, and the yielding and maximum displacements of the retrofitted beams. These equations can be used for simply supported slender beams with equal external top and bottom SMA reinforcement.

7.1.3 Flexural Behaviour of Reinforced Concrete Joints Retrofitted Using External Superelastic Shape Memory Alloy Bars.

Pre-1970s designed and built RC structures are deficient under seismic loads. Insufficient anchorage of the beam reinforcement into the joint area of the BCJ can be considered a main deficiency of these structures. Thus, there is an urgent need to retrofit these structures to ensure safety of the occupants. In addition, newly built structures may need to be retrofitted to minimize the seismic residual deformations in these structures. In chapter 5, the applicability of using the proposed retrofitting technique to retrofit beam-column joints (BCJs) is investigated.

A three-dimensional FE model is first developed using ABAQUS to simulate the behaviour of the retrofitted BCJ during the loading/unloading stages. Results of the developed model are first validated using available experimental results. Experimental results included the results of two experimentally tested BCJs that are internally reinforced with steel and SMA bars and eight externally reinforced concrete beams. Good agreement between experimental and analytical results is observed.

A retrofitted BCJ is assumed and analyzed using the developed FE model. The obtained results are compared to the results of the original BCJ. Results of the retrofitted beam show increase in the beam strength by 22% due to retrofitting. The amount of residual displacement is reduced by only 17% due to retrofitting. This small difference is attributed to the big difference in the modulus of elasticity value between steel and SMA. To improve the contribution of the SMA bars, it is proposed to cut the internal steel bars at the face of the column and replace them with

external SMA bars. The analysis is performed again for the retrofitted beam after cutting the internal bars. It is found that the residual displacement is reduced by 98%. The disadvantage of the proposed technique is the reduction in the beam strength (31%) and initial stiffness. This disadvantage can be overcome by increasing the amount of external SMA reinforcement.

Since it is a complicated process to model the BCJ in ABAQUS, a simplified model for the retrofitted BCJ is proposed. The proposed simplification is implemented in the Seismostruct software. The beams and the columns are modelled using frame elements. Two rigid arms are connected to each column to represent the angle connected in the joint area. Another two rigid arms representing the other angle are connected to the beam at a distance equal to the desired SMA length. The SMA bars are modeled between the rigid arms using truss elements. The reinforcement in the beam between the two rigid arms is cut to eliminate its contribution to the strength, stiffness, and residual deformations. Results obtained using the simplified model is validated using the ABAQUS model. Good agreement is observed between the two models. The simplified model is then used to conduct an extensive parametric study.

Results of the parametric study are then arranged in the form of a database. A total of 524 data sets are used in establishing the database. The database is then used to perform multiple linear regression analysis. After trying numerous models, the best four models for the four outputs (δ_r/δ_{max}, M_{rt}/M_{org}, ST_{rt}/ST_{org}, and EN_{rt}/EN_{org}) are presented. The four models are also summarized in the form of four simple equations to determine the optimum amount and length of the used SMA bars. The developed equations can be used for BCJs with equal column and beam dimensions, and equal top and bottom external SMA reinforcement.

7.1.4 Seismic Performance of Reinforced Concrete Frames Retrofitted Using External Superelastic Shape Memory Alloy Bars

In chapter 6, enhancing the seismic performance of RC framed structures using the suggested retrofitting technique is investigated. The simplified model previously described and validated in Chapter 5 is used to model the retrofitted BCJ of the frame structure. The steel RC frame designed by Youssef and Elfeki (2012) is used as the reference frame (Frame 1). The frame is a symmetric six-storey RC office building located in California, which is a high seismic region. The frame is modelled using the Seismostruct software.

Two potential retrofitting schemes are assumed for the retrofitted frames. The SMA bars are added to the BCJs of the first floor in one frame (Frame 2), and to the BCJs of the first and fourth floors of the other frame (Frame 3). The internal steel reinforcement of these BCJs is cut. The amount of SMA external reinforcement is chosen similar to the amount of internal steel reinforcement.

Eigen value analysis is first performed for the two retrofitted frames and compared to the results of the steel RC frame. No or negligible effect of the retrofitting technique on the fundamental period of the frame structure is observed. Incremental dynamic analysis is then performed for the three frames to observe the effect of increasing the spectral acceleration on the behaviour of the frames. The five earthquake records used by Youssef and Elfeki (2012) are used in the analysis.

Time history analysis is then performed for Frame 1 (steel RC frame) to determine the intensities of the five earthquakes at which collapse occur. The analysis is then repeated for the other two frames (Frames 2 and 3) at these collapse intensities. The performance of the three frames is then compared in terms of the damage scheme and the maximum and residual drifts.

7.2 MAJOR RESEARCH CONTRIBUTION

Developed new technique to retrofit RC frames to ensure ductility and reduced seismic deformations. This development was achieved through the following steps:

1- The flexural behaviour of RC beams internally reinforced with SMA bars during the loading and unloading stages is investigated.

2- A simple sectional analysis method to analyze RC beams internally and/or externally reinforced with SMA bars during loading and unloading stages is developed.

3- A new flexural retrofitting technique for RC beams and BCJs using external SMA bars is proposed.

4- A simplified FE model to model the behaviour of RC BCJs retrofitted using external SMA bars is developed.

5- Simple equations that can predict the changes in the flexural behaviour of beams and BCJs due to the suggested retrofitting technique are proposed.

6- The seismic performance of RC frames retrofitted using external SMA bars is investigated.

7.3 RECOMMENDATIONS FOR FUTURE STUDIES

1- Experimental investigations for RC cantilever beams internally reinforced with SMA bars in the maximum moment area.

2- Extending the developed sectional analysis method to investigate the behaviour of RC beams internally reinforced with SMA bars in conjunction with Fibre Reinforced Polymer (FRP) bars.

3- Experimental investigations for RC beams and BCJs retrofitted using external SMA bars.

4- Extending the developed simplified analysis method to investigate the behaviour of FRP RC beams and BCJs retrofitted using external SMA bars.

5- Experimental investigations for RC frames retrofitted using external SMA bars using shake table tests.

6- Investigating the behaviour of FRP RC frames retrofitted using external SMA bars.

Appendix I: Details of the Sectional Analysis Method Developed in Chapter 3

The flexural behaviour (moment-curvature) of steel and Shape Memory Alloy (SMA) Reinforced Concrete (RC) cross-sections is analytically investigated using a FORTRAN program developed by the authors. The program is based on the sectional analysis technique and it uses the fibre model methodology (Youssef and Rahman 2007; Elbahy et al. 2009). The main idea is dividing the cross-section into discrete number of horizontal fibres, **Fig. I-1**. Utilizing the one-dimensional constitutive relationship of each fibre, and taking into account the cross-section equilibrium and kinematics, the mechanical behaviour of the cross-section can be obtained.

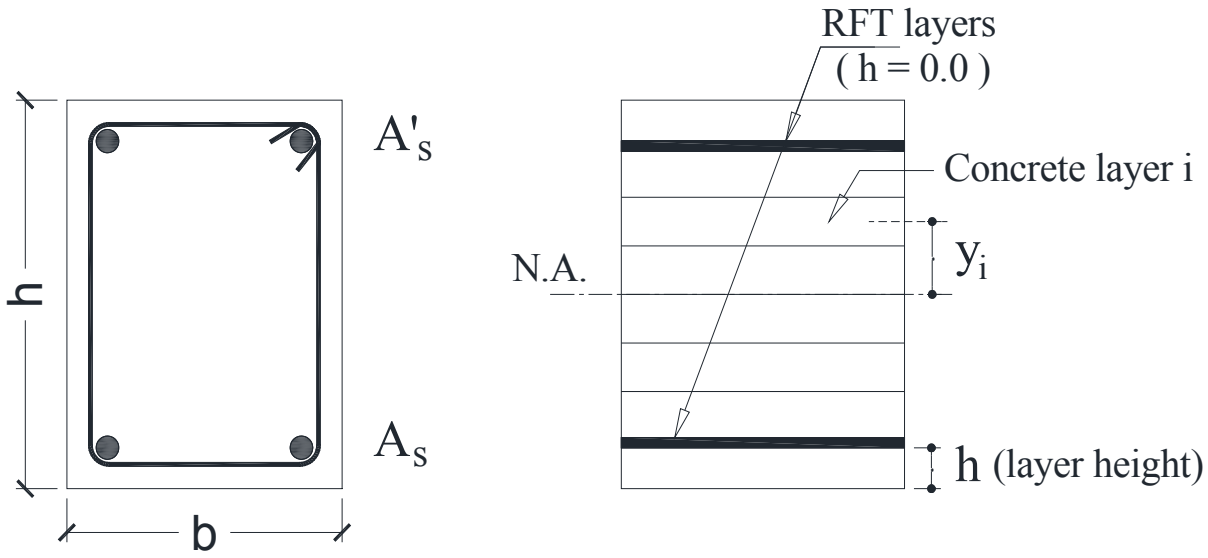

Fig. I-1: Fibre model

The developed program is capable of analyzing the cross-section under axial and/or flexural loading. Two different loading techniques can be used in the program: displacement-controlled loading and/or load-controlled loading. For both techniques, the load is applied in an incremental way. The analysis continues until one of the following conditions is achieved: (i) the desired loading level is reached; (ii) the concrete fibre in maximum compression reaches its crushing strain limit; or (iii) the used reinforcing bars reach their rupture strain limit. The relationship between the axial strain, the curvature, the moment, and the axial force can be written as:

[I-1]
$$\begin{pmatrix} \Delta M \\ \Delta P \end{pmatrix} = \begin{pmatrix} \sum E_i \, A_i \, y_i^2 & -\sum E_i \, A_i \, y_i \\ -\sum E_i \, A_i \, y_i & \sum E_i \, A_i \end{pmatrix} X \begin{pmatrix} \Delta \phi \\ \Delta \varepsilon_c \end{pmatrix}$$

where: ΔM =incremental increase in the moment acting on the cross-section, ΔP = incremental increase in the axial load force acting on the cross-section (equal to zero), $\Delta \Phi$ = incremental increase in cross-section curvature, $\Delta \varepsilon_c$ = incremental increase in the cross-section central axial strain, E_i = modulus of elasticity of layer i, A_i = area of layer i, and y_i = distance between the centre of gravity of layer i and the centre of gravity of the concrete cross-section.

The load is applied into two different stages. In the first stage (**Fig. I-2**), the axial load is applied in an incremental way while the moment is kept equal to zero. After reaching the specified axial load, stage II (**Fig. I-3**) starts by applying displacement load (curvature) in an incremental way

while keeping the axial load equal to the specified value. The steps involved in these stages can be summarized as follows.

I.1 Stage I

1) The initial axial load, concrete strain, and curvature are set to zero,
2) The initial E_i values for the concrete and steel layers are calculated,
3) A suitable load increment ΔP is chosen and applied to the cross section,
4) The incremental increase in the strain $\Delta\varepsilon_c$ is calculated using Equation [3-5],
5) The modified E_i values are calculated using the modified axial strain ($\varepsilon_c = \varepsilon_{c\text{-}previous} + \Delta\varepsilon_c$),
6) If the axial load is equal to the specified load, the values of ε_c and E_i are recorded and analysis of stage *II* starts, and
7) Analysis proceeds by repeating steps 4 to 6.

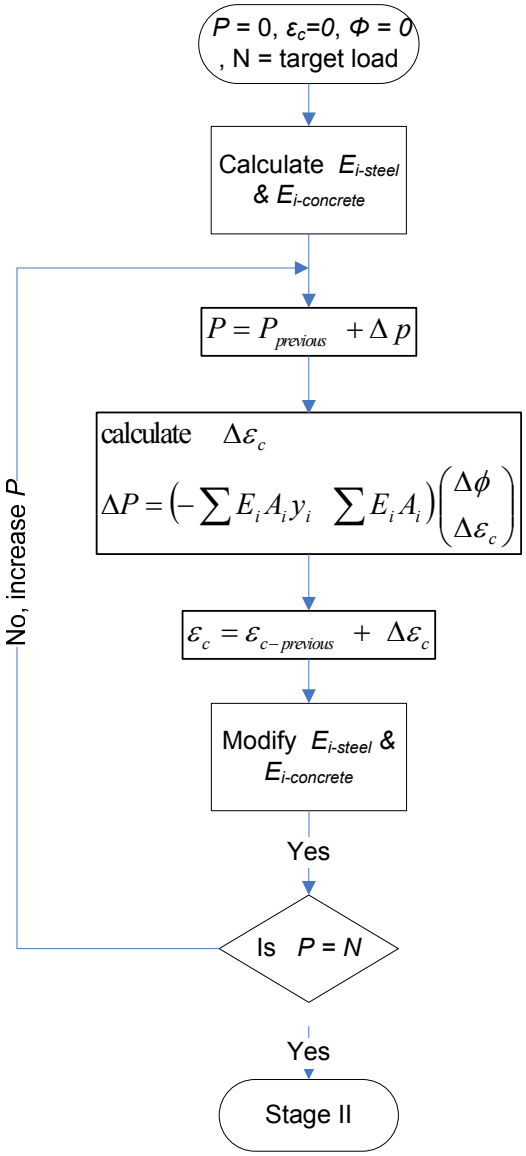

Fig. I-2: Flow chart for stage I of the fibre model analysis

I.2 Stage II:

The axial load is kept constant at the desired value recorded in stage *I* and the applied curvature is increased from zero to a specified value. A displacement approach is selected to capture the sectional behaviour after reaching the maximum compressive strength. The steps involved in this

stage have to be conducted twice to define the sectional behaviour when subjected to positive and negative curvatures and are summarized below:

1) The values of ε_c and E_i are set equal to those recorded in step 6 of analysis stage *I*,
2) A suitable curvature increment $\Delta\Phi$ is chosen and applied to the section,
3) The modified E_i values are calculated using the axial strain of each layer ($\varepsilon_{ci} = \varepsilon_{c\text{-}previous} \pm \Delta\Phi\, y_i$),
4) $\Delta\varepsilon_{ci}$ is calculated from Equation [3-5], such that ΔP is equal to zero ($\varepsilon_c = \varepsilon_{c\text{-}previous} + \Delta\varepsilon_c$),
5) $\Delta\varepsilon_c$ is checked against a predefined tolerance. If the error is higher than the tolerance, steps 3 and 4 are repeated,
6) The value of ΔM is calculated from Equation [3-5]. The total moment on the section is $M = M_{Previous} + \Delta M$. At this moment stage, the total concrete compressive forces, the forces in the steel layer and the centre of gravity of these forces are recorded, and
7) The analysis is repeated by applying a curvature increment $\Delta\Phi$ and repeating steps 3 to 6.

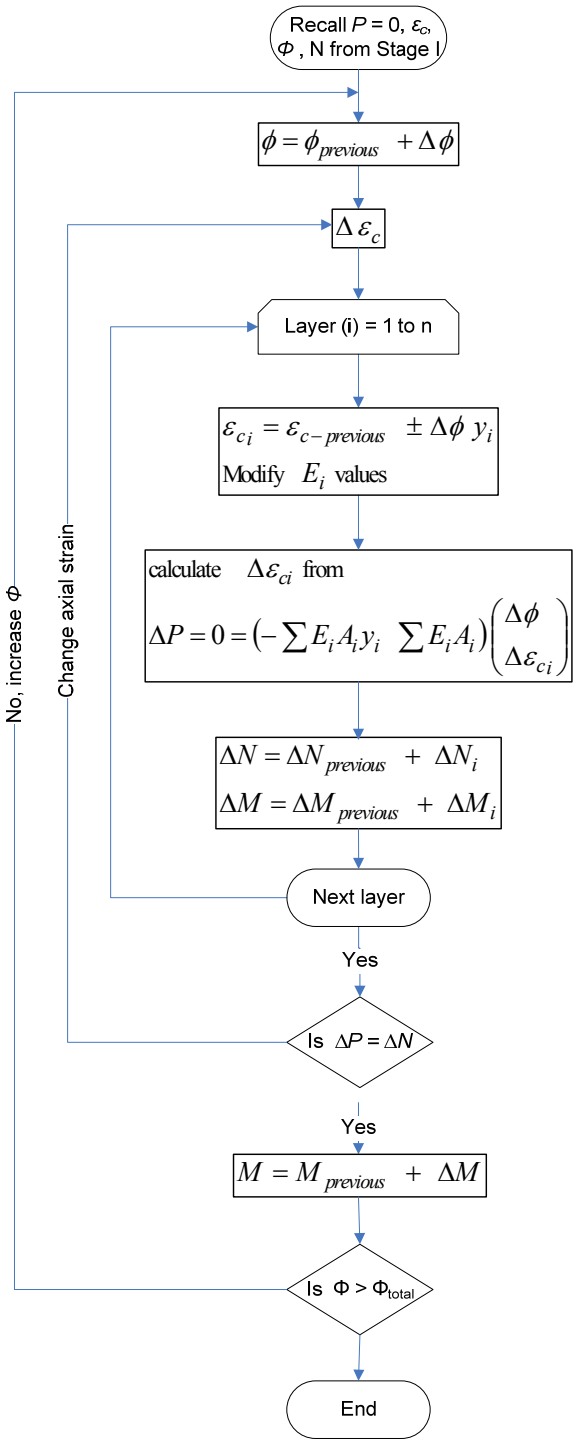

(a) Stage II

Fig. I-3: Flow chart for stage II of the fibre model analysis

Two main assumptions are used in the developed program: (i) plane sections remain plane (i.e. linear strain distribution); and (ii) perfect bond exists between concrete and the reinforcement. The program can analyze the behaviour of cross-sections reinforced with steel bars, SMA bars, or both steel and SMA bars.

For analysis performed in this study, displacement-controlled flexural loading (i.e. curvature) is used. The load is incrementally applied on the studied cross-sections while keeping the applied axial load equal to zero. Using similar technique during the unloading stage, the load (curvature) is incrementally removed from the cross-section.

I.3 CONCRETE STRESS-STRAIN MODEL UNDER COMPRESSION

Different stress-strain models are available to model the concrete behaviour under both compression and tension loadings. These models vary in their accuracy and complexity. Thus, a good balance between the desired accuracy and the model complicity is desired to achieve optimum performance. The model developed by Scott et al. (1982), **Fig. I-2**, is used to model the concrete behaviour under compression loading. The model represents a good balance between simplicity and accuracy (Youssef and Ghobarah 1999). As shown in **Fig. I-2** and given by **Eq. I-2**, the model consists of three parts: (i) pre-peak parabolic ascending part; (ii) post-peak linear descending part; and (iii) post-peak constant-stress part. Highly confined concrete is assumed in this study to allow the SMA bars to undergo large deformations before concrete crushing in compression.

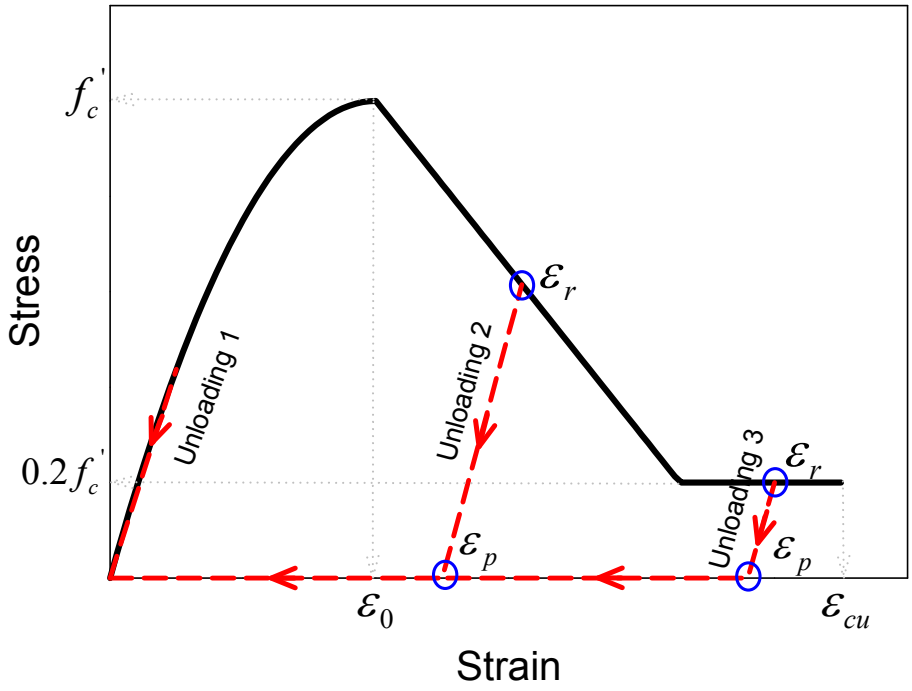

Fig. I-2: Stress-strain model for concrete in compression during loading/unloading stages.

[I-2a] $$f_c = K_h f_c' \left[2.0\left(\frac{\varepsilon_c}{0.002}\right) - \left(\frac{\varepsilon_c}{0.002}\right)^2 \right] \qquad 0 \le \varepsilon_c \le 0.002$$

[I-2b] $$f_c = K_h f_c' [1 - Z(\varepsilon_c - 0.002)] \qquad \varepsilon_c \ge 0.002 \quad and \quad f_c \ge 0.2 f_c'$$

[I-2c] $$Z = \frac{0.5}{\frac{3 + 0.29 f_c'(\text{MPa})}{145 f_c'(\text{MPa}) - 1000} + 0.75 \rho_{stirrups} \sqrt{\frac{h'}{S_h}} - 0.002 K_h}$$

[I-2d] $$K_h = 1 + \frac{\rho_{stirrups}\ f_y}{f_c'}$$

where: f_c = concrete compressive stress, Z = slope of compressive strain softening branch, ε_c = concrete compressive strain, K_h = confinement factor, h' = width of the concrete core measured to the outside of ties, S_h = centre-to-centre spacing of the ties or hoop sets, $\rho_{stirrups}$ = ratio of volume of stirrup reinforcement to volume of concrete core measured to outside of the stirrups, and f_y = reinforcement yielding stress.

Behaviour of concrete in compression during the unloading stage is assumed to follow the model proposed by Karsan and Jirsa (1969), **Fig. I-2**. This model relates the normalized loading strains to the strains at complete unloading through a quadratic formula, **Eq. [I-3a]**.When unloading starts, the unloading path follows a straight line. This line connects the unloading start strain, ε_r, to the first zero-stress strain value, ε_p. At high compression strains, **Eq. [I-3a]** exhibits unreasonable behaviour. Thus, **Eq. [I-3b]** is added to the model to ensure positive value of the unloading modulus of elasticity at high compressive levels. After reaching ε_p, the strains continue to reduce while keeping the stress value equal to zero. This continues till reaching the point of zero strain.

[I-3a] $$\frac{\varepsilon_p}{\varepsilon_0} = 0.145\left(\frac{\varepsilon_r}{\varepsilon_0}\right)^2 + 0.13\left(\frac{\varepsilon_r}{\varepsilon_0}\right)\left(\frac{\varepsilon_r}{\varepsilon_0}\right) < 2$$

[I-3b] $$\frac{\varepsilon_p}{\varepsilon_0} = 0.707\left(\frac{\varepsilon_r}{\varepsilon_0} - 2\right) + 0.834\left(\frac{\varepsilon_r}{\varepsilon_0}\right) \geq 2$$

where: ε_p = concrete strain at which unloading stress first reaches zero, ε_0 = concrete strain at maximum compressive loading stress f'_c, ε_r = concrete strain when unloading starts.

I.4 CONCRETE STRESS-STRAIN MODEL UNDER TENSION

Behaviour of concrete under tension loading is assumed to follow the model proposed by Stevens et al. (1987), **Fig. I-3**. As shown in the figure, the model is divided into two main parts: Pre-cracking zone, and post-cracking zone. For the pre-cracking zone, the concrete behaves in a linear fashion up to the cracking stress f_{cr}. As soon as the cracking stress is reached, significant reduction in the stress value is observed. Post-cracking behaviour follows the softening relationship given by **Eq. [I-4]**. This relationship is adjusted to include the simplification proposed by Youssef and Ghobarah (1999). This simplification eliminates the effect of both the amount of reinforcement and its inclination.

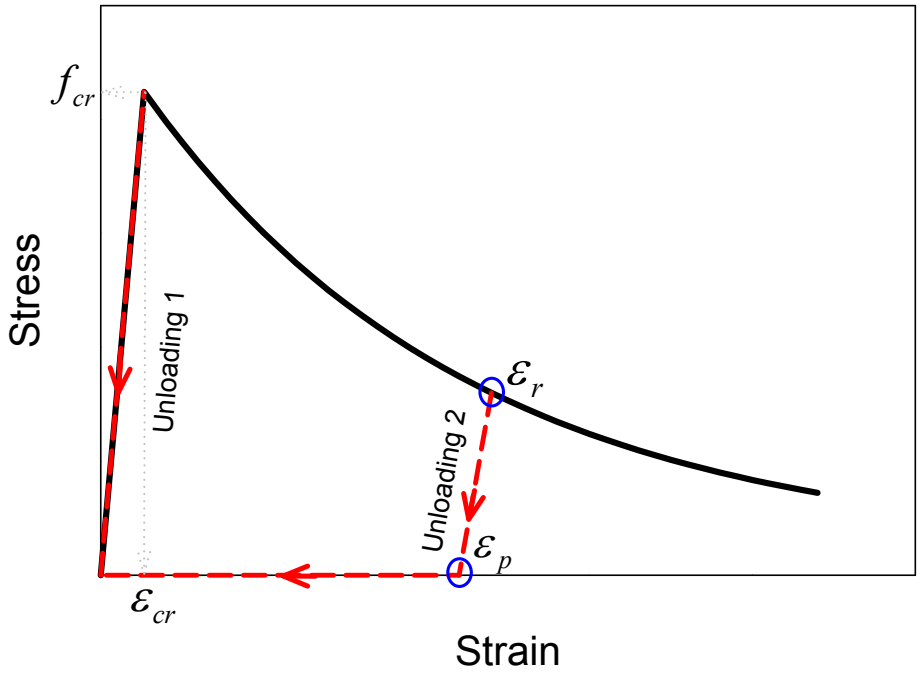

Fig. I-3: Stress-strain model for concrete in tension during loading/unloading stages.

[I-4] $$f_t = f_{cr}\left[0.95 \text{ x } e^{-1000 \text{ x } (\varepsilon_c - \varepsilon_{cr})} + 0.05\right] \qquad \varepsilon_c \geq \varepsilon_{cr}$$

where: f_t = concrete tensile stress, f_{cr} = concrete cracking stress, ε_c = concrete strain, and ε_{cr} = concrete cracking strain.

If unloading starts before reaching f_{cr}, the concrete behaves in a linear fashion exactly as the loading stage. If unloading starts after reaching f_{cr}, the unloading path is assumed to follow a straight line connecting the strain at which unloading starts, ε_r, to the point at which zero-stress value is first reached, ε_p. The unloading path slope is assumed to have a value equal to the modulus of elasticity of concrete. After reaching the zero-stress point, the strain continues to decrease while the stress is kept equal to zero. This continues until reaching the point at which zero-stress corresponds to zero-strain. It should be noted that the significant drop in the stress value after cracking makes the contribution of the concrete tensile resistant to the overall all behaviour is very minor.

I.5 STEEL STRESS-STRAIN MODEL

The behaviour of steel material is assumed to follow bilinear stress-strain under both tension and compression loading, **Fig. I-4**. The model is divided into two main regions: pre-yielding and post-yielding regions. In the pre-yielding region, the material behaves elastically with a modulus of elasticity $E_{y\text{-}s}$ until reaching its yielding strain, $\varepsilon_{y\text{-}s}$. As soon as the strain exceeds $\varepsilon_{y\text{-}s}$ (i.e. post-yielding region), the modulus of elasticity the material is significantly reduced $E_{u\text{-}s}$. The material continues to behave with $E_{u\text{-}s}$ until reaching its rupture strain, $\varepsilon_{u\text{-}s}$.

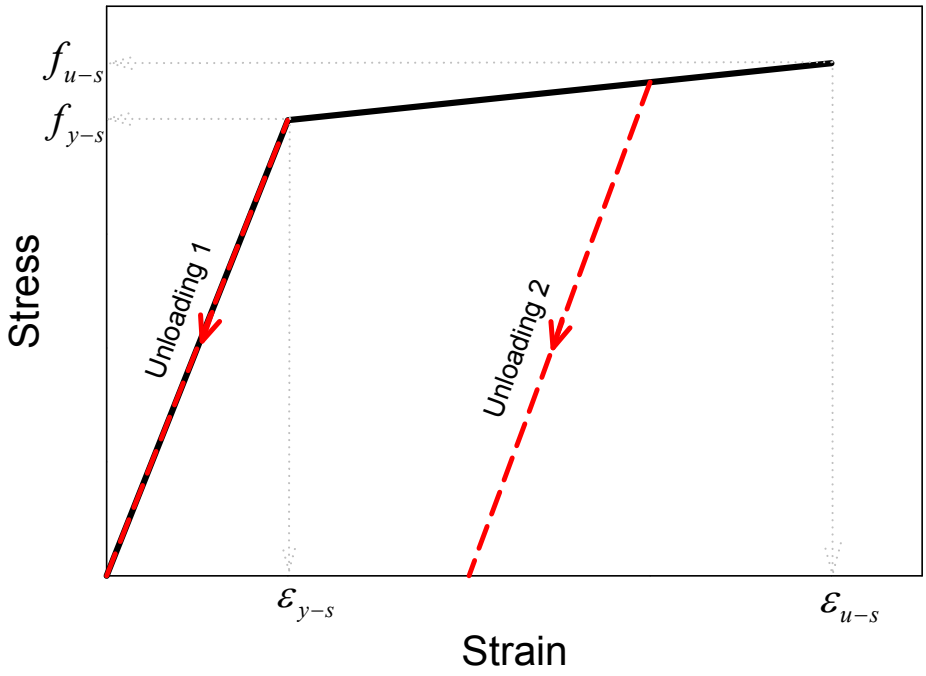

Fig. I-4: Stress-strain model for steel during loading/unloading stages.

If unloading starts with the pre-yielding zone, the material behaves elastically with a modulus of elasticity $E_{y\text{-}s}$ with no residual deformations at complete unloading, **Fig. I-4**. If the unloading starts at strain greater than $\varepsilon_{y\text{-}s}$ (i.e. post-yielding zone), the material will follow a linear unloading path that also has a slope equal to $E_{y\text{-}s}$. The material will keep following this unloading path until either unloading stops or yielding on the other side of the stress-strain relationship occurs (i.e. tension unloading up to compression yielding or compression unloading up to tension unloading). If yielding occurs on the other side, a significant reduction in the material modulus of elasticity is observed (i.e. $E_{u\text{-}s}$). Residual deformations are expected in this case. The amount of residual deformations is proportional to the strain value at which unloading starts.

I.6 SMA STRESS-STRAIN MODEL

There are different types of SMAs available in the market. These types differ in their chemical composition, which in turns changes their mechanical properties. Among these different types of SMAs, Nickel-Titanium (Ni-Ti) based SMA is found to be the most appropriate type for structural engineering applications. This is attributed to: (i) its high recoverable strain (i.e. big superelastic range); (ii) its unique behaviour under cyclic loading; (iii) its good resistance to fatigue and corrosion; and (iv) its austenite phase stability at ambient temperature (Janke et al. 2005) . Although Ni-Ti is relatively considered an expensive type of SMAs, The suggestion made by researchers to use SMA only in critical areas of the structure helps in reducing the overall cost. Thus, the term SMA in this study refers to Ni-Ti based SMA.

The stress-strain model of SMA consists of four linear branches that are connected by smooth curves (Alam et al. 2007), **Fig. I-5**. To simplify the modelling process of the SMA material, the smooth curves connecting the linear branches are ignored. Linear branches are assumed to directly intersect. As the loading starts, the material behaves elastically with a modulus of elasticity $E_{cr\text{-}SMA}$ until reaching the SMA critical stress $f_{cr\text{-}SMA}$. $f_{cr\text{-}SMA}$ is a critical stress value as it represents the start of the martensite stress induced transformation. If loading continues beyond this critical limit (i.e. strain exceeds the critical strain value, $\varepsilon_{cr\text{-}SMA}$), the material stiffness significantly reduces and it behaves with a modulus of elasticity E_{p1}. E_{p1} value is typically within the range of 10% to 15% of $E_{cr\text{-}SMA}$. As the applied strain continues to increase, the material keeps behaving with E_{p1} until reaching the martensite stress-induced strain ε_{p1}. If loading exceeds this strain limit, the material regains some of its initial stiffness because of the phase

transformation to martensite. The new stiffened modulus of elasticity E_{p2} value typically lies within the range of 50% to 60% of $E_{cr\text{-}SMA}$. If loading continues beyond this limit, the material strain is expected to reach another critical strain value $\varepsilon_{y\text{-}SMA}$ which represents real yielding of SMA. If the SMA material yields, another significant reduction in the material stiffness is observed. At this stage, the material behaves with a modulus of elasticity $E_{u\text{-}SMA}$, which has a value typically as low as 3% to 8% of $E_{cr\text{-}SMA}$.

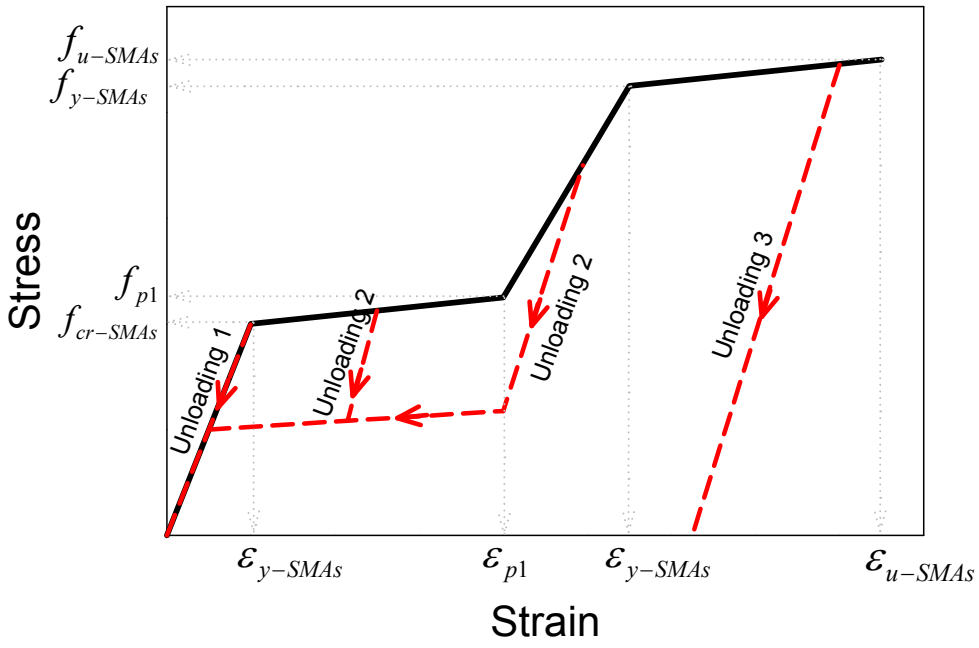

Fig. I-5: Stress-strain model for SMAs during loading/unloading stages.

The behaviour of SMA during the unloading stage is considered unique when compared to steel. Its behaviour during unloading can be divided into three main unloading paths, **Fig. I-5**. The unloading path the material will follow is mainly dependent on strain value at which unloading

starts. If unloading starts before reaching $\varepsilon_{cr\text{-}SMA}$, the material behaves elastically with $E_{cr\text{-}SMA}$ similar to the loading stage (i.e. unloading path 1). If unloading starts between $\varepsilon_{cr\text{-}SMA}$ and $\varepsilon_{y\text{-}SMA}$, the material will follow unloading path 2. The main advantage of SMA is clear during this stage (i.e. unloading path 2). The material almost recovers full deformations and return to their undeformed shape upon unloading (i.e. superelasticity property). This recovery is attributed to the reverse transformation from martensite to austenite phase.

The material will either recover the full deformations or it will keep some minor residual deformations. This can be decided from the experimental results obtained during the cyclic testing of the SMAs bars. Thus, this needs to be accounted for in the analysis. In the developed program, three values are used to define the amount of residual deformations: (i) maximum unloading strain at which zero residual deformations are obtained; (ii) maximum unloading strain at which maximum residual deformations are obtained; and (iii) maximum residual strain. Based on the strain level reached in the analysis, a linear interpolation is performed using the above mentioned three values to determine the amount of residual deformations in the analysis.

If unloading starts after reaching the SMAs real yielding, significant residual deformations are expected to be observed (i.e. unloading path 3). This is similar to the case of yielded steel. As shown in the figure, the material follows a linear unloading path that connects the point at which unloading starts to the point at which zero-stress is reached. It is very clear from the figure that loading the material beyond its real yielding limit results in full loss of the material superelastic behaviour. This causes significant undesired residual deformations. Thus, in order to benefit from the SMA superelastic behaviour, the SMs should be loaded to strain levels smaller than it is

real yielding strain. In this study, the authors ensured that the analysis performed on the SMA RC beams did not reach the real yielding limit of SMA.

I.4 REFERENCES

Elbahy Y.I., Youssef M.A., Nehdi M. (2009). "Stress Block Parameters for Concrete Flexural Members Reinforced with Superelastic Shape Memory Alloys." Journal of Materials and Structures, 42(10), 1335-1351.

Youssef, M.A., and Rahman, M. (2007). "Simplified seismic modeling of reinforced concrete flexural members." Magazine of Concrete Research, 59(9), 639-649.

Scott, B.D.; Park, R.; and Priestley, M.J.N. (1982). "Stress-Strain Behavior of Concrete Confined by Overlapping Hoops at Low and High Strain Rates." ACI journal, 79(1), 13-27.

Youssef, M., and Ghobarah, A. (1999). "Strength Deterioration due to Bond Slip and Concrete Crushing in Modeling of Reinforced Concrete Members." ACI Structural Journal, 96(6), 956-967.

Karsan, I. D., and Jirsa, J. O. (1969). "Behavior of Concrete under Compressive Loading." ASCE Journal (Structural Division), 95(12), 2543-2563.

Stevens, N.J., Uzumeri, S.M., and Collins, M.P. (1987). "Analytical Modeling of Reinforced Concrete Subjected to Monotonic and Reversed Loading." Publication No. 87-1, University of Toronto, 3634 p.

Alam, M.S., Youssef, M.A., and Nehdi, M. (2007). "Utilizing Shape Memory Alloys to Enhance the Performance and Safety of Civil Infrastructure: a Review." Canadian Journal of Civil Engineering, 34(9), 1075-1086.

Janke, L., Czaderski, C., Motavalli, M., and Ruth, J. (2005). "Applications of Shape Memory Alloys in Civil Engineering Structures - Overview, Limits and New Ideas." Materials and Structures, 338(279), 578-592.

Appendix II: Validation of The Sectional Analysis Method Developed in Chapter 3

Results of the experimental work performed by Youssef et al. (2008) are used to validate the accuracy of the results obtained by the developed method. Two large scale Beam-Column Joints (BCJs) are constructed and tested under reversed-cyclic loading applied at the free beam tip. The two joints are identical in dimensions and reinforcement details except the type of reinforcement used in the plastic hinge region, **Fig. II-1**. At the plastic hinge region, one of the two joints (BCJ1) is reinforced with regular steel bars, while the second joint (BCJ2) is reinforced with superelastic SMA bars. Since the purpose of this section is validating the accuracy of the developed program and the accuracy of using of moment-area method with SMA RC beams, the BCJs are simplified and modelled as cantilever beams. This simplification is based on the results obtained from the finite element model developed by Elbahy et al. (2010). This model is built for BCJ2 using the Seismostruct software (Seismosoft 2018), where static push-over analysis is performed for the joint.

Vertical deformation at the beam tip can be divided into three components that are associated with: (i) column flexural rotation; (ii) beam-column joint shear deformation; and (iii) beam flexural rotation. Results obtained from the finite element model showed that the column behaved in an elastic manner and had no cracks. Its rotation at the beam-column joint reached an estimated maximum value of 0.00018 rad. The joint was detailed according to the current

seismic standards and its shear deformations reached a maximum value of 0.00045 rad. The maximum contribution of those two components to the beam tip deformation is 1.14 mm which is about 3.00% of the maximum measured deformation. This insignificant contribution of the two components validates the assumption of modelling the BCJs as cantilever beams.

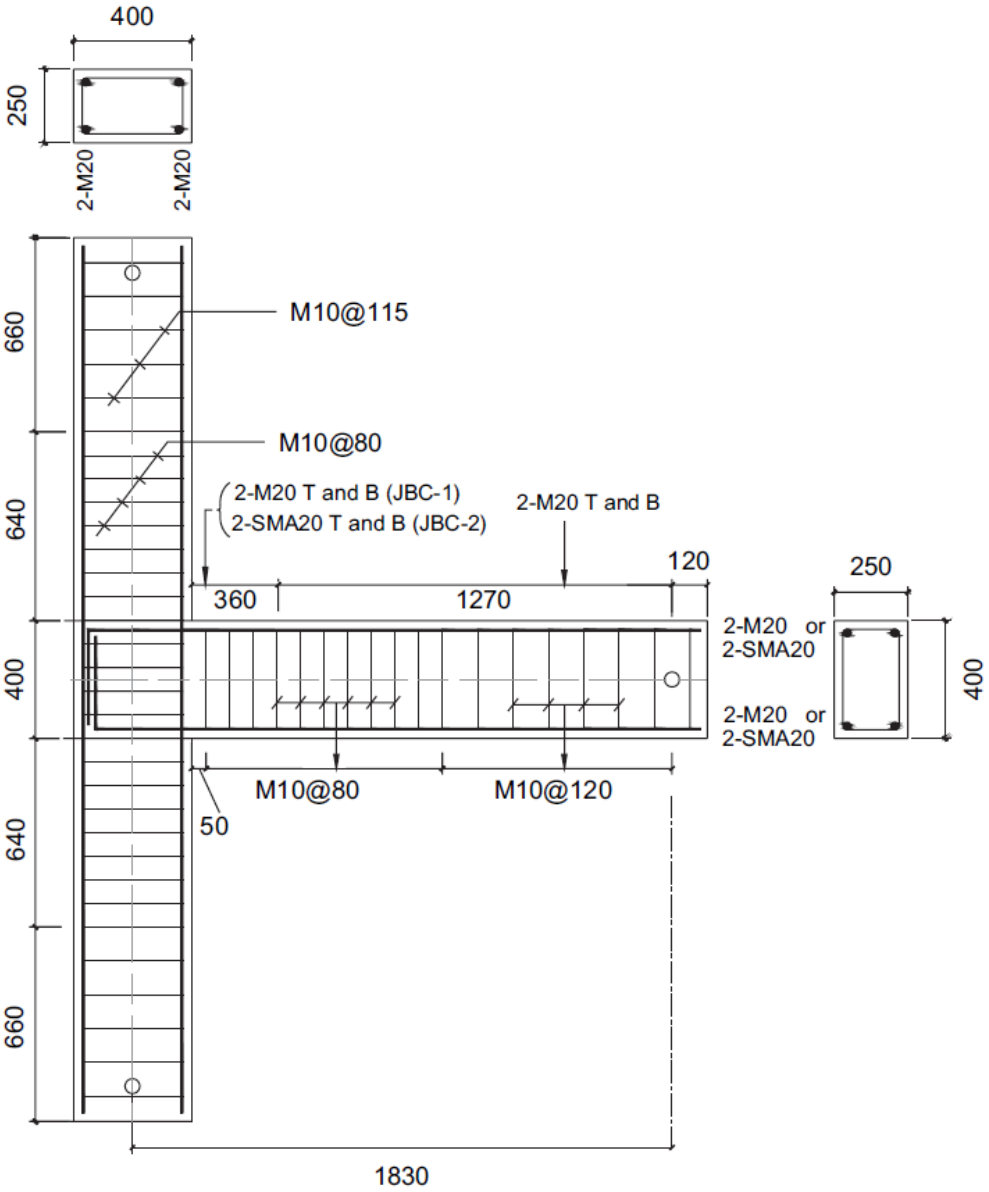

Fig. II-1: Reinforcement details of tested BCJs (Youssef et al 2008).

The geometry of the two joints beams are identical, **Fig. II-1**. The beams have 1765 mm span, 40 mm cross-section height, and 250 mm cross-section width. Amounts and arrangements of transverse reinforcement are also identical for the two beams. Stirrups are 10M in diameter and are spaced at 80 mm for 800 mm length adjacent to the support and spaced at 120 mm elsewhere. The type of longitudinal reinforcement in the plastic hinge regions of the two beams is different. Two superelastic SMAs bar (20.6 mm diameter) are used at the top and bottom of the plastic hinge region of BCJ2 beam, while 2-20M steel bars are used at the top and bottom of BCJ1 beam. The plastic hinge region length is calculated as 360 mm from the face of the column (i.e. fixed support). Regular 2-20M steel bars are used outside the plastic hinge region of BCJ2 beam. Steel couplers are used to connect the SMA bars to the steel bars.

Average concrete compressive strength is found to be 53.50 MPa for BCJ1 and 53.70 MPa for BCJ2. Average split cylinder tensile strength is found to be 3.50 MPa for the BCJ1 and 2.80 MPa for BCJ2. Steel Reinforcing bars of JBC1 beam have yield strength of 520 MPa, ultimate strength of 653 MPa, and a modulus of elasticity of 198 GPa. Steel reinforcing bars of JBC2 beam have yield strength of 450 MPa, ultimate strength 650 MPa, and a modulus of elasticity of 193 GPa. Steel of the stirrups has a yield strength of 422 MPa and ultimate strength of 682 MPa.

Youssef et al. (2008) determined the mechanical properties of the superelastic SMAs bars by experimentally testing them under cyclic loading. The SMA bars critical stress is 401 MPa at a critical strain of 0.75%. The modulus of elasticity is calculated as 62.5 GPa. The residual deformation is determined as 0.73% when the SMA bar was loaded up to 6.0% strain. In this study, envelop of the SMA test results is used to obtain an idealized stress-strain relationship,

Fig. II-2. The idealized relationship is then used in the developed program to accurately model the behaviour of the SMA bars.

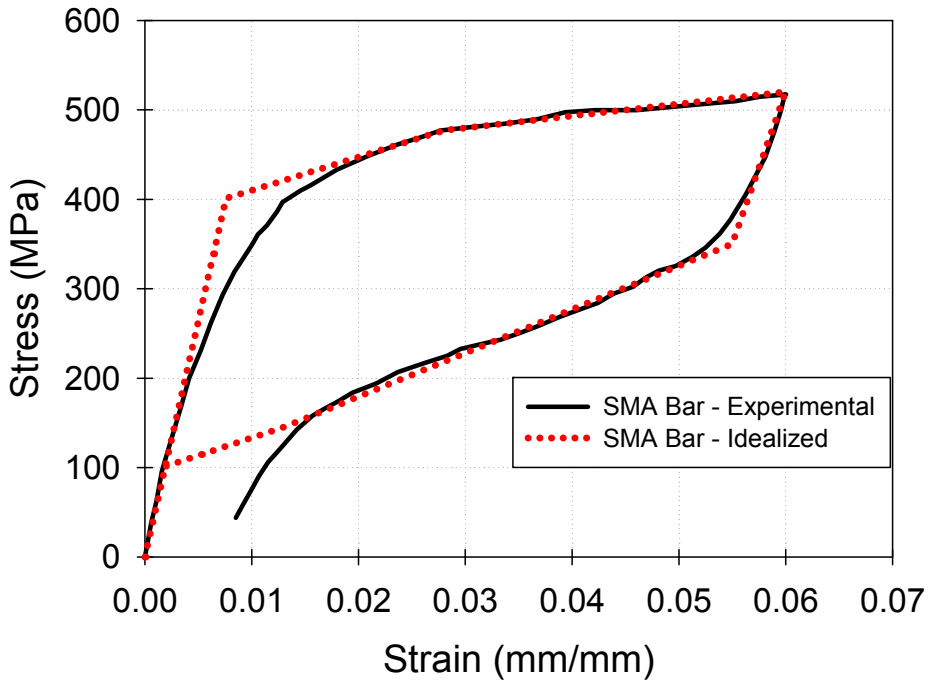

Fig. II-2: Idealized stress-strain model for SMAs bars.

Moment-curvature analysis is first performed for different cross-sections of the two beams. Considering the type of longitudinal reinforcement and taking into account the effect of concrete confinement (i.e. stirrups spacing), moment-curvature analysis is performed for two cross-sections of BCJ1 beam and for three different cross-sections of BCJ2 beam. Results of BCJ2 beam are shown in **Fig. II-3**. Obtained results are then utilized in the moment-area method to predict the load-displacement response of the two beams.

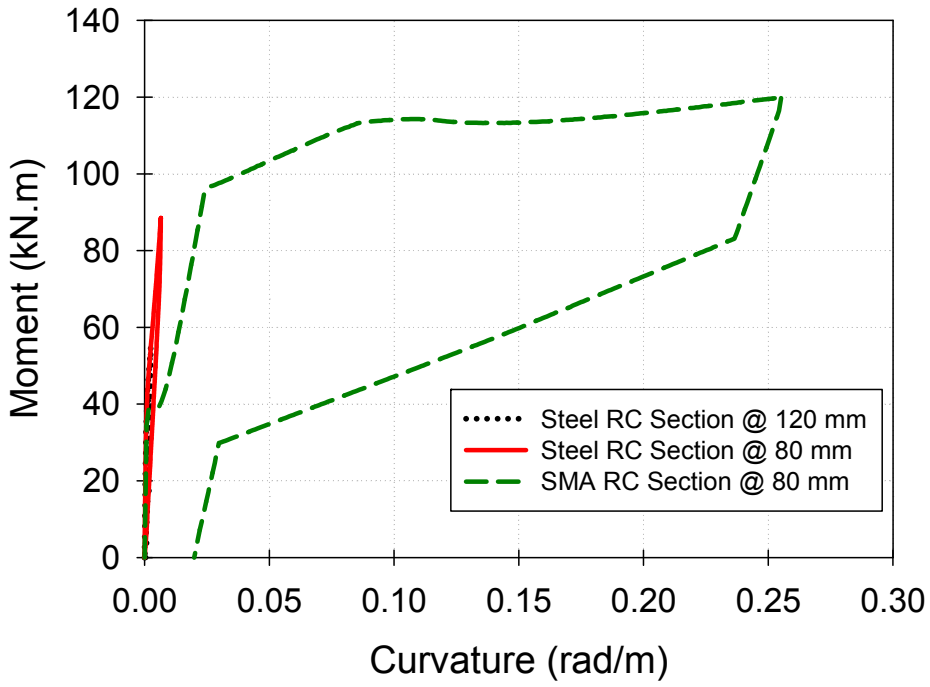

Fig. II-3: Moment-curvature analysis for steel and SMAs RC cross-sections.

Load-displacement results of BCJ1 beam are shown in **Fig. II-4**, while the load-displacement results of BCJ2 are shown in **Fig. II-5**. Good agreement can be observed for the two samples.

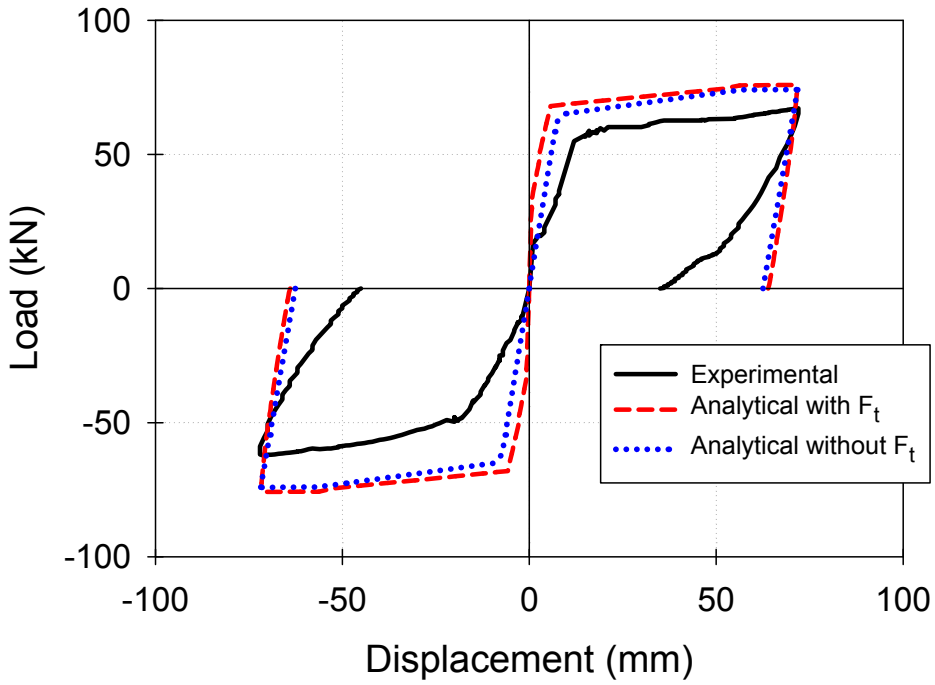

Fig. II-4: Load-displacement relationship for BCJ1.

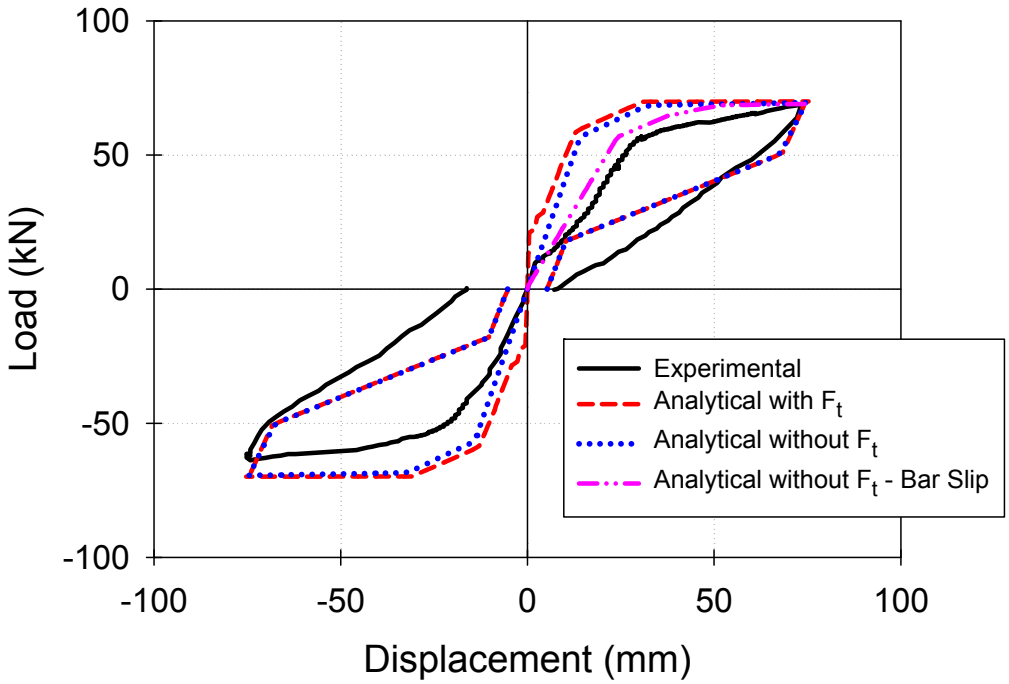

Fig. II-5: Load-displacement relationship for BCJ2.

Alam et al. (2008) reported that the significant reduction in initial stiffness at the tension side is attributed to SMA bar slip into the coupler. The load-slip relationship reported by Alam et al. (2008) is used in this study and converted to beam tip load-displacement relationship. The effect of bar slip is then subtracted from the analytical load-displacement relationship, **Fig. II-5**. As shown in the figure, a significant reduction in the initial stiffness of the analytical load-displacement relationship is observed.

II.1 REFERENCES

Youssef MA, Alam MS, Nehdi M. (2008). “Experimental Investigation on the Seismic Behaviour of Beam-Column Joints Reinforced with Superelastic Shape Memory Alloys.” Journal of Earthquake Engineering, 12(7), 454-461.

Elbahy Y.I., Youssef M.A., Nehdi M. (2010a). “Deflection of Superelastic Shape Memory Alloy Renforced Concrete Beams: Assessment of Existing Models.” Canadian Journal of Civil Engineering, 37(6), 842-854.

SeismoSoft (2018) "SeismoStruct - A computer program for static and dynamic nonlinear analysis of structures." Available from URL: http://www.seismosoft.com.

Alam, M.S., Youssef, M.A., Nehdi, M. (2008). “Analytical Prediction of the Seismic Behaviour of Superelastic Shape Memory Alloys Reinforced Concrete Elements.” Journal of Engineering Structures, 30(12), 3399-3411.

Appendix III: Validation of the Sectional Analysis Method Developed in Chapter 4

The work done by Saiidi et al. (2007) is used to validate the accuracy of the results obtained by the developed program. Saiidi et al. (2007) tested eight reinforced concrete beams under quasi-static loading. The beams have the same dimensions. The differences between the eight beams are the type and amount of reinforcement at the mid-span. Four beams are reinforced with SMA bars at mid-span, while the other four are reinforced with conventional steel bars. Details of the types and amounts of reinforcement used in the eight beams are summarized in **Table III-1**. Idealized stress-strain relationships of the used reinforcement materials are introduced in **Fig. III-1**.

Table III-1: Properties of the tested beams

Specimen	Mid-span SMAs reinforcement	Yielding (Critical) Strain (mm/mm)	Yielding (critical stress) (MPa)	Modulus of Elasticity (MPa)
BNL1	1 ϕ 6.40 mm	0.013	400	34078
BNL2	2 ϕ 6.40 mm	0.013	400	34078
BNH1	1 ϕ 9.50 mm	0.013	510	39245
BNH2	2 ϕ 9.50 mm	0.013	510	39245
BSL1	1 # 3 bars	0.0021	440	209524
BSL2	2 # 3 bars	0.0021	440	209524
BSH1	1 # 4 bars	0.0009	420	466667
BSH2	2 # 4 bars	0.0009	420	466667

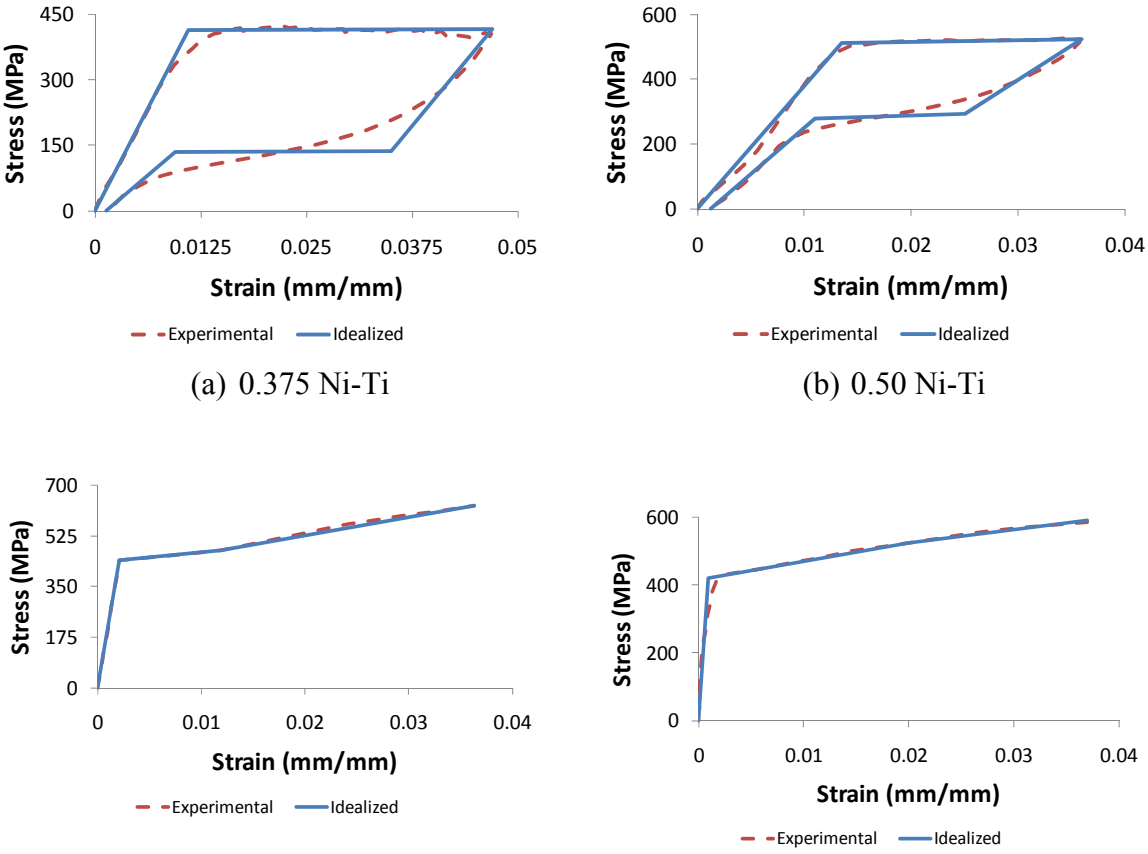

(a) 0.375 Ni-Ti

(b) 0.50 Ni-Ti

(c) #3 steel bar

(d) #4 steel bar

Fig. III-1: Experimental versus idealized stress-strain curves of the materials used as external reinforcement.

Fig. III-2 illustrates the details of the tested beams. The beams are 1530 mm long. The beams have cross-sectional dimensions of 127x152 mm at mid-span (i.e. mid-sections) and 127x305 mm at the ends (i.e. outer-sections). The beams are tested under two point symmetric loads that are placed 152 mm apart. This ensures subjecting the mid-span cross-sections to constant flexure.

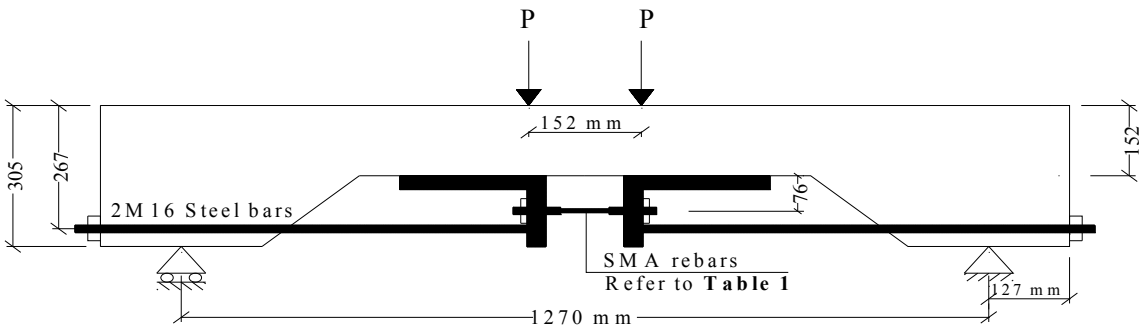

Fig. III-2: Beams dimensions and test setup

It is also shown in the figure that the reinforcement at mid-span is attached to the beam using external angles. In addition to the external reinforcement, two internal longitudinal bars are placed at the top and bottom of the mid-sections to avoid beam damage during handling. However, to ensure avoiding any contribution of the internal bars to the tensile strength, the internal bottom bar is cut before the test.

The developed program is used in this section to predict the moment-curvature and load-bar strain behaviours of the tested beams. **Fig. III-3** shows the experimental moment-curvature results of the SMA RC beams plotted versus the analytical results obtained using the developed program, while **Fig. III-4** shows the experimental and analytical load-external bar strain at mid-span. As shown in the figures, good agreements between the experimental and analytical results are observed. It should be noted that the load-bar strain results of BNH1 are not available, as the measuring strain gauge was damaged during the test (Saiidi et al.2007).

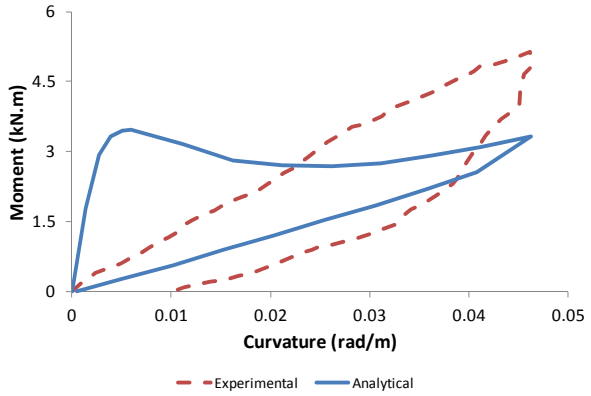

(a) BNL1

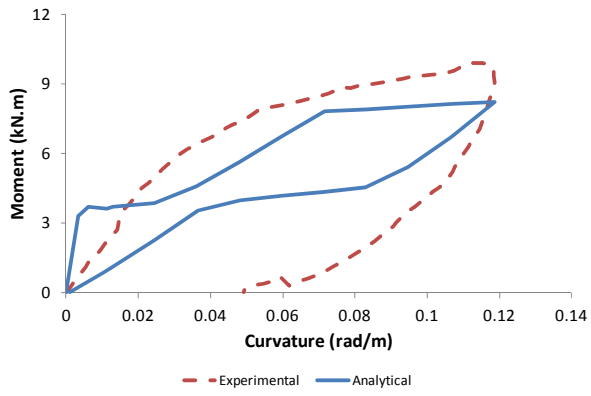

(b) BNL2

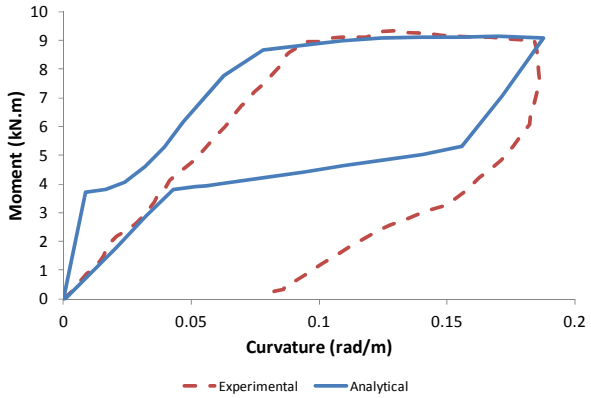

(c) BNH1

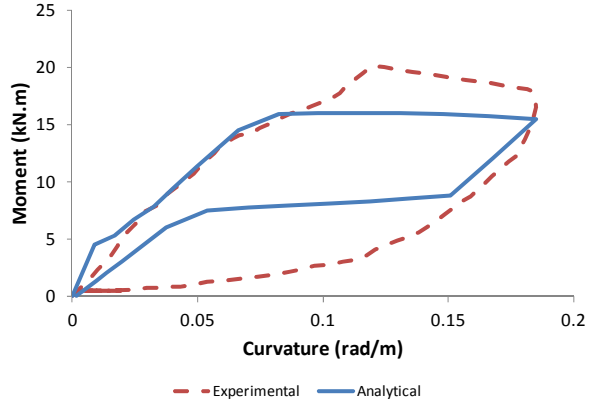

(d) BNH2

Fig. III-3: Experimental versus analytical moment-curvature results for the SMA RC beams

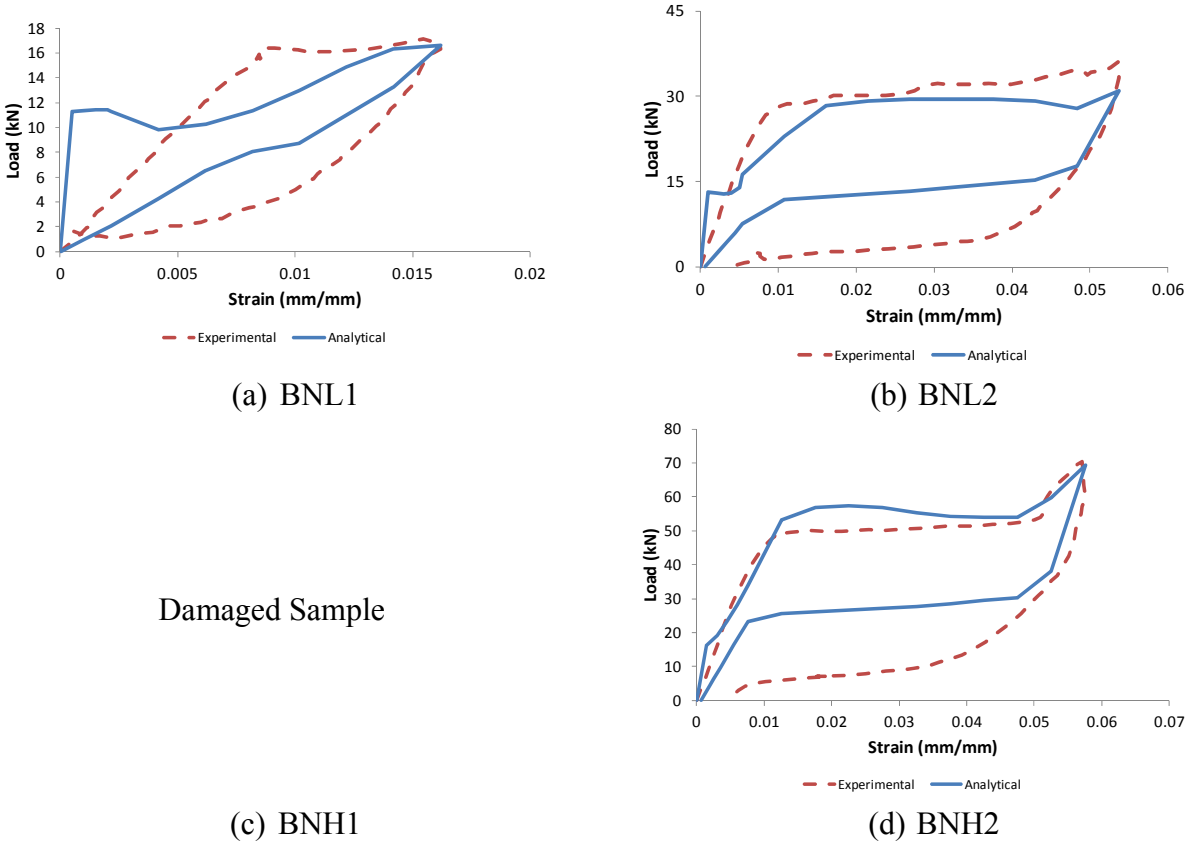

Fig. III-4: Experimental versus analytical load-bar strain results for the SMA RC beams

The program capability to predict the behaviour of RC beams strengthened using external steel bars is also investigated using the results of the other four tested beams. Similar procedure is used in the analysis (i.e. two analytical curves). **Figs. III-5** and **III-6** show the comparison between the experimental and analytical moment-curvature and load-bar strain results. As shown in the figures, good agreement between the experimental and analytical results is observed.

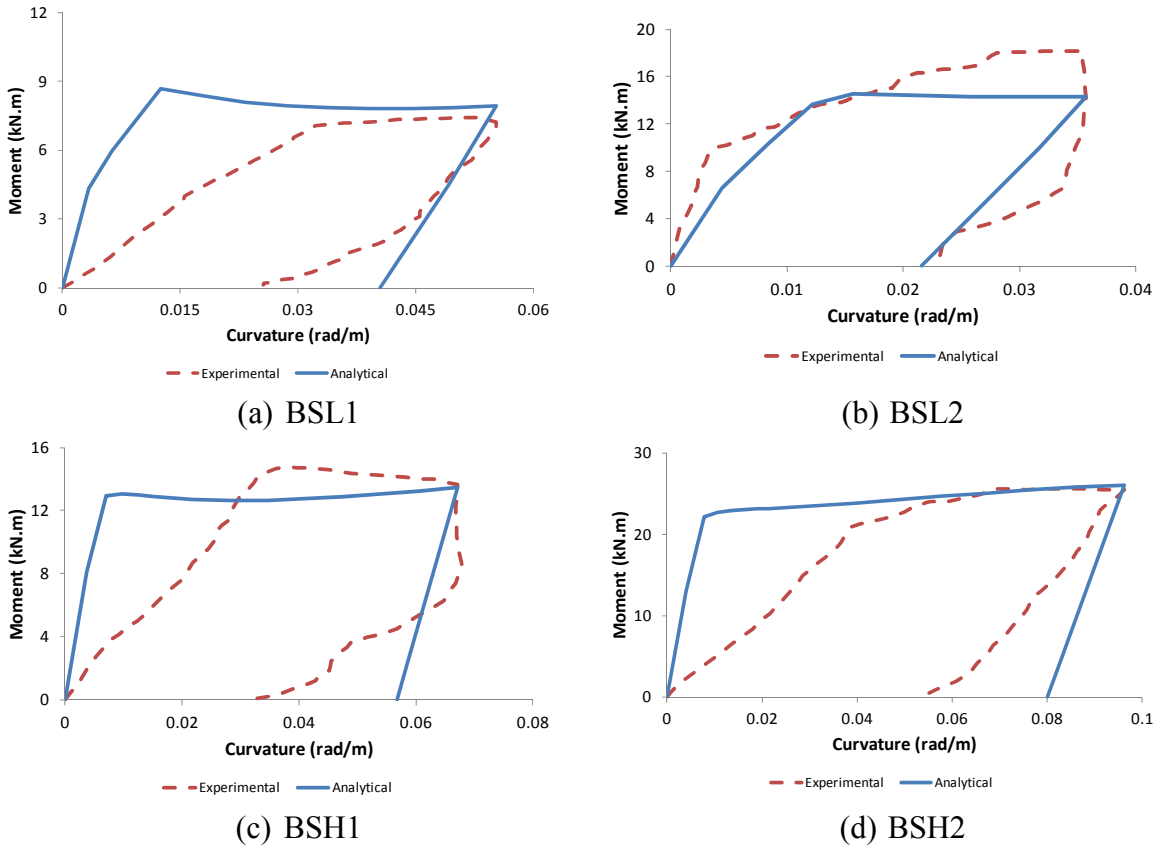

Fig. III-5: Experimental versus analytical moment-curvature results for the steel RC beams

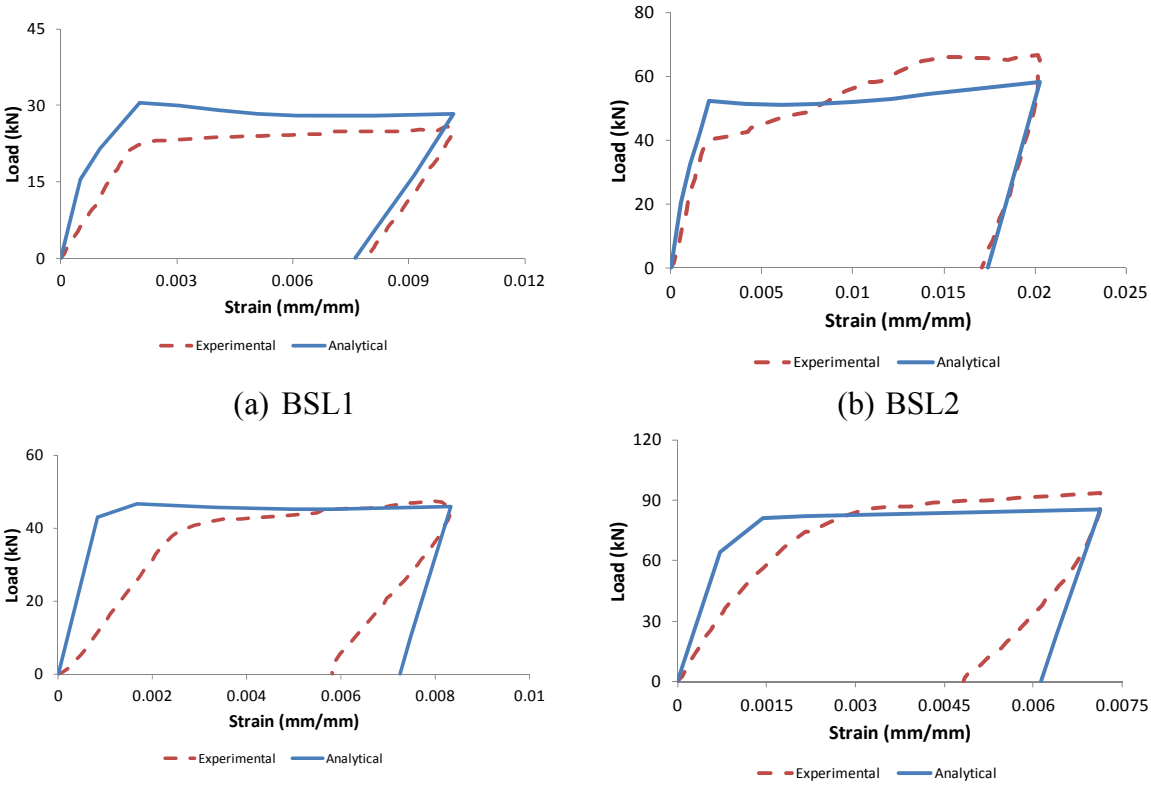

(a) BSL1 (b) BSL2

(c) BSH1 (d) BSH2

Fig. III-6: Experimental versus analytical load-bar strain results for the steel RC beams

Appendix IV: Flexural Behaviour of RC Beams Externally Reinforced with SMA Bars (internal steel is not cut)

IV.1 A_{SMA}/A_S PARAMETER

The effect of varying the ratio between the external SMA reinforcement to the internal steel reinforcement is investigated in this subsection. Seven different A_{SMA}/A_s ratios are used in the analysis. These ratios are: A_{SMA}/A_s = 0.5, 1.0, 2.0, 3.0, 4.0, 5.0, and 6.0. **Fig. IV-1(a)** shows the effect of increasing the value of the A_{SMA}/A_s ratio on the amount of residual displacement at complete unloading. Dramatic reduction in the amount of residual deformations can be obtained by increasing the A_{SMA}/A_s ratio. Increasing the A_{SMA}/A_s ratio from 0.50 to 6.0 resulted in reducing the amount of residual displacements from 95% to 5%. It is also clear from the figure that increasing the load level does not significantly change this trend. Same trend is observed when the load level increased from 1.0 δ_y to 9.0 δ_y.

Increasing the A_{SMA}/A_s ratio resulted in significant increase (400%) in the moment capacity of the beam at different loading levels, **Fig. IV-1(b)**. The increase in moment capacity occurred in a linear fashion and is not significantly affected by the loading level. Initial stiffness of the beam is also significantly increased by increasing the A_{SMA}/A_s ratio, **Fig. IV-1(c)**. Increasing the A_{SMA}/A_s from 0.50 to 6.0 resulted in 150% increase in the stiffness ratio.

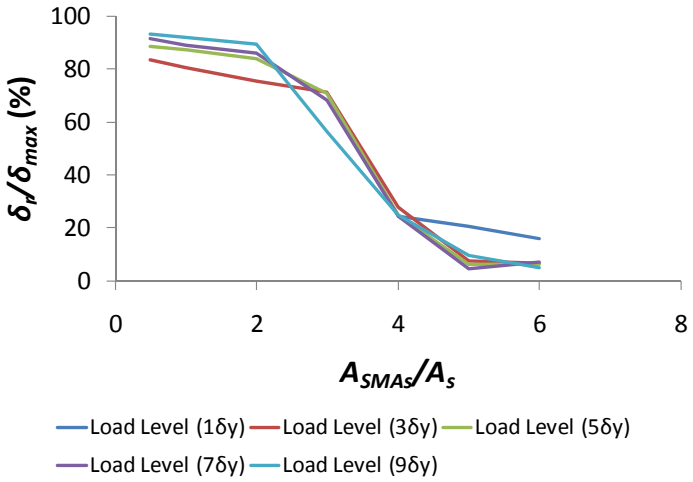

(a) Residual displacements

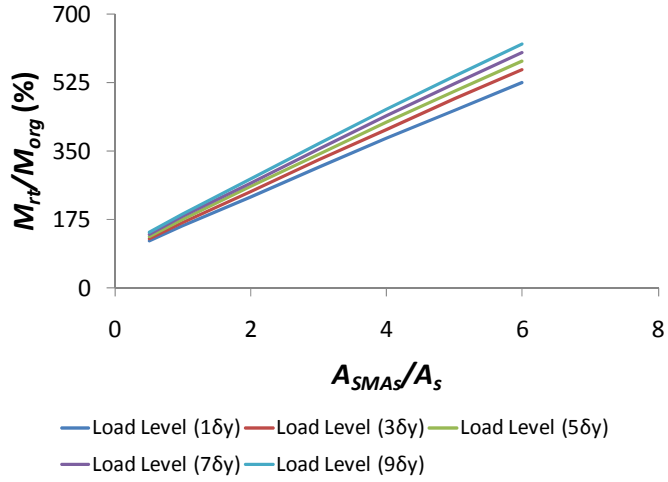

(b) Moment capacity

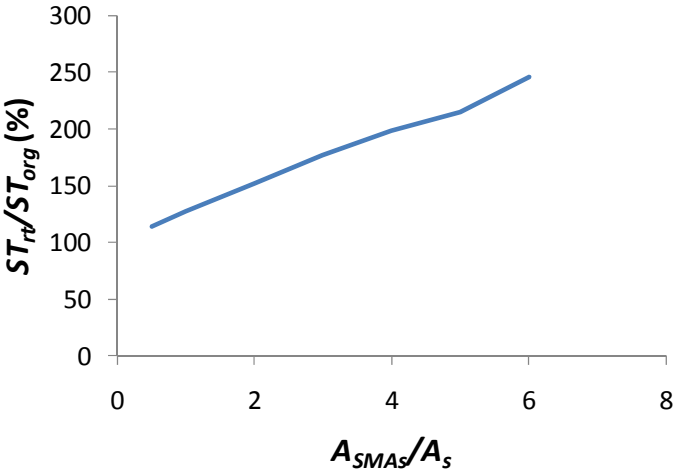

(c) Initial stiffness

Fig. IV-1: Effect of varying the A_{SMA}/A_s ratio on the strengthened beam behaviour

IV.2 LOAD LEVEL PARAMETER

The effect of varying the applied load level on the behaviour of RC beams strengthened using external SMA bars is investigated in this subsection. The analysis is performed for different values of A_{SMA}/A_s ratios. **Fig. IV-2** shows the results of the analyzed beams. It is clear from the figure that increasing the load level for low ratios of A_{SMA}/A_s (i.e. 0.5, 1.0 and 2.0) increases the amount of residual deformations, **Fig. IV-2(a)**. The δ_r/δ_{max} values increased from 40%-50% at load level = 1.0 δ_y to almost 90% at load level = 9.0 δ_y. This is attributed to the significant yielding occurs in the internal steel bars. Since the behaviour of the internal steel bars is more significant than the external SMA bars, significant residual displacements are obtained at complete unloading. Increasing the A_{SMA}/A_s ratio beyond this limit (i.e. 4.0 to 6.0) eliminated the significant effect of increasing the load level. The reason behind this is that the overall behaviour of the beam is controlled by the external SMA bars, the beam is capable of recovering almost all of the residual deformations.

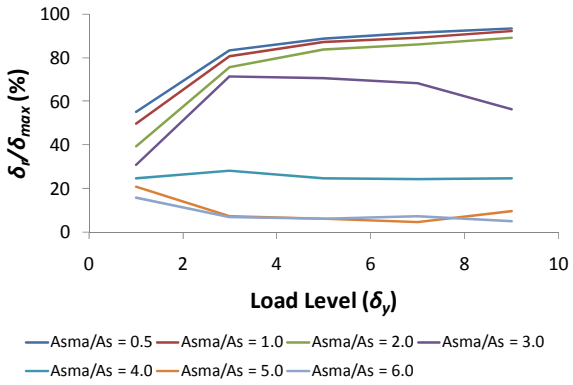

(a) Residual Displacement

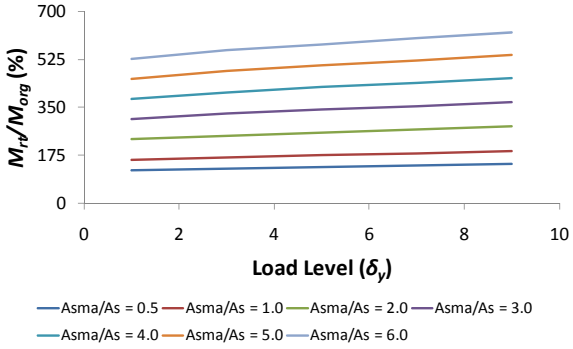

(b) Moment capacity

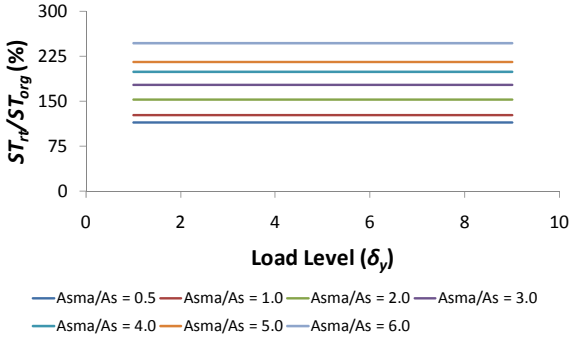

(c) Initial stiffness

Fig. IV-2: Effect of varying the applied load level on the strengthened beam behaviour

IV.3 L_{SMA}/L PARAMETER

The effect of varying the external SMA bars length on the behaviour of the retrofitted beams is investigated in this subsection. SMA bars length is represented in this study by the ratio (L_{SMA}/L) which is the ratio between the length of the used SMA bars to the total length of the beam. Nine different SMA bars length are assumed in the analysis. Each length is analyzed at different A_{SMA}/A_s ratios and at different load levels. Results of the analysis are discussed in this subsection.

Figs. IV-3 and **IV-4** show the effect of varying the L_{SMA}/L ratio on the amount of residual displacements upon unloading for different A_{SMA}/A_s ratios and for different load levels. It is clear from the figures that increasing the length of the SMA bars increases the amount of residual displacements represented by δ_r/δ_{max} values for small A_{SMA}/A_s ratios (i.e. 0.50 to 3.0). This increase in residual displacement can be attributed to the significant increase in the beam ductility gained by adding the external SMA bars to the beams. This allows the internal steel bars to undergo very large deformations beyond their yielding limits. At complete unloading, the internal steel bars keep large amounts of residual deformations, and in turns the beam keeps a large amount of residual displacement.

It can also be concluded from the figures that increasing the A_{SMA}/A_s ratio helps in reducing the amount of residual displacement caused by increasing the L_{SMA}/L ratio. For example, increasing the A_{SMA}/A_s ratio from 0.50 to 6.0 reduced the amount of residual displacement δ_r/δ_{max} from 53% to 20% at load level = 1.0 δ_y, and from 93% to 10% at load level = 9.0 δ_y.

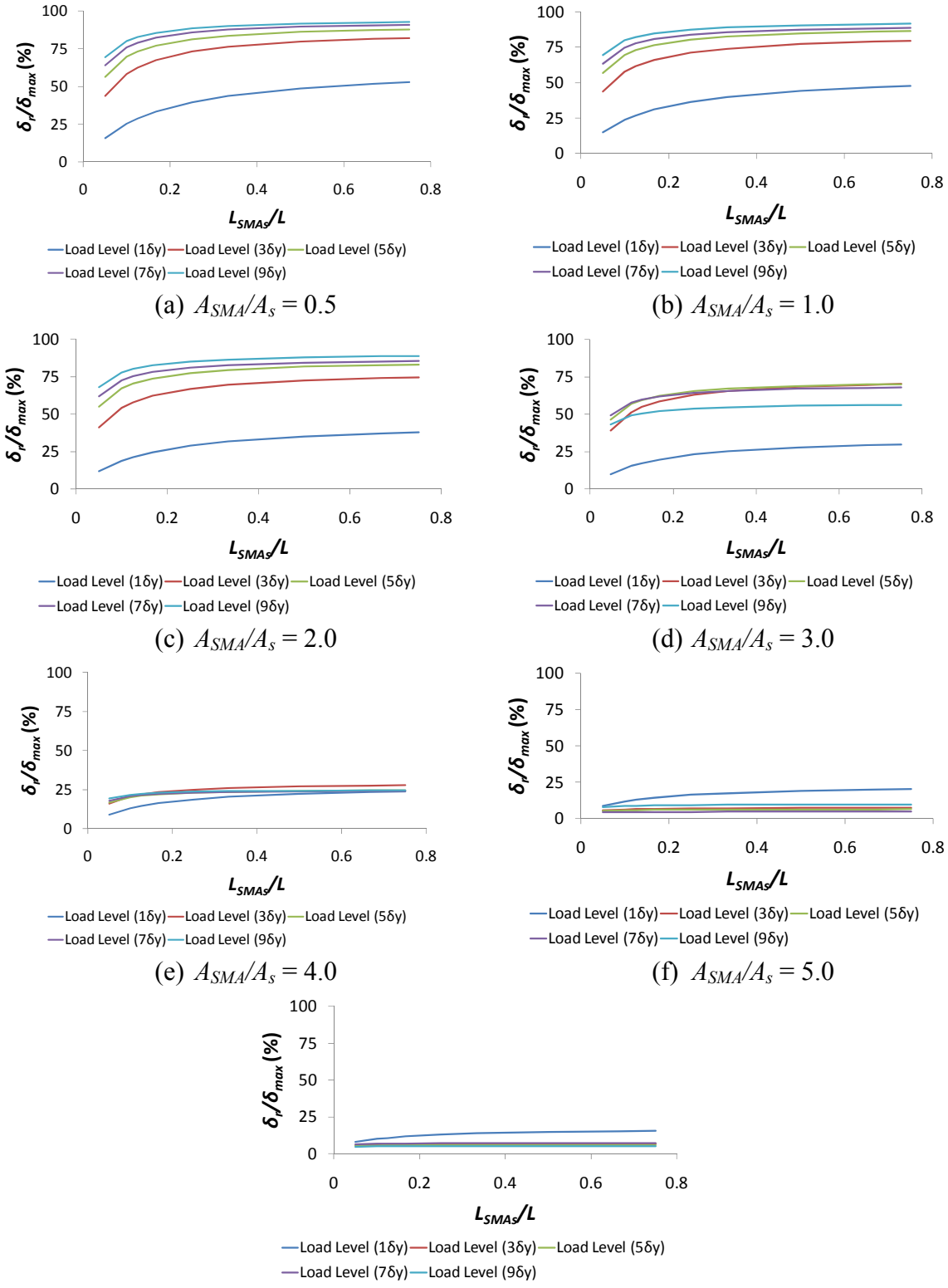

(a) $A_{SMA}/A_s = 0.5$

(b) $A_{SMA}/A_s = 1.0$

(c) $A_{SMA}/A_s = 2.0$

(d) $A_{SMA}/A_s = 3.0$

(e) $A_{SMA}/A_s = 4.0$

(f) $A_{SMA}/A_s = 5.0$

(g) $A_{SMA}/A_s = 6.0$

Fig. IV-3: Effect of varying the L_{SMA}/L ratio on the amount of residual displacements in the strengthened beams at different A_{SMA}/A_s ratios

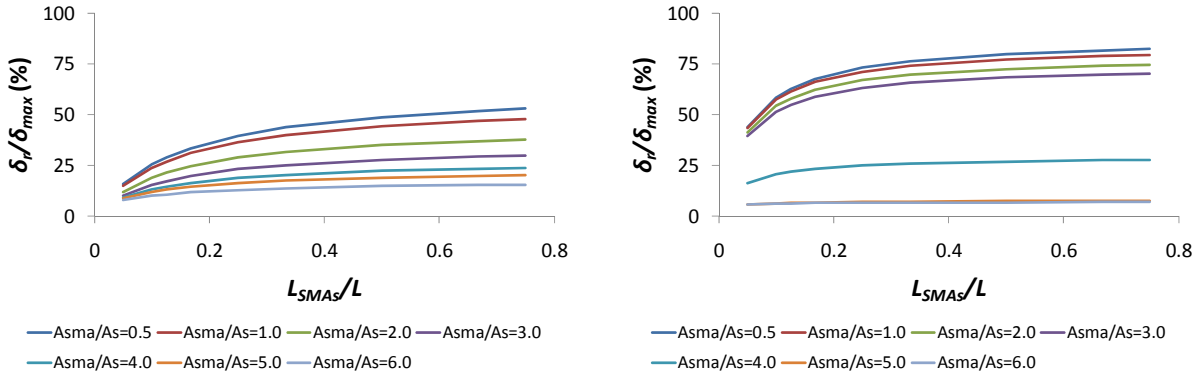

(a) Load level = 1.0 δ_y

(b) Load level = 3.0 δ_y

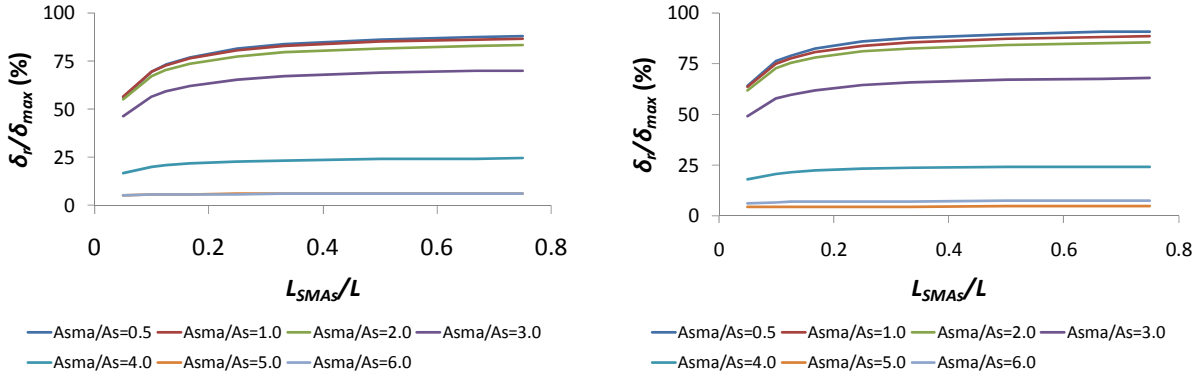

(c) Load level = 5.0 δ_y

(d) Load level = 7.0 δ_y

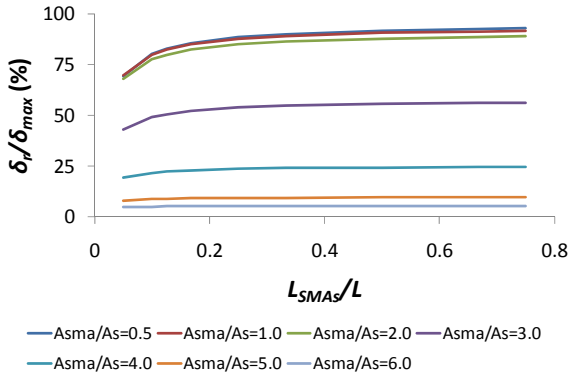

(e) Load level = 9.0 δ_y

Fig. IV-4: Effect of varying the A_{SMA}/A_s ratio on the amount of residual displacements in the strengthened beams at different load levels

Fig. IV-5 shows that the retrofitted beams strength is not affected by increasing the L_{SMA}/L ratio. The reason behind this is that the SMA bars are coupled to regular steel bars which have double the cross-sectional area to ensure that most of the deformations and failure occur in the SMA region. Thus, the maximum strength of the beam is equal to the strength of SMA RC section and is independent of the SMA bars length.

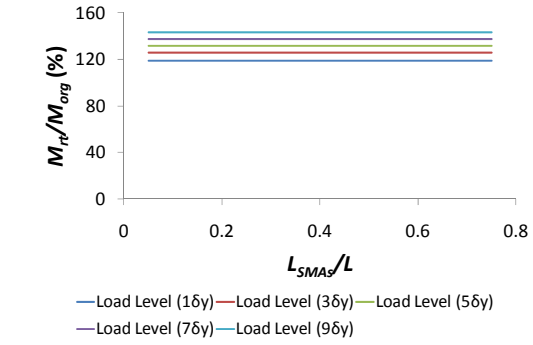

(a) $A_{SMA}/A_s = 0.5$

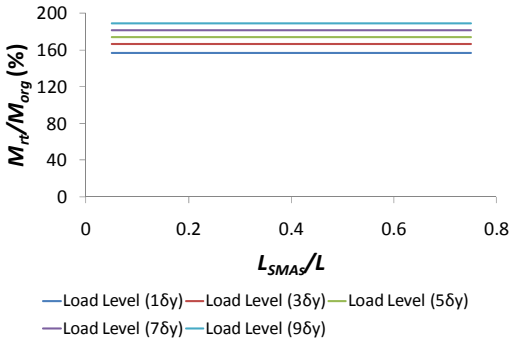

(b) $A_{SMA}/A_s = 1.0$

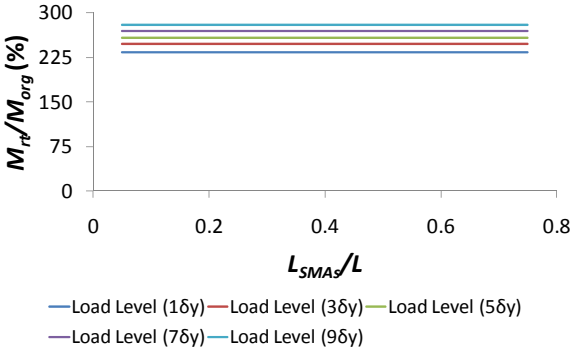

(c) $A_{SMA}/A_s = 2.0$

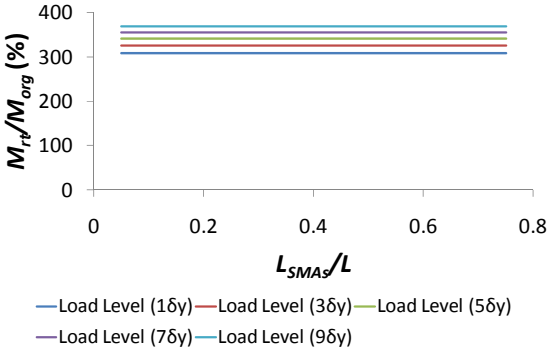

(d) $A_{SMA}/A_s = 3.0$

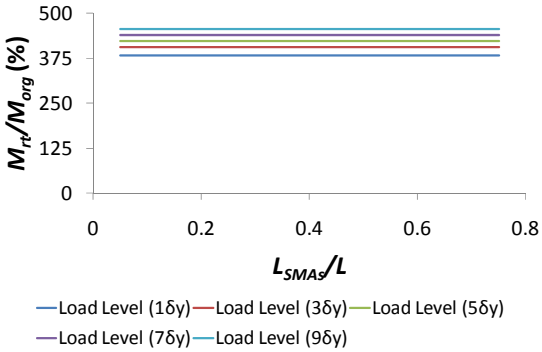

(e) $A_{SMA}/A_s = 4.0$

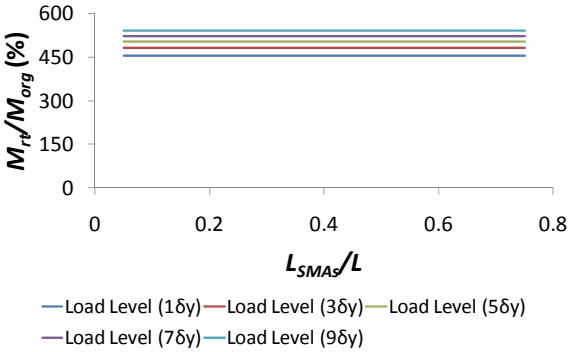

(f) $A_{SMA}/A_s = 5.0$

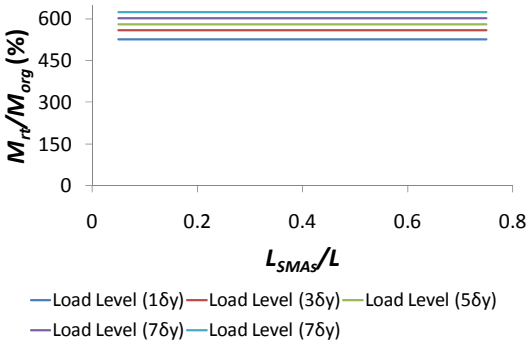

(g) $A_{SMA}/A_s = 6.0$

Fig. IV-5: Effect of varying the L_{SMA}/L ratio on the moment capacity of the strengthened beams at different A_{SMA}/A_s ratios

The effect of varying the L_{SMA}/L ratio on the initial stiffness of the beam is also studied. As shown in **Fig. IV-6**, increasing the length of the SMA bars reduces the initial stiffness of the beam. This reduction is very significant (700%) in case of low A_{SMA}/A_s ratios, and much less significant (100%) at high A_{SMA}/A_s values. This is attributed to the way the retrofitted beam is designed. The SMA bars are coupled to steel bars that have double the cross-sectional area. This results in a weaker SMA cross-section. The reason behind this is concentrating the deformations within the SMA region.

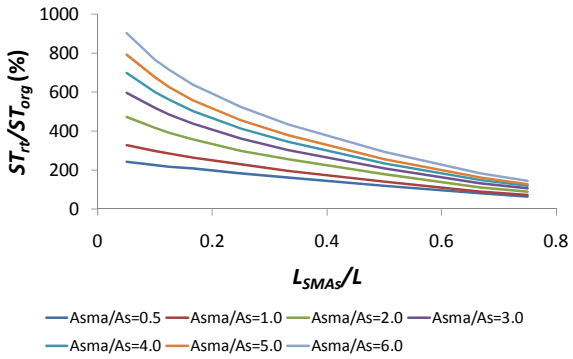

Fig. IV-6: Effect of varying the L_{SMA}/L ratio on the initial stiffness of the retrofitted beams

The effect of varying the length of the external SMA bars on the displacement at which yielding in the external SMA bars starts is also introduced. Increasing the length of the SMA bars resulted in increasing the $\delta_{y\text{-}rt}/\delta_{y\text{-}org}$ ratio, **Fig. IV-7**. This increase is insignificant at the small L_{SMA}/L values, and increases as the length of the SMA bars increase. The rate of increasing is higher (i.e. 40% to 180%) for the cases of low A_{SMA}/A_s values. The ratio $\delta_{y\text{-}rt}/\delta_{y\text{-}org}$ is independent of the load level.

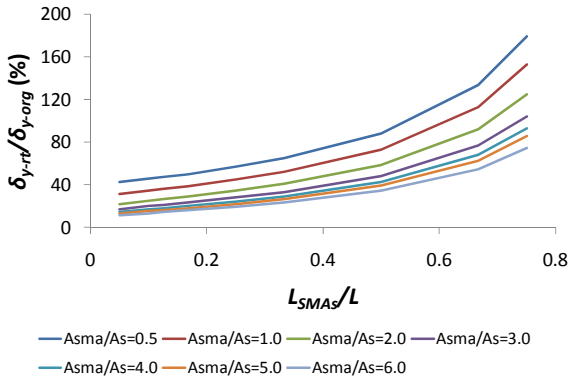

Fig. IV-7: Effect of varying the L_{SMA}/L ratio on the displacement at which yielding in the external SMA bar starts to occur in the strengthened beams

The effect of varying the length of the external SMA bars on the maximum displacement of the retrofitted beam is shown in **Fig. IV-8**. Increasing the length of the SMA bars increases the $\delta_{max\text{-}rt}/\delta_{max\text{-}org}$ ratio. This increase is more pronounced in case of low A_{SMA}/A_s ratios. Similar trend is observed at different loading levels. Similar to the yielding displacements, the rate of increase in the $\delta_{max\text{-}rt}/\delta_{max\text{-}org}$ ratio is more significant in case of low A_{SMA}/A_s ratios.

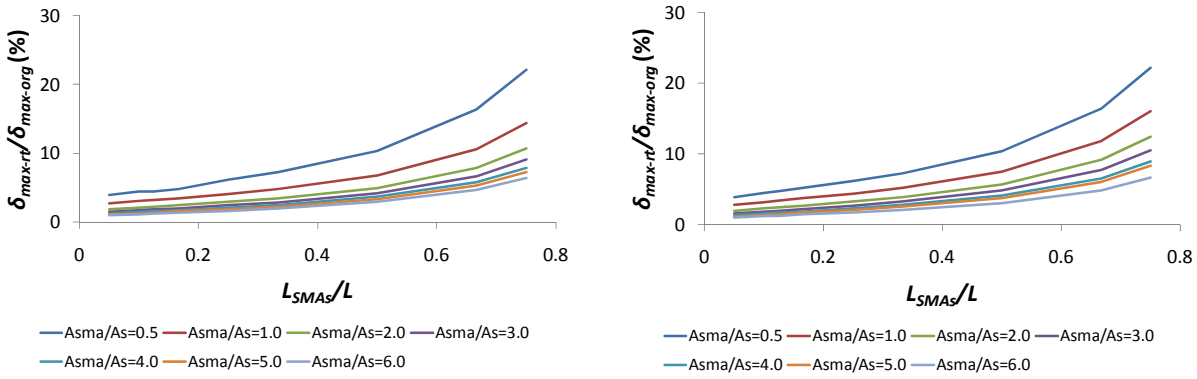

(a) Load level = 1.0 δ_y

(b) Load level = 3.0 δ_y

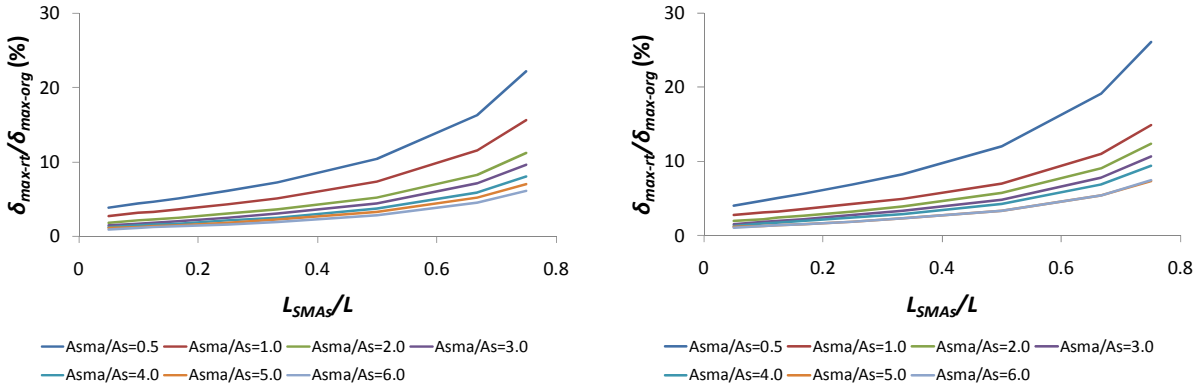

(c) Load level = 5.0 δ_y

(d) Load level = 7.0 δ_y

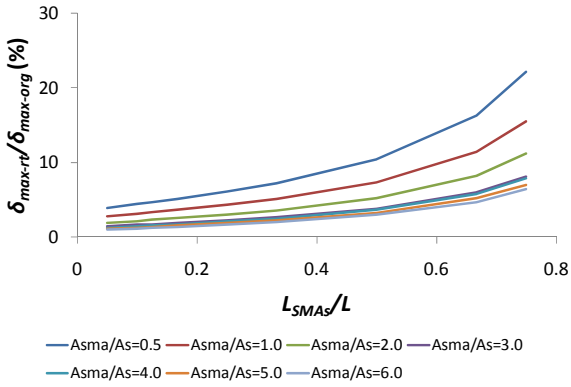

(e) Load level = 9.0 δ_y

Fig. IV-8: Effect of varying the L_{SMA}/L ratio on the maximum displacement of the strengthened beams

Appendix V: Regression Analysis for RC Beams Externally Reinforced with SMA Bars (internal steel is not cut)

Tables V-1 to **V-10** presents the final regression models developed for the five outputs (δ_r/δ_{max}, M_{rt}/M_{org}, ST_{rt}/ST_{org}, $\delta_{y\text{-}rt}/\delta_{y\text{-}org}$, $\delta_{max\text{-}rt}/\delta_{max\text{-}org}$). These models are the most statistically significant models achieved after conducting numerous numbers of trials. These trials included trying different transformations with different parameters for each output. **Equations [V-1:V-5]** represent the summary of the final regression models for the five outputs. For each output, two equations are introduced. The first equation is a general form that accounts for the status of the internal steel bars status (cut OR not cut). The second equation is for the case where the internal steel bars are not cut.

$$\ln(\delta_r/\delta_{max}) = -3.12743 \times (\text{Internal steel bar status}) + 0.299072 \times (L_{SMAs}/L) - 0.01998 \times (A_{SMAs}/A_s)^2 + 0.096038 \times (\text{Load Level}) + 3.013744 \quad \textbf{[V-1(a)]}$$

$$\delta_r/\delta_{max} = 45.95305 \times (L_{SMAs}/L) - 31.2202 \times (L_{SMAs}/L)^2 - 13.744 \times A_{SMAs}/A_s + 9.517148 \times (\text{Load level}) - 0.6793 \times (\text{Load level})^2 + 49.44006 \quad \textbf{[V-1(b)]}$$

$$M_{rt}/M_{org} = -83.1246 \times (\text{Internal steel bar status}) + 82.01286 \times (A_{SMAs}/A_s) + 6.598675 \times (\text{Load level}) + 58.1333 \quad \textbf{[V-2(a)]}$$

$$M_{rt}/M_{org} = 81.29762 \times (A_{SMAs}/A_s) + 7.423727 \times (\text{Load level}) + 56.20484 \quad \textbf{[V-2(b)]}$$

$$\ln(ST_{rt}/ST_{org}) = -0.63235 \times \ln(L_{SMAs}/L) + 0.646359 \times \ln(A_{SMAs}/A_s) - 0.68111 \times (\text{internal steel bar status}) + 4.204217 \quad \textbf{[V-3(a)]}$$

$$ST_{rt}/ST_{org} = -1306.05 \times (L_{SMAs}/L) + 847.5907 \times (L_{SMAs}/L)^2 + 74.77563 \times (A_{SMAs}/A_s) - 2.76594 \times (A_{SMAs}/A_s)^2 + 432.8192 \quad \textbf{[V-3(b)]}$$

$$\ln(\delta_{y\text{-}rt}/\delta_{y\text{-}org}) = 9.278531 \times (L_{SMAs}/L) - 11.9282 \times (L_{SMAs}/L)^2 + 0.149841 \times (A_{SMAs}/A_s) - 0.03233 \times (A_{SMAs}/A_s)^2 + 2.780991 \quad \textbf{[V-4(a)]}$$

$$\ln(\delta_{y\text{-}rt}/\delta_{y\text{-}org}) = 10.22022 \times (L_{SMAs}/L) - 12.6565 \times (L_{SMAs}/L)^2 - 0.09954 \times (A_{SMAs}/A_s) + 2.94872 \quad \textbf{[V-4(b)]}$$

$$\ln(\delta_{max\text{-}rt}/\delta_{max\text{-}org}) = 15.33261 \times L_{SMAs}/L - 18.1243 \times (L_{SMAs}/L)^2 - 0.03061 \times (A_{SMAs}/A_s)^2 + 0.269225 \times (\text{Internal steel bar status}) + 3.633697 \quad \textbf{[V-5(a)]}$$

$$\ln(\delta_{max\text{-}rt}/\delta_{max\text{-}org}) = 16.63835 \times (L_{SMAs}/L) - 18.9918 \times (L_{SMAs}/L)^2 - 0.24879 \times (A_{SMAs}/A_s) + 3.699835 \quad \textbf{[V-5(b)]}$$

Table V-1: Regression model for δ_r/δ_{max} – General model

Source	SS	df	MS	Number of obs	=	700
Model	1812.468	4	453.117	F(4, 695)	=	645.59
				Prob > F	=	0
Residual	487.795	695	0.701863	R-squared	=	0.7879
				Adj R-squared	=	0.7867
Total	2300.263	699	3.290791	Root MSE	=	0.83777

ln (δ_r/δ_{max})	**Coef.**	**Std. Err.**	**t**	**P>t**	**[95% Conf. Interval]**	
Internal steel bar status	-3.12743	0.06333	-49.38	0	-3.25177	-3.00309
L_{SMAs}/L	0.299072	0.103674	2.88	0.004	0.09552	0.502623
$(A_{SMAs}/A_s)^2$	-0.01998	0.002543	-7.86	0	-0.02497	-0.01499
Load Level	0.096038	0.011195	8.58	0	0.074057	0.118018
Constant	3.013744	0.088924	33.89	0	2.839151	3.188336

Table V-2: Regression model for δ_r/δ_{max} – Internal steel bars are not cut

Source	SS	df	MS	Number of obs	=	350
Model	275637.5	5	55127.5	F(5, 344)	=	317.85
				Prob > F	=	0
Residual	59662.16	344	173.4365	R-squared	=	0.8221
				Adj R-squared	=	0.8195
Total	335299.7	349	960.7441	Root MSE	=	13.17

δ_r/δ_{max}	**Coef.**	**Std. Err.**	**t**	**P>t**	**[95% Conf. Interval]**	
L_{SMAs}/L	45.9530	9.19569	5	0	27.86619	64.0399
$(L_{SMAs}/L)^2$	-31.2202	8.99130	-3.47	0.001	-48.905	-13.5354
A_{SMAs}/A_s	-13.744	0.37090	-37.06	0	-14.4735	-13.0145
Load level	9.51715	1.08076	8.81	0	7.391418	11.64288
(Load level)^2	-0.6793	0.10517	-6.46	0	-0.88616	-0.47244
Constant	49.4401	2.99753	16.49	0	43.54426	55.33586

Table V-3: Regression model for M_{rt}/M_{org} – General model

Source	SS	df	MS			
				Number of obs	=	700
Model	18412437	3	6137479	F(3, 696)	=	63693.9
				Prob > F	=	0
				R-squared	=	0.9964
Residual	67065.83	696	96.3590	Adj R-squared	=	0.9964
Total	18479502	699	26437.1	Root MSE	=	9.8163

M_{rt}/M_{org}	Coef.	Std. Err.	t	P>t	[95% Conf.	Interval]
Internal steel bar status	-83.1246	0.74204	-112.02	0	-84.5815	-81.6677
A_{SMAs}/A_s	82.01286	0.19549	419.53	0	81.62904	82.3967
Load level	6.598675	0.13118	50.3	0	6.341128	6.85622
Constant	58.1333	1.03247	56.3	0	56.10616	60.1604

Table V-4: Regression model for M_{rt}/M_{org} – Internal steel bars are not cut

Source	SS	df	MS			
				Number of obs	=	350
Model	8486756	2	4243378	F(2, 347)	=	49246.65
				Prob > F	=	0
				R-squared	=	0.9965
Residual	29899.54	347	86.16581	Adj R-squared	=	0.9965
Total	8516655	349	24403.02	Root MSE	=	9.2826

M_{rt}/M_{org}	Coef.	Std. Err.	t	P>t	[95% Conf.	Interval]
A_{SMAs}/A_s	81.29762	0.261432	310.97	0	80.78343	81.81181
Load level	7.423727	0.175424	42.32	0	7.078699	7.768754
Constant	56.20484	1.288521	43.62	0	53.67054	58.73913

Table V-5: Regression model for ST_{rt}/ST_{org} – General model

Source	SS	df	MS			
				Number of obs	=	700
Model	529.995	3	176.665	F(3, 696)	=	1710.6
				Prob > F	=	0
				R-squared	=	0.8806
Residual	71.8805	696	0.10328	Adj R-squared	=	0.8801
Total	601.875	699	0.86105	Root MSE	=	0.32137

$\ln(ST_{rt}/ST_{org})$	Coef.	Std. Err.	t	P>t	[95% Conf.	Interval]
$\ln(L_{SMAs}/L)$	-0.63235	0.013053	-48.45	0	-0.65798	-0.60672
$\ln(A_{SMAs}/A_s)$	0.646359	0.014458	44.71	0	0.617973	0.674745
Internal steel bar status	-0.68111	0.024293	-28.04	0	-0.72881	-0.63341
Constant	4.204217	0.027066	155.33	0	4.151077	4.257356

Table V-6: Regression model for ST_{rt}/ST_{org} – Internal steel bars are not cut

Source	SS	df	MS			
				Number of obs	=	350
Model	12795119	4	3198780	F(4, 345)	=	707.75
				Prob > F	=	0
				R-squared	=	0.8914
Residual	1559288	345	4519.676	Adj R-squared	=	0.8901
Total	14354407	349	41130.11	Root MSE	=	67.229

ST_{rt}/ST_{org}	Coef.	Std. Err.	t	P>t	[95% Conf.	Interval]
L_{SMAs}/L	-1306.05	46.94265	-27.82	0	-1398.38	-1213.72
$(L_{SMAs}/L)^2$	847.5907	45.89925	18.47	0	757.3131	937.8683
A_{SMAs}/A_s	74.77563	8.097761	9.23	0	58.84844	90.70283
$(A_{SMAs}/A_s)^2$	-2.76594	1.234135	-2.24	0.026	-5.19331	-0.33856
Constant	432.8192	13.26699	32.62	0	406.7248	458.9136

Table V-7: Regression model for $\delta_{y\text{-}rt}/\delta_{y\text{-}org}$ – General model

Source	SS	df	MS			
				Number of obs	=	700
Model	1043.18	4	260.795	F(4, 695)	=	458.96
				Prob > F	=	0
Residual	394.917	695	0.56823	R-squared	=	0.7254
				Adj R-squared	=	0.7238
Total	1438.10	699	2.05736	Root MSE	=	0.75381

$\ln(\delta_{y\text{-}rt}/\delta_{y\text{-}org})$	Coef.	Std. Err.	t	P>t	[95% Conf.	Interval]
L_{SMAs}/L	9.278531	0.372186	24.93	0	8.547788	10.00927
$(L_{SMAs}/L)^2$	-11.9282	0.363913	-32.78	0	-12.6427	-11.2137
A_{SMAs}/A_s	0.149841	0.064203	2.33	0.02	0.023785	0.275896
$(A_{SMAs}/A_s)^2$	-0.03233	0.009785	-3.3	0.001	-0.05154	-0.01312
Constant	2.780991	0.105188	26.44	0	2.574467	2.987514

Table V-8: Regression model for $\delta_{y\text{-}rt}/\delta_{y\text{-}org}$ – Internal steel bars are not cut

Source	SS	df	MS			
				Number of obs	=	350
Model	530.4985	3	176.8328	F(3, 346)	=	338.37
				Prob > F	=	0
Residual	180.8212	346	0.522605	R-squared	=	0.7458
				Adj R-squared	=	0.7436
Total	711.3197	349	2.038165	Root MSE	=	0.72291

$\ln(\delta_{y\text{-}rt}/\delta_{y\text{-}org})$	Coef.	Std. Err.	t	P>t	[95% Conf.	Interval]
L_{SMAs}/L	10.2202	0.50478	20.25	0	9.2274	11.2130
$(L_{SMAs}/L)^2$	-12.6565	0.49356	-25.64	0	-13.6273	-11.6858
A_{SMAs}/A_s	-0.09954	0.02036	-4.89	0	-0.13958	-0.05949
Constant	2.94872	0.11302	26.09	0	2.726403	3.17104

Table V-9: Regression model for $\delta_{y\text{-}rt}/\delta_{y\text{-}org}$ – General model

Source	SS	df	MS			
				Number of obs	=	700
Model	1043.18	4	260.795	F(4, 695)	=	458.96
				Prob > F	=	0
				R-squared	=	0.7254
Residual	394.917	695	0.56823	Adj R-squared	=	0.7238
Total	1438.10	699	2.05736	Root MSE	=	0.75381

$\ln(\delta_{y\text{-}rt}/\delta_{y\text{-}org})$	Coef.	Std. Err.	t	P>t	[95% Conf.	Interval]
L_{SMAs}/L	9.278531	0.372186	24.93	0	8.547788	10.00927
$(L_{SMAs}/L)^2$	-11.9282	0.363913	-32.78	0	-12.6427	-11.2137
A_{SMAs}/A_s	0.149841	0.064203	2.33	0.02	0.023785	0.275896
$(A_{SMAs}/A_s)^2$	-0.03233	0.009785	-3.3	0.001	-0.05154	-0.01312
Constant	2.780991	0.105188	26.44	0	2.574467	2.987514

Table V-10: Regression model for $\delta_{y\text{-}rt}/\delta_{y\text{-}org}$ – Internal steel bars are not cut

Source	SS	df	MS			
				Number of obs	=	350
Model	530.499	3	176.833	F(3, 346)	=	338.37
				Prob > F	=	0
				R-squared	=	0.7458
Residual	180.8212	346	0.522605	Adj R-squared	=	0.7436
Total	711.3197	349	2.038165	Root MSE	=	0.72291

$\ln(\delta_{y\text{-}rt}/\delta_{y\text{-}org})$	Coef.	Std. Err.	t	P>t	[95% Conf.	Interval]
L_{SMAs}/L	10.22022	0.504778	20.25	0	9.2274	11.21304
$(L_{SMAs}/L)^2$	-12.6565	0.493558	-25.64	0	-13.6273	-11.6858
A_{SMAs}/A_s	-0.09954	0.02036	-4.89	0	-0.13958	-0.05949
Constant	2.94872	0.113032	26.09	0	2.726403	3.171036

Appendix VI: Regression Analysis for RC Beams Externally Reinforced with Steel Bars (internal steel is not cut)

After performing the parametric study, the results are then arranged in a database format with all records of the study. Multiple linear regression technique is used to determine the relationships between the inputs and outputs of the study. Numerous number of models based on different transformations (i.e. linear transformations, quadratic power transformation, and logarithmic transformation) are first tried. The best models that relate the parametric study inputs to outputs are then chosen and reported in this study. A total of eight models for the four outputs are reported.

A total of 207 data sets are used in establishing the statistical models. These data represents all the data obtained from the parametric study. All inputs and outputs of this study are kept dimensionless. The inputs of the models are: (i) type of reinforcement (steel or SMA); (ii) internal reinforcement status (bars are cut or not cut); (iii) $A_{S\text{-}ext}/A_s$ ratio; (iv) $L_{S\text{-}ext}/L$ ratio; and (v) load level. The outputs of the parametric study are: δ_r/δ_{max}, M_{rt}/M_{org}, ST_{rt}/ST_{org}, and EN_{rt}/EN_{org}. Descriptive statistics of the used data are presented in **Table VI-1**.

Correlation analysis is first used with the data to determine the correlation between each pair of the variables and noting the highly correlated ones and their signs. The correlation matrix is determined using the STATA software V.12 and is shown in **Table VI-2**. **Tables VI-3** to **VI-10**

present the final statistical models obtained for the four outputs of the parametric study. **Equations [VI-1:VI-4]** represent the summary of the final statistical models for the four outputs. For each output, two equations are introduced. The first equation is a general form that accounts for the type of reinforcement (SMA or steel). The second equation is for the case of external steel bars.

$$(\delta_r/\delta_{max}) = -1781.73 \times (\text{Type of Reinforcement}) + 429.9668 \times (L_{S\text{-}ext}/L) - 964.33 \times (A_{S\text{-}ext}/A_s) + 350.8894 \times (\text{Load Level}) + 5758.656 \quad \textbf{[1(a)]}$$

$$(\delta_r/\delta_{max})^2 = 289.6758 \times \ln (L_{S\text{-}ext}/L) - 518.564 \times (A_{S\text{-}ext}/A_s) + 3186.173 \times \ln (\text{Load Level}) + 1851.773 \quad \textbf{[1(b)]}$$

$$(M_{rt}/M_{org}) = -15.1265 \times (L_{S\text{-}ext}/L) + 40.13077 \times (A_{S\text{-}ext}/A_s) + 7.201026 \times (\text{Load level}) + 133.8786 \quad \textbf{[2(a)]}$$

$$(M_{rt}/M_{org})^2 = -23770 \times (L_{S\text{-}ext}/L) + 23409.91 \times (A_{S\text{-}ext}/A_s) - 33875.4 \times (\text{Load level}) + 3672.185 \times (\text{Load level})^2 + 95517.42 \quad \textbf{[2(b)]}$$

$$\ln (ST_{rt}/ST_{org}) = -43.33771 \times (\text{Type of Reinforcement}) - 60.6257 \times (L_{S\text{-}ext}/L) + 56.03033 \times (L_{S\text{-}ext}/L)^2 + 55.69926 \times (A_{S\text{-}ext}/A_s) - 2.513029 \times (A_{S\text{-}ext}/A_s)^2 - 149.6919 \times (\text{Load level}) + 12.76711 \times (\text{Load level})^2 + 566.668 \quad \textbf{[3(a)]}$$

$$\ln (ST_{rt}/ST_{org}) = -0.14166 \times (L_{S\text{-}ext}/L) + 0.286813 \times (A_{S\text{-}ext}/A_s) - 0.02229 \times (A_{S\text{-}ext}/A_s)^2 - 0.45985 \times (\text{Load level}) + 0.045794 \times (\text{Load level})^2 + 6.170776 \quad \textbf{[3(b)]}$$

$$(EN_{rt}/EN_{org})^2 = 10110.78 \times (\text{Type of Reinforcement}) - 16274.1 \times (L_{S\text{-}ext}/L)^2 + 24381.64 \times (A_{S\text{-}ext}/A_s) - 1386.17 \times (A_{S\text{-}ext}/A_s)^2 + 53783.82 \times (\text{Load level}) - 4497.36 \times (\text{Load level})^2 - 112920 \quad \textbf{[4(a)]}$$

Ln (EN_{rt}/EN_{org}) = 0.227222 x $(A_{S\text{-}ext}/A_s)$ - 0.01926 x $(A_{S\text{-}ext}/A_s)^2$ + 0.168883 x (Load level) - 0.01885 x (Load level)^2 + 4.854691 **[4(b)]**

Table VI-1: Descriptive statistics of the used data

Variable	Number of Observations	Mean	Standard Deviation	Minimum value	Maximum value
Internal steel bars status	207	0.169082	0.375733	0	1
Type of Reinforcement	207	0.826087	0.379954	0	1
$L_{S\text{-}ext}/L$	207	0.328452	0.261934	0.05	0.9333
$A_{S\text{-}ext}/A_s$	207	2.879227	1.512859	0.5	5
Load level (%)	207	3.768116	0.812134	3.333333	5.833333
δ_r/δ_{max} **(%)**	207	51.47028	18.05731	18.83843	80.811
M_{rt}/M_{org} **(%)**	207	271.5901	62.80061	161.9011	385.8008
ST_{rt}/ST_{org} **(%)**	207	280.2387	69.36226	121.2801	408.0004
EN_{rt}/EN_{org} **(%)**	207	285.2922	50.92851	148.0198	428.5006

Table VI-2: Correlation coefficients between all variables

	Internal steel bars status	**Type of Reinforcement**	$L_{S\text{-}ext}/L$	$A_{S\text{-}ext}/A_s$	**Load level**	δ_r/δ_{max}	M_{rt}/M_{org}	ST_{rt}/ST_{org}	EN_{rt}/EN_{org}
Internal steel bars status	1								
Type of Reinforcement	0.21**	1							
$L_{S\text{-}ext}/L$	0.16**	0.11**	1						
$A_{S\text{-}ext}/A_s$	0.04*	-0.04*	-0.00*	1					
Load level	-0.24**	-0.46***	-0.13**	0.04*	1				
δ_r/δ_{max}	-0.13**	-0.40***	0.02*	-0.81††	0.25**	1			
M_{rt}/M_{org}	0.00*	-0.08*	-0.08*	0.971††	0.14**	-0.77†	1		
ST_{rt}/ST_{org}	0.12**	-0.05*	-0.01*	0.89††	-0.29**	-0.75†	0.85††	1	
EN_{rt}/EN_{org}	-0.10**	-0.10**	-0.16**	0.87††	0.34***	-0.65†	0.90††	0.62†	1

* None or very weak correlation (-0.1 to 0.1)

** Weak correlation (-0.3 to -0.1 or 0.1 to 0.3)

*** Moderate correlation (-0.5 to -0.3 or 0.3 to 0.5)

† Strong correlation (-0.5 to -0.8 or 0.5 to 0.8)

†† Very strong correlation (>0.8)

Table VI-3: Regression model for δ_r/δ_{max} for both steel and SMA retrofitted RC beams

Source	SS	df	MS	Number of obs	=	207
Model	5.62E+08	4	1.4E+08	F(4, 202)	=	364.84
				Prob > F	=	0
Residual	77758803	202	384944.6	R-squared	=	0.8784
				Adj R-squared	=	0.876
Total	6.4E+08	206	3104488	Root MSE	=	620.44

δ_r/δ_{max}	Coef.	Std. Err.	t	P>t	[95% Conf.	Interval]
Type of Rft	-1781.73	128.4904	-13.87	0	-2035.09	-1528.38
$L_{S\text{-}ext}/L$	429.9668	166.6478	2.58	0.011	101.3745	758.5591
$A_{S\text{-}ext}/A_s$	-964.33	28.60543	-33.71	0	-1020.73	-907.926
Load level	350.8894	60.26099	5.82	0	232.0682	469.7107
Constant	5758.656	311.51	18.49	0	5144.427	6372.884

Table VI-4: Regression model for δ_r/δ_{max} for steel retrofitted RC beams

Source	SS	df	MS	Number of obs	=	36
Model	4455916	3	148531	F(3, 32)	=	75.46
				Prob > F	=	0
Residual	6298652	32	196833	R-squared	=	0.8762
				Adj R-squared	=	0.8645
Total	5085781	35	145308	Root MSE	=	443.66

$(\delta_r/\delta_{max})^2$	Coef.	Std. Err.	t	P>t	[95% Conf.	Interval]
ln $(L_{S\text{-}ext}/L)$	289.6758	76.66331	3.78	0.001	133.5177	445.8338
$A_{S\text{-}ext}/A_s$	-518.564	45.28071	-11.45	0	-610.798	-426.33
ln (Load level)	3186.173	354.1277	9	0	2464.838	3907.507
Constant	1851.773	568.5884	3.26	0.003	693.5962	3009.95

Table VI-5: Regression model for M_{rt}/M_{org} for both steel and SMA retrofitted RC beams

Source	SS	df	MS	Number of obs	=	207
Model	777458.5	3	259152.8	F(3, 203)	=	1503.58
				Prob > F	=	0
Residual	34988.42	203	172.3567	R-squared	=	0.9569
				Adj R-squared	=	0.9563
Total	812446.9	206	3943.917	Root MSE	=	13.128

M_{rt}/M_{org}	Coef.	Std. Err.	t	P>t	[95% Conf.	Interval]
$L_{S\text{-}ext}/L$	-15.1265	3.520577	-4.3	0	-22.0681	-8.18493
$A_{S\text{-}ext}/A_s$	40.13077	0.605179	66.31	0	38.93753	41.32402
Load level	7.201026	1.136518	6.34	0	4.960132	9.44192
Constant	133.8786	4.914939	27.24	0	124.1877	143.5694

Table VI-6: Regression model for M_{rt}/M_{org} for steel retrofitted RC beams

Source	SS	df	MS	Number of obs	=	36
Model	5.35E+10	4	1.34E+10	F(4, 31)	=	295.89
				Prob > F	=	0
Residual	1.40E+09	31	45231786	R-squared	=	0.9745
				Adj R-squared	=	0.9712
Total	5.49E+10	35	1.57E+09	Root MSE	=	6725.5

$(M_{rt}/M_{org})^2$	Coef.	Std. Err.	t	P>t	[95% Conf.	Interval]
$L_{S\text{-}ext}/L$	-23770	6088.94	-3.9	0	-36188.5	-11351.6
$A_{S\text{-}ext}/A_s$	23409.91	686.414	34.1	0	22009.96	24809.86
Load level	-33875.4	14844.8	-2.28	0.03	-64151.7	-3599.16
(Load level)^2	3672.185	1614.11	2.28	0.03	380.1874	6964.183
Constant	95517.42	33093.9	2.89	0.007	28022.05	163012.8

Table VI-7: Regression model for ST_{rt}/ST_{org} for both steel and SMA retrofitted RC beams

Source	SS	df	MS			
Model	934848.14	7	133549.7	Number of obs	=	207
				F(5, 165)	=	472.53
				Prob > F	=	0
Residual	56243.2405	199	282.6293	R-squared	=	0.9433
				Adj R-squared	=	0.9413
Total	991091.382	206	4811.123	Root MSE	=	16.812

ln (ST_{rt}/ST_{org})	Coef.	Std. Err.	t	P>t	[95% Conf.	Interval]
Type of Rft	-43.33771	3.581911	-12.1	0	-50.40108	-36.27434
$L_{S\text{-}ext}/L$	-60.6257	15.90945	-3.81	0	-91.99844	-29.25296
$(L_{S\text{-}ext}/L)^2$	56.03033	17.00542	3.29	0.001	22.49638	89.56428
$A_{S\text{-}ext}/A_s$	55.69926	3.709661	15.01	0	48.38397	63.01455
$(A_{S\text{-}ext}/A_s)^2$	-2.513029	0.627414	-4.01	0	-3.750262	-1.275795
Load level	-149.6919	23.12186	-6.47	0	-195.2872	-104.0966
(Load level)^2	12.76711	2.578975	4.95	0	7.68148	17.85273
Constant	566.668	50.26954	11.27	0	467.5386	665.7973

Table VI-8: Regression model for ST_{rt}/ST_{org} for steel retrofitted RC beams

Source	SS	df	MS			
Model	2.424268	5	0.484854	Number of obs	=	36
				F(5, 30)	=	373.03
				Prob > F	=	0
Residual	0.038993	30	0.0013	R-squared	=	0.9842
				Adj R-squared	=	0.9815
Total	2.463262	35	0.070379	Root MSE	=	0.03605

ln (ST_{rt}/ST_{org})	Coef.	Std. Err.	t	P>t	[95% Conf.	Interval]
$L_{S\text{-}ext}/L$	-0.14166	0.03264	-4.34	0	-0.20832	-0.075
$A_{S\text{-}ext}/A_s$	0.286813	0.019471	14.73	0	0.247049	0.326577
$(A_{S\text{-}ext}/A_s)^2$	-0.02229	0.003187	-6.99	0	-0.0288	-0.01578
Load level	-0.45985	0.079577	-5.78	0	-0.62236	-0.29733
(Load level)^2	0.045794	0.008653	5.29	0	0.028123	0.063465
Constant	6.170776	0.178547	34.56	0	5.806134	6.535418

Table VI-9: Regression model for EN_{rt}/EN_{org} for both steel and SMA retrofitted RC beams

Source	SS	df	MS			
				Number of obs	=	207
Model	1.5735e+11	6	2.62E+10	F(6, 200)	=	239.1
				Prob > F	=	0
Residual	2.1937e+10	200	1.1E+08	R-squared	=	0.8776
				Adj R-squared	=	0.874
Total	1.7929e+11	206	8.7E+08	Root MSE	=	10473

$(EN_{rt}/EN_{org})^2$	Coef.	Std. Err.	t	P>t	[95% Conf. Interval]	
Type of Rft	10110.78	2230.51	4.53	0	5712.439	14509.1
$(L_{S\text{-}ext}/L)^2$	-16274.1	3009.97	-5.41	0	-22209.4	-10338.7
$A_{S\text{-}ext}/A_s$	24381.64	2310.97	10.55	0	19824.66	28938.6
$(A_{S\text{-}ext}/A_s)^2$	-1386.17	390.852	-3.55	0	-2156.886	-615.447
Load level	53783.82	14396.7	3.74	0	25395	82172.6
(Load level)^2	-4497.36	1605.97	-2.8	0.006	-7664.167	-1330.56
Constant	-112920	31312.7	-3.61	0	-174664.9	-51174.1

Table VI-10: Regression model for EN_{rt}/EN_{org} for steel retrofitted RC beams

Source	SS	Df	MS			
Model	1.25091	4	0.312728	Number of obs	=	36
				F(4, 31)	=	551.92
				Prob > F	=	0
Residual	0.017565	31	0.000567	R-squared	=	0.9862
				Adj R-squared	=	0.9844
Total	1.268475	35	0.036242	Root MSE	=	0.0238

ln (EN_{rt}/EN_{org})	Coef.	Std. Err.	t	P>t	[95% Conf.	Interval]
$A_{S\text{-}ext}/A_s$	0.227222	0.012855	17.68	0	0.201003	0.253441
$(A_{S\text{-}ext}/A_s)^2$	-0.01926	0.002104	-9.15	0	-0.02355	-0.01497
Load level	0.168883	0.052541	3.21	0.003	0.061725	0.27604
(Load level)^2	-0.01885	0.005713	-3.3	0.002	-0.0305	-0.0072
Constant	4.854691	0.117746	41.23	0	4.614547	5.094834

VITA

Name Yamen Ibrahim Elbahy

Post-Secondary Education and Degrees

- University of Western Ontario
  London, Ontario, Canada
  2010 – 2018, PhD
- University of Western Ontario
  London, Ontario, Canada
  2006 – 2008, M.E.Sc.
- Information Technology Institute
  Giza, Egypt
  2005 - 2006, Software Development Diploma
- Ain Shams University
  Cairo, Egypt
  1999 – 2004, B.E.Sc.

Memberships:

- Engineer in Training (EIT), Professional Engineers of Ontario (PEO)
- ACI student membership
- Engineers Syndicate of Egypt

Honors and Awards:

- 2011-2014, Canada Graduate Scholarship (NSERC-CGS),
- 2011-2012, Ontario Graduate Scholarship (OGS) – Declined by the applicant
- 2010 - 2014, Western Engineering Scholarship
- 2008, Best paper award, 2nd Canadian conference on effective design CCEDS-II, McMaster University, Hamilton, Ontario, Canada.
- 2007, Nominated for one of the top ten abstracts in CAC-Ontario Exchange Forum at The University of Waterloo
- 2006 - 2008, Western Engineering Scholarship
- 2005 – 2006, Egyptian Ministry of Communications and Information Technology Scholarship, Information Technology Institute, Giza, Egypt.
- 1999 - 2004, The Government Award of Excellence in undergraduate studies, Ain Shams University, Cairo, Egypt. 1999-2004

Related Work Experience:

- Teaching and Research Assistant
  The University of Western Ontario,
  London, Ontario, Canada
  2010-2018 & 2006 – 2008

- Research Assistant

  The British University in Egypt (BUE),

  Cairo, Egypt

  2009-2010

- Junior Structural Engineer

  Arab Consulting Engineers (MOHARRAM BAKHOUM), Giza, Egypt

  2005

Publications:

- Elbahy Y.I., Youssef M.A., Nehdi M. (2010). "Deflection of Superelastic Shape Memory Alloy Reinforced Concrete Beams: Assessment of Existing Models." Canadian Journal of Civil Engineering, 37(6), 842:854.
- Elbahy Y.I., Nehdi M., Youssef M.A. (2010). "Artificial Neural Network Model for Deflection Analysis of Superelastic Shape Memory Alloy Reinforced Concrete Beams." Canadian Journal of Civil Engineering, 37(6), 855:864.
- Elbahy Y.I., Youssef M.A., Nehdi M. (2009). "Stress Block Parameters for Concrete Flexural Members Reinforced with Superelastic Shape Memory Alloys." Materials and Structures Journal, 42(10), 1335:1351. DOI: 10.1617/s11527-008-9453-z.

- Elbahy Y.I., Youssef M.A., Nehdi M. (2008). “Flexural Behaviour of Concrete Members Reinforced with Shape Memory Alloys.” 2nd Canadian Conference on Effective Design of Structures CCEDS-II, Sustainability of Civil Engineering Structures, Hamilton, ON, Canada, pp. 477-486.
- Elbahy, Y.I., El-Feki, M.A., El-Fitiany, S.F., Siddique, M., and El-Naggar, M. (2008). Big Beam Contest. Report Submitted to Precast/Prestressed Concrete Institute, Chicago, IL, June, 2008.